Field-based measurement and characterization of transport and turn-over of wastewater contaminants in streams

Dissertation

der Mathematisch-Naturwissenschaftlichen Fakultät

der Eberhard Karls Universität Tübingen

zur Erlangung des Grades eines

Doktors der Naturwissenschaften

(Dr. rer. nat.)

vorgelegt von

Gaëlle Guillet

aus Saint-Germain-en-Laye, Frankreich

Tübingen

2021

Gedruckt mit Genehmigung der Mathematisch-Naturwissenschaftlichen Fakultät der Eberhard Karls Universität Tübingen.

Tag der mündlichen Qualifikation:	30.06.2021
Dekan:	Prof. Dr. Thilo Stehle
1. Berichterstatter:	Prof. Dr. Beate Escher
2. Berichterstatter:	Dr. Marc Schwientek

Abstract

The present work investigated the spatio-temporal variability of the input and fate of common wastewater contaminants (e.g. pharmaceuticals, flame retardants, personal-care products, etc.) in three contrasting rivers in the area of Tübingen, southern Germany. Field sampling particularly focused on assessing reactive transport and key parameters affecting contaminant removal in streams, as well as their association to particles during high-discharge events. Among the three investigated catchments, River Steinlach was the main investigation site with a catchment characterized by mixed land use. River Ammer exhibits a mainly agricultural and slightly more urbanized catchment and River Goldersbach drains a primarily forested catchment devoid from treated wastewater discharge or heavy traffic.

Reactive transport was investigated during two sampling campaigns using novel approaches of the Lagrangian sampling scheme in a segment of River Steinlach downstream of a wastewater treatment plant (WWTP). For optimal results, environmental conditions favorable for natural attenuation were chosen – i.e. baseflow conditions, sunny and dry weather. One sampling approach, the so-called "tracer-based sampling", coupled a conservative-tracer test with water sampling at four monitoring sites during a day- and a night-time experiment. The tracer breakthrough curves were deconvoluted to calculate transfer functions, mathematical operators describing the travel time distribution of a water parcel flowing between the measuring stations. The transfer functions served to disentangle conservative transport processes affecting observed concentrations from degradation of compounds investigated and fit first-order decay constants for photo-dependent and -independent elimination. The other approach, the so-called "24 h sampling", monitored mass fluxes along a 24 h-water parcel at two sampling sites. A mass balance of studied compounds was calculated during a winter campaign to serve as a comparison to a previous identical study conducted during the summer season. The length of the water parcel was chosen to minimize biases by inaccuracies from timing and dispersion effect and to integrate complete diurnal patterns in contaminant input and removal. Since concentrations of suspended sediments are typically low during baseflow conditions in the investigated rivers, particle-associated transport was assessed by sampling of turbid water during flood events in Rivers Steinlach and Ammer. Linear correlations between total contaminant and particle concentrations were tested as it had previously been done for polycyclic aromatic hydrocarbons (PAHs). Finally, contaminant fluxes were monitored during a monthly sampling in River Steinlach, Ammer and Goldersbach and yearly loads were estimated and compared.

Contaminants observed in River Steinlach exhibited conservative (e.g. carbamazepine) to highly reactive behaviors (e.g. oxcarbazepine was completely removed during the tracer-based sampling). The comparison between day- and night-time, and summer and winter conditions, highlighted the occurrence of photo-dependent and -independent elimination processes as well as their seasonal dependence. In winter, reactivity was reduced, with an absence of photo-dependent elimination and limited or no photo-independent elimination of most analyzed compounds. Contaminant removal was higher in the tracer-based study compared to the summer 24 h sampling or previous field studies. Enhanced photo-dependent and independent elimination observed during the tracer-based sampling were linked to local parameters such as the high proportion of treated wastewater, water temperature, dissolved organic carbon and nitrate concentrations, as well as low flow conditions with a larger flow fraction through the hyporheic zone. During day-time, photo-dependent degradation was highly efficient for metoprolol, bisoprolol or venlafaxine in the tracer-based study, but its impact on contaminant removal was comparatively similar or lower than photo-independent processes when averaged over 24 hours.

A linear correlation between total contaminant and particle concentration was only found for six of the fourteen contaminants analyzed during the flood sampled in River Ammer. The method is based on the assumption that the dissolved concentration of contaminants and their average concentration on the particles does not vary over time. But the simultaneous input of dissolved contaminants during combined-sewer overflows parallel to the mobilization of particles may have led to such apparent

correlations between total concentrations of contaminants and particle concentration. Without analyzing directly compounds onto the sediments, particle-associated transport could not be confirmed, nor a constant loading of the contaminants on suspended particles. If any, less than 51% for carbamazepine, diclofenac, naproxen, TCPP and triclosan and less than 67% for lidocaine was associated to particles for suspended sediment concentration around 300 mgL^{-1} during the Ammer event sampled.

Fluxes calculated during the sampling campaigns identified the WWTP as the main source of wastewater contaminants in River Steinlach during dry-weather conditions. Yearly load estimations were challenged by contaminant input variability from the WWTP, the contaminant degradability and the erratic activation of additional contaminant sources by precipitation. While loads of individual contaminants in the pristine part of the Goldersbach catchment were negligible, they reached up to 10 $kg\ a^{-1}$ (for HHCB-lactone and TCPP) in the Steinlach and Ammer catchments downstream of WWTPs. In comparison, PAHs, that are mainly released into rivers sorbed to particles during precipitation events, exhibited loads of 4 and 6 $kg\ a^{-1}$ in River Steinlach and Ammer, respectively.

In conclusion, contaminants released continuously by WWTPs can undergo no to complete natural attenuation in receiving rivers. But attenuation processes, particularly photo-dependent elimination, are strongly governed by prevailing environmental conditions and follow their variability in time. This variability is yet to be fully assessed, further than day and night or season alternation, to capture a more representative picture of compound reactivity according to environmental parameters met in single streams. Also, higher fluxes of contaminants are released during episodic precipitation events and sorption to particles in turbid waters during floods may occur, but remains to be demonstrated.

Zusammenfassung

Die vorliegende Arbeit untersuchte die räumlich-zeitliche Variabilität des Eintrags und des Verbleibs gängiger abwasserbürtiger Schadstoffe (z.B. Pharmazeutika, Flammschutzmittel, Körperpflegemittel, etc.) in drei kontrastierenden Flüssen im Raum Tübingen, Süddeutschland. Die Probennahmen konzentrierten sich insbesondere auf die Bewertung des reaktiven Transports und der Schlüsselparameter, die den Schadstoffabbau in den Fließgewässern beeinflussen, sowie auf die Assoziation der Schadstoffe mit Partikeln bei Hochwasserereignissen. Von den drei untersuchten Einzugsgebieten war die Steinlach das Hauptuntersuchungsgebiet, das durch gemischte Landnutzung gekennzeichnet ist. Die Ammer weist ein hauptsächlich landwirtschaftlich genutztes und etwas stärker urbanisiertes Einzugsgebiet auf, und der Goldersbach entwässert ein hauptsächlich bewaldetes Einzugsgebiet ohne Abwassereinleitungen oder starken Verkehr.

Der reaktive Transport wurde während zweier Beprobungskampagnen mit neuartigen Ansätzen des Lagrangeschen Beprobungsschemas in einem Flussabschnitt der Steinlach flussabwärts einer Kläranlage untersucht. Für optimale Ergebnisse wurden Umweltbedingungen gewählt, die eine natürliche Attenuierung begünstigen - d.h. Basisabfluss, sonniges und trockenes Wetter. Ein Probennahmeansatz, die sogenannte "tracerbasierte Probennahme", koppelte einen konservativen Tracerversuch mit Wasserproben an vier Messstellen während eines Tag- und eines Nachtexperiments. Die Tracer-Durchbruchskurven wurden entfaltet, um Transferfunktionen zu berechnen, mathematische Operatoren, die die Fließzeitverteilung eines zwischen den Messstationen fließenden Wasserpakets beschreiben. Die Transferfunktionen dienten dazu, konservative Transportprozesse, die die beobachteten Konzentrationen beeinflussen, vom Abbau der untersuchten Verbindungen zu entkoppeln und Abbauratenkonstanten erster Ordnung für die photoabhängige und -unabhängige Elimination zu bestimmen. Der andere Ansatz, die so genannte "24 h-Beprobung", beobachtete die Massenflüsse entlang eines 24 h-Wasserpakets an zwei Probenahmestellen. Eine Massenbilanz der untersuchten Verbindungen wurde während einer Winterkampagne berechnet und diente als Vergleich zu einer früheren identischen Studie während der Sommersaison. Die Länge des Wasserpakets wurde gewählt, um Ungenauigkeiten aufgrund von Timing- und Dispersionseffekten zu minimieren und um vollständige tageszeitliche Muster im Schadstoffeintrag und -abbau zu integrieren. Da die Konzentrationen von Schwebstoffen in den untersuchten Flüssen während des Basisabflusses typischerweise niedrig sind, wurde der Partikel-assoziierte Transport durch die Beprobung von trübem Wasser während Hochwasserereignissen in Steinlach und Ammer untersucht. Lineare Korrelationen zwischen Gesamtschadstoff- und Partikelkonzentrationen wurden getestet, wie es zuvor für polyzyklische aromatische Kohlenwasserstoffe (PAK) gemacht wurde. Schließlich wurden die Schadstoffflüsse während einer monatlichen Probenahme in der Steinlach, der Ammer und dem Goldersbach beobachtet und die Jahresfrachten abgeschätzt und verglichen.

Die in der Steinlach beobachteten Schadstoffe zeigten ein konservatives (z.B. Carbamazepin) bis hochreaktives Verhalten (z.B. wurde Oxcarbazepin bei der tracerbasierten Beprobung vollständig eliminiert). Der Vergleich zwischen Tag- und Nachtzeit sowie Sommer- und Winterbedingungen verdeutlichte das Auftreten von photoabhängigen und -unabhängigen Eliminationsprozessen sowie deren saisonale Abhängigkeit. Im Winter war die Reaktivität reduziert, mit einer fehlenden photoabhängigen Elimination und einer begrenzten oder keiner photounabhängigen Elimination der meisten analysierten Verbindungen. Die Schadstoffentfernung war in der tracerbasierten Studie höher als bei der 24-Stunden-Probenahme im Sommer oder bei früheren Feldstudien. Die erhöhte photoabhängige und -unabhängige Elimination, die während der tracerbasierten Beprobung beobachtet wurde, stand in Zusammenhang mit lokalen Parametern wie dem hohen Anteil an gereinigtem Abwasser, der Wassertemperatur, den gelösten organischen Kohlenstoff- und Nitratkonzentrationen sowie den niedrigen Durchflussbedingungen mit einem größeren Durchflussanteil durch die hyporheische Zone. Während des Tages war der photoabhängige Abbau für Metoprolol, Bisoprolol oder

Venlafaxin in der tracerbasierten Studie hocheffizient, aber sein Einfluss auf die Schadstoffentfernung war vergleichsweise ähnlich oder geringer als die photounabhängigen Prozesse, wenn über 24 Stunden gemittelt wurde.

Ein linearer Zusammenhang zwischen Gesamtschadstoff- und Partikelkonzentration wurde nur für sechs der vierzehn analysierten Schadstoffe während der Hochwasserbeprobung in der Ammer gefunden. Die Methode basiert auf der Annahme, dass die gelöste Konzentration der Schadstoffe und ihre durchschnittliche Konzentration auf den Partikeln nicht über die Zeit variiert. Aber der gleichzeitige Eintrag von gelösten Schadstoffen bei Mischwasserüberläufen parallel zur Mobilisierung von Partikeln kann zu solchen scheinbaren Korrelationen zwischen Gesamtkonzentrationen von Schadstoffen und Partikelkonzentration geführt haben. Ohne eine direkte Analyse der an den Sedimenten sorbierten Verbindungen konnte weder ein partikelassoziierter Transport noch eine konstante Beladung der Schadstoffe auf suspendierten Partikeln bestätigt werden. Wenn überhaupt, waren weniger als 51% für Carbamazepin, Diclofenac, Naproxen, TCPP und Triclosan und weniger als 67% für Lidocain bei einer Schwebstoffkonzentration um 300 mgL^{-1} während des beprobten Ammer-Ereignisses mit Partikeln assoziiert.

Die während der Beprobungskampagnen berechneten Flüsse identifizierten die Kläranlage als Hauptquelle für Abwasserschadstoffe in der Steinlach bei Trockenwetterbedingungen. Jährliche Belastungsabschätzungen wurden durch die Variabilität der Schadstoffeinträge aus der Kläranlage, deren Abbaubarkeit der Schadstoffe und die erratische Aktivierung zusätzlicher Schadstoffquellen durch Niederschläge erschwert. Während die Frachten einzelner Schadstoffe im naturbelassenen Teil des Goldersbach-Einzugsgebietes vernachlässigbar waren, erreichten sie in den Einzugsgebieten von Steinlach und Ammer flussabwärts der Kläranlagen bis zu 10 $kg\ a^{-1}$ (für HHCB-Lacton und TCPP). Im Vergleich dazu wiesen PAK, die hauptsächlich bei Niederschlagsereignissen an Partikel sorbiert in die Flüsse gelangen, Frachten von 4 bzw. 6 $kg\ a^{-1}$ in Steinlach und Ammer auf.

Zusammenfassend lässt sich sagen, dass Schadstoffe, die kontinuierlich aus Kläranlagen freigesetzt werden, in den aufnehmenden Flüssen keine bis keine vollständige natürliche Attenuierung erfahren. Die Abbauprozesse, insbesondere die photoabhängige Elimination, werden jedoch stark von den vorherrschenden Umweltbedingungen bestimmt und folgen deren zeitlicher Variabilität. Diese Variabilität muss noch vollständig bewertet werden, über den Tag- und Nacht- oder Jahreszeitenwechsel hinaus, um ein repräsentativeres Bild der Reaktivität von Verbindungen in Abhängigkeit von den in einzelnen Strömen angetroffenen Umweltparametern zu erhalten. Außerdem werden bei episodischen Niederschlagsereignissen höhere Schadstoffflüsse freigesetzt, und bei Überschwemmungen kann es zu einer Sorption an Partikel in trübem Wasser kommen, was jedoch noch nicht nachgewiesen ist.

Acknowledgement

I would like to thank all the people who accompanied me through these years in Tübingen. First of all, I want to thank Prof. Dr. Peter Grathwohl for giving me my chance with a master thesis and later with a PhD position in his department at Tübingen University. I particularly want to express my gratitude to Dr. Marc Schwientek, for his supervision and guidance throughout my work. His continuous availability and advises helped me get through this work. Also, his support, when I needed it, helped me complete these years despite difficult events. Another very important person through my years in Tübingen was Dr. Julia Knapp, who was of a great help regarding the modelling part of my thesis as well as a great co-worker and office companion. I would also like to thank Dr. Hermann Rügner, who accompanied us in field campaigns and was always available for discussion. I want to address thanks to Prof. Dr. Olaf Cirpka for his great input in a late part of my work and the paper that it yielded. Further thanks go to our chemistry partners, without whom none of my samples would have been analyzed. During our meetings, Dr. Bertram Kuch and Dr. Sylvain Merel always showed enthusiasm to talk about my compounds and the results I was observing in my test sites. I would also like to acknowledge the technical crew of Tübingen lab (Thomas, Annegret, Bernice, Renate and Sara). I particularly interacted with Sara, Renate and Thomas, who offered me their help and advises at many occasions and always welcomed me in a warm atmosphere to work in.

I also want to thank the people from Keplerstrasse 17, with whom I could always have a nice chat when passing by. The lunch crew to the Mensa (Zhongwen, Reynold, Matthias, Bo, Jeremy, Yan) always offered me a fun and relaxed break time when I was joining them. And I particularly thank my office companions, again Julia and Yan, as well as Marie-Sophie, Jens, Astrid and Katharina. I, of course, do not forget the other members of the Grathwohl work group, in particular Jana and Sven, whit whom I had always enjoyable chats. At my return to the office in the late months, I got to join our PhD team Ran, Victor, Elena and her son Yarik, Veronika, Oscar, Clarissa and Phillip, with whom I had great times that gave me the last push to finish this thesis.

I finally want to thank Monique Baqué, who hosted me when I arrived in Germany and helped me through the German paperwork to start a new life in Tübingen. She remained a close friend ever since.

This work would have of course not been possible without the financial support from joint grant from the Helmholtz Center for Environmental Research, Leipzig (UFZ) and the Ministry of Science, Research and Arts of Baden-Württemberg (AZ Zu 33-721.3-2) as well as the EU FP7 Collaborative Project GLOBAQUA (Grant Agreement no 603629). Additional support was provided by the Collaborative Research Center 1253 CAMPOS (Project P1: Rivers), funded by the German Research Foundation (DFG, Grant Agreement SFB 1253/1 2017).

Table of Contents

List of figures

List of tables

List of tables and figures in the Appendix

1 Introduction

Wastewaters produced by households, industries and other urban structures, are collected but treated incompletely by wastewater treatment plants (WWTPs), that release many chemical species into surface waters (Bester, 2004; Leclercq et al., 2009; Reemtsma et al., 2006; Simonich et al., 2002; Ternes, 1998). Due to their increasing diversity and use in modern societies, organic wastewater contaminants, pharmaceuticals, personal care products and flame retardants among others, have become ubiquitous in the environment (Bester, 2005; Heberer et al., 1999; Loos et al., 2009; Ternes, 1998). The persistence of contaminants determines how far they spread within the river network, raising concerns regarding their environmental impact (Adolfsson-Erici et al., 2002; la Farré et al., 2008; Seeland et al., 2012; van der Veen and de Boer, 2012) and the risk for drinking water exploitations (Benotti et al., 2009; Kuehn and Müller, 2000; Mompelat et al., 2009; Nödler et al., 2013; Webb et al., 2003).

In addition to wastewater, sewer systems particularly in southern Germany often collect run-off water from urban surfaces during rain events. These "combined sewers" are equipped with outlets that can discharge the excess mixture of run-off and raw wastewater into the river network in case the sewers' volume capacity gets submerged by incoming water. Though WWTPs are widely recognized as primary sources of wastewater contaminants in surface waters during dry-weather conditions (Baker and Kasprzyk-Hordern, 2013; Heberer et al., 1999; Lindström et al., 2002; Moreno-González et al., 2014; Schultz et al., 2010; Schwientek et al., 2016), they can be by-passed during sufficiently intense rain events, as combined-sewer overflows (CSOs) become consequent contaminant sources for a short period of time (Gasperi et al., 2010; Launay et al., 2016; Musolff et al., 2010; Radke et al., 2010). They also release land-surface particles that were dragged into the sewers by rain, wastewater solid phase as well as old sewer sediments simultaneously with untreated wastewater into receiving rivers. These particles may contain sorbed contaminants and add up to remobilized river sediments that can also have a share of contaminated particles from previous waste- or treated water discharge (Lahti and Oikari, 2011; Schultz et al., 2010; Yang et al., 2015). Sorption to particles protects contaminants to a certain degree from degradation processes such as bio or photo-degradation (Bouwer et al., 1994; Huang et al., 2015). Where soluble compounds may be quickly flushed through the river network, particles and contaminants that are bound to them will represent a source of contamination as they settle down into the riverbed and release adsorbed contaminants over time or transfer them to the fauna feeding on sediment (Landrum, 1989; Sangster et al., 2014).

1.1 State of the art

1.1.1 Assessing reactive transport of compounds in rivers

Contaminants dissolved in the water column can undergo various physico-chemical or biological processes – e.g. hydrolysis, sorption, photo- and bio-degradation – that will attenuate their concentration in the water column as travel time increases from the source. The persistence of wastewater contaminants has mainly been studied in the laboratory to assess their respective susceptibilities to natural attenuation processes (Andreozzi et al., 2002; Baena-Nogueras et al., 2017; Durán-Álvarez et al., 2015; Lin et al., 2010; Lindström et al., 2002; Yamamoto et al., 2009). While these susceptibilities relate to the intrinsic physico-chemical properties of the contaminant, environmental conditions play an important role in triggering reaction processes. The anticonvulsant carbamazepine, as an example, was demonstrated to undergo indirect photodegradation in laboratory experiments (Andreozzi et al., 2002; Matamoros et al., 2009) while being well known to be persistent in the environment (Kunkel and Radke, 2012; Li et al., 2016; Schwientek et al., 2016). Such contrast highlights how the site-specific environmental conditions combined with the intrinsic properties of investigated compounds can be decisive for contaminant transport and the occurrence of transformation processes. How these field

conditions impact the compounds is however not well understood so far, as discrepancies also occur between different field studies (Li et al., 2016). As an example, Fono et al. (2006), Kunkel and Radke (2011) and Lin et al. (2006) found varying half-lives of the anti-inflammatory drug ibuprofen ranging from 4.6 days to 5.4 hours in the River Trinity (USA), the River Säva (Sweden) and the River Santa Ana (USA), respectively. Kunkel and Radke (2011) highlighted the lack of "holistic mechanistic understanding which allows predicting micropollutant attenuation based on […] site-specific parameters". Furthermore, Kunkel and Radke (2012) and Li et al. (2016) compared the same river system and showed differences in contaminant attenuation. Environmental conditions thus do vary in time, from one year or season to another, to scales as small as day and night alternation (Lin et al., 2006) or even within minutes as sunlight is shielded by cloud cover. This calls for improved field assessment methods to multiply environmental observations and gather clues on which and how field parameters influence the fate of contaminants in streams.

To assess the fate of wastewater contaminants in rivers, one must take into account the temporal variability of the input from WWTPs as well as elimination processes – e.g. typically, the variation of photodegradation according to solar radiation – and river transport characteristics – e.g. advection, dispersion or dilution. Among the numerous methods designed to assess the fate of solutes in rivers, the Lagrangian sampling scheme takes into account the constraints previously cited. In Lagrangian sampling schemes (Meade and Stevens, 1990; Moody, 1993), the same water parcel is repeatedly sampled on its way down the river, thus separating effects of advection from those of mixing and reaction on solute concentrations.

To time their sampling, some authors estimated velocities by hydrodynamic modeling (Bertani et al., 2016; Cladière et al., 2014; Ruff et al., 2015) while others used tracer tests prior to their campaign (Barber et al., 2013, 2011; Brown et al., 2009; Mandaric et al., 2019; Schultz et al., 2010). However, even small inaccuracies in the travel time (e.g., due to changing river discharge) can bias the interpretation of the observations, as WWTP inputs fluctuate in time (e.g., Writer et al. (2013) found a 300% variation of effluent discharge within 4 h).

One solution is to label the water parcel with a tracer compound and sample it as it passes the respective control sections (Morrall et al., 2004; Schaper et al., 2018). However, in addition to fluctuation of contaminant input, dispersion can cause a biased interpretation of the contaminant concentrations. While some researchers neglected this bias (Lin et al., 2006; Morrall et al., 2004), others adapted their sampling methodology to limit them (e.g., normalization to the concentration of a conservative compound (Antweiler et al., 2014; Barber et al., 2013), introduction of correcting factors based on conservative-compound measurements (Writer et al., 2013), or increasing the sampling interval along the investigated river section to counter dispersion effect (Antweiler et al., 2014; Writer et al., 2013)). A straightforward method is the coupled artificial input of reactive and conservative contaminants as tracers (Kunkel and Radke, 2011; Writer et al., 2012). However, injecting contaminants into rivers is not always compatible with local environmental regulations. It can also yield unrealistic concentrations in the studied river stretch, while microbial communities are not adapted to degrade them. At last, averaging long concentration time series at each control plane limits the impact of inaccuracies (Glaser et al., 2020b; Hanamoto et al., 2018; Radke et al., 2010; Ruff et al., 2015; Schaper et al., 2018; Schwientek et al., 2016).

1.1.2 Importance of particle-associated transport

Sorption of hydrophobic compounds to the organic phase of sediments and suspended particles in waterbodies has been well documented, particularly for highly sorbing compounds, such as polycyclic aromatic hydrocarbons (PAHs), polychlorinated biphenyls (PCBs) or pesticides (Gasperi et al., 2010; Navarro et al., 2009; Readman et al., 1982; Rügner et al., 2019; Schwientek et al., 2013b). But as

research focused more and more on emerging contaminants, studies started investigating the sorption of wastewater contaminants onto environmental particles (Hanamoto et al., 2018; Huang et al., 2015; Lahti and Oikari, 2011; Sangster et al., 2015; Stein et al., 2008; Winkler et al., 1998). Among those latter, compounds such as pharmaceuticals or personal care products count many ionizable species that can bind to particles through other processes than partitioning to organic matter (Al-Khazrajy and Boxall, 2016; Burke et al., 2013; Lahti and Oikari, 2011; Lin et al., 2010; Yamamoto et al., 2009). Non-hydrophobic sorption includes electrostatic interactions with charged mineral surfaces or natural organic matter, ion exchange, complexation to mineral surfaces or electron donor-acceptor interactions. Sorption of organic contaminants depends not only on the compound ionization or hydrophobicity, but also on the nature and characteristics of sediments such as cationic-exchange capacity, complexation sites or carbon content (Al-Khazrajy and Boxall, 2016; Gao and Pedersen, 2005; Huang et al., 2014; Lahti and Oikari, 2011; Sangster et al., 2015; Schaffer et al., 2012a). Environmental parameters can also influence sorption of wastewater contaminants. pH as an example, determines their degree of ionization within water and their inclination towards non-hydrophobic interaction – or repulsion (Al-Khazrajy and Boxall, 2016; Hari et al., 2005; Lahti and Oikari, 2011; Schaffer et al., 2012b).

In streams such as the low order rivers investigated in this work, particle load is generally deemed negligible as turbidity, and thus particle concentration, remains low outside of high discharge events (Rügner et al., 2013). Major fluxes of highly sorbing organic compounds such as PAHs, PCBs and polybrominated diphenyl ether (PBDEs) have been observed to be released in surface waters during high discharge events, as their concentrations were clearly correlated to particle concentrations in rivers (Gasperi et al., 2014; Gilbreath and McKee, 2015; Schwientek et al., 2013b). Wastewater contaminants have been found sorbed onto riverbed sediments, particularly downstream of WWTPs, as well as onto sewer sediments (Launay et al., 2016; Schultz et al., 2010). They thus can also constitute reserves that can be mobilized during high discharge conditions, as precipitation events induce CSOs and particle resuspension. CSOs are also consequent sources of dissolved contaminants (Buerge et al., 2006; Launay et al., 2016; Musolff et al., 2010; Radke et al., 2010), particularly those that are highly degraded in WWTP (Weyrauch et al., 2010) or washed off of urban surfaces (Chebbo and Gromaire, 2004; Rabiet et al., 2010). These dissolved wastewater contaminants might be found in high amounts in the presence of mobilized particles during high discharge events, with the possibility to sorb to those latter.

Unlike bed-sediment sampling, that can show spatial disparities in contaminant concentrations (Lu et al., 2015; Schultz et al., 2010; Walling et al., 2003), sampling suspended sediment during flood conditions expects an averaging of the overall-catchment particles (Schwientek et al., 2013b). Thus, monitoring turbidity events induced by floods is essential to give more insight on the particle-associated transport of wastewater contaminants. Precipitation events and the resulting floods and CSOs being sparse and hardly foreseeable, contaminant fluxes released during such events can be easily missed for the estimation of annual loads, urging to an adapted monitoring or the use of a proxy (Madrid and Zayas, 2007; Rabiet et al., 2010; Rügner et al., 2013).

1.2 Research questions

In the context previously described, the following questions arise:

- How can elimination processes and transport of wastewater contaminants be assessed during a field study?
- How do degradation processes affect the transport of wastewater contaminants in rivers impacted by WWTP effluent discharge?
- Which environmental parameter(s) determine the fate and transport of contaminants in streams?

1.3 Objectives and structure of the thesis

This work investigates how wastewater contaminants discharged into surface waters are transported along river segments.

The first part focuses on reactive transport of wastewater pollutants introduced through WWTP effluent discharge into a segment of River Steinlach during dry-weather conditions. New sampling approaches were tested in order to assess the fate of wastewater contaminants under various environmental conditions and highlight key parameters or combinations of key parameters that will hinder or foster contaminant removal in streams. The so-called "*tracer-based sampling*", tested a new tracer-based approach to isolate conservative transport, measured through the monitoring of a tracer, from reactive turnover by using computation. Transfer functions of reactive compounds were used to fit first-order decay constants by comparing measured concentrations of wastewater constituents to simulated concentrations from convoluting transfer functions of the conservative tracer. The comparison of day- and night-time experiments allowed to discriminate between photo-dependent and -independent elimination processes. The so-called "*24 h sampling*" followed the Lagrangian sampling scheme by monitoring contaminant loads of a 24 h-long water parcel to calculate a mass balance that palliates inaccuracies from timing and dispersion effect from regular Lagrangian sampling. Observing 24 h cycles was meant to demonstrate diurnal patterns in contaminant release and removal – e.g. photodegradation during day-time. The sampling was operated during a winter campaign to investigate seasonal differences in contaminant removal as a comparison from previous identical works performed in the summer season before.

The second part investigates the particle-associated transport of wastewater contaminants, discharged into rivers through CSOs or remobilized from storages in the bed-sediment. During wet-weather conditions, reactive turnover in the water column is neglected, assuming that turbulences, turbidity, short residence time and cloud cover will hinder major degradation processes such as bio- or photodegradation. Sampling of turbid water was performed in two rivers presenting contrasting sediment natures, River Steinlach and Ammer. The course of a complete flood event, which presents the interest of gathering mixed sediment types from across the catchment, was monitored at one spot for each river. Samples were taken to measure concentrations of contaminants and particles in the bulk water and determine a correlation that would allow calculating the average concentration of contaminants on the floating particles.

In a third part, the fluxes of wastewater contaminants monitored during the various campaigns as well as a monthly sampling performed in River Goldersbach, Steinlach and Ammer between 2009 and 2011 by the WESS competence cluster are used to assess spatio-temporal variability of contaminant release and transport. Yearly loads were estimated for example wastewater contaminants and compared to PAHs that are transported almost exclusively on particles mobilized during wet-weather conditions.

2 Investigated river systems

The research in this thesis was performed in tributaries of River Neckar, in the vicinity of Tübingen, south-west Germany (see Figure 1).

2.1 River Steinlach

The main investigation field-site was River Steinlach, a 4th-order stream taking its source in the Swabian Alb at 700 m above sea level (a.s.l.) and entering River Neckar at 320 m a.s.l. in the city of Tübingen. River Steinlach is 25 km long, draining a 142 km² hilly catchment in the northern foreland of the Swabian Alb Mountains. With a precipitation of 900 mm yr^{-1} (1980–2009) in the catchment, which maximum intensity occurs in summer, River Steinlach exhibits an average discharge of 1.7 m^{3}s^{-1}.

Concerning the lithologic features of the Steinlach watershed, Mesozoic formations cross diagonally the catchment. The Upper "White" Jurassic in south-east of the catchment begins with marls shifting to massive limestone banks at the highest altitudes of the catchment. Further downstream, the stream crosses clayey marls to thick limestone banks from Middle "Brown" Jurassic followed by limestone banks and organic rich clayey marls from the Lower "Black" Jurassic formation. The oldest formations in the northern and downstream part are constituted by marls and sandstones from the Middle Keuper. In the river bed, the sediment deposits consist mainly of limestone gravels constituting a shallow alluvium in the downstream part. These modern formations are locally subject to bank erosion and thus are an important source of bedload material (Osenbrück et al., 2013). Finally, the hills, topped by limestone of the base of the "Black" Jurassic (lα), are covered by a vast Quaternary loess formation.

Only a minor part of the Steinlach headwaters develops in karstic formations. The majority of the stream networks flows through formations characterized by low hydraulic conductivity (Schwientek and Selle, 2016). The thin alluvial aquifer and limited karstic formations allowing only limited storage, the hydrology of the Steinlach is characterized by relatively low baseflow. This hydrogeological characteristic coupled with the steep hill slopes of the Middle Jurassic formation often generates flashy stream flow peaks during the summer season as a result of both convective precipitation events and the generation of fast runoff components along the land surface (Schwientek and Selle, 2016).

The land-use in River Steinlach catchment is to 49% agriculture, 39% forest, while the remaining 12% are urban areas, with a population density of approximately 340 inhabitants per km². Apart from combined-sewer overflows, occurring only during strong precipitation events, and minor leaks from the sewer system, the Steinlach-Wiesaz WWTP in Dußlingen is the only source of wastewater compounds in the catchment. The WWTP is situated 4.3 km upstream of the confluence to River Neckar and treats a 99,000 population equivalent (wastewater from 50,000 inhabitants, the rest from industrial and commercial origin). It is equipped with a secondary and tertiary treatment stage, largely eliminating nitrogen and phosphorous loads. The effluent enters the stream with a mean flow rate of 260 Ls^{-1}. On average, treated wastewater represents 15% of the Steinlach discharge at the catchment outlet.

Finally, River Steinlach is monitored by two gauging stations. The first one is situated 200 m upstream of the effluent of the Steinlach-Wiesaz WWTP. The gauge is maintained by the University of Tübingen and will be further referred to as "*Steinlach WESS gauge*". The second gauging station is situated about a kilometer downstream of the WWTP, right above the Mühlbach deviation. This latter being ran by the Environmental Agency of the State of Baden-Württemberg (LUBW), it will be referred further as the "*Steinlach State gauge"* to differentiate it from the "*Steinlach WESS gauge*".

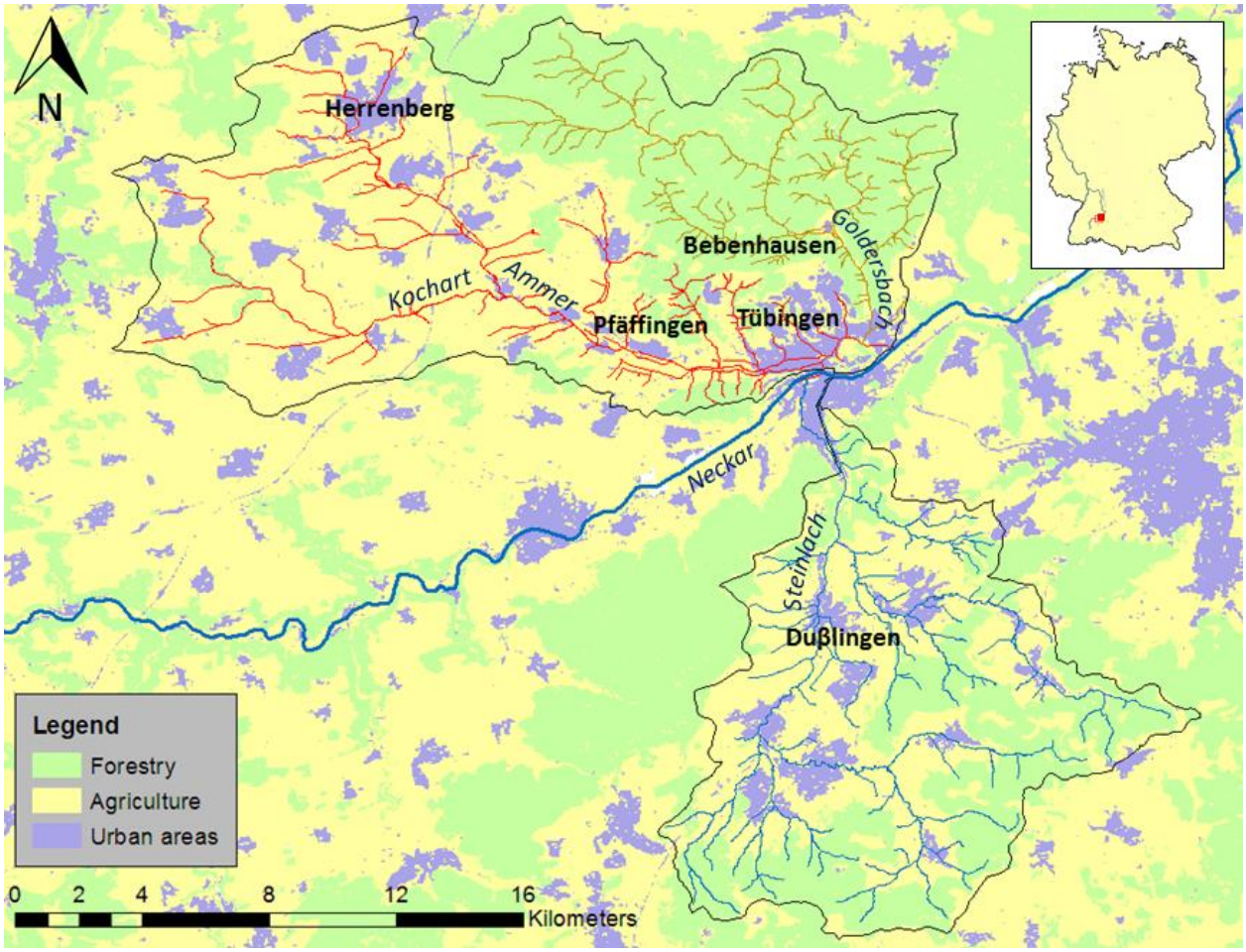

Figure 1. Map and land-use of the studied area.

2.2 River Ammer

The Ammer overall catchment comprises the sub-catchment of River Goldersbach which joins River Ammer 1 km above its mouth into the Neckar. As the Ammer above River Goldersbach and the Goldersbach sub-catchments have contrasting characteristics, these were separately investigated and will be described as independent systems. In the following sections, the terms "*Ammer catchment*" or "*River Ammer*" refer to the Ammer sub-catchment and corresponding river network devoid from the Goldersbach.

River Ammer is a 4th-order stream with an average discharge of 1 m^3s^{-1} dominated by groundwater flow (Selle et al., 2013a; Villinger, 1982). The watershed extends from its source 400 m a.s.l. north-west of Tübingen to its outlet 320 m a.s.l. in the east of the city. Its catchment receives 700 to 800 mm annual precipitation on average with maximum amounts during the summer season (Selle et al., 2013b, 2013a). The main stem spreads over 12.5 km before reaching the village of Pfäffingen, situated east of Tübingen and about 10 km upstream of the confluence of River Ammer with River Neckar. The only gauge of River Ammer, maintained and used by both the University of Tübingen and the LUBW, is situated in Pfäffingen and monitors a topographic catchment of 134 km^2. Due to the strong karstification, the subsurface catchment deviates from the topographic one and was estimated with an area of 180 km^2 (Selle et al., 2013b, 2013a).

The catchment groups the oldest geological units of the area with Triassic to Jurassic formations (Selle et al., 2013a, 2013b). The headwaters of the Ammer, situated north-west, are fed by springs from the

massive karstic limestones of the upper Muschelkalk formation from the middle Triassic. The land surface in the valley downstream crosses Lettenkeuper under Gipskeuper formations. The Gipskeuper is characterized by gypsum layers that can be subject to karstification like the Muschelkalk formation. This karstification provides numerous springs feeding the river network with high electrical-conductivity water. Underneath the gypsum formations, the organic rich clays of the Lettenkeuper constitute the base of the Keuper formation. Towards east, the Keuper continues to younger clayey marls and sandstones formations as the downstream part of the Ammer catchment gets narrower with the clayey marls from the Lower "Black" Jurassic sitting on top. The Alluvium of the Ammer is constituted by silty to clayey sediments with high carbon content, locally.

The discharge of the Ammer river network is primarily fed by springs from the Upper Muschelkalk and the Gipskeuper aquifer systems. The Upper Muschelkalk represents the main aquifer of the catchment. It has also a substantial storage capacity that provides a constant contribution through large karstic springs in the upper part of the catchment. Consequently, discharge is rather stable and significantly increased flow occurs only from the direct runoff in urban areas during rainfall events (Schwientek et al., 2013a). A secondary source of discharge for River Ammer stems from groundwater extraction of the Upper Muschelkalk, producing an average of 150 Ls^{-1} of drinking water for the Ammertal-Schönbuchgruppe water provider.

The Ammer catchment is mainly covered by agriculture (71%) and characterized by a higher urbanization than the Steinlach with 17% of urban areas and 12% of forests. The Gäu-Ammer WWTP in Gültstein, situated 7.6 km upstream of Pfäffingen, treats the water of an 80,000 population equivalent, among which the city of Herrenberg and its 31,000 inhabitants. The major tributary of River Ammer, the Kochart, also receives the treated water of the Bondorf-Hailfingen WWTP, situated about 8 km upstream of Pfäffingen and treating 9,000 population equivalent**.** All municipalities downstream of these WWTPs are connected to the WWTP of Tübingen, which effluent is discharged into River Neckar. During rain events, the combined sewer system situated upstream of Pfäffingen can easily get overwhelmed by run-off water and quickly discharge the exceeding volume of mixed rain and untreated wastewater into River Ammer.

2.3 River Goldersbach

The 4^{th}-order stream Goldersbach takes its source in the hills of the Schönbuch natural reserve, at approximately 500 m a.s.l. north-west of Tübingen, and flows towards the southeast to join River Ammer at 320 m a.s.l. in Tübingen City. River Goldersbach extends along 18.6 km in total, draining a 73 km² catchment when joining River Ammer. The catchment receives an average precipitation of 810 mm yr^{-1} (1980-2009) for an average discharge of 0.25 m^3s^{-1} at the gauge (Grathwohl et al., 2013).

The sandstones of the Keuper and the Lower "Black" Jurassic draw the steep hills of the Goldersbach catchment (Einsele and Agster, 1986). River Goldersbach has rather gravelly sediments that turn sandier in the lower part of the Goldersbach catchment. The "km4" sandstone formation hosts the main aquifer of the Schönbuch. River Goldersbach is fed by springs, mainly situated at the basis of these sandstones. Upstream of Bebenhausen, the catchment of River Goldersbach is covered at 97% by forestry and is completely devoid of any urbanization or heavy traffic.

A gauging station, ran by the University of Tübingen, is situated upstream of the Bebenhausen village. Due to the absence of treated wastewater discharge and urban area above the gauge, the 37 km² Goldersbach catchment at this location represents a pristine catchment as reference for the two others.

3 Overview on considered transport and natural attenuation processes

An overview of the main transport and natural-attenuation processes expected to impact the transit of wastewater contaminants, and factors driving them, are given to better grasp results exposed in section 5.

3.1 Advection

Advection is the transport of a solute by the bulk movement of a flowing fluid, such as a river. Through advection, solutes and water molecules flow with the same average velocity.

3.2 Dispersion

Dispersion in a river is a combination of processes causing the spreading of solutes in the flowing water. In this work, only longitudinal dispersion is considered to spread and smooth contaminant concentration profiles along the river segments. Longitudinal dispersion occurs mainly due to heterogeneities in flow velocity within the river channel, particularly due to shear forces exerted by solid boundaries of the waterbody (e.g. roughness of river banks and bottom), turbulences or low velocity zones.

3.3 Biodegradation

Biodegradation is the decomposition of organic substances by microorganisms. Atop and in riverbed sediments, bacterial and algae mats can develop and form symbiotic community mats that can act as a reactive contact surface. Microorganisms can sit on suspended particles but generally, the concentration of micro-organisms floating in the water column remains low in comparison with the riverbed. Winkler et al. (1998) mentioned also that algae represented the majority of suspended material in rivers in summer.

Almost any organic contaminant can be biodegraded but the biodegradation rate determines whether its disappearance is achieved within days, months or years. This latter is determined by numerous factors among which its bioavailability (i.e. the rate at which it is absorbed or made available at the site of physiological activity of an organism) as well as the presence of micro-organisms adapted to degrade it (Grenni et al., 2013; Nödler et al., 2014; Wilson et al., 2003). Warmer temperatures influence bacterial activity positively until a certain threshold, and seasonality in bacterial growth and composition of the bacterial community was observed in river ecosystems (Freese et al., 2006; García-Armisen et al., 2014). Photosynthesis makes algae sensitive to sunlight exposure in addition to temperature. Their activity thus undergoes seasonal variations similarly to bacteria, with the winter season as an unfavorable development period.

3.4 Photodegradation

Photodegradation comprises two mechanisms, photolysis and indirect photodegradation. During photolysis, a given molecule absorbing a photon shifts to an excited state that is not stable in presence of ambient dioxygen or water. The molecule thus gets oxidized or hydrolyzed, respectively, and decomposes. The reaction can produce unstable fragments such as singlet oxygens, hydroxyl ($^{\bullet}OH$) or carbonate ($^{\bullet}CO_3^-$) radicals that will react with other chemical species in their environment. The

decomposition of a substance by reacting with a reactive product issued from photolysis is defined as indirect photodegradation, as the photon did not interact directly with the substance considered. Indirect photodegradation can also occur through photosensitization, meaning the transfer of energy from a photosensitizer in excited state after absorption of a photons, to a distinct molecule at ground state, leading to its decomposition.

Penetration of sunlight into water is determined by the tree and cloud cover as well as the absorbance of the water. Photodegradation is thus more efficient in open shallow waters. Light absorbance of water can increase with the presence of particles or dissolved constituents. Dissolved organic matter (DOM) can create a light screening effect by absorbing solar radiations (Lam and Mabury, 2005). DOM and nitrate can yield reactive intermediates when photo-degraded but also act as photosensitizers (Lam and Mabury, 2005; Niu et al., 2013; Yamamoto et al., 2009). Finally, river pH determines the dissociation and thus the absorbance spectra of chemicals (Chowdhury et al., 2010; Niu et al., 2013; Tixier et al., 2002). pH also regulates the quantity of hydroxyl radicals present in the water, which are the most reactive photodegradation intermediates due to their non-selectivity and highly electrophilic nature (Lam and Mabury, 2005).

In this work, the term photo-dependent elimination will be used and refers to any degradation process that occurs exclusively during day-time and thus directly or indirectly implying reaction to sunlight occurrence. This includes direct and indirect photodegradation, but also biodegradation performed by photosensitive organisms such as aquatic plants, algae or algae and bacterial communities acting in symbiosis.

3.5 Hydrolysis

Hydrolysis involves the breaking of one or several covalent bonds in a molecule, with a water molecule as a reactant. Hydrolysis can concern reactions directly with water or enzymatic reactions consuming a water molecule during biodegradation as well as the molecule splitting through photodegradation process. In this work, the term hydrolysis in rivers only refers to the action of river water itself.

3.6 Sorption

Sorption refers to the physical or chemical process through which a chemical – named "sorbate" – becomes associated to a solid phase – named "sorbent". One should differentiate adsorption from absorption, as the first concerns the attachment of the chemical to a surface while the second refers to the incorporation of the chemical into a material's matrix.

In this work, we consider sorption to suspended particles in rivers. The solid-water distribution coefficient K_d [L^3M^{-1}] denotes the ratio between the concentration of a given chemical sorbed to the suspended solids C_{sus} [$M\ M^{-1}$] and dissolved in the aqueous solution C_w [ML^{-3}] at equilibrium in the considered system:

$$K_d = \frac{C_{sus}}{C_w} \quad (1)$$

Chemicals that sorb to DOM being considered to remain in the dissolved phase, C_w comprehends both the concentrations of the freely dissolved contaminants and those sorbed onto DOM. C_{sus} is the mean contaminant concentration on the solids, resulting from the sum of each contaminant concentration

obeying a specific sorption process weighed by the fraction of the contaminant binding through this process.

In river sediments, partitioning of organic compounds can occur between aqueous and organic phases in presence. Additionally, a sorbate can interact with any solid surface by gathering at its periphery through London dispersive forces and polar or electrostatic interactions. These interactions are described as "*physisorption*", as sorbates accumulating in the near-surface water layer, tightly associated with the solids, only appear "sorbed" but do not chemically bind to the solid. If sorbates exhibit moieties that can react with the surface of the sorbent, they can establish covalent bonds through so called "*chemisorption*", that are stronger than interaction involved in "*physisorption*".

Sorption processes depend on the sorbate and the sorbent properties. The sorbates considered in this work are wastewater contaminants that comprehend neutral and charged, highly hydrophobic to very soluble compounds. The sorption of neutral contaminants can be reduced to the partitioning to organic matter while charged species will have more complex interactions with mineralogically heterogeneous river sediments (Al-Khazrajy and Boxall, 2016; Hou et al., 2010; Kile et al., 1995; Mader et al., 1997; Schwarzenbach et al., 2003). Generally, the number of available sorption sites can increase with concentration of particles – or solid to liquid ratio – or surface area, while sorption can decrease due to competition between sediment constituents, ions and sorbates in presence (Hou et al., 2010; Schwarzenbach et al., 2003).

3.6.1 Hydrophobic sorption

Hydrophobic substances are substances that are not attracted by water molecules. Water molecules are polar and interact with each-other or with other polar and ionic species or surfaces through hydrogen bonds. By contrast, hydrophobic molecules or hydrophobic moieties are incapable of forming hydrogen bonds with water. Hydrogen bonds between water molecules being highly dynamic, the water phase has a high entropy compared to hydrophobic phases. Thus, hydrophobic substances will disturb hydrogen bonds between water molecules and migrate towards more ordered structures such as solid surfaces and organic phases to have a minimal contact with water (Schwarzenbach et al., 2003).

When partitioning of an organic compound into an organic phase is the dominant process, C_{sus} in equation ((1)) simplifies to the product of the compound concentration in the organic fraction of the particles C_{oc} [ML^{-3}] and of the organic carbon fraction of the particles f_{oc} [-]. The K_d of a compound becomes the product of f_{oc} times the organic carbon-water partitioning coefficient K_{oc} [L^3M^{-1}]:

$$K_d = f_{oc} \cdot \frac{C_{oc}}{C_w} = f_{oc} \cdot K_{oc} \tag{2}$$

K_{oc} is often approximated by the octanol-water partitioning coefficient K_{ow} [-], determined in laboratory and usually given in logarithmic form. For ionizable species, $\log K_{ow}$ is completed to account for pH of the water and the dissociation constant of the compound in its negative $\log pK_a$ and expressed as the logarithmic octanol-water distribution coefficient $\log D_{ow}$. $\log D_{ow}$ approximates hydrophobicity of compounds considering both its ionized and unionized form in presence at a given pH.

The type and quality of organic matter available to contaminants (e.g. vegetal debris, organic content in mineral phases, black carbon, etc.) will influence their sorption. Moreover, contaminant partitioning to organic phase is rather insensitive to temperature while adsorption to organic surfaces can increase by a factor of 2 for a 10°C decrease in temperature (Schwarzenbach et al., 2003).

3.6.2 Electrostatic interactions between charged contaminants and surfaces: physisorption

Electrostatic interactions occur as two charged molecules interact with each other. Electrostatic interactions discussed in this section do not create any covalent bond and are a type of "*physisorption*".

In aqueous media, most mineral surfaces as well as particulate organic matter are charged (Schwarzenbach et al., 2003). At river pH, particulate organic matter is negatively charged, primarily due to the ionization of carboxyl groups (-COOH), and phenols at higher pH. The excess of accessible divalent cations or of CO_3^{2-} on the solid wet-surface of carbonate particles will also induce charges. The wet-surface of oxides and oxyhydroxides (e.g. quartz, hematite, gibbsite, etc.) is covered by hydroxyl groups (-OH) that can undergo proton exchange with the aqueous phase similarly to acid-base reactions, leading to the formation of either $-OH_2^+$ or $-O^-$ moieties at the material's surface. The total amount of available charged sites on the surface will be translated by either cationic or anionic exchange capacity (CEC or AEC) of a net negatively or positively charged material, respectively. Finally, clay minerals possess two types of charges and can attract both anionic and cationic species (CEC and AEC at the same time). The first type occurs at the edges of clay layers, as the interruption of the tetra- and octahedral chains is compensated by protonation from the environing water to create hydroxyl moieties. The second type of charge in clays is caused by isomorphic substitutions within the mineral structure (e.g. substitution of a Si^{4+} by an Al^{3+} in tetrahedral layers and of an Al^{3+} by Fe^{2+} or Mg^{2+} in octahedral layers). The amount of substitutions varies with the clay type but induces a fixed and permanent negative charge within the clay structure that will attract cationic compounds at its surface and between its layers.

Electrostatic interactions will thus concern organic contaminants exhibiting charges in water, particularly cationic sorbates as most natural surfaces are negatively charged at common river pH. Electrostatic interactions being non-selective for species of similar charge, the hydrophobic character of some organic substances encourages them more than hydrophilic or inorganic species to accumulate in the more ordered near-surface water layer (Schwarzenbach et al., 2003). Also, pH determines the ionization of dissociating organic contaminants as well as the charge at the material's surface by controlling the (de)protonation of hydroxyl and carboxyl groups. As an example, the negative charge of natural organic matter will increase with increasing pH (Schwarzenbach et al., 2003).

3.6.3 Adsorption of non-ionic species due to electron donor-acceptor interaction

Electron donor-acceptor interactions are the exchange of an electronic charge between an electron donor – such as carboxyl ($-COO^-$) or hydroxyl ($-O^-$) functional groups – and an electron acceptor, without formation of a covalent bond in order to stabilize a complex of two molecules under excited state. The force of this charge transfer leads to an unstable bond between the complex molecules that also accounts as "*physisorption*".

That process can be found in highly clay-rich layers in soils and glass or metal sampling and laboratory material but is deemed negligible whenever organic matter is present (Schwarzenbach et al., 2003).

3.6.4 Electrostatic interactions between charged contaminants and surfaces: chemisorption

Chemisorption concerns sorbates either forming covalent bonds to natural organic matter (e.g. on carbonyl moieties (-C=O)) or displacing existing ligands (e.g. H_2O or OH^-) to form a complex with other ions, particularly metals, exposed on the surface of inorganic solids.

Bonding to natural organic matter is particularly prominent for organic bases at common water pH (Schwarzenbach et al., 2003) but involves rather long reaction times (hours to years). Complexation can occur on metal oxides, carboxylic acids (-COOH) and phenols being reactive moieties commonly found in the sorbates involved.

Those reactions are dependent on the type of mineral involved as well as pH, since it influences the number of reactive moieties both on the sorbate and the sorbent surface.

3.7 Volatilization

In this work, volatilization refers to the transfer of dissolved contaminants into the air phase. More precisely called evaporation at non-boiling temperatures, the process is driven by the partitioning of the contaminant between air and the aqueous phase to reach an equilibrium.

Henry's law defines the equilibrium of a compound between air and water phase by the proportionality between its partial pressure p [ML^{-2}] in the air phase and its concentration C_w [NL^3] in the water phase. The Henry's law volatility constant, K_H [LMN^{-1}], is given by:

$$K_H = \frac{p}{c_w} \tag{3}$$

p being in the numerator, the higher the K_H the more volatile the compound is. The source of contaminants being treated-water discharge, the concentration gradient and atmosphere-water exchange should be oriented from aqueous to gas phase.

Since vapor pressure is highly temperature-dependent, temperature in the atmosphere will have an impact on the distribution of a given contaminant in order to reach equilibrium (Buerge et al., 2003). Evaporation being a surface phenomenon, the higher the contact surface, the higher the transfer fluxes. Contaminant volatilization can be facilitated in the case of turbulent zones or during high discharge conditions, where water droplets are stirred into the atmosphere, increasing the contact surface for water-vapor exchange. Turbulences also maintain the concentration gradient at the water-air interface that ensures phase transfer.

4 Material and methods

Field studies investigated a wide selection of contaminants, but particularly focused on a small group of commonly found contaminants presenting various uses and properties in studied streams (see Table S1 in the Appendix). In the category of pharmaceuticals, the focus was made particularly on the anticonvulsant drugs carbamazepine and oxcarbazepine, the anti-inflammatory drugs diclofenac, naproxen and ibuprofen and the local anesthetic lidocaine, beside the anti-depressant venlafaxine and the antibiotic sulfamethoxazole. The flame retardants tris(2-chloroethyl)phosphate (TCEP), tris(1-chloro-2-propyl)phosphate (TCPP) and tris(1,3-dichloroisopropyl)phosphate (TDCPP) were also in the mainly investigated compounds next to the artificial musk fragrances 7-acetyl-1,1,3,4,4,6-hexamethyl-1,2,3,4-tetrahydronaphthalene (AHTN), 1,2,3,4,5,6,7,8-octahydro-2,3,8,8-tetramethylnaphthalen-2yl]ethan-1-one (OTNE) and 1,3,4,6,7,8-hexahydro-4,6,6,7,8,8-hexamethylcyclopenta-(g)-2-benzopyran (HHCB), with HHCB-lactone the metabolite of HHCB. The herbicide mecoprop, the pesticide atrazine and its metabolite desethylatrazine were used as indicators from urban and agricultural land surfaces, respectively. Finally, the stimulant caffeine, the biocide triclosan, the insect repellent N,N-Diethyl-meta-toluamide (DEET) and the bleaching agent Tetraacetylethylenediamine (TAED) were the only representatives of their use category. The transport and fate of these compounds were described in this work to show the variety of organic contaminant behaviors in the streams studied.

4.1 General approach

4.1.1 Description of conservative transport by transfer functions

The method has previously been used to correct the effects of dispersion on the estimation of reaeration rate coefficients from gas-tracer concentrations (Knapp et al., 2015). Linear transport of a solute between an input and output can be described by the convolution of the input time series $C_{in}(t)$ [ML^{-3}] with the transfer function $g(\tau)$ [T^{-1}]:

$$C_{out}(t) = \int_0^t g(\tau) C_{in}(t-\tau) d\tau \quad (4)$$

in which t [T] is time, τ [T] is a time offset or travel time, and $C_{out}(t)$ [ML^{-3}] is the predicted output signal. The transfer function describes the linear response of the system to a perfect unit pulse at time zero.

In the case of a conservative tracer, the transfer function $g(\tau)$ only reflects conservative transport processes such as advection, dispersion, transient-storage processes and dilution by inflows in the river section between two measurement stations. It is thus the travel time distribution multiplied with the tracer recovery. As an example, the concentration breakthrough curve (BTC) of a conservative tracer test, introduced by pulse injection, is the transfer function between the injection and observation points times a constant scaling factor. To obtain transfer functions between two observation points downstream of the injection, a non-parametric deconvolution (Cirpka et al., 2007) of conservative-tracer time series was applied. This latter does not predefine the parametric shape of the transfer function, thus, facilitating unconventional features such as multiple peaks, extended tailing, etc. The approach merely constrains the transfer function to be non-negative for all values of τ and exhibits a certain degree of smoothness.

By convoluting the conservative-tracer transfer function with the concentration time series of a contaminant as input signal (equation (4)), the concentration time series of the contaminant at the downstream location can be predicted under the assumption that the contaminant behaves like the tracer.

To retrieve a meaningful estimate, the duration of contaminant sampling at the first observation point, used as input signal $C_{in}(t)$ in equation (4), must be sufficiently long to cover all travel times, and the temporal resolution must be fine enough to capture the trend in the data.

The mean travel time τ_m between two sampling locations is determined by calculating the first moment of corresponding transfer functions $g(\tau)$ following the equation:

$$\tau_m = \frac{\int_0^\infty g(\tau)\tau d\tau}{\int_0^\infty g(\tau) d\tau} \tag{5}$$

4.1.2 Transport of reactive compounds

The method of transfer functions was further explored for the data of the sampling methodology based on a tracer test (see section 4.2), which results were published in Guillet et al. (2019). In this application, the signals $C_{in}(t)$ and $C_{out}(t)$ are BTCs at up- and downstream control planes. The transport of a compound undergoing a first-order decay process with the time-dependent decay constant k [T^{-1}] can also be described by convolution:

$$C_{out}(t) = \int_0^t h(\tau, t) C_{in}(t - \tau) d\tau \tag{6}$$

in which the reactive-compound transfer function $h(\tau, t)$ [T^{-1}] relates to the conservative-compound transfer function $g(\tau)$ by:

$$h(\tau, t) = g(\tau) \exp\left(-\int_0^\tau k(t - \tau + \tau_*) \mathrm{d}\tau_*\right) \tag{7}$$

with the integration variable τ_*. The dependence of $h(\tau, t)$ on time t stems from potential temporal variations of the decay constant k. The latter reflects the first-order reactivity of the compound in the river, which may be affected by environmental conditions.

While there are several decay processes acting on micropollutants, disentangling their contribution to contaminant degradation from measured concentrations alone requires distinct patterns of these processes in time. In this regard, photodegradation or biodegradation by micro-organisms that require light, are the only elimination processes that can be clearly distinguished from all other elimination processes as they do not occur at night. Assuming that the overall elimination of a contaminant is the sum of several elimination processes following first-order decay, the day-time decay constant k_{day} [T^{-1}] can be expressed as:

$$k_{day} = k_{photo} + \underbrace{k_{non-photo}}_{=k_{night}} \tag{8}$$

in which k_{photo} [T^{-1}] is the rate constant of photo-dependent elimination processes and $k_{non-photo} = k_{night}$ [T^{-1}] is the sum of all decay constants from photo-independent, not specifically identified

elimination processes. $k_{non-photo}$ is the apparent decay constant at night-time. Assuming no significant temporal variation of the efficiency of the photo-independent processes (which requires environmental conditions with the exception of solar radiation to remain more or less constant), the photo-dependent decay can be separated from the day-time decay by subtracting k_{night} from k_{day}, in which both coefficients are determined by fitting equations (6) and (7) to measured contaminant concentrations at day and night time, respectively.

If environmental conditions besides solar radiation (H_G) do not change significantly over the sampling day, k_{photo} can be assumed to be proportional to H_G [MT^{-3}]:

$$k_{photo}(t) = k_i \cdot H_G(t). \tag{9}$$

Thus, k_{photo} is the rate constant for photo-dependent elimination processes and k_i [T^2M^{-1}] the specific constant determined under the present environmental conditions scaled by solar radiation. k_i is obtained by fitting the model to day-time data.

As solar radiation changes over time, the overall decay of a compound undergoing photo-dependent elimination processes is achieved by integrating the solar radiation $H_G(t)$ over time, multiplying it with the compound-specific coefficient k_i, adding the photo-independent contribution, and substituting the resulting expression into equations (6) and (7):

$$C_{out}(t) = \int_0^t g(\tau)\exp\left(-\int_0^\tau \left(k_{night} + k_i H_G(t-\tau+\tau_*)\right) d\tau_*\right) C_{in}(t-\tau)d\tau. \tag{10}$$

This way, the concentration of a compound degraded by photo-dependent elimination processes is predicted for a downstream observation point, accounting for the time series of its concentrations further upstream, dispersion and dilution (via $g(\tau)$ obtained from the conservative tracer), photo-independent degradation (via fitting night-time data), and variations of solar radiation.

The ratio of zeroth moments of the transfer functions $h_i(\tau)$ of the reactive compound i and $g(\tau)$ of the conservative tracer yields the remaining fraction RF_i [-] of the compound. The relative mass loss R_i [-] of compound i by elimination processes can be computed by:

$$R_i = 1 - RF_i = 1 - \frac{\int_0^\infty h_i(\tau)d\tau}{\int_0^\infty g(\tau)d\tau} = 1 - \frac{\int_0^\infty g(\tau)\exp\left(-\int_0^\tau \left(k_{night}+k_i H_G(t-\tau+\tau_*)\right)d\tau_*\right)d\tau}{\int_0^\infty g(\tau)d\tau} \tag{11}$$

Like RF_i, the reactive removal R_i depends on the full distribution of travel times.

4.1.3 24 h-mass balance calculation

The methodological approach was published in Schwientek et al. (2016), reporting the results of the summer 24 h-sampling campaign performed in July 2013. A winter campaign was operated in February 2014 (see section 4.3).

The Lagrangian sampling scheme was modified to investigate an extended parcel of water, here 24 h-long similarly to Ahel et al. (1994). The choice of a large water parcel, compared to the travel time,

minimized the impact of uncertainties from the estimation of this latter, prior to the experiment, and of dispersion effects. To calculate a mass balance and evaluate contaminant loss in the water column, mass fluxes must be monitored at the various inputs and output(s) of the investigated segment (i.e. upstream end of the segment and entering tributaries against segment outflow(s), respectively). WWTPs' effluent often presents a diurnal cycle due to varying use of water from the households and industries that are connected to the sewer system. This diurnal pattern is reflected in the contaminant concentrations in the river downstream, as it results from the proportion of effluent water on the total river flow downstream of the WWTP. The sampling campaign must provide discharge and concentration measurements at a sufficient temporal resolution to capture this temporal variability and calculate an accurate mass balance for each investigated compound over the whole length of the water parcel according to:

$$\int_{t0}^{t1} \sum_{i=1}^{n} (Q_i C_i)_{in} dt = \int_{t0+\tau}^{t1+\tau} (QC)_{out} + \Delta S \quad (12)$$

where Q [L^3T^{-1}] and C [ML^{-3}] represent the volumetric water flow rate – or discharge – and the compound concentration, respectively. The left-hand side of equation (12) sums up the various input terms i of the compound balance obtained at the upstream end of the investigated river segment and from the tributaries joining the reach over the whole sampling period (from $t0$ to $t1$). The right-hand side of equation (12) represents the output measured during the same duration after the travel time τ plus the sink term ΔS [MT^{-1}]. ΔS represents the missing mass load at the output and denotes the overall elimination of the investigated compound from the water column during its travel through the investigated river segment. In later chapters, ΔS normalized to the input mass load will quantify the "net removal" of each compound over the investigated reach during the studied period.

To fairly compare removals from different campaigns, the decay constant of a reactive compound can be calculated to give the compound's reactivity independently from the residence time τ. Assuming the investigated compound undergoes a first-order decay, its mass load $M(\tau)$ [MT^{-1}] at the output of the system after the travel time τ is given by:

$$M(\tau) = M_0 \exp(-k\tau) \quad (13)$$

where M_0 [MT^{-1}] is the total mass load, comprising all inputs, of the investigated compound entering the system. k [T^{-1}] is the apparent decay constant, quantifying the kinetics of all elimination processes gathered. The half-life time $t_{1/2}$ can then be calculated following the expression:

$$t_{1/2} = \frac{\ln 2}{k} \quad (14)$$

4.1.4 Particle-associated transport

The assessment of particle-associated transport of wastewater contaminants follows the works on PAHs performed by the WESS competence cluster in the same streams investigated as in this study (Rügner et al., 2014, 2013; Schwientek et al., 2013b). In these previous works, PAHs were found to be transported mainly onto particles in rivers. PAH total concentration in a water sample $C_{w,tot}$ [ML^{-3}] comprised its freely dissolved concentration C_w [ML^{-3}] and the concentration of the compound sorbed

to particles C_{sus} [M M^{-1}] multiplied by the particle concentration TSS [ML^{-3}] (for total suspended solids), as shown in equation (15):

$$C_{w,tot} = C_w + C_{sus} \cdot TSS \quad (15)$$

With C_w and C_{sus} being constant over time, the correlation between $C_{w,tot}$ and TSS was found to be linear for PAHs in the streams studied, indicating a constant particle loading of PAHs specific to each of the investigated catchments. Considering equilibrium between the solid and the aqueous phase of a water sample, the slope C_{sus} and the intercept C_w from the $C_{w,tot}$ - TSS linear correlations allow calculating the distribution coefficient K_d given by equation ((1)).

Rügner et al. (2013) demonstrated a linear correlation between TSS and turbidity, according to:

$$TSS = m \cdot Turbidity \quad (16)$$

Turbidity quantifies the scattering of light caused by the presence of particles in the water. This relationship between turbidity and TSS depends on many parameters, such as the size, the density, the shape and the nature of the particles, as well as the water color. It was, however, shown to hardly vary, both spatially and temporally, within one system (Rügner et al., 2013). Through high-resolution monitoring of turbidity using an optical backscattering sensor, turbidity is a parameter easier to measure than TSS and can serve as a proxy for this latter. When inserting equation (16) into equation (15):

$$C_{tot} = C_w + C_{sus} \cdot m \cdot Turbidity \quad (17)$$

For a contaminant mainly transported with particles, $C_w \ll C_{sus} \cdot TSS$ in turbid waters and contaminant fluxes occur mainly during the mobilization of suspended solids in the river water – e.g. during high discharge events. After estimating yearly particle loads using turbidity monitoring, Rügner et al. (2013) estimated yearly fluxes of PAHs in rivers of Tübingen area from the determined constant C_{sus} and by neglecting C_w.

In this work, these investigations were pursued for wastewater contaminants in turbid waters sampled during two flood samplings and the Steinlach pre-sampling campaign (see section 4.4 and 4.5, respectively).

4.1.5 Assessment of contaminant fluxes

Concentration and discharge data collected through the various sampling campaigns detailed further, including a monthly sampling between 2009 and 2011 (see section 4.6), were used to assess contaminant fluxes during the studied conditions.

Moreover, the contribution of the Steinlach-Wiesaz WWTP to fluxes of analyzed compounds in River Steinlach was estimated for the tracer-based and 24 h-sampling campaigns (see sections 4.2 and 4.3, respectively). The calculation was made by comparing fluxes measured downstream of the WWTP to fluxes monitored in water inputs that did not receive WWTP effluent discharge and were assumed to be constant over the duration of the given campaign (upstream of the WWTP and in the various

tributaries joining the investigated segment). Estimations constituted only "minimum" contributions as the fluxes were not measured directly in the WWTP effluent but at a station downstream which could have allowed compound elimination, particularly in the case of the tracer-based sampling, situated further downstream than in the 24 h-sampling campaigns. When concentrations were under the limit of quantification (LOQ), half of the LOQ was used. During the summer 24 h-sampling campaign, the period of the effluent stop was not considered and during the winter sampling, the 4th tributary was not used for the calculation as it was assumed to receive water from the main stem through the Mühlbach deviation (see section 4.2.1). For estimations of the WWTP contribution to fluxes measured during the tracer-based sampling, the discharge of the State gauge was used with concentrations measured at MS1. The calculation did not account for the Mühlbach deviation, as this did not impact concentrations measured at MS1.

4.2 The tracer-based sampling

The so-called the "*tracer-based sampling*" was performed on the day of August 7, 2015 and repeated during the following night. The following was modified from Guillet et al. (2019).

4.2.1 Site description

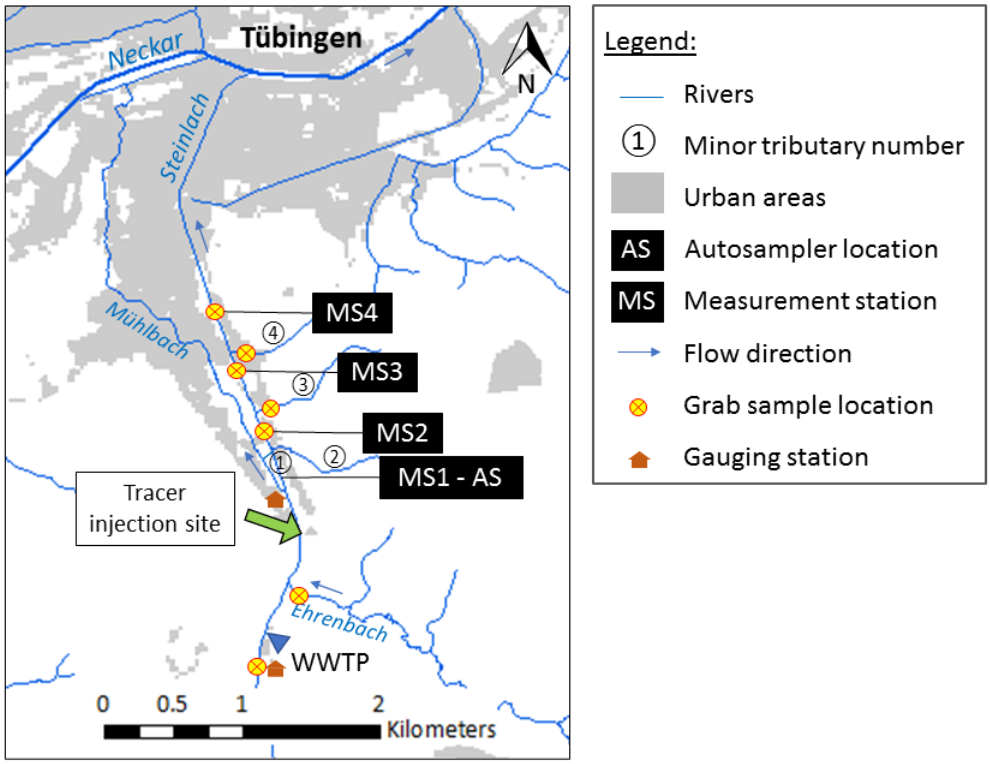

Figure 2. Sampling map of the tracer-based sampling campaign in River Steinlach.

The tracer-based study was performed in River Steinlach in Derendingen, south of Tübingen city, downstream of the Steinlach-Wiesaz WWTP. After the WWTP, River Steinlach receives water from the Ehrenbach creek and four minor tributaries numbered from ① to ④ from south to north, free of any treated wastewater discharge. The Mühlbach, a constructed diversion, leaves the main channel 3.3 km above the river mouth and does not return to River Steinlach. In the Steinlach main stem, the river

flows through a straightened channel with a mean slope of 7‰, though higher gradients are locally created by ~1.5 and ~0.5 m high weirs, situated shortly after the Mühlbach deviation, as well as various artificial steps along the river segment, about one or a couple of decimeters high. The river bed consists of medium sized gravel with large limestone blocks placed into the river as bed-armoring material. At baseflow, the average width of the study section is 7 m and the sparse tree and bush cover on the overbanks cause very little shading of the river.

The injection of the fluorescent tracer fluorescein was performed 660 m downstream of the WWTP outlet (see Figure 2) at a sufficient distance from the first measurement station (MS1) to ensure complete lateral mixing of the tracer with the river water.

MS1 was located 40 m downstream of a 1.5 m high weir situated right downstream the Mühlbach deviation and marked the beginning of the study stretch. The study stretch was defined as three nested sub-segments, all starting from MS1. The first sub-segment was 410 m-long between MS1 and MS2, the second was 885 m-long from MS1 to MS3 and the third started once again at MS1 and ended after 1310 m at MS4.

The environmental conditions are summarized for both day- and night-time samplings in Table 1. The sampling occurred during a particularly dry summer and year. Weather conditions on the day were dry and sunny with few clouds. The drought led to striking differences in water and air temperature, discharge and proportion of treated wastewater in River Steinlach downstream of the WWTP, compared to the milder conditions met during the 24 h-summer sampling campaign in July 2013 (see Table 2 in section 4.3.1). Discharge was relatively stable within the day- and night-time experiment. Among the minor tributaries between MS1 and MS4, the two southern ones were dried-up. The discharge contribution from the minor tributaries ③ and ④ entering the investigated segment was negligible, with less than 0.3% of the discharge flowing through the main stem for each of them during both day- and night-time samplings. The water was of a yellowish color, and numerous filamentous debris and algae mats were floating in the river water.

Table 1. Summary of sampling conditions during the day- and night-time experiments of the tracer-based sampling.

	DAY-TIME SAMPLING	**NIGHT-TIME SAMPLING**
	7-8 August 2015	
Weather conditions	Sunny with few clouds	
Minimum/maximum air temperature (LUBW data)	+ 27 °C / + 36 °C	+ 20 °C / + 25 °C
Minimum/maximum water temperature (divers data)	+ 20.1 °C / + 24.9 °C	+ 19.5 °C / + 21.3 °C
Mean discharge (State gauge)[1]	180 Ls^{-1}	160 Ls^{-1}
Mean travel time τ_m from MS1 to MS4	146 min	156 min
Proportion of treated wastewater	77%	74%
Ehrenbach discharge	2.5 Ls^{-1}	
Tributary ① discharge	/	
Tributary ② discharge	/	
Tributary ③ discharge	0.1 Ls^{-1}	
Tributary ④ discharge	0.5 Ls^{-1}	

[1]Discharge monitored before the Mühlbach deviation.

4.2.2 Fluorescent tracer test

Simultaneous to the sampling of wastewater compounds, two tracer tests were performed on August 7, 2015 as 13.9 g and 10.8 g of sodium-fluorescein were injected as a slug across the width of the stream, in the morning and after nightfall for the day- and night-time experiment, respectively. Time series of tracer concentrations were recorded at all four measurement stations (MS1-MS4) downstream of the injection point (see Figure 2) with the help of online fluorometers (GGUN-FL30, Albillia Sàrl, Neuchâtel) at 10 s intervals. To verify recorded tracer concentrations, a small number of grab samples was collected over the course of the tracer breakthrough at each measurement station and analyzed on a high-precision laboratory spectrofluorometer (FluoroMax-4, Horiba Scientific, Japan).

4.2.3 Sampling procedure for inorganic ions and wastewater contaminants

An ISCO 3700 autosampler (Teledyne ISCO, USA) containing twelve 950 mL glass bottles was installed at MS1. The Teflon tubing used for sampling of the river water was set close to the sensors of the fluorometer, slightly downstream to avoid creating turbidity effects while pumping. The autosampler was programmed to collect one-hour composite samples (150 mL every 10 min) over six hours. The autosampler started at 8:00 and sampled until 14:00 during the day experiment and sampled from 20:00 until 02:00 for the night experiment. For sample preservation, the autosampler was filled with ice to limit biodegradation in the sample bottles at the summerly air temperatures. Aliquots of each sample from the autosampler were transferred to 500 mL brown glass bottles, previously rinsed with sample water, within two hours of sampling and placed into cool boxes filled with ice. Samples were stored in the dark at 4°C until analysis.

At all other locations (MS2, MS3, and MS4), grab samples were taken with 250 mL brown glass bottles, after rinsing them with river water. The grab sampling targeted a time close to the peak of fluorescein at each location, i.e. at 12:22, 13:14 and 14:24 on the 7th of August for the day experiment and at 0:28, 1:52 and 2:58 on the 8th of August for the night experiment. Like the autosampler samples, grab samples were stored in the dark at 4°C until analysis. MS3 and MS4 sampling consisted in a single grab sample, while at MS2, a triplicate sample was collected to assess analytical uncertainty.

Additional grab samples were taken upstream of the WWTP effluent, in the Ehrenbach and the two minor tributaries to check organic pollutants sources other than the WWTP while assuming steady-state conditions regarding discharge and concentrations at these locations.

As a field blank, a sample of distilled water was taken after the experiment in order to check cross-contamination in the autosampler as well as sample handling and analysis. The blank was collected by the autosampler installed at MS1 through the same sampling routine as for the input function. Before the blank collection, the autosampler and its bottles and tubing were rinsed with 5 L of distilled water from a clean polyethylene canister. The operation was repeated with a second 5 L canister, also filled with distilled water, and the sample was kept as a blank. The blank was transported, stored and analyzed along with the 26 other samples collected during the campaign.

4.2.4 Measurement of environmental parameters

Complete mixing of stream and treated wastewater was verified at MS1 twice, at the beginning and the end of the whole experiment, by a lateral profile of specific electrical conductivity (EC) (for 25°C) using a handheld WTW LF340 device (WTW GmbH & Co.KG, Germany).

Water-level probes (AquaTROLL®200, In-Situ Inc., USA) were placed at MS1 and MS4 for water stage check and river temperature measurements. CTD divers (Schlumberger Water Sciences Technology, Canada) were set at MS2 and MS3 to measure river temperature. Discharge was given by the Steinlach State gauge (www.hvz.baden-wuerttemberg.de) while data on air temperature and global solar radiation was provided by a LUBW station in Derendingen (http://udo.lubw.baden-wuerttemberg.de).

The pH of the river was continuously recorded at MS1 over the course of the experiment with a multi-parameter probe (HI9828, HANNA instruments, USA).

A schematic map of all measurements and samplings is given in Figure 3.

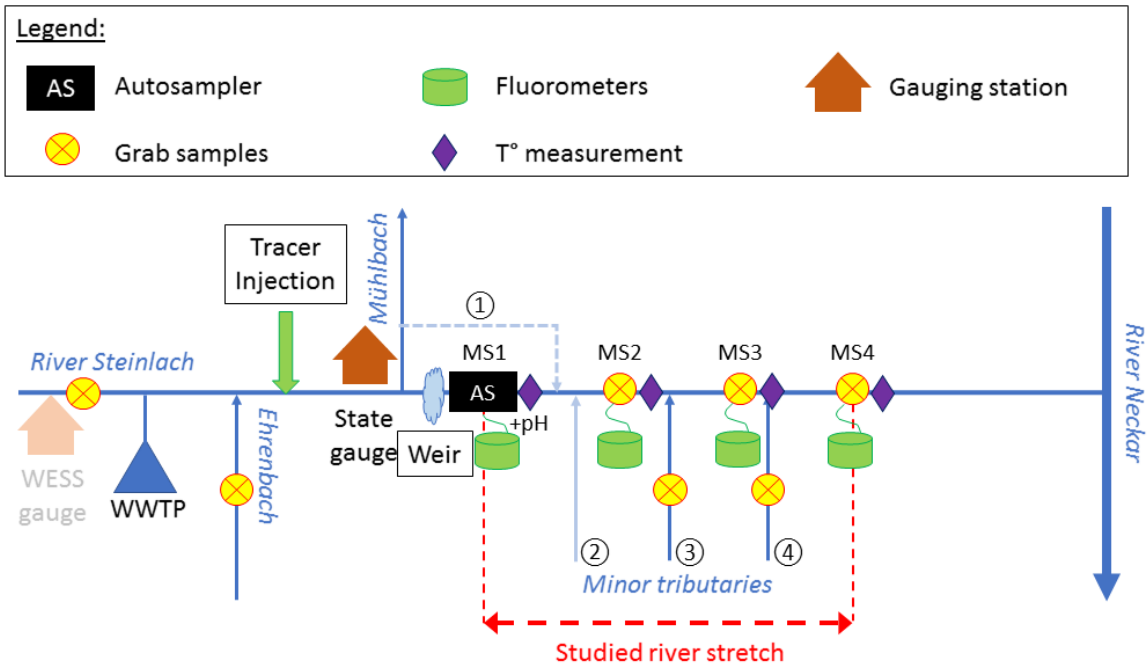

Figure 3. Schematic map of sampling and measurements operated during the tracer-based sampling.

4.2.5 Analytical work

At Tübingen University, pH and turbidity of the raw samples were measured with a Multical® pH 540GLP pH meter (WTW GmbH, Germany) and 2100N a turbidimeter (HACH, USA), respectively. An aliquot of the samples was filtered through 0.45 µm cellulose-acetate filters into two separate 25 mL glass vials for the analysis of inorganic ions and DOC. Concentrations of inorganic ions were measured using an ion chromatograph (DX 500, DIONEX, USA). DOC was determined after acidification to pH 2 and purging with nitrogen gas using a TOC analyzer (Elementar HighTOC, Germany; thermal oxidation at 680 °C and CO2 quantification by an infrared detector). The measurement on raw samples as well as sample filtration for analysis of DOC, inorganic and organic compounds were performed by the author, the rest by the laboratory of Tübingen and Dr. Sylvain Merel.

A large set of common wastewater contaminants (thirty-eight compounds which properties and usage are shown in Table S1 in the Appendix) were quantified by liquid chromatography coupled to tandem mass spectrometry (HPLC-MS/MS) at the laboratory of Tübingen University. For the procedure, an aliquot of each sample was filtered by the author through a 0.2 µm regenerated cellulose syringe filter

(Captiva, Agilent Technologies, Germany) into 2 mL glass vials for analysis using successive liquid chromatography and mass spectrometry. Liquid chromatography was performed with an Agilent device combining a 1260 infinity solvent degasser, binary pump and column compartment with a 1290 infinity sampler. Without previous enrichment, 100 µL of sample were injected onto an Agilent Poroshell 120 EC-C18 column (2.1 x 100 mm with 2.7 µm particle size). While the temperature of the column was kept at 40 °C, the analytes were eluted with 0.4 $mLmin^{-1}$ of a gradient of water at 1mM ammonium acetate (solvent A) and acetonitrile (solvent B), both acidified with 0.1% acetic acid. The portion of solvent B was linearly increased from 2% to 80% within 17 min, then immediately increased to 100% and held for 5 min. Finally, solvent B was set to 2% and held for 9 min in order to equilibrate the column before the next analysis. Following chromatographic separation, compounds were detected with an Agilent 6490 triple quadrupole mass spectrometer. Analytes were ionized by positive and negative electrospray with fast polarity switching, 16 $Lmin^{-1}$ drying gas (N2) at 150 °C, 12 $Lmin^{-1}$ sheath gas (N2) at 400 °C, a nebulizer pressure of 35 psi, and a capillary/nozzle voltage of 2500V/300V in positive mode and 3000V/1500V in negative mode. For each compound, the precursor ion was isolated for collision induced dissociation and two specific product ions (quantifier and qualifier) were monitored.

4.2.6 Convolution of the concentrations time series and k fitting

As discharge provided by the State gauge was stable during each experiment and as changes in discharge along the study section were deemed insignificant, night BTCs were normalized to yield recoveries of 100%. Normalization thus eliminated measurement errors associated with the fluorometers that could potentially bias further calculations. Night-time transfer functions between MS1 and the other measurement stations were obtained from the deconvolution procedure. The night-time transfer functions were normalized to obtain a recovery of 100% to correct uncertainties of the deconvolution, still considering insignificant changes in discharge along the study section.

Day-time BTCs could not directly be used to compute conservative-tracer transfer functions between the individual measurement stations, because fluorescein undergoes photodegradation during the day. Under night conditions, by contrast, fluorescein was expected to behave like an ideal tracer at the slightly alkaline pH-values of River Steinlach (Gutowski et al., 2015). As discharge conditions changed to some degree between the day- and night-time experiments, night-time conservative transfer functions had to be transformed to represent day-time conditions. Schmadel et al. (2016) showed that varying discharge conditions mainly affect advective time scales. We therefore scaled the night-time transfer functions of the conservative tracer, by a dimensionless factor f [-] to yield the day-time transfer functions:

$$g_{day}(\tau) = \frac{1}{f} g_{night}(f \cdot \tau) \tag{18}$$

in which the scaling factor f was fitted together with the specific photo-decay coefficient k_i of fluorescein, further referred as k_{Fluo}. The thus determined day-time conservative transfer functions $g_{day}(\tau)$ were used in the analysis of the wastewater contaminants.

A smooth concentration distribution $C_{fine}(t)$ [ML^{-3}] was reconstructed from the hourly averages of the input function from MS1 C_i^{meas} [ML^{-3}] by finding the strictly non-negative concentration distribution that minimizes the squared concentration gradient and meets the hourly averages by constrained optimization:

$$C_{fine}(t) = \underset{C_i^{meas}(t)\geq 0 \forall t}{\arg\min} \int_0^T \left(\frac{dC_i^{meas}(t)}{dt}\right)^2 dt \tag{19}$$

subject to

$$\frac{1}{\Delta t}\int_{(i-1)\Delta t}^{i\Delta t} C_{fine}(t)dt = C_i^{meas} \; \forall i \tag{20}$$

in which the non-negativity constraint and the constraint of meeting the time-averaged measurements are implemented by the method of Lagrange multipliers. In equation (20), $\Delta t = 1h$ is the duration of averaging, and C_i^{meas} is the concentration value of the i-th measurement increment. The final smooth reconstruction with a 1 min interval thus meets the hourly averages C_i^{meas} with a minimum temporal gradient of the signal.

The application of transfer functions produces a signal of a smaller length than the initial input time series used. To compensate the up to 1.2% missing data, depending on the location considered, extrapolation had to be performed to remove any bias that might affect the reaction constants calculated. After testing extrapolation using the minimum, maximum, mean and neighboring values, the mean value for the two missing samples was chosen after concluding insignificant differences in the calculated constants.

Photo-independent decay constants k_{night} were determined for each compound and section using the night-time conservative transfer function $g_{night}(\tau)$ and reconstructed concentration time-series at MS1, $C_{in}(t)$. The constants were calculated using equations (6) and (7) to fit the night-time grab sample measurements of the triplicate mean at MS2 and the single concentrations at MS3 and MS4 as $C_{out}(t)$. The same was repeated with the day-time data and $g_{day}(\tau)$, this time fitting k_i for each compound and section. The decay constants were only fitted to a single value per MS in the present study, as mentioned before, in order to minimize the logistical and analytical effort as much as possible. Nevertheless, this represents a potential source of uncertainty in the obtained constants, though the reliability for analytical accuracy was demonstrated (section 5.2.2). The reactive removal was subsequently computed for day- and night-time conditions and each compound and section by equation (11).

The results of the computational procedure are illustrated in Figure 4 for the antidepressant venlafaxine. Figure 4a shows the concentration time series from the 1 h composite samples measured at MS1 and the reconstructed input functions obtained from equation (19) and (20) for the day- and night-time campaign. The transfer functions $g(\tau)$ and $h(\tau, t)$, representing conservative transport calculated from tracer BTCs and reactive transport calculated using fitted k_{night} and k_i (equation (10)), respectively, are compared to each other in Figure 4b. Figure 4c shows the prediction of the venlafaxine time series at MS2-M4 using the conservative transfer function $g(\tau)$, while Figure 4d shows the same prediction using the reactive transfer function $h(\tau, t)$, both for the day- and night-time campaigns. The concentrations of the grab samples are plotted in Figure 4c and d to show the misfit of the conservative transport model to the measurements and the fit of the reactive transport model, respectively. The step-like increase and decrease of the predictions is an artifact of having only a limited time series at MS1.

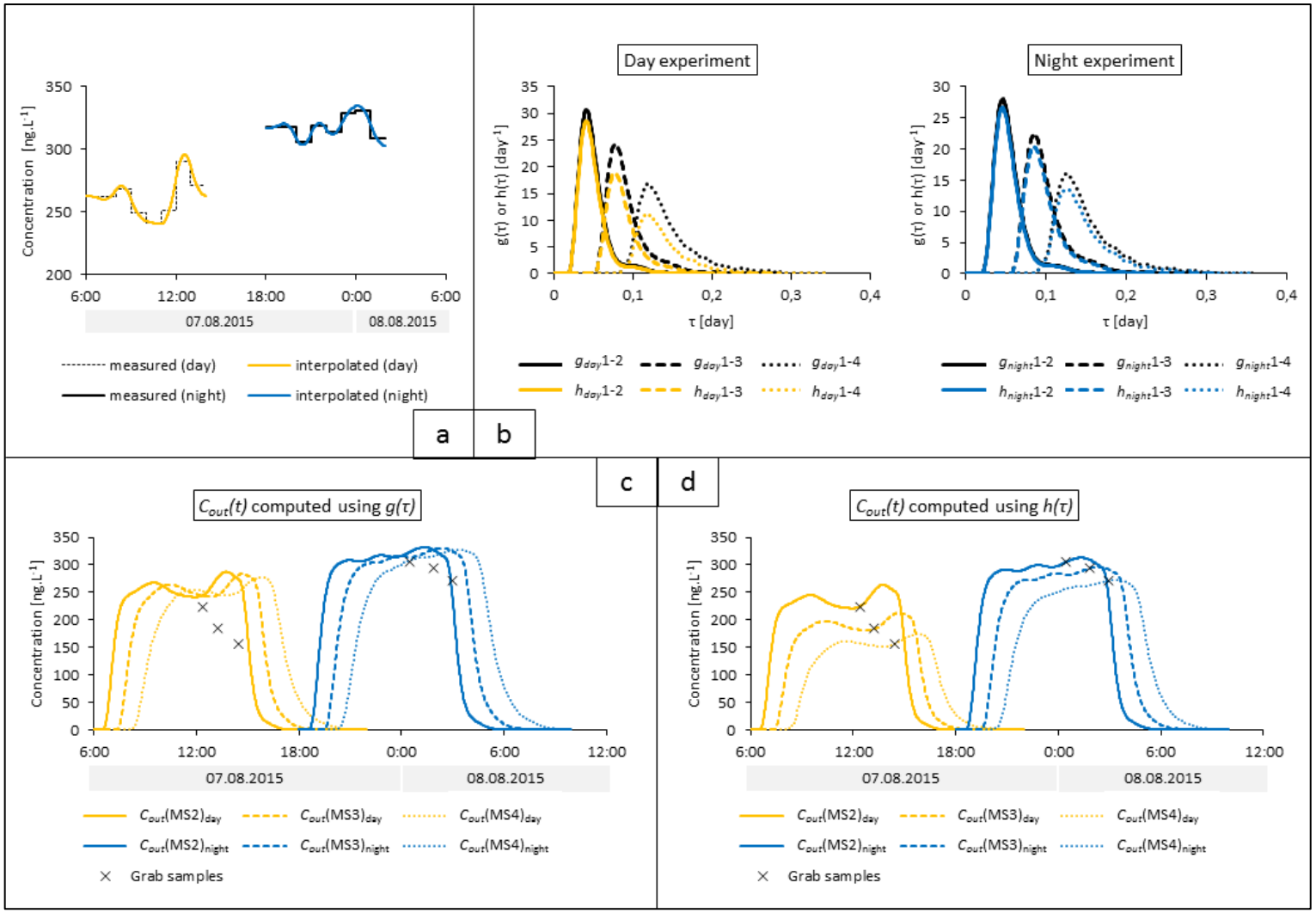

Figure 4. Model outcome for venlafaxine. a: reconstructed input functions at MS1 compared to measured 1 h-composite samples. b: reactive and conservative transfer functions, h(τ,t) and g(τ) between MS1 and MS2, MS3 and MS4 for the day- (h or g_{day}1-2, 1-3, 1-4, respectively) and night-time campaigns (h or g_{night}1-2, 1-3, 1-4, respectively). c and d: computed $C_{out}(t)$ at the different measurement stations downstream of MS1 using g(τ) and h(τ,t), respectively, and comparison to grab sample concentrations.

4.2.7 Extrapolation of elimination processes

Since solar radiation $H_G(t)$ shows a clear diurnal signal, the reactive removal computed by equation (11) depends on the observation time t. In order to evaluate the mean degradation over the entire day, the reactive removal was averaged over the period T of one day:

$$\bar{R}_i = 1 - \frac{\frac{1}{T}\int_0^T \int_0^\infty g(\tau)\exp\left(-\int_0^\tau \left(k_{night} + k_i H_G(t-\tau+\tau_*)\right)d\tau_*\right)d\tau dt}{\int_0^\infty g(\tau)d\tau} \quad (21)$$

The same expression, dropping photodegradation, yields the contribution of photo-independent processes on the degradation of compound i and reversely. The calculation used water parcels departing every minute from MS1 on the 7th of August 2015 starting from 00:00 until 23:59. For photodegradation, the solar radiation signal H_g covering all the widths of the corresponding transfer functions was used (see Figure S1 in the Appendix).

4.3 The 24 h-sampling campaigns

The 24 h mass-balance calculation was applied during the so-called "24 h-sampling" campaigns, operated during a summer campaign on July 2-3, 2013 and a winter campaign on February 12-13, 2014.

4.3.1 Site description

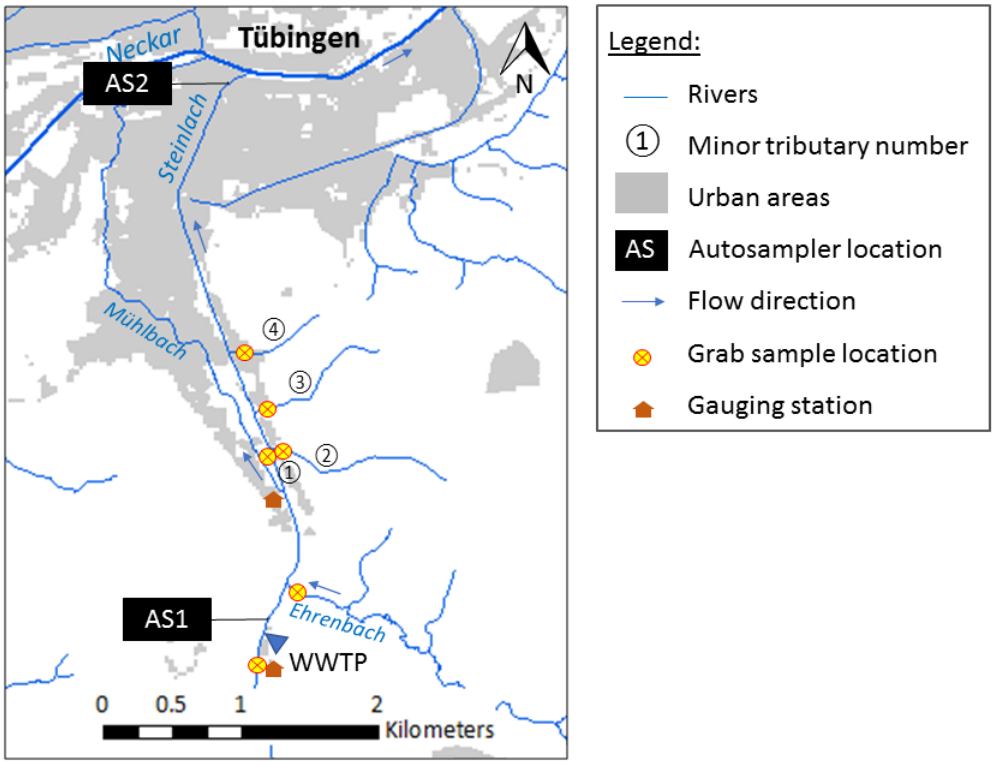

Figure 5. Sampling map of the 24 h-sampling campaigns in River Steinlach.

Mass flux time series were monitored at two control cross-sections delimiting a 4 km-long segment in River Steinlach in Derendingen, starting 90 m downstream of the WWTP effluent and ending 100 m before the confluence of River Steinlach with River Neckar (see Figure 5). Mass fluxes in the Ehrenbach and the four minor tributaries downstream were also monitored to take into account dilution or contaminant input from diffuse sources. From contaminant concentration measurements (see section 5.1.1), the minor tributary ① was assumed to drain water partly from the Mühlbach deviation, itself derived from the studied Steinlach reach. Several combined sewer overflows bordered the segment but remained dry in the absence of precipitation.

The environmental conditions are summarized for both summer and winter campaigns in Table 2. Discharge conditions were rather stable during both campaigns, except for an effluent stop that interrupted contaminant input during the summer campaign (for more details, see next paragraph). The minor tributary ① was dried up during the summer sampling but was flowing into the main stem in winter. The contribution of each minor tributaries did not exceed 0.3% of the discharge in the main stem during both campaigns, with a maximum of 4% for the Ehrenbach and a 4.6% maximum contribution from all gathered tributaries. In both campaigns the tree cover was almost absent, and the water was clear and deprived of vegetation, allowing sunlight to penetrate the water column.

Table 2. Summary of sampling conditions during the summer and winter 24 h-sampling campaigns.

	SUMMER CAMPAIGN 2-3 July 2013	**WINTER CAMPAIGN 12-13 February 2014**
Weather conditions	Sunny	Sunny
Day length	16 h (6:00-22:00)	10 h (8:00-18:00)
Minimum/maximum air temperature (LUBW data)	+ 12.2 °C / + 28.0 °C	- 1.5 °C / + 9.4 °C
Minimum/maximum water temperature (divers data)	+ 14.0 °C / + 20.9 °C	+ 3.8 °C / + 6.3 °C
Mean discharge (over the 24 h period)[1]	604 Ls^{-1}*	974 Ls^{-1}
Mean travel time τ_m	233 min*	155 min
Mean proportion of treated wastewater	23%*	22%
Ehrenbach discharge	13 Ls^{-1}	35 Ls^{-1}
Tributary ① discharge	/	1.5 Ls^{-1}
Tributary ② discharge	1 Ls^{-1}	1.5 Ls^{-1}
Tributary ③ discharge	1 Ls^{-1}	1.5 Ls^{-1}
Tributary ④ discharge	1 Ls^{-1}	2 Ls^{-1}

[1]Calculated for the lower control cross-section, after addition of the tributaries and subtraction of the Mühlbach discharge.
*Calculated by discounting the effluent stop period.

Unexpected events occurred during the sampling campaigns. The major event was the interruption of treated wastewater discharge due to maintenance works from the WWTP. The interruption occurred on July 2, 2013 between 15:40 and 17:10, where the WWTP's effluent discharge decreased rapidly until becoming inexistent. In addition, a small rain, initially forecasted for the afternoon of July 3, 2013, started around 6:30 on that day and intensified from 9:00 on. As it happened at the end of the campaign and did not affect the hydrograph, no consequences on the measurement were assumed. Another light rain event happened on February 13, 2014 at 3:00 during the winter campaign. The rain was too light to be recorded by the weather station from the LUBW and did not affect the hydrograph either.

4.3.2 Determination of the travel time prior to and during the experiment

The travel time was estimated prior to the experiment using EC signals and by timing recognizable EC patterns measured with CTD divers (Schlumberger Water Sciences Technology, Canada) placed at the AS locations. The treated wastewater discharged by the WWTP presents a significantly higher EC than River Steinlach water while the effluent/river discharge ratio is high enough to reflect the diurnal cycle of the WWTP effluent in the EC signals measured downstream (see section 5.2.1). The estimated travel time was used to program the start of the autosampler at the lower control cross-section (AS2) of the investigated segment. The divers were left during the experiment to determine the actual mean travel time τ_m during sampling (see Table 2) using equation (5). Though 3 h were expected during each experiment, τ_m was 53 min longer during the summer sampling and 25 min shorter during the winter sampling.

4.3.3 Sampling procedure for inorganic ions and wastewater contaminants

Autosamplers (ISCO 3700) equipped with a Teflon tube fixed on the riverbed were placed at both ends of the studied segment (see Figure 5). The upstream (AS1) and downstream (AS2) autosamplers started sampling for both campaigns at 6:00 and 9:00 in the morning, respectively, and were run for 23h45. Sub-samples were collected every 15 min, filling half a 950 mL glass bottles at a time, each autosampler bottle representing a 30 min-time span that would be mixed into 2 h-composite samples. Every 6 hours, 2 h-composite samples collected were transferred to 5 L clean polyethylene canisters through a rinsed steel funnel after shaking them to re-suspend the settled matter at their bottom. During the summer campaign, an aliquot representing a 2 h-time span from each 5 L canisters was transferred after shaking into 100 mL brown glass bottles, using the same fennel. During the winter campaign, the aliquot was directly taken from the autosampler bottles after shaking, thus representing 30 min-time spans. In the case of the summer campaign, an extra 2 h-composite sample was collected by both autosamplers at the end of the experiment, and was used for the extrapolation of the 24 h-time series, as explained in section 4.3.8.

As other water bodies joining the studied stretch do not receive treated wastewater discharge, the contaminant fluxes they provided were assumed not to undergo significant temporal variations over the experiment. Single grab samples were thus taken at the WESS gauge upstream of the WWTP, in the Ehrenbach and in each of the four minor tributaries joining the investigated segment.

A triplicate was collected at the upper control cross-section of the investigated segment. Three polyethylene canisters and brown glass bottles were rinsed with Steinlach water and filled directly in the river at the right and left banks and in the middle of the cross-section, next to the inlet of the AS1 tubing, within a few minutes.

The canisters and glass bottles were brought immediately to Tübingen laboratory. The brown glass bottles were stored in the dark at 4 °C for inorganic ion and DOC analysis as well as pH (only the summer samples) and turbidity measurement in Tübingen laboratory while the canisters were shipped within 24 h to the Institute of Sanitary Engineering, University of Stuttgart, for the analysis of organic micropollutants.

4.3.4 Measurement of environmental parameters

Lateral EC profiles were measured repeatedly at the two cross-sections delimiting the segment using again a WTW LF340 device to ensure complete mixing of the effluent water and various tributaries with the Steinlach water at the sampling locations.

CTD divers were set at the upper and lower control cross-sections to measure specific EC, river temperature and total pressure every 5 min. Global solar radiation data during summer 2013 and data on air temperature were found on the LUBW website, from the measurement station situated in Derendingen (http://udo.lubw.baden-wuerttemberg.de). This latter did not monitor solar radiation during the whole 2014 year. Another station, based in Unterjesingen, 6 km west of Tübingen, was chosen to provide the solar radiation data used in the interpretation of the winter campaign's results (www.wetter-bw.de). Both stations recorded solar radiations during the tracer-based sampling (August 7-8, 2015) described in section 4.2 and the fit of both measurements was checked to ensure that winter solar data from the Unterjesingen station could be compared to the summer values from Derendingen.

The upper control cross-section, where AS1 was set, did not allow discharge measurements to provide mean discharge data for the calculation of mass loads from the twelve consecutive 2 h-composite samples taken at that location. EC time series, measured every 5 min by CTD divers set at the AS1 location, upstream and in the WWTP effluent, and discharge time series Q_{up}, measured at the WESS gauge (see Figure 6), supplied the mixing equation (24) in section 4.3.6 to calculate discharge time series at the AS1 location. Discharge upstream of the WWTP Q_{up} was determined from converting water stage measurements, acquired at the WESS gauge during the samplings, by a rating curve established at this location.

The lower control cross-section, where AS2 was set, did not allow discharge recording either. Though the cross-section was ideal for discharge measurement, perturbations of the water stage were observed and attributed to backwater effect from the Neckar weir, 470 m downstream of the confluence of River Steinlach. As this perturbation was only identified during the summer campaign, the discharge at the AS2 cross-section had to be calculated for the July 2013 sampling (see section 4.3.6). During the winter campaign, this problem was anticipated, and a rating curve was built at a cross-section shortly before a railway bridge 170 m upstream of the AS2 section, where water stage was not affected. A CTD diver was placed in the river flowing under the bridge and a water stage time series with a 5 min interval was obtained by subtracting the atmospheric pressure measured by a CTD baro-logger, set at the WESS gauge, from the total pressure measured by the diver.

Discharge was also checked at both control cross-sections during each experiment to ensure the fit of the calculated time series. Those discharge measurements as well as measurements in the Ehrenbach and the Mühlbach were performed using an OTT C2 flow meter or an ADC acoustic current meter (both OTT Hydromet GmbH & Co.KG, Germany). Discharge in the minor tributaries was estimated due to the impossibility to perform measurements and, as for the Ehrenbach and the Mühlbach, assumed constant for the mass load calculation.

A schematic map of measurements and samplings is given in Figure 6.

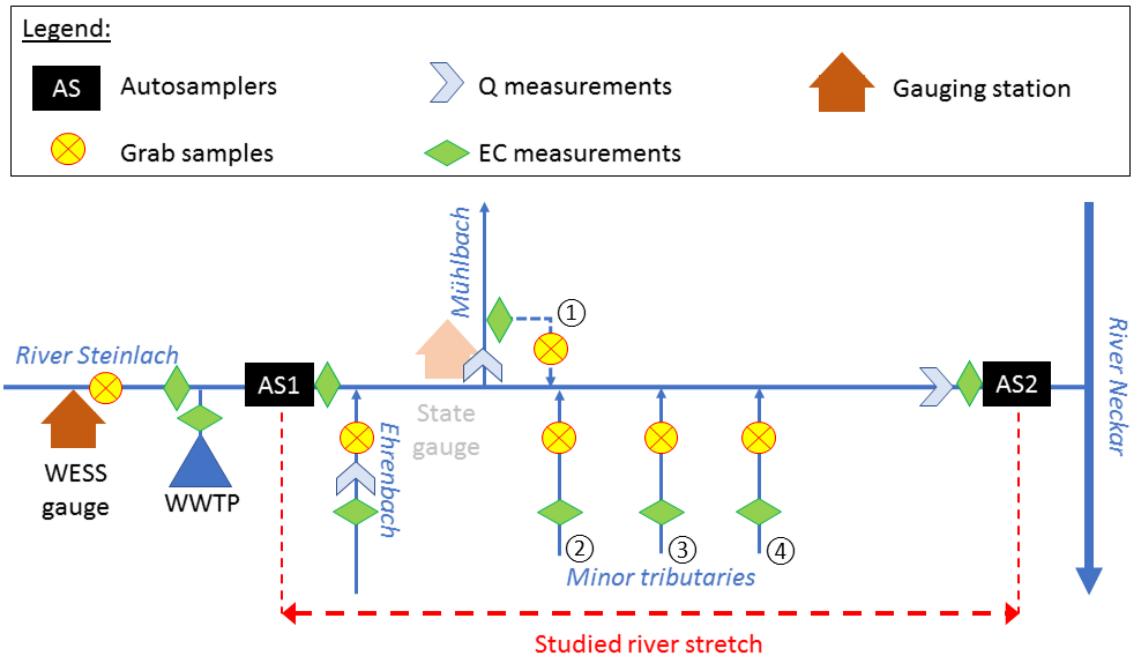

Figure 6. Schematic map of sampling and measurements operated during the 24 h-sampling campaigns.

4.3.5 Analytical work

pH, only for the summer campaign, turbidity, DOC and concentrations of inorganic ions were analyzed by the laboratory of Tübingen as described in 4.2.5.

The list of the eighteen organic compounds analyzed by Dr. Bertram Kuch in Stuttgart University during the summer and winter 24 h campaigns and their respective properties are presented in Table S1 in the Appendix.

For the analysis of diclofenac, naproxen, mecoprop and triclosan, the internal standards diclofenac-d4 (50 µL, 4 ng μL^{-1} in dichloromethane), naproxen-d3 (50 µL, 4 ng μL^{-1} in dichloromethane), mecoprop-d3 (20 µL, 1 ng μL^{-1} in methanol) and triclosan-d3 (50 µL, 1 ng μL^{-1} in methanol) were added in the non-filtered water samples (~2 L) and the pH-value was adjusted to pH 2.5 using sulfuric acid (96%). The analytes were extracted via liquid/liquid-extraction (dichloromethane, 2 × 80 mL). The combined organic phases were rotavaporated to approximately 2 mL and dried with sodium sulfate. Prior to GC/MS-analysis the extracts were concentrated with a nitrogen stream (40 °C) to dryness and re-dissolved in a solution of the derivatization agent TMSH (20 µL trimethylsufoniumhydroxide, 0.25 M in methanol).

For the analysis of the other organic compounds, the non-filtered water samples (~2 L) were spiked with internal standards (100 µL AHTN-d3, 1 ng μL^{-1} in dichloromethane; 50 µL carbamazepine-d10, 2 ng μL^{-1} in dichloromethane). Liquid/liquid extraction with dichloromethane and further steps were performed as described above. Prior to GC/MS-analysis the extracts were concentrated in a nitrogen stream at 25 °C to a volume of 50 µL.

GC/MS-analysis was performed on a high-resolution gas chromatograph Agilent 6890 directly coupled with a low-resolution mass selective detector Agilent 5975. The analytes were quantified directly via the isotope dilution method or external calibration with internal standards.

4.3.6 Determination of discharge at the control cross-sections

The mass balance principle was also applied to deduct the discharge Q_{AS1} at the upper control cross-section by using EC as a conservative tracer. A distinct sub-segment was defined, starting at the Steinlach WESS gauge and ending at the beginning of the investigated segment of River Steinlach. Within this new sub-segment, the only known inflow comes from the WWTP effluent with the effluent pattern being observable in the EC signal in the river downstream. EC presents the advantage of being recordable at high temporal resolution by CTD divers. In the case of a conservative parameter such as EC, the ΔS term equals zero and the input equals the output. The mixing equation (22) for a conservative parameter such as EC yields:

$$Q_{up}EC_{up} + Q_{WWTP}EC_{WWTP} = Q_{AS1}EC_{AS1} \tag{22}$$

where $Q_{up/WWTP/AS1}$ [L^3T^{-1}] and $EC_{up/WWTP/AS1}$ [$A^2T^3M^{-1}L^{-3}$] are discharge and specific electrical conductivities measured upstream of the WWTP, in the WWTP effluent and at the upper control cross-section of the investigated segment – AS1 location (see Figure 6), respectively. AS1 was set far enough downstream from the WWTP to ensure complete mixing of the two input terms of equation (22). Q_{up} and all EC terms being known, Q_{WWTP} can be calculated following equation (23), after transformation of equation (22):

$$Q_{WWTP} = Q_{up}\frac{EC_{up}-EC_{WWTP}}{EC_{AS1}-EC_{WWTP}} \tag{23}$$

The discharge Q_{AS1} is finally obtained by summing measured Q_{up} and calculated Q_{WWTP}:

$$Q_{AS1} = Q_{up} + Q_{WWTP} = Q_{up}\left(1 + \frac{EC_{up}-EC_{WWTP}}{EC_{AS1}-EC_{WWTP}}\right) \tag{24}$$

Because these locations are separated by a certain transit time, the various Q and EC time series recorded for equation (22) were shifted to their theoretical arrival at the WWTP effluent site for equation (23) and to the AS1 cross-section for equation (24), according to observed velocities in the sub-segment for EC and water stage, obtained from measurements by the CTD divers during the campaigns.

To calculate the discharge at the AS2 cross-section for the summer campaign, the discharge time series at AS1 and the discharge of the different contributing inflows were summed up while subtracting the Mühlbach's, assuming no additional input along the segment. The obtained discharge time series was then shifted according to the kinetic wave approach. Dingman (1984) demonstrated theoretically for a rectangular cross-section that the ratio of the wave over the water flow velocity was equal to 5/3, assuming that Q and water depth are related by the Manning equation. During the summer campaign, water stage and EC time series could be compared only between the WESS gauge and a spot right above the WWTP effluent, representing a 330 m distance. The ratio of the measured Q wave and EC velocities yielded values between 1.5 and 2.1 close to the 5/3=1.67 ratio from Dingman (1984). However, this was upstream of the investigated segment and for a short distance. The diver set at the railway bridge during the winter campaign allowed comparing the water height and EC time series over 3.8 km. The ratio obtained was 1.63. Thus, the use of the 5/3 ratio was assumed accurate also for summer discharge conditions and kept for the shifting of the calculated discharge to the AS2 site during the summer campaign. During the winter campaign, the mean velocity of the kinetic wave between the AS1 and the railway bridge was used to shift discharge measured at the railway bridge to the AS2 location.

4.3.7 Mass balance calculation

To calculate the mass balance according to equation (12), mass loads of analyzed compounds at the autosamplers cross-sections were calculated for each 2 h – or 30 min for inorganic ions in winter – sample from integrating the corresponding mean discharge values over the sample respective sampling interval and multiplying it by the measured concentration. The load contribution from the tributaries was assumed constant over the sampling and was added as input term according to equation (12).

As it receives the water from the main stem and should observe the same temporal concentration pattern, loads leaving the investigated segment through the Mühlbach had to be calculated at the same temporal resolution as the AS samples. To simplify the calculation, only one discharge measurement was made in the Mühlbach, assuming that discharge variations were negligible in comparison to the main channel. To avoid recording a 24 h time series in the Mühlbach, no sample was taken but the output through the Mühlbach was calculated as the sum of the corresponding loads at the AS1 and the Ehrenbach, weighed by the ratio between the Mühlbach discharge and the mean discharge during the time span of the sample. This assumes that the mixed concentration in the river reach remains constant upstream of the Mühlbach, meaning no significant elimination within the kilometer separating the upstream control cross-section from the Mühlbach deviation. For each time increment, the corresponding loads exiting through the Mühlbach were subtracted from the left side of equation (12), as they do not represent reactive turnover.

For the balance over 24 h, all output loads were subtracted from summed up inputs over the 24 h campaigns in order to determine ΔS according to equation (12). ΔS was then normalized to the sum of all inputs (minus loads exiting through the Mühlbach) to provide a relative net removal in percent and the constant k was finally calculated using equation (13) for both summer and winter campaigns.

4.3.8 Convolution of the concentration time series

If τ is known, corresponding mass loads at the input and output can be directly compared. In the case of strong variations of concentrations over time, dispersion effects along the flow path can become more important and cause bias in the observation of actual elimination of investigated compounds. The upstream time series of compound concentrations from the winter campaign was processed through the method described in section 4.1.1 to observe temporal variations of elimination processes over one day. For fair comparison, the same procedure was applied to result from Schwientek et al. (2016).

For each campaign, the transfer function $g(\tau)$, obtained by deconvoluting EC signals between the two control cross-sections of the investigated segment, was used to compute the 24 h-time series expected at the AS2 location if only conservative transport occurred. In the investigated segment of River Steinlach, the C_{in} term used in equation (4) was calculated by summing up the EC value of the various inputs – through the main reach at AS1 location and from the tributaries – weighed by their respective discharge. The calculated transfer function of each campaign was corrected from unrealistic peaks in the raising limb and in the tailing. It was then normalized to obtain a recovery of 100% and correct uncertainties from the deconvolution, considering the conservativeness of EC and insignificant changes in discharge along the study section.

To convolute the contaminant time series with the transfer function and visually compare it to the downstream sampling location, the temporal resolution from the 2 h- or 30 min-composite samples at both cross-sections was refined. The smooth concentration distribution $C_{fine}(t)$ [ML^{-3}] was reconstructed as for the tracer-based sampling (see section 4.2.6), only for the 24 h sampling was the duration of averaging $\Delta t = 2$ h or 30 min in equation (20). For the upper control cross-section, the term

C_i^{meas} was calculated by summing up the various inputs weighed by their respective discharge, as it was done for EC.

To recover a 24 h-long time series and compare it to the 24 h-signal downstream of the investigated segment, the input time series had to be extrapolated due to the use of transfer function like in the tracer-based sampling. During the 24 h samplings, 3.7% and 1.3% of the concentration signal for the summer and winter sampling were missing, respectively. While the extra sample measured at the end of the 24 h-cycle during the summer sampling was used, the extrapolation before the 24 h-time series of both summer and winter campaigns and after the 24 h-time series of the winter sampling used the concentration C_i^{meas} of the neighboring sample. The choice of the neighboring concentration value was due to the input time series being much longer and generally more variable than in the tracer-based sampling.

For both campaigns, the extrapolated data for each analyzed compound was then interpolated at a 1 min interval using equation (19) and (20), convoluted with the corresponding transfer function and compared graphically to the concentrations measured at the AS2 location (see section 5.3.2).

4.4 The flood sampling

4.4.1 Sites description

Two floods were sampled at single observation points in River Steinlach and Ammer, at the location of the WESS gauge upstream of the Steinlach-Wiesaz WWTP and at the Ammer gauge in Pfäffingen city downstream of two WWTPs, respectively (see Figure 7).

The flood captured in River Steinlach occurred in the night of August 9, 2015, one day after the end of the tracer-based sampling, after a high-intensity precipitation event in the late afternoon, typical for a summer season in the Suabian Alb region. No station for precipitation measurement was situated in the upper part of the Steinlach catchment but the LUBW provided a map interpolating the precipitation measured by neighboring stations (see Figure S2 in the Appendix). In River Steinlach, the main discharge peaks ①, ② and ③ – 6, 6 and 23 m^3s^{-1} – were reached within 30-45 min compared to baseflow, a dynamic response typical from the river's hydrological characteristics, detailed in section 2.1. Peak ③ was the 2nd biggest of the year 2015 in terms of discharge recorded at the WESS gauge and was followed by three secondary peaks on its falling limb (see Figure 8).

The discharge event captured at the Ammer gauge occurred on the night of February 9, 2016. The precipitation event at the origin of the Ammer flood was typical of the winter season where more gradual rainfalls occur. One measurement station from the LUBW in Herrenberg, in the upstream part of the catchment, provided precipitation data for the Ammer (see Figure S3 in the Appendix). The Ammer "flood" was constituted by a main peak followed by a secondary peak on its falling limb – 1.4 and 1.1 m^3s^{-1} for peak ① and ②, respectively (see Figure 8). Both were rather small compared to the Steinlach event, but still provided significant particle concentrations (up to 317 mg L^{-1}).

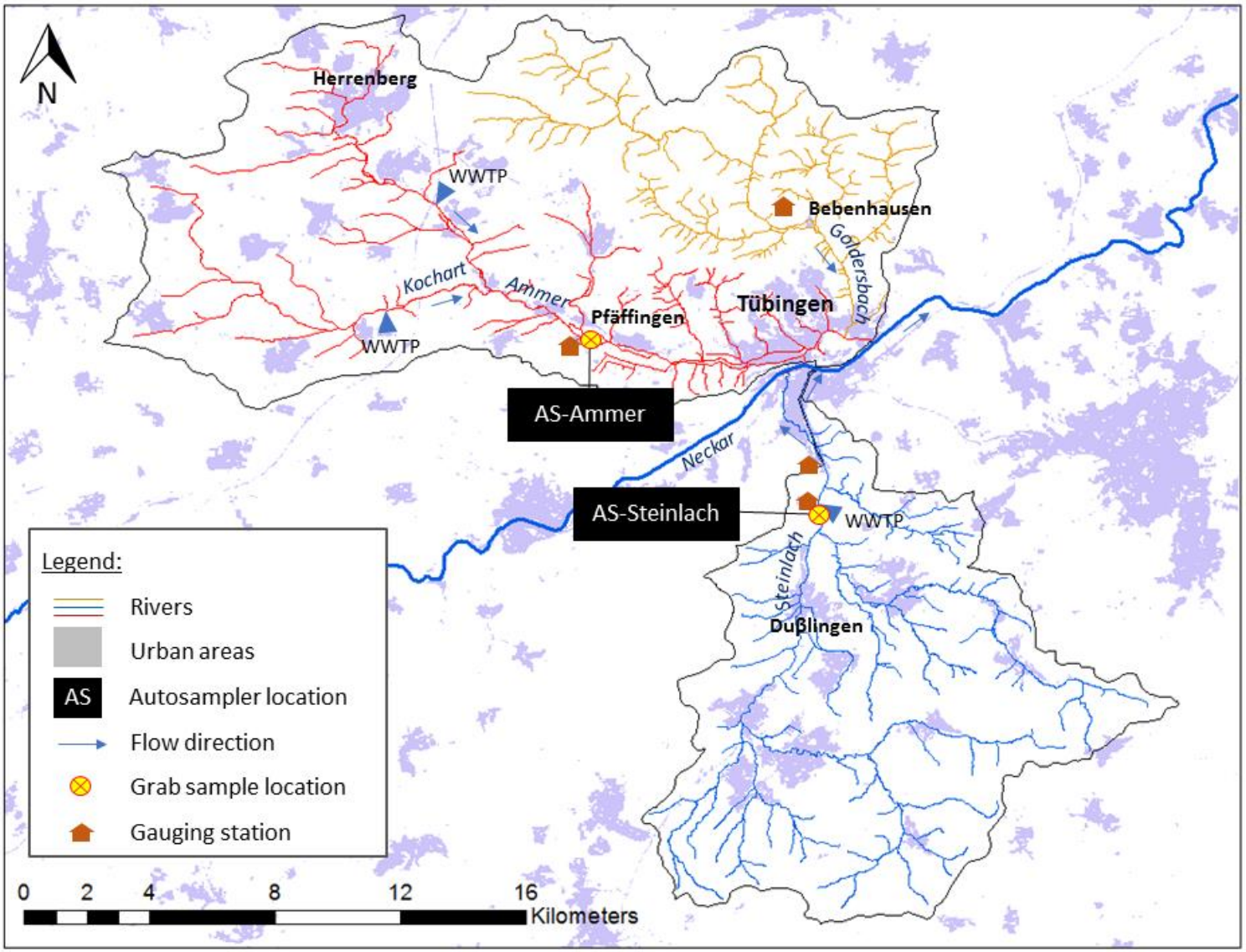

Figure 7. Sampling locations for flood sampling campaigns in River Steinlach and Ammer.

4.4.2 Sampling procedure

For each sampling, two ISCO 3700 autosamplers containing each twelve 950 mL glass bottles were set at the corresponding gauge with Teflon tubes set into the river water at the right bank. A liquid detector set about 10 cm above the water level was connected to the autosamplers to start them as soon as the water head rose. The autosamplers were programmed to collect each simultaneously three bottles per sampling event. The hydrographs of the Steinlach and Ammer flood events as well as the corresponding sampling are displayed in Figure 8.

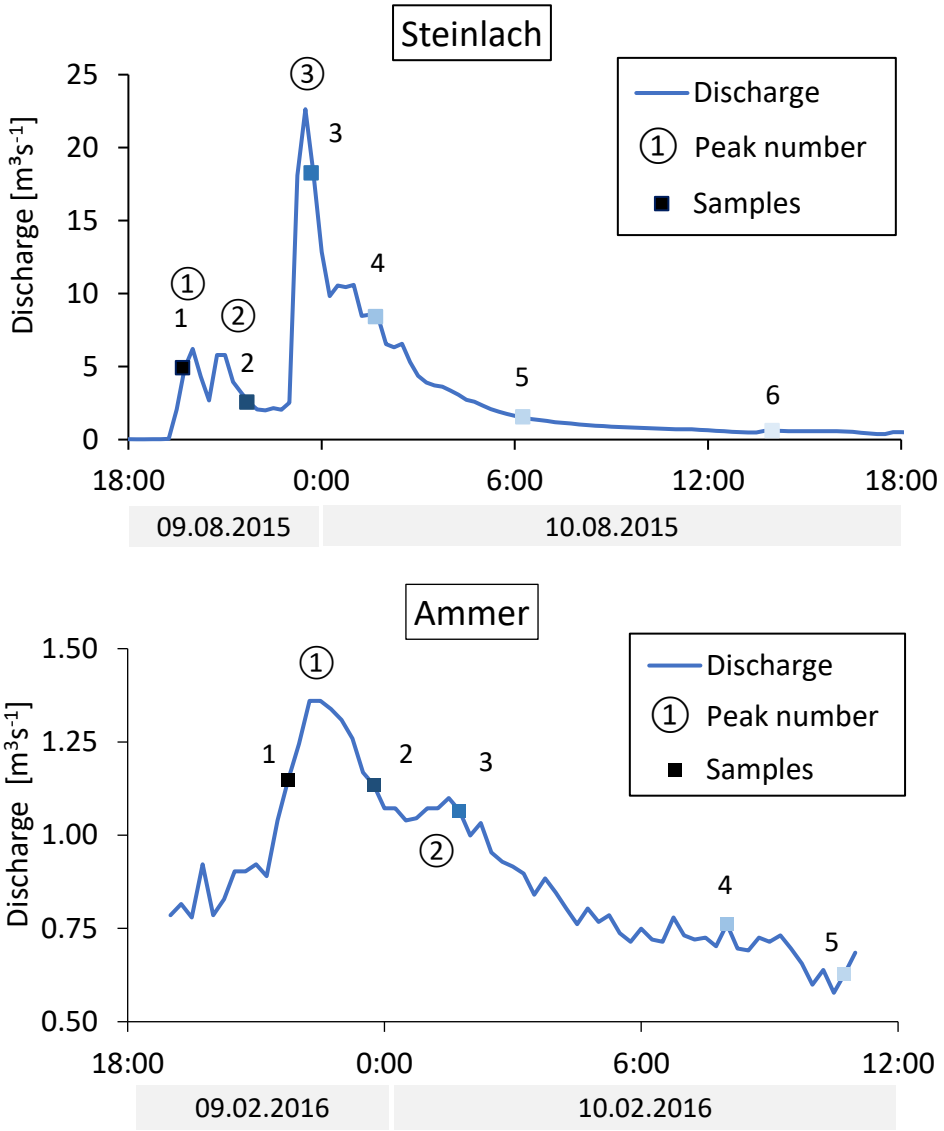

Figure 8. Hydrographs of floods captured in River Steinlach and Ammer and associated samples.

The two autosamplers in place in River Steinlach started sampling at 19:41 on August 9, 2015 and collected three more samples during the night, each separated by 2 h. They were reactivated once the previous samples were recovered to collect two more samples at 6:15 and 14:00 on August 10, 2015. A hand triplicate to test the analytical procedure was taken in the river 3 m upstream of the gauge. For the analysis of wastewater contaminants, the triplicates were taken at 6:15 using three 5 L polyethylene

canisters, in the same time as the 5th sample from the autosamplers. Due to practical reasons, the sampling of the triplicate was made by rinsing and filling first two canisters before doing the third one immediately after, within the following 3 min. Due to handling problems, the triplicate for environmental parameters and inorganic ion analysis was taken using three 1 L brown glass bottles at 7:07.

The sampling in River Ammer was initiated by the liquid detector on February 9, 2016 at 21:38, followed by two other samples separated by 2 h. Due to a technical problem of the ASs, the following samples consisted in a triplicate taken by hand on the February 10, at 08:03 and a grab sample later at 10:42 directly in the Ammer water, 50 cm upstream of the tubing. The triplicate sampling was operated again within a few minutes using three 5 L polyethylene canisters and three 1 L brown glass bottles.

As rain persisted overnight parallel to the flood events, autosampler samples were transferred at dawn for safety reasons into canister and bottles, and into cool boxes containing ice. To maximize preservation of samples, the autosamplers were filled with ice. For each sample, the corresponding three bottles of one autosampler and two from the other were transferred through a rinsed steel funnel into 5 L polystyrene canisters, rinsed with distilled water, for organic contaminant analysis. The third bottle of the second autosampler was transferred into a clean 1 L brown glass bottle. All autosampler bottles were shaken to ensure that no particles remained at the bottom.

Before the sampling in River Ammer, a field blank of ultrapure water was taken in order to identify contamination by the autosampler, transport, sample manipulation and analysis. Before the blank collection, the autosampler and its bottles and tubing were rinsed with 7.5 L of ultrapure water from a clean 5 L polyethylene canister that was refilled from another canister during the pumping procedure. The operation was repeated using another 5 L polystyrene canister filled with ultrapure water to fill six AS bottles with the blank sample. The blank sample was then transferred into a final 5 L polystyrene canister and a brown 1 L glass bottle as for the other samples.

All samples were directly brought to Tübingen laboratory and stored in the dark at 4 °C until analysis of inorganic ions and environmental parameters from brown-glass bottle samples or shipping of the canisters to Stuttgart University for organic contaminant analysis.

4.4.3 Measurement of environmental parameters

Turbidity sensors at the Steinlach and Ammer gauges met technical problems and could not provide consistent turbidity data for the flood events sampled. Both gauges gave however water stage data that were transformed into discharge using predefined rating curves.

4.4.4 Analytical work

Concentrations of inorganic ions and organic contaminants, DOC, pH and turbidity in the samples were measured as detailed in section 4.3.5. The author conducted the measurements of pH and turbidity on the raw samples as well as the filtration of samples for the analysis of inorganic ions and DOC. The use and properties of organic contaminants investigated during the flood campaigns are displayed in Table S1 in the Appendix.

TOC was measured on raw samples after grinding of the particles by the author with the “Ultra Turrax” (IKA-Werke GmbH & Co. KG, Deutschland) during 1 Minute at a rate of 15000 rounds/min before acidification of samples at pH<2 to remove all inorganic carbon. TOC was measured on liquid samples

by Tübingen laboratory staff by thermal oxidation (1200°C) and CO2 quantification with a Vario TOC cube (Elementar Analysensysteme GmbH, Deutschland).

Tübingen laboratory staff measured total suspended solid concentration (TSS) after filtrating samples through glass microfiber membrane (pore diameter of 1.5 µm) and weighing dried residues for the given sample volume, according to the DIN38409-2 (1987) .

For the analysis of grain size distribution, a small aliquot of raw samples obtained after shaking was injected by the author using a plastic pipette into the dispersion module of a Malvern Mastersizer 2000 (Malvern Panalytical Ltd, UK). Based on laser diffraction analysis of the particles, the particle sizes distribution in volume % per particle size between 20 nm and 2 mm as well as the d50 (grain size at which 50% of the particles volume is found in the samples) were obtained. Grain size distribution was measured by the author on all Steinlach samples and in sample 1, 2, 3 and one of the triplicates of sample number 4 from the Ammer flood. The fifth sample collected in River Ammer could not be measured due to the too high volume required given the low turbidity of the sample.

4.4.5 Calculation of the organic content

The calculation of organic content f_{oc} was performed using the environmental parameters measured in Tübingen laboratory according to the equation:

$$f_{oc} = \frac{TOC - DOC}{TSS} \tag{25}$$

4.5 The Steinlach "pre-sampling" campaign

The comparison of filtered and unfiltered samples analyzed during a sampling campaign operated on June 12, 2013 was used to support data analysis for particle-associated transport. This "pre-sampling" campaign was initially a preparation step prior to the later works on reactive transport in the Steinlach study segment.

4.5.1 Site description

Grab samples were taken following a longitudinal profile along the Steinlach segment downstream of the WWTP (see Figure 9). The pre-sampling campaign occurred ten days after an approximately 100 m^3s^{-1} flood event (of a twenty-year return period). The additional occurrence of precipitation in the days preceding the campaign induced a 3.2 m^3s^{-1} discharge in the segment downstream of the Steinlach-Wiesaz WWTP, according to the State gauge, and the WWTP retention basin was seen overflowing during the sampling.

4.5.2 Sampling procedure

Grab samples were collected 0.9, 1.7, 2.7, 3.5 and 4.2 km downstream of the WWTP effluent, by filling 5 L polystyrene canister and 500 mL brown glass bottles previously rinsed with river water, for analysis of organic contaminants and inorganic ions, respectively. Samples were recovered by following approximately the same water parcel thanks to water velocity prior estimations from EC measurements, similarly to 4.3.2.

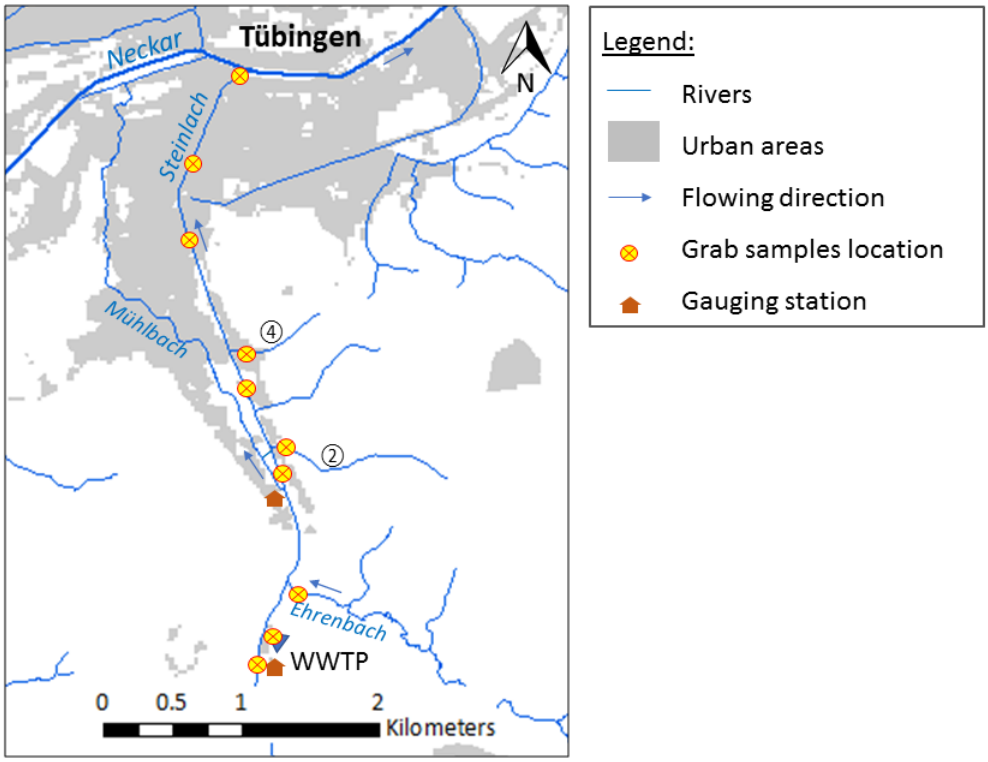

Figure 9. Sampling map of the "pre-sampling" in River Steinlach.

A grab sample was taken 5 m upstream of the WWTP effluent and two were recovered in the WWTP effluent (at the beginning and at the end of the profile sampling). A grab sample was also collected in the Ehrenbach, the tributary ② and ④, the other tributaries being unfound at the time (see Figure 9).

Samples were brought back to Tübingen and stored in the dark at 4°C before analysis of turbidity, DOC and concentration of inorganic ions in Tübingen laboratory and shipping to Stuttgart University for organic contaminant analysis.

4.5.3 Analytical work

Turbidity, DOC, inorganic ion and organic contaminant concentrations were analyzed the same way as for the 24 h-sampling campaigns (see section 4.3.5). The analysis of organic contaminants was this time performed on both filtered, using 0.45 µm cellulose acetate filters, and unfiltered samples.

4.6 The monthly sampling

The data from a monthly sampling performed between 2009 and 2011 by the WESS competence cluster was used for the estimation of fluxes in the Steinlach, Ammer and Goldersbach catchments.

4.6.1 Site description

The monthly sampling monitored 48 locations in total, from which only five situated in the three studied catchments were used for the comparison of both temporal and spatial variations of wastewater contaminant fluxes (see Figure 10).

Two locations were chosen in the Goldersbach catchment, at a WESS gauge upstream of Bebenhausen and at the mouth of the river before its confluence with River Ammer in Tübingen City. The locations provided comparison between the pristine Schönbuch forest and the lightly urbanized portion of the catchment with Bebenhausen village and eastern Tübingen city. River Goldersbach does not receive WWTP discharge nor is there any CSO outlet upstream of Bebenhausen but CSOs can be expected in the urban areas in case of precipitation event.

Two locations in the Steinlach catchment, up- and downstream of the WWTP effluent, were used as comparison with the data recovered from the 24 h- and flood-sampling campaigns. The upstream location, unlike in the other sampling campaigns, was situated upstream of the confluence of River Wiesaz with River Steinlach.

A single location in the Ammer catchment was selected at the WESS gauge in Pfäffingen, 8 km downstream of both Gäu-Ammer and Bondorf-Hailfingen WWTPs and downstream of urban areas, more consequent than in the Steinlach catchment, with CSOs releases expected during rainy conditions.

The monthly sampling captured mostly baseflow conditions in the three rivers. Two snow-melting events during December 2010 and January 2011, respectively (Rügner et al., 2013), yielded higher discharge conditions in the three rivers. In River Goldersbach, discharge was estimated at 1.5 m^3s^{-1} at the WESS gauge and 3 m^3s^{-1} at the Goldersbach mouth in December 2010 and at 0.5 m^3s^{-1} and 1 m^3s^{-1}, respectively, in January 2011. Discharge in River Goldersbach captured by the rest of the sampling ranged from 0.07 to 0.2 m^3s^{-1} at the WESS gauge and 0.15 to 0.4 m^3s^{-1} at the mouth. In River Steinlach, the snow-melting events in December 2010 and January 2011 induced discharges of 12 and 4.5 m^3s^{-1} upstream of the WWTP and 15 and 5.7 m^3s^{-1} downstream of the WWTP. A 4 m^3s^{-1} event was also captured upstream of the WWTP in June 2010 but the other samples were taken during rather low flow, with 0.2 to 1 m^3s^{-1} upstream of the WWTP and 0.3 to 1.3 m^3s^{-1} downstream of the WWTP. In River Ammer, discharge conditions captured in December 2010 and January 2011 were 2.0 and 2.1 m^3s^{-1}, respectively. In the other samples, discharge varied from 0.6 to 1.4 m^3s^{-1}.

4.6.2 Sampling procedure

Ten to thirteen grab samples were collected on an almost monthly basis at the desired locations in the neighboring catchments, in the same order and usually at the same time of the day between October 6, 2009 and May 9, 2011 (Lange et al., 2015). Grab samples were expedited directly to Stuttgart laboratory for analysis of organic contaminants.

4.6.3 Measurement of environmental parameters

There were no gauges monitoring the investigated cross-sections of studied rivers at the time of the sampling. Discharge was retrieved from nearby gauges and scaled by catchment area to obtain data for all locations.

4.6.4 Analytical work

Concentrations of organic contaminants were analyzed at Stuttgart University by Dr. Bertram Kuch and turbidity was measured in Tübingen laboratory, with the same methodology as described in section 4.2.5.

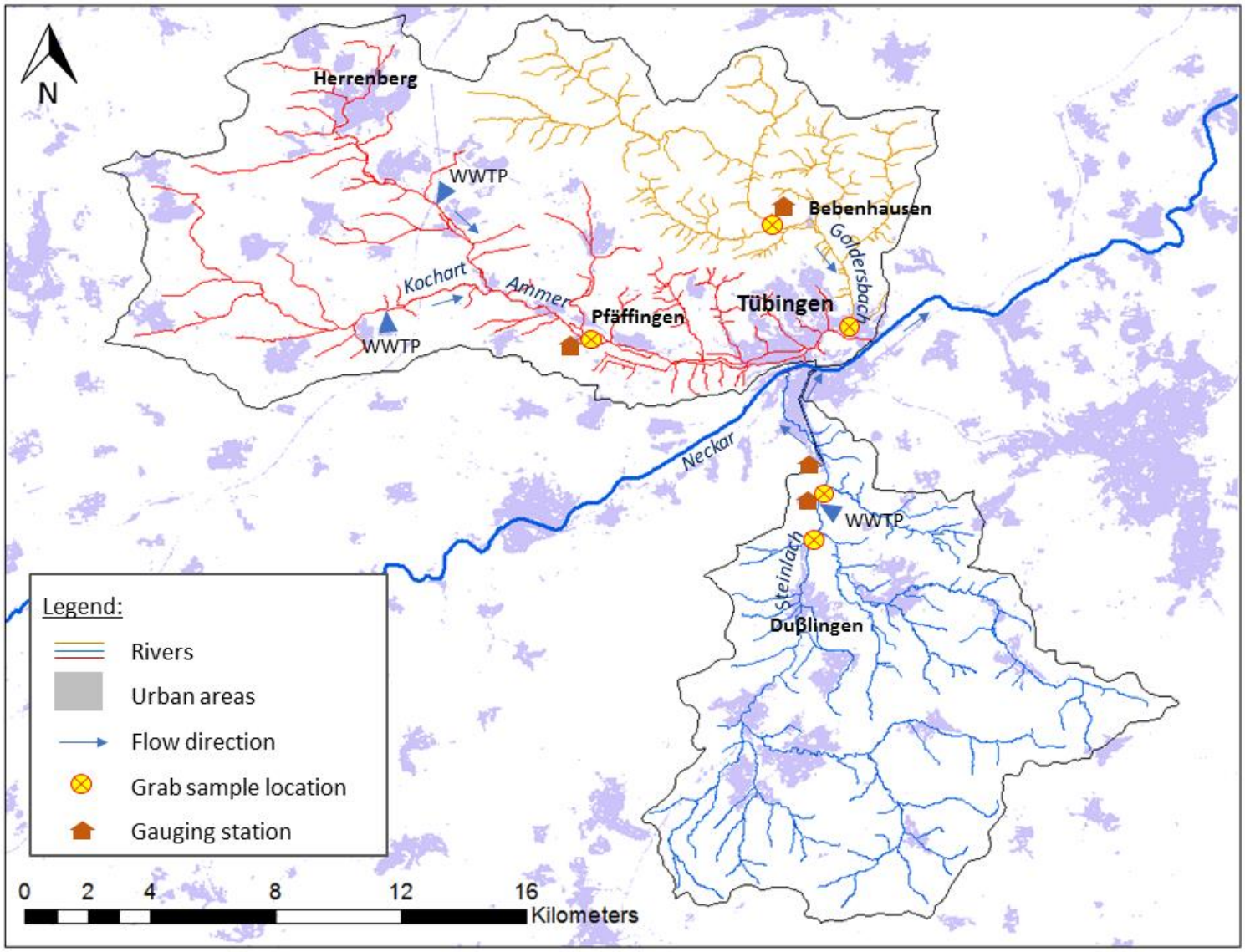

Figure 10. Locations of the monthly grab sampling in Rivers Steinlach, Ammer and Goldersbach.

5 Results and discussion

5.1 Measured concentrations and environmental parameters

5.1.1 Reactive transport in River Steinlach

The pH measured in River Steinlach indicated slightly basic water, with a pH of 8.0 and 7.6 to 7.8 during the day and night experiment of the tracer-based sampling and 7.6 to 8.6 during the summer 24 h-sampling campaign, respectively. pH was not measured during the winter 24 h-sampling campaign but was assumed to be of similar value.

Turbidity stayed negligible in the main reach for all samplings during dry weather conditions with 3-6 NTU, 1-2 NTU and 1-4 NTU for the tracer-based, the 24 h-summer and 24 h-winter samplings, respectively, as stable and relatively low discharge conditions were targeted.

DOC upstream of the WWTP effluent and in the different tributaries joining River Steinlach downstream of the WWTP ranged between 1.5 and 3.2 mgL^{-1} in all baseflow-campaigns. DOC ranged between 2.9 and 4.1 mgL^{-1} (but went down to 2.2 mgL^{-1} during the effluent stop) in the main reach during the summer 24 h-sampling campaign and between 2.4 and 3.8 mgL^{-1} during the winter sampling. DOC values during the tracer-based sampling campaigns were notably higher with 7.1 to 8.6 mgL^{-1}, originating from the high fraction of treated wastewater in the river during the experiment (92 to 94% of DOC fluxes originated from the WWTP against 56 to 69% and 49 to 61% for the summer and winter 24 h samplings, respectively).

During the tracer-based sampling, the mean water temperature varied only by 1.8 Kelvin between the day- and night-time experiments. Hence, the assumption of no major change in biodegradation over the duration of the experiment justified the calculation of k_i and k_{night}, as described in section 4.1.2. A similar amplitude of water temperature variation was observed during the summer 24 h-sampling campaign. But minimum and maximum temperature in the river water during the tracer-based samplings was about 6 Kelvin higher than the minimum and maximum observed during the summer 24 h-sampling campaign.

The wide set of analytes measured during the tracer-based sampling in River Steinlach in August 2015, provided concentrations of the investigated wastewater contaminants ranging between 2 ngL^{-1} (atrazine, salbutamol) and 5000 ngL^{-1} (sucralose) in the main stem (see Table 3). Concentrations upstream of the WWTP were mostly below the limit of quantification (LOQ) or even the limit of detection (LOD). A few compounds had however notable concentrations. The artificial sweetener acesulfame displayed a concentration of 76 ngL^{-1} while concentration of the corrosion inhibitor benzotriazole was 43 ngL^{-1}. Diatrizoic acid and TCPP were measured at 26 ngL^{-1}. The insect repellent DEET was measured at 29 ngL^{-1} and the herbicide atrazine had a concentration of 2 ngL^{-1} upstream of the effluent, similar to the 2-3 ngL^{-1} measured downstream.

As upstream of the WWTP in the absence of treated wastewater discharge, most organic compounds were not detected or under the LOQ in the tributaries joining the investigated segment during the tracer experiment. The contrast agent diatrizoic acid was an exception with a concentration of 263 ngL^{-1} in the minor tributary ④. No diatrizoic acid was detected in the minor tributary ③ and reasons could not be found to explain its presence at such concentrations (but low fluxes) in the minor tributary ④.

Concentrations of inorganic ions were generally higher in the main stem than in the tributaries, except for fluoride and magnesium, and only fluoride had a higher concentration upstream of the WWTP, though it remained close to the LOQ. Phosphate was observable only in the main reach downstream of the WWTP.

Table 3. Concentration ranges[1] measured during the tracer-based sampling in the minor tributaries ③ and ④, at MS1 and at MS4 for both day- and night-time campaigns.

		2-Aminobenzimidazole	Acesulfame	Amisulpride	Atenolol	Atrazine	Benzotriazole	Bisoprolol
Day	MS1 time series (n=6)	10-12	499-609	94-109	10-13	2-3	2519-2873	176-211
	MS4 grab sample (n=1)	11	506	86	8	3	2551	102
Night	MS1 time series (n=6)	12	545-663	114-123	10-13	2	2842-3131	209-232
	MS4 grab sample (n=1)	11	586	112	9	2	2829	177
Trib. ③ (n=1) ; trib. ④ (n=1)		n.d.[2] ; n.d.	<1 ; 13	n.d. ; n.d.	n.d. ; n.d.	<1 ; 1	4 ; 10	<1 ; <1
		Candesartan	Carbamazepine	Carbendazim	DEET	Denatonium	Desvenlafaxine	Diatrizoic acid
Day	MS1 time series (n=6)	1097-1268	418-508	54-88	103-173	334-400	624-686	328-367
	MS4 grab sample (n=1)	1122	434	67	97	339	507	349
Night	MS1 time series (n=6)	1210-1315	473-530	89-100	154-163	384-402	706-785	372-408
	MS4 grab sample (n=1)	1279	503	86	133	364	693	385
Trib. ③ (n=1) ; trib. ④ (n=1)		n.d. ; n.d.	<1 ; <1	n.d. ; <1	2 ; 4	3	<1 ; <1	n.d. ; 263
		Diclofenac	Gabapentin	Iopamidol	Irbesartan	Lamotrigine	Lidocaine	Metoprolol
Day	MS1 time series (n=6)	811-886	3301-4066	392-901	384-446	1340-1701	81-94	813-910
	MS4 grab sample (n=1)	483	3450	712	302	1455	80	460
Night	MS1 time series (n=6)	996-1163	3932-4256	1049-1312	463-535	1604-1732	100-112	955-1075
	MS4 grab sample (n=1)	1053	3769	1198	486	1415	101	830
Trib. ③ (n=1) ; trib. ④ (n=1)		<2 ; <2	n.d. ; n.d.	<60 ; <60	<2 ; <2	n.d. ; n.d.	<1 ; <1	n.d. ; n.d.
		Olmesartan	Oxcarbazepine	Primidone	Salbutamol	Sitagliptine	Sotalol	Sucralose
Day	MS1 time series (n=6)	827-1252	9-101	120-159	2-3	1375-1746	34-40	4543-4822
	MS4 grab sample (n=1)	921	<2	118	2	1402	30	4971
Night	MS1 time series (n=6)	1277-1439	67-140	141-156	3	1676-1811	42-46	4586-4754
	MS4 grab sample (n=1)	1270	136	141	3	1513	40	4749
Trib. ③ (n=1) ; trib. ④ (n=1)		n.d. ; n.d.	n.d. ; n.d.	n.d. ; n.d.	n.d. ; n.d.	<2 ; <2	n.d. ; n.d.	<40 ; <40

[1]Concentrations are given in [ngL^{-1}] for organic contaminants and in [mgL^{-1}] for inorganic ions.
[2]n.d.: not detected.

Table 3 (continued). Concentration ranges[1] measured during the tracer-based sampling in the minor tributaries ③ and ④, at MS1 and at MS4 for both day- and night-time campaigns.

		Sulfamethoxazole	Sulpiride	TAED	TCPP	Tiapride	Torasemide	Tramadol
Day	MS1 time series (n=6)	643-832	95-110	179-309	1067-1401	74-92	246-353	372-424
	MS4 grab sample (n=1)	723	94	73	1238	72	267	264
Night	MS1 time series (n=6)	816-853	106-113	223-331	1337-1485	93-101	310-402	508-535
	MS4 grab sample (n=1)	734	101	242	1344	85	331	472
Trib. ③ (n=1) ; trib. ④ (n=1)		n.d.[2] ; n.d.	n.d. ; n.d.	n.d. ; n.d.	<8 ; <8	n.d. ; n.d.	n.d. ; n.d.	<1 ; <1
		Trimethoprim	Valsartan	Venlafaxine	Calcium	Chloride	Fluoride	Nitrate
Day	MS1 time series (n=6)	132-166	56-76	241-290	114-117	85-96	<0.1-0.1	43-50
	MS4 grab sample (n=1)	130	54	157	110	89	0.1	44
Night	MS1 time series (n=6)	154-166	51-63	306-330	113-114	96-97	<0.1-0.1	50-52
	MS4 grab sample (n=1)	131	45	271	112	95	0.1	48
Trib. ③ (n=1) ; trib. ④ (n=1)		n.d. ; n.d.	1 ; 1	<1 ; <1	76 ; 103	9 ; 50	0.1 ; 0.2	8 ; 8
		Magnesium	Potassium	Phosphate	Sodium	Sulfate		
Day	MS1 time series (n=6)	19-20	16-18	0.9-1.2	84-93	84-93		
	MS4 grab sample (n=1)	19	15	0.9	82	86		
Night	MS1 time series (n=6)	19	17-18	1.0-1.2	88-89	92-93		
	MS4 grab sample (n=1)	19	16	1.0	83	91		
Trib. ③ (n=1) ; trib. ④ (n=1)		77 - 64	4 ; 2	<0.4 ; <0.4	21 ; 12	18 ; 18		

[1]Concentrations are given in [ngL^{-1}] for organic contaminants and in [mgL^{-1}] for inorganic ions.
[2]n.d.: not detected.

The concentrations measured at the two autosampler locations are shown for both summer and winter 24 h campaigns in Table 4. Concentrations of the more limited selection of organic contaminants in the main reach ranged from under the compounds' limit of quantification (atrazine at <1 ngL^{-1} in winter 2014) to 482 ngL^{-1} (diclofenac in summer 2013). Generally higher concentrations of wastewater contaminants in the main reach in summer can easily be attributed to the lower flow and consequent higher proportion of treated wastewater in the river compared to the winter campaign. Seasonal differences in contaminant fluxes released by the WWTP however exist and are detailed in section 5.5.3.

Table 4. Concentration ranges measured at the input and output of the studied segment for the summer and winter 24 h campaigns.

		Summer campaign (2-3.7.2013)		**Winter campaign (12-13.2.2014)**	
		AS WWTP	AS Conf.	AS WWTP	AS Conf.
		n[1]=(12)[2] 10	n=(12) 10	n=12 (i. ions: 24)[3]	n=12 (i. ions: 24)[3]
Concentrations [ngL^{-1}]	AHTN	(5) 9-14	5-13	13-18	8-14
	Atrazine	/		0-1	1
	Carbamazepine	(35) 118-172	(65) 93-163	75-106	72-100
	DEET	(18) 48-83	(38) 47-85	4-6	4-7
	Desethylatrazine	/		2-3	2-3
	Diclofenac	(82) 328-482	(112) 212-419	/	
	HHCB	(26) 56-95	(27) 31-71	106-136	65-90
	HHCB-lactone	(108) 280-402	(168) 207-326	140-245	176-223
	Lidocaine	/		15-33	19-31
	Mecoprop	(14) 21-36	17-34	9-14	11-19
	Naproxen	(23) 58-85	(27) 49-78	51-79	52-75
	OTNE	(49) 104-186	27-118	239-367	141-219
	Oxcarbazepine	(5) 22-86	5-37	11-19	7-17
	TAED	(3) 8-20	4-18	7-18	3-19
	TCEP	(37) 48-90	(35) 50-72	/	
	TCPP	(41) 122-211	(97) 128-194	75-113	86-133
	TDCPP	(12) 35-48	(29) 32-44	14-26	17-25
	Triclosan	(19) 16-25	(7) 6-20	11-19	10-17
Concentrations [mgL^{-1}]	Calcium	(94) 105-94	(102) 98-109	111-120	106-121
	Chloride	(36) 48-59	(43) 46-59	35-42	35-41
	Magnesium	(9) 10	(12) 12-13	11-12	12-13
	Nitrate	(13) 18-23	(14) 16-22	18-23	17-22
	Potassium	(3.2) 5.4-7.2	(4.4) 4.9-7.1	4.3-5.7	4.2-5.3
	Sodium	(23) 33-44	(29) 32-44	25-32	26-31
	Sulfate	(57) 63-69	(62) 64-70	64-69	65-68

[1]n is the number of samples from which the range was measured.

[2]In summer, the two samples concerned by the effluent stop were discarded from the range calculation. The minimum value reached during this period was indicated in brackets.

[3]i. ions for inorganic ions.

Upstream of the WWTP, the concentrations of wastewater contaminants were in the order of a few ngL^{-1} or beneath the LOQ. The highest concentrations were observed for TCEP and HHCB-lactone with 15 and 13 ngL^{-1} in summer, respectively, followed by OTNE with 7 ngL^{-1} in winter. Concentrations upstream of the WWTP in winter were similar or inferior to summer's. In the absence of WWTP effluent discharge in the upstream part of the Steinlach catchment, the concentrations in wastewater contaminants measured presumably stemmed from leaks of the sewer system (Rutsch et al., 2006). But unlike acesulfame, benzotriazole or diatrizoic acid during the tracer-based sampling, these rather hydrophobic substances might also stem from contaminated sediment storages, constituted during precipitation events as PAHs would, from which they might have desorbed. Concentrations of inorganic ions upstream of the WWTP were lower or in the same range as what was observed in the investigated segment.

Concentrations of wastewater contaminants in the minor tributary ① were significantly higher than in other tributaries or in the range of the studied reach, as it was assumed to partly receive water from the Mühlbach deviation of the Steinlach studied reach.

The other tributaries showed concentrations in the order of a few ngL^{-1} or beneath LOQ for the other organic contaminants during the 24 h samplings, with the exception of musk fragrances. The minor tributary ④ displayed 11 to 22 ngL^{-1} for artificial musk fragrances OTNE, HHCB and HHCB-lactone in summer while HHCB-lactone exhibited between 10 and 22 ngL^{-1} in all tributaries sampled but the minor tributary ①. HHCB-lactone and OTNE displayed 9 and 7 ngL^{-1} in minor tributary ④ in winter. Concentrations of inorganic ions in tributaries joining River Steinlach were in the same range or lower than concentrations in the investigated reach at the exception of magnesium, concentrations of which were significantly higher with 24 to 63 mgL^{-1} in tributaries during both seasons.

Concentration of Atrazine was 2 ngL^{-1} upstream of the WWTP and similar or inferior concentrations were measured in the tributaries, but tributary ② stood out with its 60 ngL^{-1} (see Table 4). Atrazine being a pesticide banned since 1991 in Germany, observed quantities were assumed to be the legacy left in agricultural soils and groundwater of the catchment. The low desethylatrazine concentration in the tributary ② sample could indicate a fresh illegal use of atrazine in the watershed of the southern tributary. The too low concentrations of both contaminants will be used for flux calculations, but their removals will not be discussed in this thesis.

During the 24 h-sampling campaigns, ammonium, nitrite and phosphate were not measured above LOQ in any of the samples recovered during both sampling campaigns. Fluoride was measured above LOQ only in the minor tributaries ②, ③ and ④ during the summer campaign, and upstream of the WWTP, in the Ehrenbach and the minor tributaries ③ and ④, as well as occasionally in the samples taken in the main reach during the winter campaign.

The effluent stop overlapped 1/8 and 5/8 of the 14:00-16:00 and 16:00-18:00 composite samples taken by AS1, respectively, and 6/8 and 1/8 of the 17:00-19:00 and 19:00-21:00 composite samples collected by AS2, respectively. The minimum concentration of organic contaminants during the summer campaign was reached in these samples, while the drop of concentration was less significant for the inorganic ions, as these have consequent input from the Steinlach catchment itself (see section 5.5.1), but also surprisingly for triclosan.

5.1.2 Particle-associated transport in various catchments

5.1.2.1 Floods in River Steinlach and Ammer

The pH range was similar for both floods sampled, with values ranging between 7.8 and 8.2 in River Steinlach and between 7.6 and 8.0 in River Ammer. Turbidity and TSS ranged from 147 to 2176 NTU and from 120 to 2614 mgL^{-1} in the samples collected during the Steinlach flood and from 41 to 205 NTU and 45 to 317 mgL^{-1} in the samples collected during the Ammer flood, respectively. DOC in the flood samples ranged between 4.4 and 6.1 mgL^{-1} for River Steinlach and between 2.6 and 3.1 mgL^{-1} in River Ammer. TOC ranged between 12 and 110 mgL^{-1} in the Steinlach flood samples and between 5 and 17 mgL^{-1} in the Ammer flood samples. In the Steinlach flood, TOC was 2 to 20 times higher than DOC while in the Ammer flood TOC was only 1.5 to 5.5 times higher. Mean organic content of particles were similar between the two investigated rivers with 4.5 and 4.7% in River Steinlach and Ammer, respectively.

Concentration ranges of wastewater contaminants and inorganic ions measured during the floods sampled in River Steinlach and Ammer are displayed in Table 5. In both floods, the ratio between the maximum and minimum concentrations was not the same for all compounds, indicating that some compounds displayed more variability in their release compared to others.

During the flood sampled in River Steinlach, concentrations of organic contaminants went clearly higher than what was measured upstream of the WWTP during dry-weather conditions. During the tracer-based and 24 h samplings, most organic contaminants were measured close or under the LOQ at few exceptions (see section 5.1.1). Concentrations of the same organic contaminants went up to several hundreds of ngL^{-1} (see ibuprofen, mecoprop or TCPP in Table 5), highlighting the activation of contaminant sources upstream of the WWTP due to precipitation, most likely CSOs releasing untreated wastewater into River Steinlach. The concentrations of wastewater contaminants measured during the Steinlach flood did not have systematically higher or lower ranges than what was measured downstream of the WWTP during the 24 h samplings, presumably due to the high dilution of highly concentrated raw wastewater released during the flood event. But concentration ranges were all wider during flood sampling for a similar sampling duration. Concentrations of wastewater contaminants measured during the Steinlach flood stayed however in the same order of magnitude as what was measured downstream of the WWTP during baseflow sampling. Concentrations of inorganic ions were lower in the samples of the Steinlach flood compared to the samples of the 24 h-sampling, implying dilution presumably from rainwater. Though phosphate and ammonium were found under the LOQ, nitrite could be quantified in some of the samples of the Steinlach flood, contrary to the campaigns performed during dry weather conditions.

The flood captured in River Ammer exhibited higher concentrations for all analytes but DEET, ibuprofen, mecoprop and TCPP, but still in the same order of magnitude, as in the Steinlach flood. Also, all analyzed inorganic ions, including phosphate, ammonium and nitrite, were measured above LOQ in the samples of the Ammer flood. Only potassium was unrealistically under LOQ in the first two samples captured, which was linked to an error of measurement in Tübingen laboratory.

Table 5. Concentration[1] ranges measured during the floods sampled in River Steinlach and Ammer.

	AHTN	Atrazine	Caffeine	Carbamazepine	DEET	Desethylatrazine
Steinlach flood (09-10.08.15)	7-46	/	55-699	11-48	7-26	/
Ammer flood (09-10.02.16)	31-53	1	149-901	81-151	9-15	3-4
	Diclofenac	HHCB	HHCB-lactone	Ibuprofen	Lidocaine	Mecoprop
Steinlach flood (09-10.08.15)	23-136	7-82	54-148	33-386	4-22	15-513
Ammer flood (09-10.02.16)	210-320	170-274	314-489	39-133	18-40	22-26
	Naproxen	TAED	TCEP	TCPP	TDCPP	Triclosan
Steinlach flood (09-10.08.15)	9-30	5-62	37-83	46-230	/	2-25
Ammer flood (09-10.02.16)	47-78	37-313	80-138	95-189	20-26	20-37
	Ammonium	Calcium	Chloride	Fluoride	Magnesium	Nitrate
Steinlach flood (09-10.08.15)	<0.4-<1	40-83	8-28	0.1	3-13	5-9
Ammer flood (09-10.02.16)	0.3-0.7	115-165	58-79	0.1-0.2	23-35	20-24
	Nitrite	Phosphate	Potassium	Sodium	Sulfate	
Steinlach flood (09-10.08.15)	<0.1-0.4	<0.3	3-4	7-19	19-105	
Ammer flood (09-10.02.16)	0.6-0.9	0.6-0.8	< 0.1-4.5	31-48	124-217	

[1]Concentrations of organic contaminants and inorganic ions are given in [ngL^{-1}] and [mgL^{-1}], respectively.

5.1.2.2 Pre-sampling

In the pre-sampling operated before the summer 24 h-sampling campaign in River Steinlach, highest values of DOC and lowest values of turbidity – 4.5 and 4.7 mgL^{-1} and 0.9 and 1.0 NTU, respectively – were found in the two WWTP effluent samples, showing that the Steinlach-Wiesaz WWTP was a source of organic substances but not of particles. DOC ranged between 1.8 and 3.6 mgL^{-1} upstream of the WWTP and in the tributaries of River Steinlach and was stable at 2.2-2.3 mgL^{-1} downstream of the WWTP. Turbidity in the investigated segment, upstream of the WWTP and in tributary ② ranged between 10 and 13 NTU while it was only 4 NTU in tributary ④.

The lowest concentrations were found in the tributary ④ for all organic contaminants while the highest were measured in effluent samples, one to twelve times what was found in the main stem, except for caffeine (see Table 6). Concentrations in water bodies that did not receive WWTP effluent discharge were found close to the LOQ only for carbamazepine, AHTN and DEET. The other compounds showed significant concentrations upstream of the WWTP and in the Ehrenbach, though lower than what was measured in the main stem. Due to the rainy conditions in the days preceding the sampling, some CSOs might have been activated upstream of the WWTP and in the Ehrenbach, inducing those high concentrations.

Highest concentrations of inorganic ions were again found in the WWTP effluents although calcium concentrations were very close to what was measured in the main stem (see Table 7). Magnesium was particularly high in the tributaries compared to the main stem up- and downstream of the WWTP (22-55 mgL^{-1} compared to 9-10 mgL^{-1}, respectively). The Ehrenbach was also quite rich in sulfate (77 mgL^{-1}), and tributary ④ in chloride (38 mgL^{-1}). Fluoride concentration could be seen above the LOQ everywhere but upstream of the WWTP effluent while phosphate concentration was above the LOQ only in the WWTP effluent, though concentration remained quite low for both ions. Ammonium and nitrite remained under LOQ in all samples.

Table 6. Concentrations of wastewater contaminants [ngL^{-1}] measured on unfiltered samples during the "pre-sampling" in River Steinlach.

	AHTN	Caffeine	Carbamazepine	DEET	HHCB	HHCB-lactone	TAED	TCEP	TCPP
Up. WWTP effluent	3	66	3	< 1	9	27	7	27	5
Dn. WWTP effluent	4-7	55-109	24-30	28-32	36-47	80-102	14-20	35-41	27-37
1st Effluent sample	40	118	179	230	258	690	42	166	190
2nd Effluent sample	42	123	172	282	269	680	53	161	249
Ehrenbach	4	651	4	5	22	33	326	22	26
Tributary ②	2	44	3	< 1	7	15	< 1	11	3
Tributary ④	2	13	< 1	< 1	2	4	< 1	12	2

Table 7. Concentrations of inorganic ions [mgL^{-1}] measured on filtered samples during the "pre-sampling" in River Steinlach.

	Calcium	Chloride	Fluoride	Magnesium	Nitrate	Phosphate	Potassium	Sodium	Sulfate
Up. WWTP effluent	107	18	<0.1	9	11	<0.5	2	12	41
Dn. WWTP effluent	114-116	29	<0.1-0.1	9-10	14	<0.5	3	19-20	47-48
1st Effluent sample	119	93	0.1	14	35	1	11	67	83
2nd Effluent sample	122	93	0.1	14	34	1	11	65	85
Ehrenbach	133	29	0.2	22	16	<0.5	2	23	77
Tributary ②	104	12	0.1	44	5	<0.5	2	20	51
Tributary ④	112	38	0.2	55	9	<0.5	2	12	19

5.1.3 Monthly sampling

The monthly sampling captured mostly low turbidities at the exception of some samples, particularly the December 2010 and January 2011 ones, taken during snow-melting events. These latter yielded turbidities of 88 and 42 NTU in the December 2010 and January 2011 samples at the Goldersbach WESS gauge, respectively, and 75 and 21 NTU at the mouth. In River Steinlach 136 and 18 NTU were measured in samples of December 2010 and January 2011 upstream of the WWTP and 85 and 84 NTU downstream of the WWTP, respectively. The snow-melting events in December 2010 and January 2011 yielded turbidities of 50 and 11 NTU in River Ammer. At the exception of the June 2010 sample at the Goldersbach WESS gauge that exhibited 20 NTU, 1 to 10 NTU were measured in all the other samples of the monthly campaign in River Goldersbach. The June 2010 sample upstream of the Steinlach-Wiesaz WWTP also exhibited 25 NTU, but other measurements in River Steinlach stayed in the 0.4 to 5 NTU range. Turbidity in all Ammer samples but the snow-melting events ranged between 1 and 7 NTU. Interestingly, some of the discharge conditions captured in River Ammer and Steinlach were similar or higher than what was observed during the flood samplings, but turbidity measured were comparatively lower.

Ranges of concentrations obtained from the monthly sampling during years 2009 to 2011 are given in Table 8. Except for caffeine, TCEP and TCPP, concentrations of analyzed contaminants were close to or under LOD in most samples taken in River Goldersbach at the WESS gauge and at the mouth. Contrary to the lower portion of the Goldersbach, the water flowing at the WESS-gauge location drains a pristine forest area deprived from urban influence. No contaminant source being known in the upper part of the Goldersbach catchment, the detection of wastewater contaminants during the monthly sampling may be explained by a cross-contamination problem in the samples analyzed. Flame retardants could stem from sampling and analysis materials and caffeine is a product commonly found in working environments. The random measurement of higher concentrations of the bleaching agent TAED, the biocide triclosan and musk fragrances in some samples taken at this location hints towards this conclusion. A wide variety of organic contaminants analyzed in River Goldersbach was indeed found under the LOQ in a more recent study (Müller et al., 2018). In the absence of blank samples, it is also hard to know if cross-contamination impacted samples of the mouth location as well, which could explain high concentrations of caffeine outside of the snow melting events, or even samples from the other rivers investigated by the monthly sampling.

Like in the 24 h and tracer-based campaigns, concentrations measured in River Steinlach during the monthly sampling were significantly higher downstream of the WWTP compared to upstream. Concentrations upstream of the WWTP were measured close to or below LOD for HHCB, AHTN, DEET, triclosan, lidocaine, diclofenac and carbamazepine in most samples. The other compounds exhibited comparable or higher concentrations than what was found upstream of the WWTP during the 24 h and tracer-based samplings. In samples of the snow-melting events, the concentrations of almost all compounds were for both locations in the average or in the lower range of what was measured the rest of the monthly sampling. Only caffeine, TAED and triclosan in the December 2010 sample up- and downstream of the WWTP and in the January 2011 downstream of the WWTP exhibited significantly higher concentrations.

The concentration range measured at the WESS gauge in River Ammer during the monthly sampling was comparable to the one downstream of the WWTP in River Steinlach. By comparing concentrations of a single compound in both rivers, samples recovered the same day would show inconsistently lower or higher concentrations in River Ammer compared to River Steinlach. The two WWTPs from the Ammer catchment cumulating 89,000 population equivalent against 99,000 for the Steinlach WWTP, similar concentration ranges in both rivers imply that water treatment facilities have a similar impact on the river quality of both catchments.

Table 8. Concentrations in [ngL^{-1}] of wastewater contaminants investigated during the monthly sampling in River Goldersbach, Steinlach and Ammer.

		AHTN	Caffeine	Carbamazepine	DEET	Diclofenac	HHCB	HHCB-lactone
Goldersbach	WESS gauge	n.d.-4	n.d.-81	n.d.-<1	n.d.-3	n.d.-<1	n.d.-7	n.d.-23
	Mouth	n.d.-6	n.d.-750	n.d.-<1	n.d.-3	n.d.-<1	n.d.-5	n.d.-12
Steinlach	upstream of the WWTP	n.d.-5	13-346	n.d.-15	n.d.-26	n.d.-<1	n.d.-11	1-32
	downstream of the WWTP	8-109	8-760	6-156	5-105	3-114	36-298	15-1084
Ammer	WESS gauge	12-90	10-716	38-352	6-105	7-115	55-228	13-816

		Lidocaine	TAED	TCEP	TCPP	TDCPP	Triclosan
Goldersbach	WESS gauge	n.d.-<1	n.d.-22	n.d.-61	n.d.-15	n.d.-5	n.d.-6
	Mouth	0-1	n.d.-20	7-69	n.d.-70	n.d.-10	n.d.-<1
Steinlach	upstream of the WWTP	n.d.-2	<1-134	6-136	n.d.-30	n.d.-45	n.d.-4
	downstream of the WWTP	n.d.-56	8-259	34-253	36-732	12-194	n.d.-11
Ammer	WESS gauge	6-68	n.d.-497	27-236	120-719	13-246	n.d.-13

5.2 Corrections and quality control of measured data

5.2.1 Mixing at the upper control cross-sections

During the tracer-based sampling, coefficients of variation (CVs) of the discrete measurements across MS1 were 0.006 (10 measurements) and 0.002 (9 measurements) at the beginning and end of the experiment, respectively. Despite technical problems of the divers used to measure conductivity, the EC endmembers were observed around 830 μScm^{-1} upstream of the WWTP and 1200 μScm^{-1} in the WWTP effluent during the sampling campaign. Thus, considering the significant difference between EC endmembers and the resulting low CVs at MS1, the cross-section and segment downstream were thus deemed sufficiently mixed for the calculations exposed in section 4.2.6.

During the 24 h-sampling campaigns, coefficients of variation (CVs) of discrete measurements across the AS1 location were 0.004 for the summer 2013 sampling (9 measurements, EC endmember upstream of the WWTP = 572 ± 5 μScm^{-1} and in the WWTP effluent = 1101 ± 41 μScm^{-1}) and 0.001 for the winter 2014 sampling (6 measurements, EC endmember upstream of the WWTP = 585 ± 9 μScm^{-1} and in the WWTP effluent = 1122 ± 7 μScm^{-1}). The AS1 location and segment downstream were thus deemed completely mixed and suitable for the calculations from section 4.3.

5.2.2 Quality control of measured concentrations

Quality of the concentration measurements was approached by using CVs of the triplicate samples, assessing the deviation between concentrations measured for each compound.

CVs of the triplicate samples taken at MS2 during the tracer-based sampling indicated a deviation below 5% in concentrations of most compounds (see Table 9), indicating a good reproducibility of the measured concentrations. Data for oxcarbazepine, valsartan (0.15 and 0.10 CVs for day triplicates, respectively) and atenolol (night triplicate, 0.11) should be regarded more cautiously as they exceeded the 10% analytical uncertainty for organic contaminants given by the Tübingen laboratory. CVs for all inorganic ions showed also a deviation below 5% with the exception of phosphate, with 6% and 15% during the day- and night-time experiment, respectively, presumably due to its detection close to the LOQ.

As the upstream cross-section was deemed completely mixed at the AS1 location during the two 24 h campaigns, the samples taken across the section were considered as triplicates and were used to assess analytical uncertainty. CVs of the triplicate samples during the summer 24 h sampling at the upstream cross-section (see Table 10) also revealed a concentration deviation below 5% for the majority of the wastewater contaminants and below 2% for inorganic ions. Except for calcium, chloride, magnesium, nitrate, TAED and TDCPP, the CVs of the winter triplicates were higher than for the summer data. But triplicate deviation for organic contaminants remained mostly below the assumed 10% analytical uncertainty given by Stuttgart laboratory. Only the winter triplicates for AHTN, atrazine, and desethylatrazine exhibited CVs of 0.12, 0.29 and 0.11, respectively.

Table 9. Coefficients of variation of the triplicates sampled at MS2 during the day- and night-time experiments of the tracer-based sampling.

	2-Aminobenzimidazole	Acesulfame	Amisulpride	Atenolol	Atrazine	Benzotriazole	Bisoprolol	Candesartan
Day	0.021	0.051	0.036	0.046	0.032	0.028	0.006	0.046
Night	0.041	0.028	0.018	0.110	0.087	0.001	0.050	0.031
	Carbamazepine	Carbendazim	DEET	Denatonium	Desvenlafaxine	Diatrizoic acid	Diclofenac	Gabapentin
Day	0.024	0.026	0.013	0.046	0.059	0.036	0.034	0.016
Night	0.032	0.024	0.032	0.023	0.026	0.034	0.030	0.018
	Iopamidol	Irbesartan	Lamotrigine	Lidocaine	Metoprolol	Olmesartan	Oxcarbazepine	Primidone
Day	0.042	0.016	0.025	0.023	0.047	0.031	0.153	0.058
Night	0.068	0.008	0.021	0.037	0.018	0.051	0.017	0.003
	Salbutamol	Sitagliptin	Sotalol	Sucralose	Sulfamethoxazole	Sulpiride	TAED	TCPP
Day	0.040	0.025	0.028	0.027	0.025	0.003	0.068	0.043
Night	0.024	0.047	0.025	0.021	0.038	0.013	0.048	0.136
	Tiapride	Torasemide	Tramadol	Trimethoprim	Valsartan	Venlafaxine	Calcium	Chloride
Day	0.043	0.019	0.028	0.035	0.104	0.020	0.035	0.002
Night	0.033	0.068	0.011	0.029	0.011	0.018	0.017	0.002
	Magnesium	Nitrate	Phosphate	Potassium	Sodium	Sulfate		
Day	0.052	0.009	0.057	0.019	0.019	0.003		
Night	0.007	0.006	0.147	0.006	0.007	0.003		

Table 10. Coefficients of variation of the triplicates sampled during the 24 h-sampling campaigns.

	AHTN	Atrazine	Carbamazepine	DEET	Desethylatrazine
Summer campaign	0.010	/	0.007	0.020	/
Winter campaign	0.124	0.292	0.010	0.047	0.112
	Diclofenac	HHCB	HHCB-lactone	Lidocaine	Mecoprop
Summer campaign	0.011	0.013	0.010	/	0.019
Winter campaign	/	0.086	0.084	0.025	0.159
	Naproxen	OTNE	Oxcarbazepine	TAED	TCEP
Summer campaign	0.021	0.014	0.001	0.040	0.028
Winter campaign	0.069	0.024	0.059	0.030	0.009
	TCPP	TDCPP	Triclosan	Calcium	Chloride
Summer campaign	0.003	0.024	0.010	0.006	0.007
Winter campaign	0.008	0.010	0.091	0.001	0.004
	Magnesium	Nitrate	Potassium	Sodium	Sulfate
Summer campaign	0.011	0.009	0.015	0.011	0.001
Winter campaign	0.003	0.005	0.017	0.017	0.001

CVs of triplicates for flood sampling (see Table 11) were low in River Ammer with a maximum of 0.04 at the exception of TCEP. For the triplicates taken during the Steinlach flood, the CVs were very high for most compounds. Of 14 organic compounds, only four showed a CV inferior to 0.05 while inorganic ions displayed very low CVs inferior to 1%. No obvious explanation was found to justify the high CVs in the Steinlach flood. The triplicate concentrations for organic compounds rarely matched the sample taken by the autosampler at the same moment (data not shown). It is possible that, at the time of the triplicate sampling, a source of pollutants (CSO) was not well mixed with the river water or that its temporal variability was very high, as it was already observed for sewer releases (Launay et al., 2016). The triplicates being taken a few meters upstream of the autosampler first with two bottles followed by the third one, this high temporal variability could also explain the differences with the sample from the autosampler and also be responsible for the high CVs, making the triplicate invalid. The data of the Steinlach flood was still analyzed in the further sections, but conclusions should still be considered with caution.

Blank samples were only taken during the tracer-based sampling and the Ammer flood. In the blank from the tracer-based sampling, all compound concentrations were below the LOD, under the LOQ or at negligible concentrations compared to the main reach (<2%). The blank for DEET stood out by representing up to 15 % of concentrations measured in the main reach. Such issue was already reported by studies highlighting challenges of DEET quantification (Merel et al., 2015; Merel and Snyder, 2016). Blank concentrations of inorganic ions were not always under LOQ but represented less than 2% of what has been measured during the tracer-based sampling except for sodium (with up to 6%).

The concentration in the blank sample of the Ammer flood for inorganic ions was always under the LOQ except for sodium, calcium and magnesium where it represented less than 2% of the concentrations measured during the flood. The blank concentration of wastewater contaminants was under the LOQ or representing maximum 4% of the other measured concentrations along the event. Only exceptions were DEET again (up to 7%), TCEP (up to 9%) and desethylatrazine and atrazine (up to 9% and 11%, respectively) which displayed low concentrations during the event (see Table 5). The polyethylene canisters were used for the flood but also for the 24 h-sampling campaigns due to the amount of water that had to be transported from Tübingen to Stuttgart while avoiding any risk of breaking. Despite the bottles being previously used, sorption to or desorption from the polyethylene

canisters was not deemed a significant risk for monitored concentrations, according to Stuttgart laboratory tests. The blank concentrations from the Ammer flood confirmed the negligible desorption.

Table 11. Coefficients of variation of the triplicates sampled during the Steinlach and the Ammer floods.

	AHTN	Atrazine	Caffeine	Carbamazepine	DEET	Desethylatrazine
Steinlach	0.448	/	0.015	0.325	0.183	/
Ammer	0.023	0.033	0.010	0.011	0.006	0.013
	Diclofenac	HHCB	HHCB-Lactone	Ibuprofen	Lidocaine	Mecoprop
Steinlach	0.090	0.742	0.144	0.215	0.052	0.034
Ammer	0.013	0.019	0.028	0.012	0.007	0.024
	Naproxen	TAED	TCEP	TCPP	TDCPP	Triclosan
Steinlach	0.257	0.020	0.295	0.157	/	0.074
Ammer	0.019	0.039	0.095	0.035	0.055	0.005
	Ammonium	Calcium	Chloride	Fluoride	Magnesium	Nitrate
Steinlach	/	0.012	0.005	0.059	0.011	0.006
Ammer	0.050	0.006	0.004	0.036	0.003	0.005
	Nitrite	Phosphate	Potassium	Sodium	Sulfate	
Steinlach	0.022	/	0.024	0.009	0.002	
Ammer	0.021	0.049	0.008	0.003	0.020	

5.2.3 Tracer-based sampling: correction of breakthrough curves

Day-time BTCs of fluorescein were employed to highlight photo-dependent elimination processes in addition to being used to time the sampling and help compute day-time transfer functions. The tracer fluorescein was previously found to be highly photodegradable but not readily biodegradable (Gutowski et al., 2015). Indeed, 105% of the mass measured at MS1 was recovered at MS4 during the night against only 28% during the day. We thus confirmed that the loss of fluorescein was an indicator for photo-dependent elimination processes.

The set of day- and night-time BTCs of fluorescein with the associated samples for contaminant analysis are displayed in Figure 11. The BTCs measured at MS1 yielded a somewhat particular shape that was attributed to the particular flow conditions at the weir. Additional corrections were needed as the variations in turbidity in the river caused noise and artifacts in the fluorescence measurements, in particular at low fluorescein concentrations. Finally, the measurement of the night-time BTC at MS2 was biased due to extremely high turbidity readings (attributed to floating material clogging the sensor). Corrections of the night-time BTC at MS2 were done using night-time BTC at MS3 as a reference curve and yielded very satisfying results, as the recreated part of the BTC fitted the concentrations of the tracer grab samples. Night-time BTCs at MS2, MS3 and MS4 showed mass recoveries of 91%, 102% and 105%, respectively. The lower recovery at MS2 was imputed to the fitting of the tracer grab samples using BTC3, the tail of which did not decline to zero at late times (see the sharp drop at the end of BTC2 in Figure 11). The recoveries slightly above 100% at MS3 and MS4 were attributed to the removal of the fluorometer at MS1 before the end of the night-time BTC1 tailing (see the same sharp drop at the end of the night-time BTC1 in Figure 11). The tail of BTC1 presenting the same problem as the corrected BTC2 and the mass of tracer deviated through the Mühlbach being unknown, we assumed

that most of the mass in the main stem was recovered at MS1 before removal of the fluorometer and normalized all BTCs to obtain a recovery of 100%.

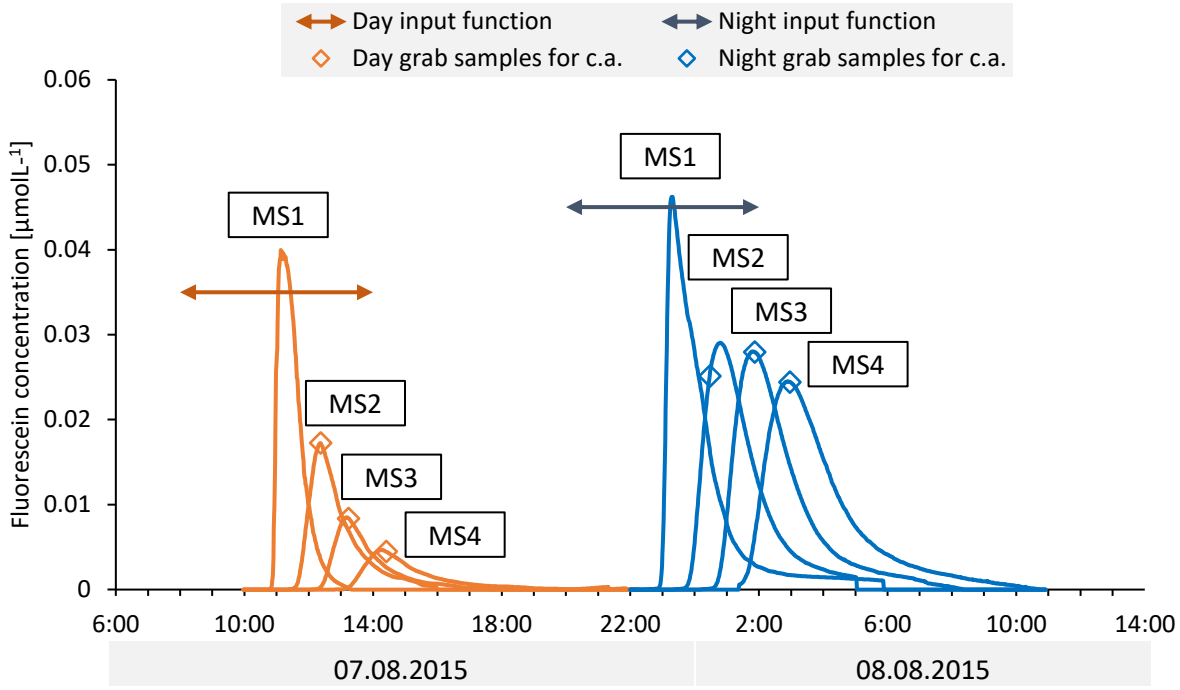

Figure 11. Corrected day and night BTCs with corresponding sampled times series and grab samples for chemical analysis (c.a.) from the tracer-based sampling in River Steinlach.

Non-parametric deconvolution was applied on night-time BTCs to obtain night-time transfer functions. Day-time transfer functions were obtained according to equation (18) (section 4.2.6). The example of day- and night-time transfer functions for fluorescein are displayed in Figure 12 with the scaling factor f and the specific photo-decay constants k_{Fluo} (also displayed among contaminant specific constants k_i in Table S2 in the Appendix).

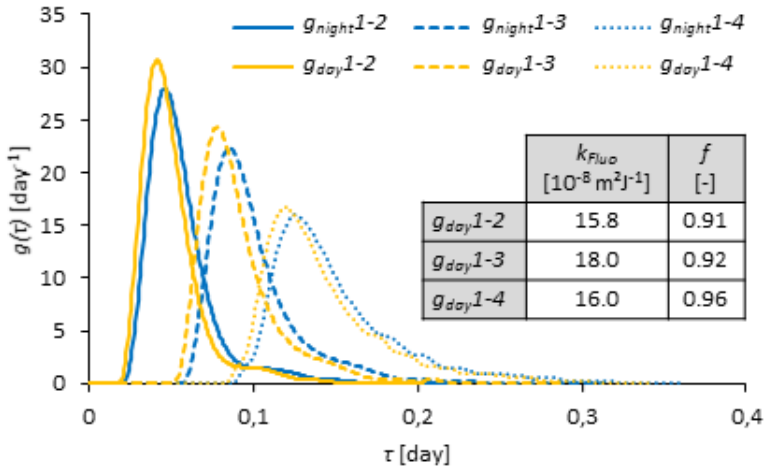

	k_{Fluo} [10^{-8} m^2J^{-1}]	f [-]
$g_{day}1\text{-}2$	15.8	0.91
$g_{day}1\text{-}3$	18.0	0.92
$g_{day}1\text{-}4$	16.0	0.96

Figure 12. Transfer functions g(τ) for fluorescein between MS1 and MS2, MS3 and MS4 for the day ($g_{day}1\text{-}2$, $g_{day}1\text{-}3$, $g_{day}1\text{-}4$, respectively) and the night ($g_{night}1\text{-}2$, $g_{night}1\text{-}3$, $g_{night}1\text{-}4$, respectively) experiments with the constants k_{Fluo} and scaling factor f.

5.2.4 24 h sampling: checking the fit of transfer functions on the EC signal

Non-parametric deconvolution was also applied on EC input and output time series to obtain transfer functions in the investigated segment during the summer and winter 24 h samplings (see Figure 13).

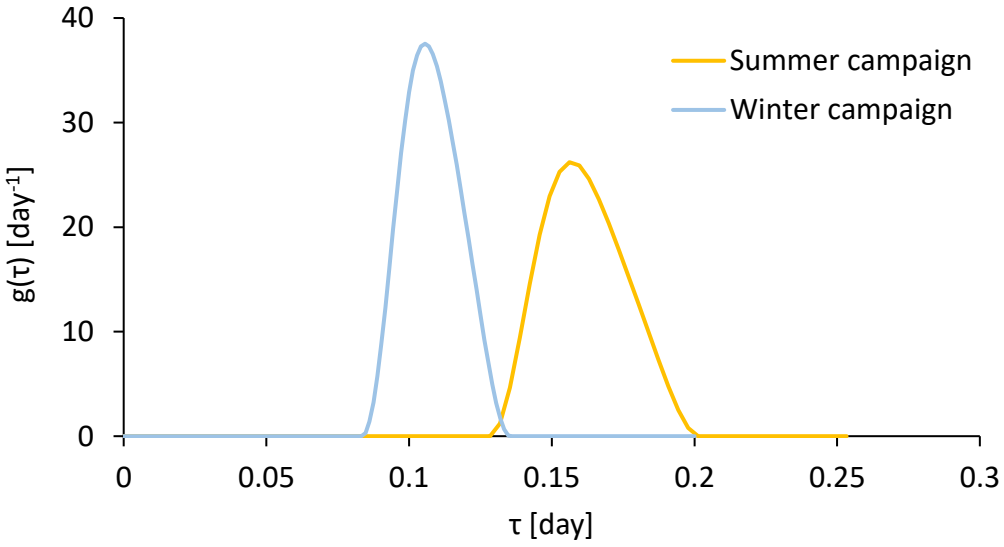

Figure 13. Normalized transfer functions for the summer and the winter 24 h samplings in River Steinlach.

The corrected transfer functions were convoluted with the EC input time series used for their calculations to check if the corrections and normalizations lead to reasonable tools for the later calculations. The computed EC time series are compared to the measured output time series at the lower control cross-section in Figure 14 for both summer and winter samplings. The computed EC time series fitted quite well the measurements. Some offsets were however locally observed, in particular for the

summer sampling. These latter could stem from errors in EC measurements, but did not affect the good fit of the variations and thus the time distribution of the signal. For the summer campaign, it is also possible that the effluent stop was a determining fitting signal to calculate the transfer function, despite the assumption of steady state conditions. It is thus possible that the calculated transfer function and travel time averaged the discharge conditions monitored, including the effluent stop period. In addition, while EC was assumed conservative, this sharp decrease in ion concentrations in the river may have triggered ion exchange processes between the water column and the porewater in the river bed and led to the higher measured concentrations as the ones expected from the computation (data not shown). Overall, the fit was deemed satisfying enough to further use the calculated transfer functions to observe diurnal patterns in the recorded 24 h-time series.

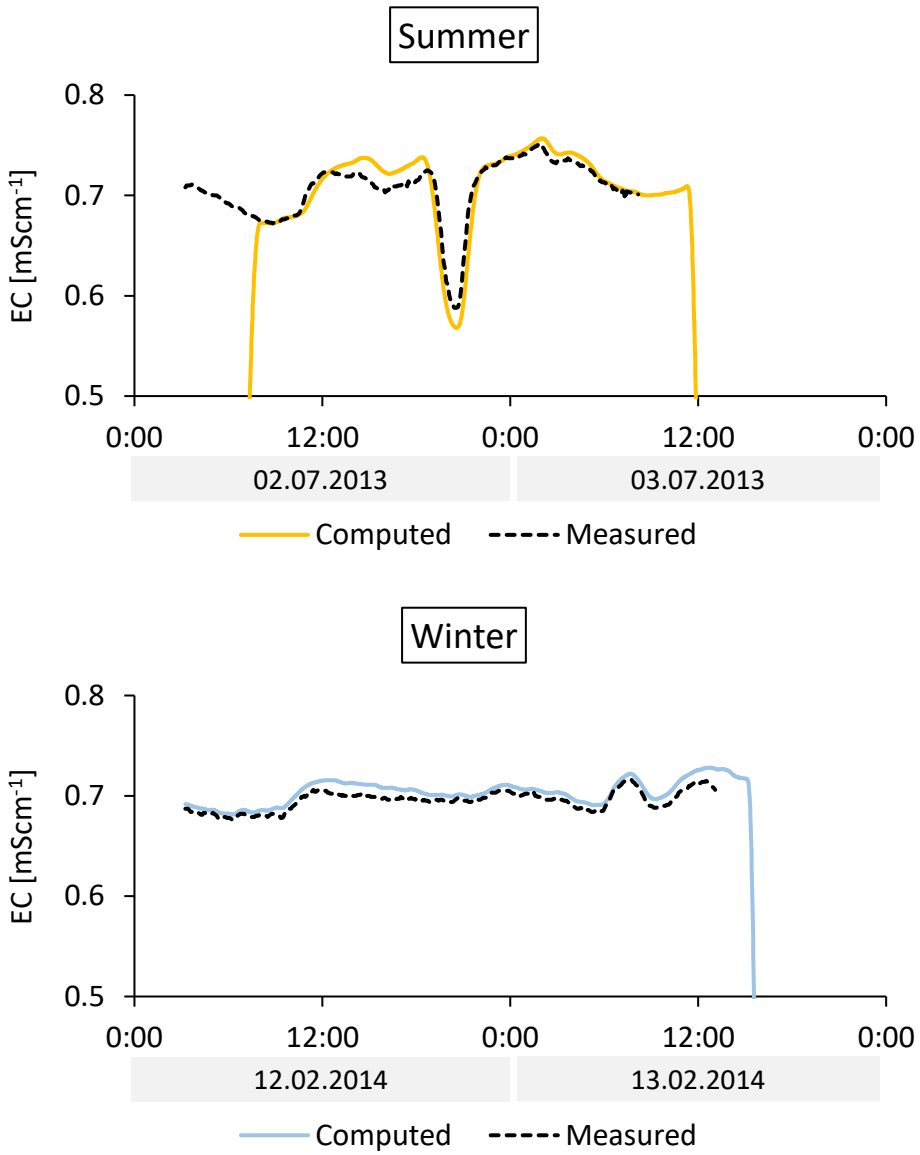

Figure 14. Measured and expected electrical conductivity (EC) computed using the transfer functions at the lower control-cross-section of the investigated segment during the summer and winter 24 h samplings.

5.3 Assessment of reactive transport

5.3.1 The tracer-based sampling

5.3.1.1 In-stream attenuation of contaminants

During the tracer-based sampling, the removal of chloride and sulfate, considered to be conservative species, as well as magnesium was negligible with less than 1.6% over the whole river section during both day- and night-time samplings. Other inorganic ions had clearly larger removals. Calcium exhibited 5 and 2% removals at MS4 during day- and night-time experiments, respectively, nitrate and sodium 6-7% and potassium 8%. Considering the low analytical uncertainty of inorganic ion analysis and in agreement with previous works in the same river for nitrate (Schwientek and Selle, 2016), these removals were clearly larger than for the conservative ions. Nitrate is a well investigated reactive ion that can be consumed by micro-organisms during denitrification process or by plant uptake (Birgand et al., 2007). Calcium and potassium can also act in the latter process. Nevertheless, their reactivity was comparable to those of the persistent organic contaminants investigated (see Figure 15a). In comparison, the high removals observed for reactive wastewater compounds stress their potential for attenuation in River Steinlach.

Organic contaminant reactivity ranged from conservative to highly reactive with an almost complete elimination of oxcarbazepine observed at MS4. Higher contaminant removals observed during the day-time experiment compared to night-time also highlighted the occurrence of photodegradation processes for some compounds. Three representative organic contaminants for observed reactive transport behaviors will be discussed in the following. Carbamazepine represented the group of persistent contaminants while sulfamethoxazole illustrated compounds that were degraded solely by photo-independent elimination processes. Venlafaxine reflected compounds that were attenuated by both photo-dependent and -independent elimination processes. Their longitudinal profiles, built by plotting RF_i against the mean travel time, are shown in the lower section of Figure 15a.

The anticonvulsant carbamazepine was persistent over the studied stretch. This confirms outcomes from previous field studies (Aymerich et al., 2016; Kunkel and Radke, 2012; Li et al., 2016; Nödler et al., 2011; Schaper et al., 2018) while other works showed some reactivity of the compound in Spanish and Greek surface waters (Acuña et al., 2015; Mandaric et al., 2019; Matamoros and Rodríguez, 2017).

The antibiotic sulfamethoxazole illustrated the involvement of one or several elimination processes that were assumed stable over the sampling day. k_{night} and k_i were equal to 1 day^{-1} and 0 $m^2.J^{-1}$ over the study segment, respectively (see Table S2 in the Appendix), yielding similar longitudinal profiles at day- and night-time (see Figure 15b).

A negligible elimination of sulfamethoxazole was observed in three Swedish rivers (Li et al., 2016) and in an English and Japanese river (Hanamoto et al., 2018). Kunkel and Radke (2012) and Li et al. (2016) found an elimination by 26% and 18% for sulfamethoxazole in River Gründlach (Germany) for an estimated travel time of 18 h and 50 h, respectively. The 13% elimination during both day- and night-time experiments in River Steinlach, for 3.4 and 3.6 h mean travel times, respectively, are much higher in terms of reaction rate than River Gründlach values, indicating very favorable conditions for the degradation of this contaminant. River Gründlach presented similar features to the River Steinlach (pH, sediment type, shallow depth, low turbidity, period of high insolation and a high proportion of treated wastewater). Kunkel and Radke (2012) attributed the elimination of sulfamethoxazole to microbial activity in the hyporheic zone. The Steinlach segment features steps, a higher topographical gradient and a large grain size of the bed substrate; these properties may enhance fast flow through the shallow hyporheic zone. Transient storage also occurred in the river itself because parts of the river were practically stagnant at the given low discharge. Furthermore, conditions during the experiment could

promote the biodegradation of sulfamethoxazole. The high proportion of treated wastewater in the investigated segment ensures the presence of bacteria that are adapted to sulfamethoxazole degradation. It also provides easily degradable carbon or nitrogen sources, found to trigger co-metabolism (Alexy et al., 2004; Drillia et al., 2005; Herzog et al., 2013; Kassotaki et al., 2016; Larcher and Yargeau, 2011) or diauxie mechanisms (Müller et al., 2013) leading to the biodegradation of sulfamethoxazole. Sulfamethoxazole has a very small octanol-water partitioning coefficient at the Steinlach pH (see Table S1 in the Appendix) and sorption was demonstrated to be small (Barber et al., 2009; Gao and Pedersen, 2005; Hou et al., 2010; Stein et al., 2008). During control tests, many studies also deemed sulfamethoxazole resistant to hydrolysis (Boreen et al., 2004; Lam et al., 2004; Niu et al., 2013; Radke et al., 2009).

Photo-dependent degradation was not observed for sulfamethoxazole although indirect photodegradation in WWTP effluent water was previously identified and attributed to the photosensitizing effect of effluent dissolved organic matter (Ryan et al., 2011). Here, the effluent DOM did not seem to act as a photosensitizer in the Steinlach segment, despite the high proportion of treated wastewater. Sulfamethoxazole was also shown to be prone to direct photolysis (Boreen et al., 2004; Niu et al., 2013) but the yellow color of the segment water and potentially the natural DOM could have hindered light penetration at the required wavelength (Lam et al., 2004; Lam and Mabury, 2005). Kunkel and Radke (2012) indicated that the basic pH of the river water was also a critical parameter, as the anionic form of sulfamethoxazole present at the Steinlach pH is more resistant to photolysis than in acidic media (Boreen et al., 2004; Niu et al., 2013).

The antidepressant venlafaxine was affected by both photo-dependent and -independent elimination processes with a clear elimination during night-time, with a k_{night} of 1.2 day^{-1} at MS4, and an elimination about twice higher during day-time (see Figure 15b, k_i of $3.2 \cdot 10^{-8}$ $m^2.J^{-1}$ in Table S2 in the Appendix). Writer et al. (2013) and Aymerich et al. (2016) found that venlafaxine was conservative in Boulder Creek, United States, and in the Segre River, Spain, respectively. The Spanish experiment was performed in October, when, despite a lower latitude, solar radiation is expected to be weaker than in German summer. Conversely, radiation should be close to the year's maximum for the River Steinlach sampling campaign in August as well as for Writer et al. (2013)'s experiment in May. Travel times were not a limiting factor either, as these were 5.4 h in the Boulder Creek study and 3.4 h in the River Segre study, against 3.1 h and 3.6 h during the day- and night-time experiment in River Steinlach, respectively. In a laboratory study using ultrapure and river water samples, Rúa-Gómez and Püttmann (2013) demonstrated a preferential degradability by indirect photodegradation while biodegradation and photolysis had a negligible impact on the persistence of venlafaxine. Only slight indirect photodegradation was demonstrated by Li et al. (2013) in a similar experiment, hinting toward a more persistent character of venlafaxine. Although indirect photodegradation did not occur for sulfamethoxazole, it is possible that venlafaxine reacted to intermediates created by photodegradation of other species in presence, or to photosensitizers such as the elevated nitrate concentrations or species contained in the measured DOC, as it was seen for other compounds (Bahnmüller et al., 2014).

Rühmland et al. (2015) found no degradation of venlafaxine in a constructed wetland without the presence of sediment, that they considered as imperative substrate for the development of microbial communities, similarly to the statement of Kunkel and Radke (2012) regarding sulfamethoxazole. This conclusion is carried further by Schaper et al. (2018), who linked the observation of a significant removal of venlafaxine in the River Sturt, Australia, to a higher hyporheic exchange in their study than in Writer et al. (2013).

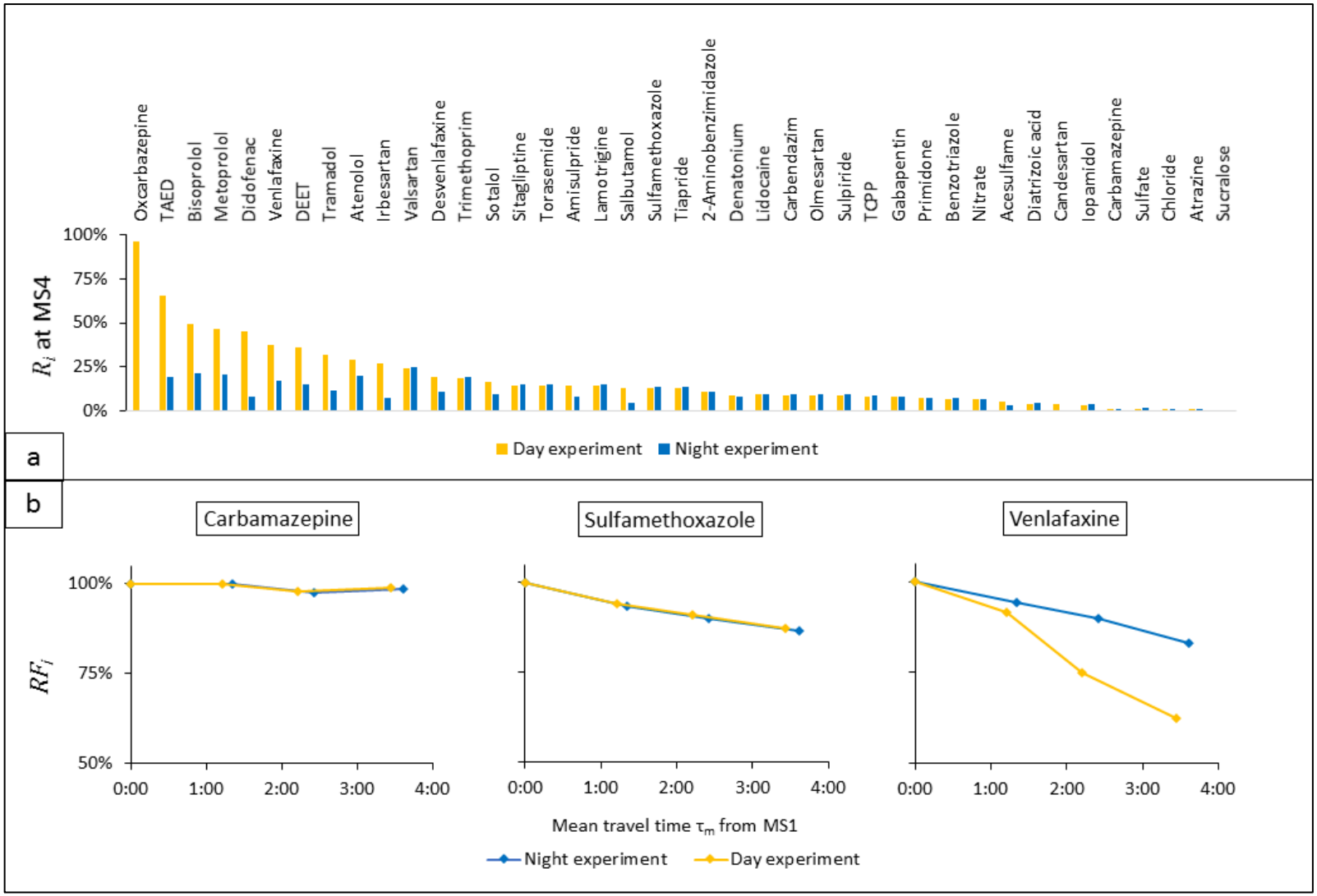

Figure 15. a: calculated removals R_i over the investigated segment (MS1 to MS4). b: representative examples of longitudinal profiles obtained by plotting the remaining fractions RF_i according to the mean travel time at each MS.

Finally, according to its octanol-water partitioning coefficient at the pH during the tracer-based sampling (see Table S1 in the Appendix), venlafaxine is presumably capable to sorb to the organic phase of the bed sediment and particles transported in the water column. Sorption was indeed assumed to be the main attenuation mechanism for venlafaxine in Acuña et al. (2015). However, measured concentrations only slightly changed along the 6 hours recorded at MS1 during both day- and night-time experiments and a relative equilibrium is assumed between the sediment and river water.

In a nutshell, carbamazepine reflected conservative transport in River Steinlach. Sulfamethoxazole underwent only photo-independent elimination that may be attributed to biodegradation, mainly in the hyporheic zone. Venlafaxine also seemed to be prone to biodegradation in the sediment and presumably indirect photodegradation.

5.3.1.2 Environmental implications

Night-time removals never exceeded 25 % (see the antihypertensive agent valsartan in Figure 15a) for a mean 3.6 h travel time while the concomitance of photo-dependent elimination processes enhanced the elimination of some contaminants up to total removal for a mean 3.4 h travel time during day-time (see the antihypertensive agents metoprolol, bisoprolol or the anticonvulsant oxcarbazepine in Figure 15a).

The 24 h-averaged removals by photo-dependent and -independent elimination processes calculated from equation (21) were compared using the travel-time distribution given by the night-time transfer function between MS1 and MS4 (Figure 16).

Oxcarbazepine left aside, TAED and diclofenac were the only contaminants where the efficiency of photo-dependent elimination processes was higher than photo-independent elimination when averaged over 24 h. For the other compounds analyzed, photo-dependent elimination processes resulted in a calculated removal comparable or inferior to the photo-independent elimination processes when averaged over a whole day (Figure 16). Photodegradation is very sensitive to environmental conditions such as cloud and vegetation cover or day-night alternation. In the day-time experiment, conditions for photodegradation were optimal with very low water stage, intense summer insolation, little or no shading of the river stretch, long day-time duration and good weather conditions; with the exception of the high measured DOC and the color of the water that could have had an impact on light penetration. If photo-independent elimination processes are governed by less variable factors such as river temperature, they will be less variable than photodegradation over time and methods identifying them should be developed.

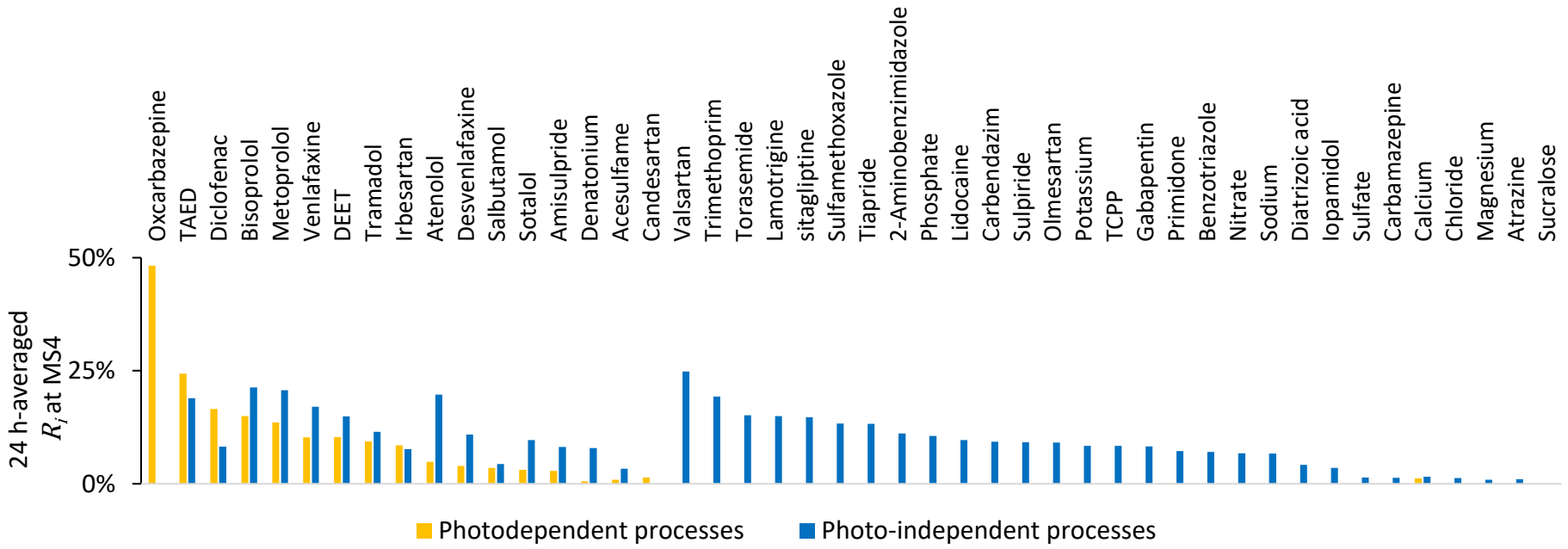

Figure 16. 24 h-averaged removals R_i computed for photo-dependent and -independent processes between MS1 and MS4.

5.3.2 Seasonal differences in the 24 h samplings

The relative net removals by mass balance calculation (equation (12)) for both summer and winter 24 h samplings are presented in Figure 17 for investigated organic contaminants and inorganic ions.

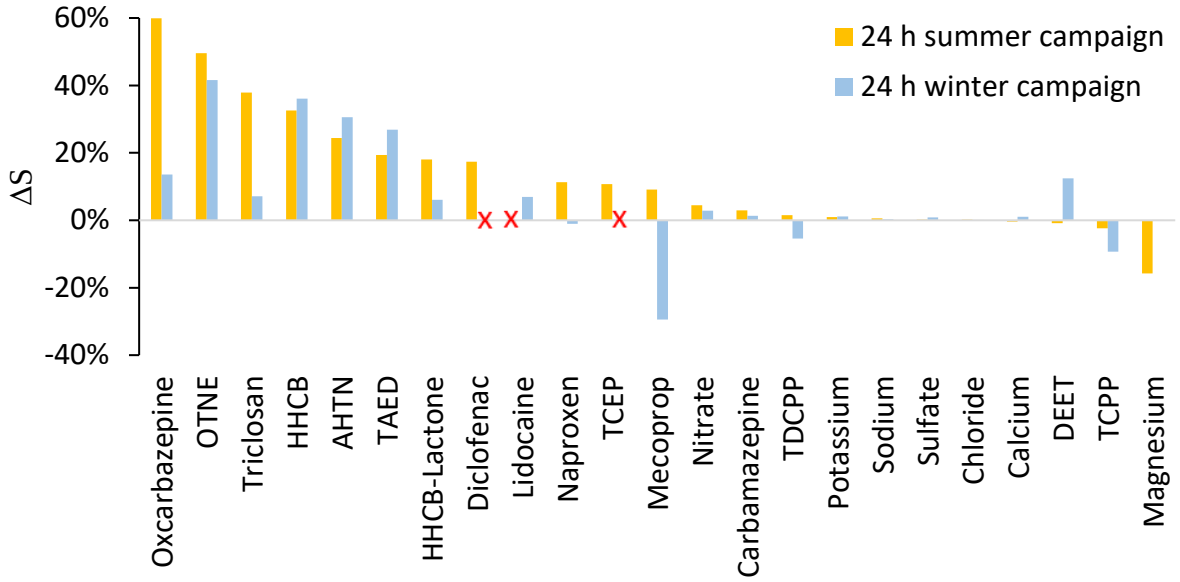

Figure 17. Relative net removals ΔS during the summer and winter 24 h-sampling campaigns. Red crosses indicate that no data were available for the compound during the concerned campaign.

As in Schwientek et al. (2016), balances of conservative sodium, chloride and sulfate calculated during the winter sampling exhibited very low relative net removals with $0.1\%<\Delta S<0.8\%$ over the 4 km-long stretch, potassium and calcium reaching both ΔS 1.1%. With a ΔS of 0.1% in winter, magnesium did not show the same 16% nor absolute mass difference as during the summer sampling. The relative net removal ΔS for nitrate was 4.5% in summer and 2.8% during the winter sampling. Again, nitrate reactivity was comparable to those of the persistent organic contaminants investigated but, considering the uncertainty of inorganic ion analysis, both summer and winter removals were deemed significant.

In Schwientek et al. (2016), wastewater organic contaminants investigated during the summer sampling showed very variable reactivities compared to one another, as it was observed in the tracer-based sampling. In Figure 17, compounds were ordered from the highest to the lowest removal during the summer campaign. On the left-hand side, the anticonvulsant oxcarbazepine showed the highest removal in summer (60% on average over 24 h, for the 3h53 residence time in the river) while ΔS decreases towards the right-hand side, where compounds with nearly nil removals are. The anticonvulsant carbamazepine, flame retardants TCPP and TDCPP and insect repellent DEET are the only contaminants situated on the right-hand side of nitrate in summer with no significant removals, among chloride and sulfate. The drastically higher removals of the anticonvulsant oxcarbazepine, the biocide triclosan or the artificial musk fragrances compared to nitrate highlight again the potential of the contamination introduced via the WWTP for natural attenuation in River Steinlach. During the winter season, the herbicide mecoprop showed a consequent input within the investigated river segment (ΔS of -30%). Considering that mecoprop presented one of the highest CV in the triplicates taken during the winter sampling (0.159 in Table 10) and its rather low concentration, this input could be an artifact due

to measurement error. The flame retardants TCPP and TDCPP exhibited an input as well, but more minor, with ΔS of -10% and -6%, respectively, within the 10% of analytic error.

The 24 h-time series, divided into 2 h-composite samples, detailed the temporal evolution of natural attenuation, allowing to observe the occurrence and temporal variability of photo-dependent elimination of investigated compounds. Expected concentrations were computed using transfer functions to represent the compound's concentration at the lower control cross-section if this latter behaved conservatively (see section 4.3.8). In Figure 18 and 20, expected concentrations are compared to actual measurements at the lower control cross-section for both summer and winter campaigns during the complete 24 h cycles. As computed concentrations only reflect conservative transport, differences between computed and measured time series were interpreted as the occurrence of storage or elimination processes within the investigated river segment.

In the summer 24 h-sampling campaign, four types of reactive transport behaviors could be identified from the comparison of the expected and measured 24 h time series (see Figure 18 and 20). The anti-convulsant drug carbamazepine represented the group of persistent contaminants. The biocide triclosan was solely degraded by photo-dependent elimination processes and the anti-convulsant drug oxcarbazepine, showed the highest reactive behavior by undergoing both photo-dependent and independent elimination processes in summer. The only analyzed compound exhibiting solely photo-independent elimination was HHCB-lactone, the metabolite of HHCB that can be produced from HHCB biodegradation, a photo-independent process as well. The winter 24 h sampling only showed two behaviors, attenuation by solely photo-independent processes for oxcarbazepine or conservativeness for carbamazepine but also triclosan and HHCB-lactone. For this latter, it is though not known whether HHCB-lactone might have been produced in winter, covering any degradation that might have happened.

Before assessing the seasonal variability of compound reactivity based on 24 h patterns, one must acknowledge that the lower quality of the analytics during winter seemed to impact the measured concentrations and slightly impair the interpretation of winter data. The problem is easily visible when looking at carbamazepine data in Figure 18, where the computed and measured concentration time series fitted well in summer but systematically mismatched each other in winter, though both average trends fitted perfectly. It is also reflected by the rather negative removals (=inputs) of flame retardants along the segment in winter. While the use of transfer functions was not to blame, as these misfits were also observable in raw concentration data, one can only interpret seasonal differences with caution.

As a striking example of seasonal contrast in contaminant removal, oxcarbazepine was the most reactive of the investigated compounds during the summer campaign (see Figure 17). In Figure 18, the offset between computed and measured concentration was bigger during the day-time (average $\Delta S = 85\%$) than during the night-time (average $\Delta S = 46\%$), highlighting the occurrence of both photo-dependent and independent elimination processes. During the winter experiment, the offset was $\Delta S = 11\%$ and 12% during day- and night-time, respectively.

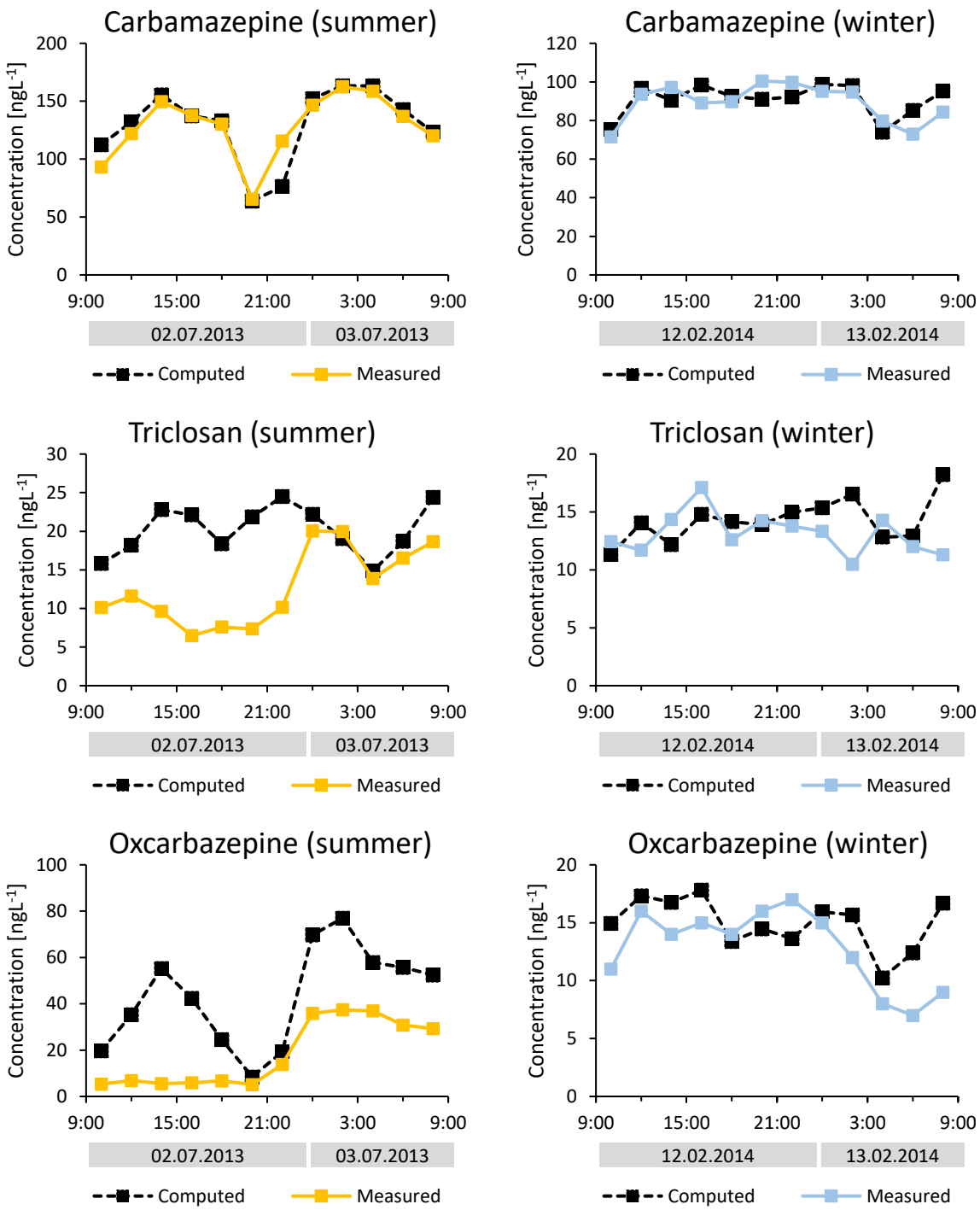

Figure 18. Computed and measured 24 h-time series of example compounds carbamazepine, triclosan and oxcarbazepine during the summer and winter 24 h-sampling campaigns.

Higher discharge during winter due to more humid conditions in the catchment is an important factor for reactivity assessment, as it reduces the residence time of contaminants in the 4 km-long river segment. The reactivity of investigated compounds from both summer and winter 24 h samplings cannot be directly compared, as transit time in summer was 50% longer than in winter. The decay constant *k* was calculated for each compound measured during both campaigns, assuming first-order reaction

between the two control cross-sections (see Figure 19, and Table S4 with *k* and half-life values in the Appendix).

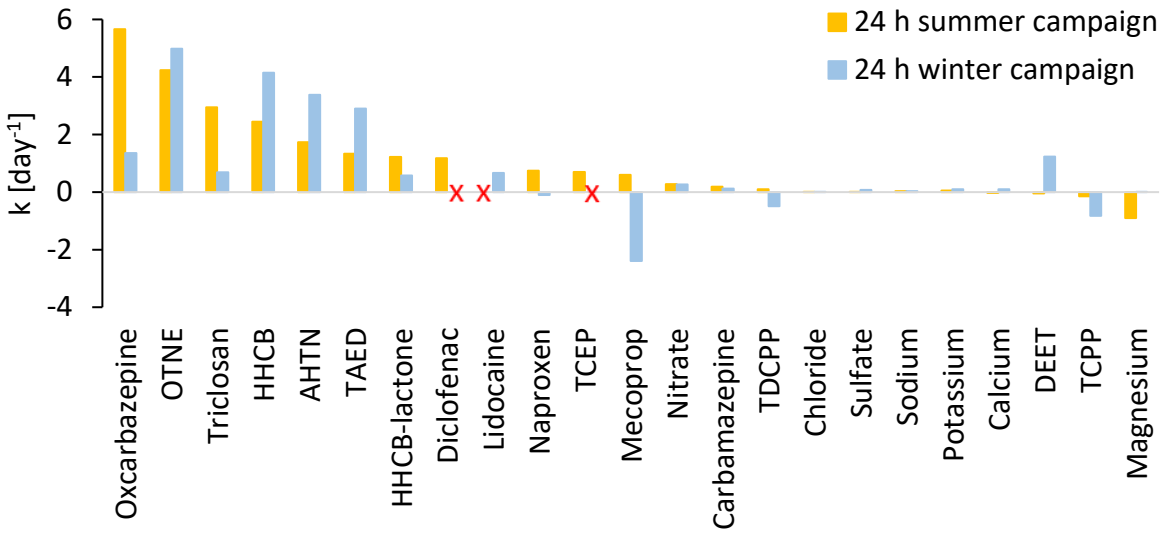

Figure 19. Calculated decay constants k from 24 h-mass balances during the summer and winter 24 h-sampling campaigns. Red crosses indicate that no data were available for the compound during the concerned campaign.

While calculated rate constants *k* were comparable between summer and winter for some compounds, particularly little reactive ones as well as nitrate, differences in rate constants for other compounds highlighted seasonal variability of contaminant elimination processes in addition to day-night alternation. Considering higher water stage, lower temperatures, less solar radiations, lower bacterial activity and disappearance of algae mats during the winter season, photo- and biodegradation were expected to have lower efficiencies in winter compared to summer. Smaller decay constants in winter were indeed observed for oxcarbazepine, triclosan, HHCB-lactone and the anti-inflammatory drug naproxen with inexistent photo-dependent elimination and limited photo-independent processes affecting the investigated compounds. But nitrate showed almost identical decay constants of 0.27 and 0.28 day^{-1} in winter compared to summer, respectively. This goes against the observations of Schwientek and Selle (2016) upstream of the studied segment, questioning the impact of the change in chemistry due to WWTP effluent discharge.

For artificial musk fragrances AHTN and HHCB and the bleaching agent TAED, reactivity was up to twice higher during winter while the insect repellent DEET exhibited reactivity only during that season.

Artificial musk fragrances are volatile compounds prone to volatilization into the air in particular in turbulent water (see HHCB Henry's constant in Table S3 in the Appendix). The investigated Steinlach segment contained various steps and weirs creating turbulences capable of vaporizing water droplets into the atmosphere. Indeed, a musk smell was noted at the 1.5 m weir in the investigated River Steinlach segment. Volatilization being photo-independent, it could be involved in HHCB removal during night-time during both seasons (see Figure 20). According to Buerge et al. (2003), the negligible impact of other elimination processes during winter leaves losses to the atmosphere and outflowing water as the only two removal processes in Lake Zurich. The process is dependent on temperature as well as the compound's concentration (Buerge et al., 2003; Lu et al., 2015; McDonough et al., 2016). In regard to temperature, volatilization of artificial musk fragrances from the water column should decrease in winter, just as biodegradation but the higher concentrations observed in winter could have

led to an increase of the process. The 50% higher discharge during the winter sampling could have increased the turbulences created at the various steps and weirs, leading to more vaporization of the compound into the air. Turbulences within the water column also ensure mixing of the river water and maintains the concentration gradient with the atmosphere. This would explain the consequently higher photo-independent elimination observed in winter for artificial musk fragrances. The stirring of artificial musk fragrances into the atmosphere could in fact be a major process in the compound removal in River Steinlach and be in that case only local, not obeying any 1st order kinetics along the investigated segment during both summer and winter seasons. HHCB-lactone is a metabolite of HHCB and exhibited solely photo-independent elimination during the summer sampling. Unless production of HHCB-lactone occurred in the studied segment, the absence of elimination of HHCB-lactone in winter (see Figure 20) would indicate that the compound was not affected by volatilization unlike its parent compound.

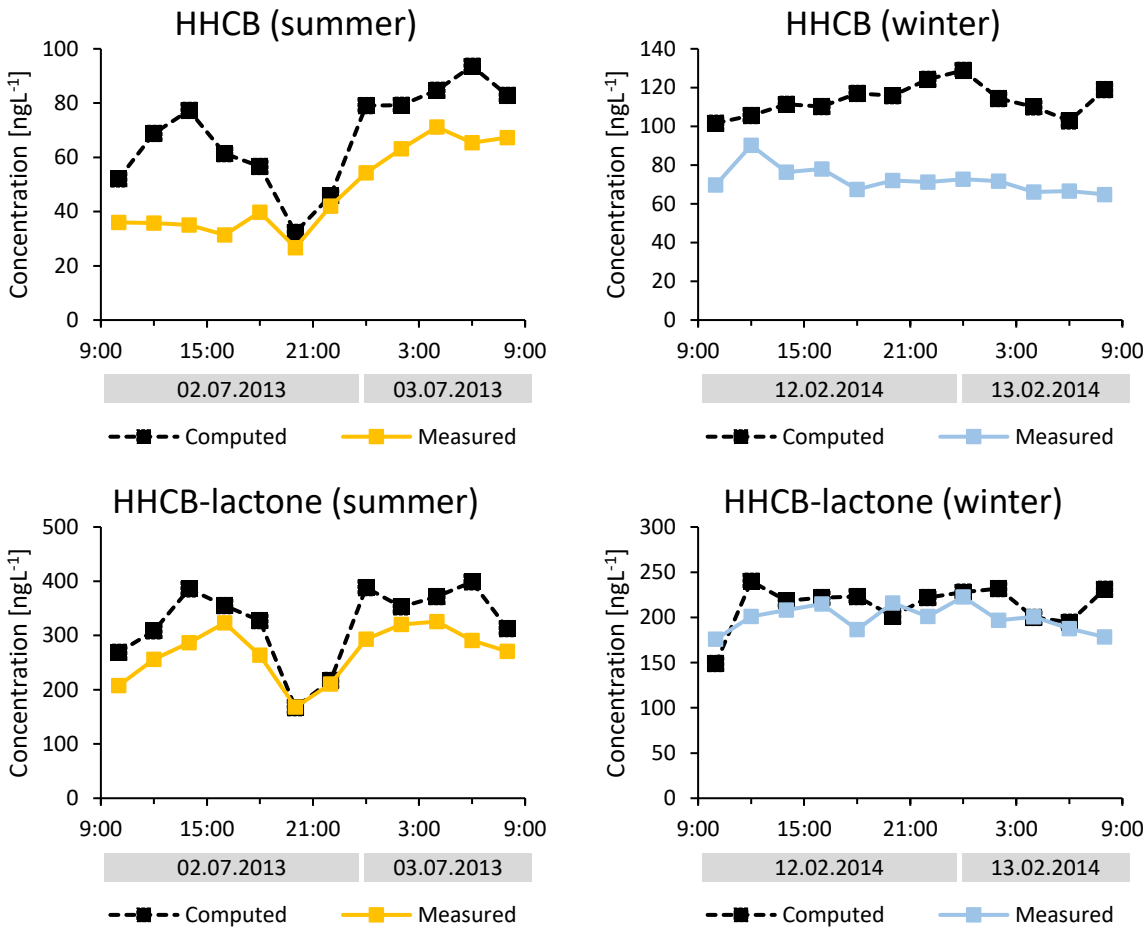

Figure 20. Computed and measured 24 h-time series of HHCB and HHCB-lactone for the summer and winter 24 h-sampling campaigns.

Unlike musk fragrances, TAED and DEET do not have a high tendency to partition into the air (see Table S3 in the appendix). Their higher removal in winter, despite unfavorable conditions for photo-dependent elimination or biodegradation, thus cannot be explained by the same volatilization mechanism as for musk fragrances. Unexplainable patterns for TAED and DEET during the winter sampling observed in Figure S5 and S6 in the Appendix, respectively, were thus attributed to higher

analytical uncertainty in winter. Though it was not reflected in the CVs from winter triplicates (see Table 10), the problem was already stressed out for DEET (see section 5.2.2.) while both compounds were measured at rather low concentrations.

The computed and measured 24 h-time series for both seasons are displayed for the rest of the compounds in Figure S5, S6, S7 and S8 in the Appendix).

The contrasts observed in reactive removals of example compounds between summer and winter, both for photo-dependent and independent elimination processes, implied a correlation with seasonal parameters such as solar radiation or temperature. As temperature changes according to solar radiation within one day or one year, the impact of temperature on some photo-independent processes (e.g. biodegradation) would invalidate the assumption that photo-independent processes do not follow a diurnal pattern, making them impossible to disentangle from photo-dependent processes. To discuss this issue, mean water temperature and solar radiation, under which each water parcel was exposed during its transit time in the studied segment, were plotted in Figure 21 with the computed/measured concentration ratios of HHCB over the sampling day for both summer and winter campaigns. Those ratios express the difference between concentrations expected at the output of the studied segment if contaminants were conservative and measured ones. Always equal or superior to one, a higher ratio implies a higher elimination observed for the compound considered.

During the summer sampling, the ratio between computed and measured concentrations of HHCB clearly followed variations of solar radiations but not temperatures. The stable ratio of 1.1-1.5 during night-time coincided quite well to the absence of solar radiations during that period, while temperature was still decreasing. In winter, the ratio between computed and measured concentrations of HHCB were rather stable, at the exception of the second sample, and did not follow any of both parameter variations. Photo-dependent degradation did not occur in winter implying that solar radiation did not cause HHCB removal during that period.

As winter data did not show any temporal pattern in compound elimination, only the summer 24 h-time series were plotted for contaminants presenting manifest patterns in Figure 22. As for HHCB, the computed/measured concentrations ratio for oxcarbazepine and OTNE was rather constant during night-time and thus photo-independent elimination did not follow any temporal pattern during that period. Triclosan ratio fitted best the temporal pattern of temperature and appeared offset compared to solar radiation. However, unlike oxcarbazepine and OTNE, triclosan underwent elimination exclusively during day-time in summer, thus ruling out photo-independent elimination processes for the removal of the compound. In Figure 22, the triclosan ratio was already 1.6 for the first two samples of the summer sampling, at the lowest temperatures of the day, against 1 to 1.1 during night-time, at median temperatures. Thus, the reason why the temperature pattern seemed to fit triclosan's better remains unclear. Unlike the other investigated compounds, triclosan concentration did not show the same sharp drop in the samples affected by the effluent stop, which corresponds to the second peak in computed/measured concentrations ratio that fits the falling limb of the temperature signal, letting presume that this fit was rather an artifact.

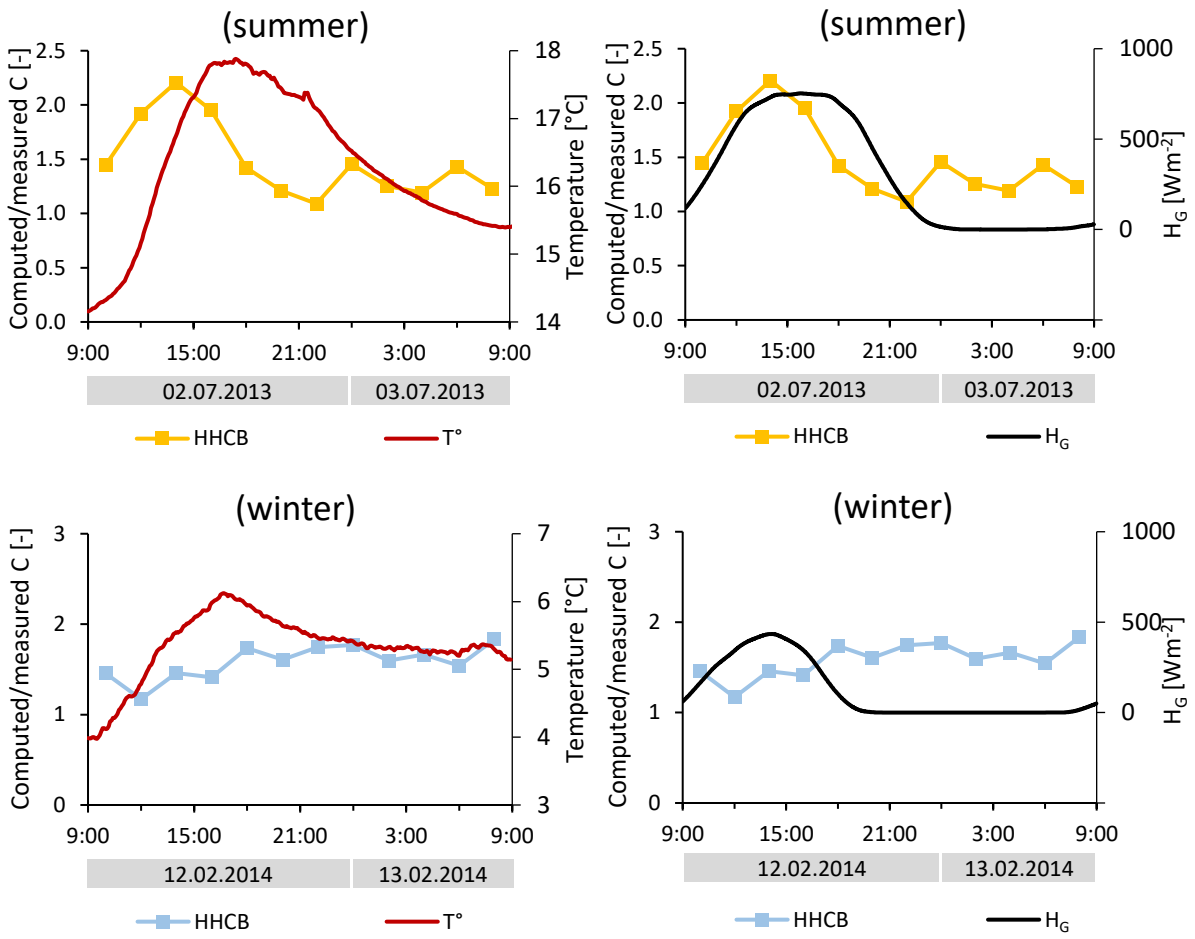

Figure 21. Comparison of mean water temperature (T°) and mean solar radiation (H_G) over the studied segment with the ratio of computed over measured concentrations (C) of HHCB at the lower control cross-section of the summer and winter 24 h samplings.

From these observations, we can conclude that variations in mean temperatures of a few degrees over a single day did not affect significantly the elimination of investigated compounds. Bigger temperature differences between summer and winter seasons may however be responsible for differences in reactivities of some photo-independent elimination processes, as the one(s) affecting oxcarbazepine or HHCB-lactone. The mean water temperature along the studied segment of River Steinlach during the recorded 24 h ranged over 4°C between the minimum and maximum values during the summer sampling and 2°C during the winter sampling. In comparison, there was an 11°C difference between mean water temperatures from summer and winter samplings (16.2 and 5.3 °C, respectively). This greater difference is expected to have a more significant impact on biodegradation efficiency, for example.

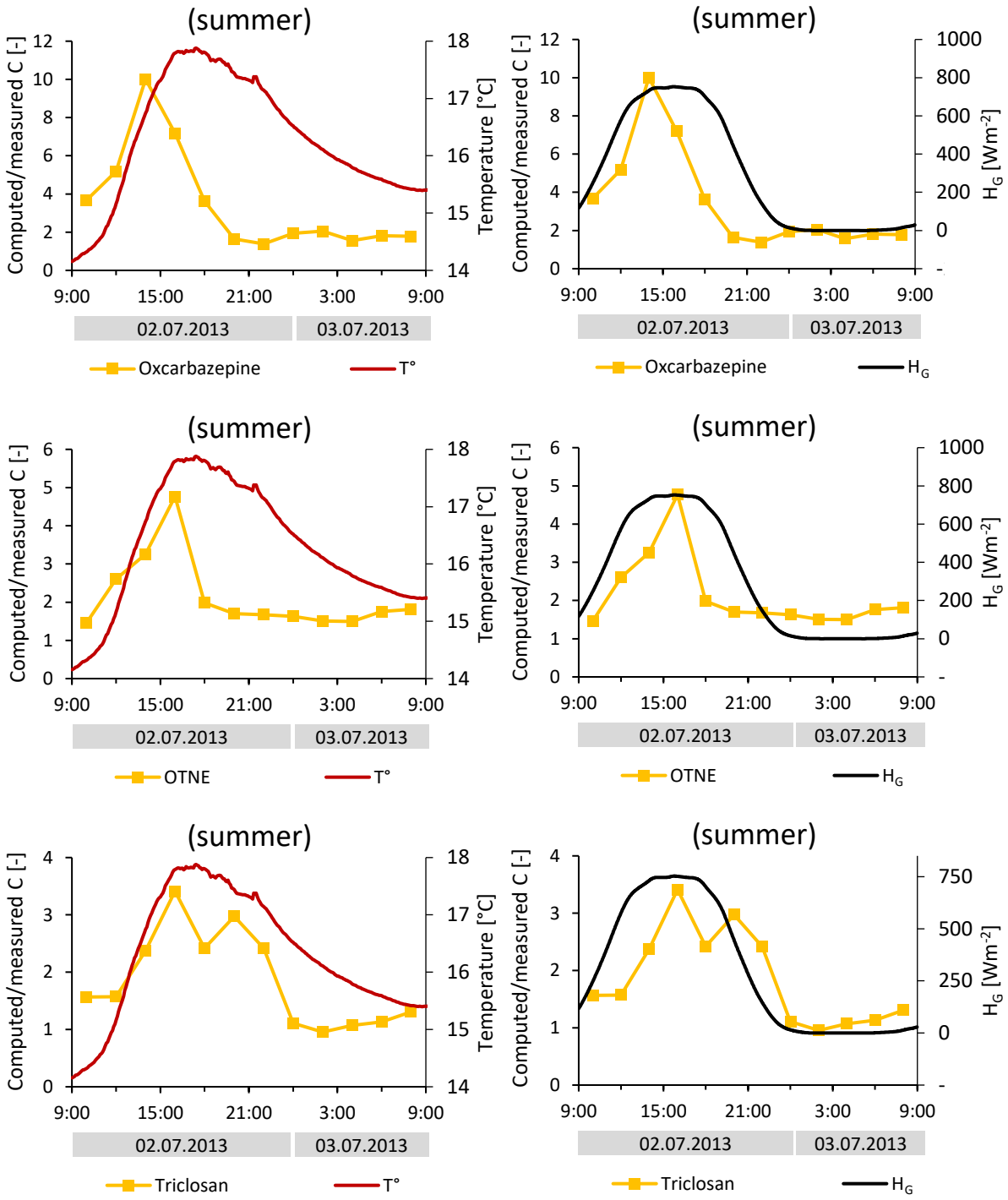

Figure 22. Comparison of mean water temperature (T°) and mean solar radiation (H_G) over the studied segment with the ratio of computed over measured concentrations (C) of oxcarbazepine, OTNE and triclosan at the lower control cross-section of the summer 24 h sampling.

During the summer sampling, an increase of the ratio between measured and computed concentrations of HHCB was already observable at a mean solar radiation of 251 Wm^{-2} for the first sample (9:00-11:00). The early drop of the HHCB ratio as solar radiation started decreasing after stabilizing at its highest mean value corresponded to the samples touched by the effluent stop. These transient conditions being unusual, it is hard to guess what should be observed during that time. During the winter sampling,

the peak of mean solar radiation over the studied segment reached 435 Wm^{-2}. Solar radiation was measured a couple of meters above the ground, and the same amount should reach River Steinlach surface. That this amount of solar radiation did not trigger photo-dependent elimination of HHCB or any photodegradable compound investigated in winter implied the absence or concomitance of other parameters.

Outside of the effluent stop, HHCB concentration was equal or up to 2.5 times higher in winter compared to summer in River Steinlach. Turbidity, that can act as a light filter, was low for both campaigns and DOM and nitrate, that can act as photosensitizers (Andreozzi et al., 2002; Rühmland et al., 2015) or DOM having also a light screening effect (Niu et al., 2013) were rather similar between both samplings. The higher water depth could lower the amount of contaminant photodegraded as the proportion of light decreases with depth, though River Steinlach waters remained quite shallow in both campaigns. If phototrophic organisms were responsible for HHCB removal, their absence due to cold temperatures could explain that no photo-dependent degradation of HHCB could be observed in winter. This can however not be the case for all compounds that underwent photo-dependent elimination in summer.

In winter, radiation has to cross a longer path through the atmosphere to reach the Earth surface, leading to higher absorption of sunlight by the atmosphere which affects the resulting light spectrum. The photolysis of a compound depending on its absorption spectrum (Lindström et al., 2002; Tixier et al., 2002), it can be reduced if sunlight spectrum do not overlap this latter anymore. Hypotheses can also be made regarding the optical properties of river water in winter, for example the higher density of River Steinlach water at 4 to 6°C in winter compared to its 14 to 18°C in summer can have an incidence on light absorbance or reflectivity. Sun rays reaching the water surface at a low angle like in winter have also better chances to get reflected by the water surface of River Steinlach compared to sunrays reaching the Earth surface at an angle close to 90° (Kirk, 1981).

In a nutshell, compound reactivity highly decreased or shifted to conservativeness during the winter sampling, as photo-dependent elimination processes disappeared and photo-independent processes displayed a lower efficiency. Only artificial musk fragrances, which have the particular property to be volatile, showed comparable or higher elimination, that is assumed to stem from volatilization into the atmosphere at local high turbulences zones enhanced by the higher discharge during the winter sampling. Finally, temperature dependence of photo-independent elimination processes was deemed insignificant within one sampling day but was presumed to cause the lower removals of wastewater contaminants in winter compared to summer. Lower solar radiation could not explain entirely the absence of photodegradation during winter-time and additional environmental parameters were proposed to explain the observations. Overall, winter-time showed to be a rather unfavorable period for contaminant natural attenuation in streams such as River Steinlach, in comparison to summer season.

5.3.3 Discussion: contaminant reactivity and influencing factors

The work presented above showed the complexity of compound elimination in surface waters. Despite compound families like musk fragrances that show the same tendency to evaporate from the water phase, it could be seen that contaminants of the same category, with a similar structure or use would not necessarily have the same reactivity. Carbamazepine and oxcarbazepine, both anticonvulsant drugs, the structure of which differs by an additional carbonyl group in the latter compound (see Figure 23a-b), displayed opposite reactivities, the first being persistent while the latter showed to be highly reactive, being photo- and biodegraded during summer conditions in River Steinlach. Similarly, HHCB displayed a photo-sensibility during the summer 24 h sampling that was absent in its daughter compound HHCB-lactone, the structure of which also differs by an additional carbonyl group (see Figure 23c-d). HHCB-

lactone also seemed to be deprived of volatility unlike its parent compound. The single presence of a functional group did not dictate which behavior the investigated compounds had and stressed the influence of the structure of the rest of the molecule. Bayer et al. (2014) observed that sartan compounds that possessed amide groups underwent fast biotransformation. Here, the carbonyl group present in oxcarbazepine and HHCB-lactone seemed to support biodegradation of both compounds compared to carbamazepine and HHCB, respectively. But with compounds with such different structures, it also had as an effect to enhance photodegradability for oxcarbazepine while suppressing it, as well as volatility, for HHCB-lactone, in comparison to carbamazepine and HHCB, respectively.

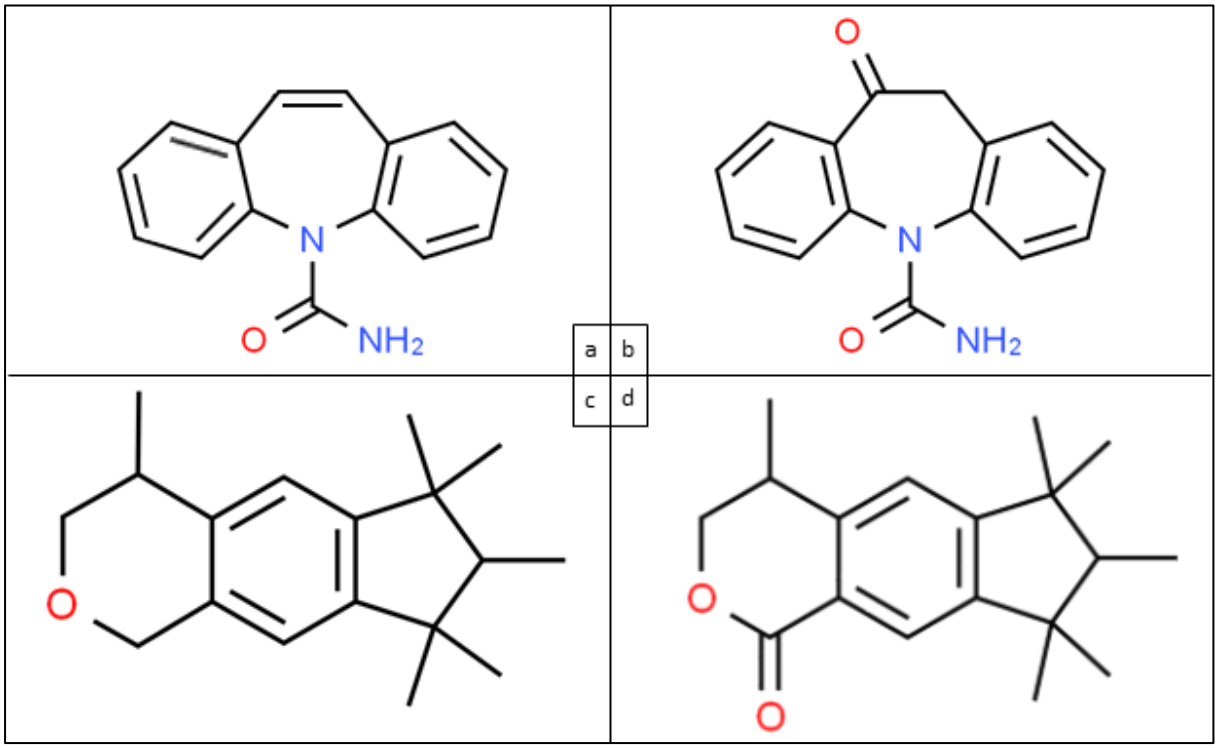

Figure 23. Molecular structure of the anticonvulsant drugs a: carbamazepine and b: oxcarbazepine, the artificial musk fragrance c: HHCB and its metabolite d: HHCB-lactone (www.chemspider.com).

To compare decay constants and the 4 and 1.5 km-long segments investigated during the 24 h and tracer-based samplings, respectively, we assume that the difference of analytical procedures did not impact calculated removals and that the segment downstream of the Steinlach-Wiesaz WWTP was homogeneous. Artificial musk fragrances being the only compounds that were assumed to be eliminated locally within the investigated segment of the 24 h campaigns, first-order kinetic applies to all compounds compared further.

The elimination of wastewater contaminants, though they possess intrinsic vulnerabilities to specific elimination processes, will also be triggered by present environmental conditions. Seasonal differences were already presented in section 5.3.2. Differences could also be observed between the summer 24 h sampling in July 2013 and the tracer-based sampling from August 2015. Nitrate, though poorly degraded in comparison to reactive organic contaminants, was eliminated at 4.5% during the 3h53 travel time along the Steinlach investigated segment in summer 2013 (and 2.8% in winter, at the same rate with $k = 0.3$ day^{-1}, see Table S4 in the Appendix), and at 6-7% during the 3h26 and 3h36 travel time during the day- and night-time experiments in summer 2015, respectively (with $k = 0.5$ day^{-1}, see Table S2 in the Appendix). Here, where comparison of summer 2013 and winter data did not show any

difference in nitrate removal, summer 2015 offered conditions that could have enhanced nitrate reactivity. Investigated contaminants analyzed in both studies showed similar or enhanced reactivity in August 2015 compared to July 2013. Within the Steinlach segment downstream of the WWTP, carbamazepine showed to be conservative in both studies and the flame retardant TCPP remained in the error margin of the chemical analyses. The differences in method and travel time did not allow a direct comparison of day- or night-time removals of the summer 24 h sampling to the tracer-based sampling. Still removals calculated for 8 h spans representing exclusively day- or night-time during the 24 h sampling were juxtaposed to the tracer-based sampling data. The insect repellent DEET was also conservative in July 2013 but exhibited a 36 % and 15 % removal during day- and night-time in August 2015, respectively. The anti-inflammatory drug diclofenac showed 19% and 12% removals during day- and night-time in July 2013, respectively, against 45% and 8% during day- and night-time experiments of August 2015, respectively. The bleaching agent TAED had 52% and -4% removal during day- and night-time of the July 2013 sampling against 65% and 19% during the day- and night-time experiments of August 2015, respectively. Contrary to summer 2013, no contaminant was deemed prone exclusively to photo-dependent elimination processes in August 2015. In July 2013, the anticonvulsant oxcarbazepine showed an average elimination of 46% during night-time and 85% during day-time. No removal was attained for oxcarbazepine during night-time while the compound was already under LOQ at MS3 during day-time in August 2015. However, the results for night-time data of August 2015 appeared to be questionable as an increase of concentration occurred between MS1 and 2 while the grab samples measurements downstream showed a decreasing trend with concentrations that remained above C_{in} (see Figure S4 in the Appendix). The correction of the night-data by the coefficient calculation yielded zero removal, as contaminant input was excluded. But assuming concentration of oxcarbazepine was underestimated at MS1, this trend during the night-time experiment would indicate photo-independent elimination and corroborate findings from the July 2013 sampling.

August 2015 clearly offered more favorable conditions for photo-dependent and independent elimination processes. Solar radiation was similar between the two studies but photodegradation might have been enhanced in August 2015 by the lower water level allowing better light penetration and the higher DOC and nitrate concentrations that can contribute to indirect photodegradation of contaminants. The higher proportion of treated wastewater yielding higher concentrations of contaminants and biomass adapted to degrade them, the higher water temperature and the lower flow velocity could have fostered biodegradation besides.

The comparison of August 2015 data to other published field work highlighted particularly optimal conditions leading to the unusually high removals in the investigated Steinlach segments, which can also apply to summer 2013 data. Photodegradation and biodegradation in the sediment appeared to be important elimination processes for the example compounds, though musk fragrances presented the particularity to volatilize into the atmosphere.

Predicting the reactivity of a compound within another water body reveals to be even more challenging as environmental conditions can highly differ from one river to another. Key factors shall however be identified. Lower water depth – or the larger water surface to volume ratio –, particularly, could be an important factor for enhancing photodegradation, despite a similar solar radiation. An increasing number of studies reports the action of stream bed biofilms and biodegradation in the sediment as a determining factor for contaminant removal in rivers (Kunkel and Radke, 2011; Matamoros and Rodríguez, 2017; Rühmland et al., 2015; Schaper et al., 2018; Writer et al., 2013). The warm temperatures, a large fraction of water flowing through the hyporheic zone enhanced by coarse sediment and steep gradients, retention in surface transient storage, and high contaminant concentrations may be additional key parameters explaining the large removals through photo-independent elimination processes in River Steinlach.

These properties are regularly found in small streams but to a smaller extent in larger rivers, where turbidity and depth would prevent light penetration and the lower surface to volume ratio would reduce the importance of degradation in the sediment. Low order streams, thus, seem to have a strong potential for contaminant attenuation (Schwientek and Selle, 2016).

Latitude could also represent an important factor for differences in photodegradation. Where photodegradation was shown to be dependent on highly variable factors such as simple day-night alternation, the variation of day-time duration due to day-night alternation or season will depend on latitude. At lower latitudes, sunrays angle of incidence would also vary less along the year and penetrate water bodies more evenly.

5.3.4 Investigation method discussion

The disentangling of reactive elimination processes relied on the use of transfer functions fitted to a conservative tracer, to rid the measured signal from effect of conservative river transport such as advection and dispersion. The use of the transfer functions was mainly aimed at observing transport of shorter parcels, such as the 2 h-composite samples. To assess how the method impacts the obtained results, removals calculated from measured raw concentrations and concentrations modelled using transfer functions were compared. The same error in the travel time estimation was kept to compare the two signals. Figure 24 and 25 show the relative net removals calculated the same way for the day- and night-time samples – covering 8 h time spans each – during the summer and winter campaigns.

Differences between balances using raw data and data computed using transfer functions did not exceed 0.2% for all compounds in both campaigns, at the exception of TAED that exhibited a 1.1% difference during summer nigh-time. Thus, the use of an 8 h-long (24 h-long too) water parcel to compensate inaccuracies from dispersion effect yielded almost identical results as with using transfer functions.

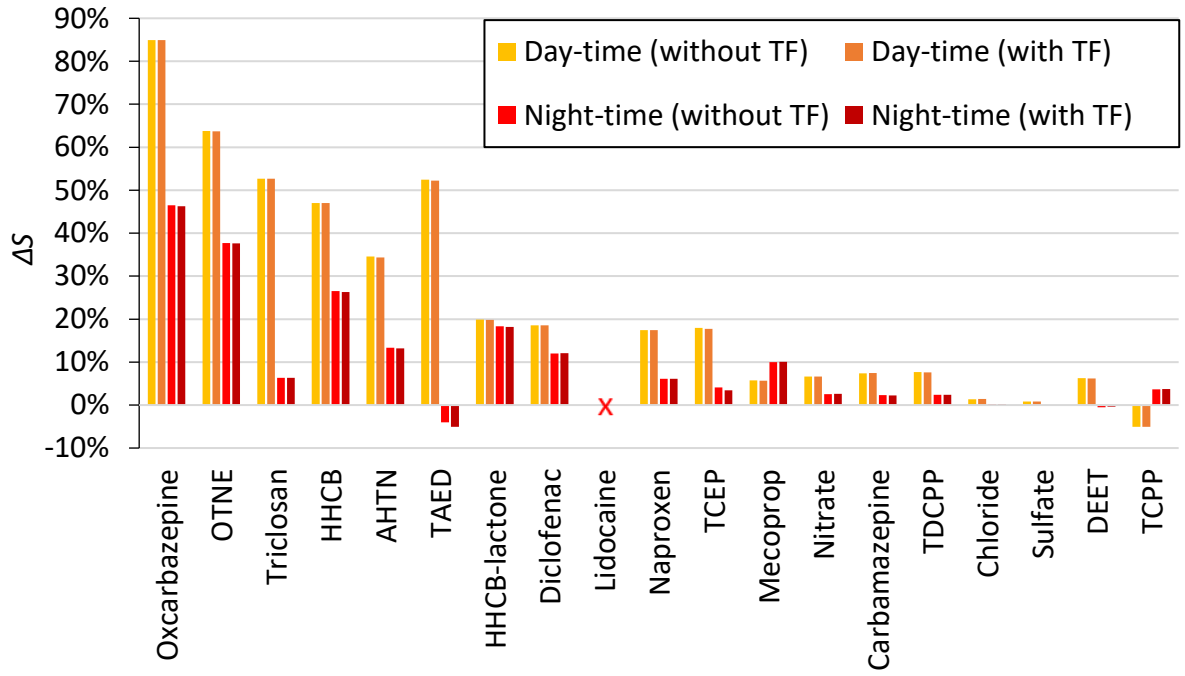

Figure 24. Comparison of removals calculated over the day- and night-time periods (each covering n=4 samples) during the summer 24 h-sampling campaign, using or not the transfer functions (TF).

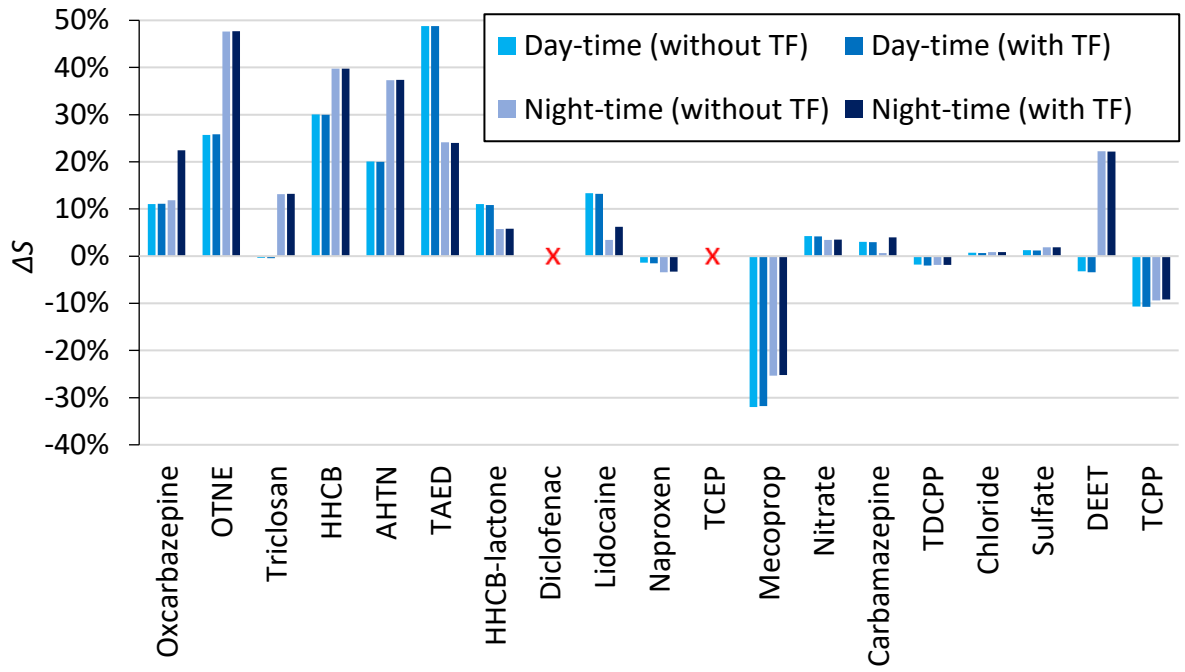

Figure 25. Comparison of removals calculated over the day- and night-time periods (each covering n=4 samples) during the winter 24 h-sampling campaign, using or not the transfer functions (TF).

The impact of using transfer function on shorter – 2 h-long – water parcels was also checked. "Measured" concentrations of 2 h-composite samples C_i^{meas}, as calculated in section 4.3.8, shifted by τ_m as well as computed concentrations were compared for oxcarbazepine, triclosan and TAED in Figure 26 for summer and winter samplings. For a variable signal such as the discharge of wastewater contaminants by WWTPs, the effect of dispersion would smooth out the concentration time series monitored downstream of a WWTP effluent. Therefore, the effect of dispersion on compound concentration signal shall be more pronounced for compounds displaying strong temporal variabilities in their input. During the summer, including the effluent stop, and winter samplings, the variability of oxcarbazepine concentration time series was 49% and 15%, respectively, according to CV calculation of the measured 24 hours at the upper control cross-section. Variability of triclosan concentration time series was in the lowest, with 16% during both seasons. The biggest differences between shifted measured concentrations and computed ones were observed for oxcarbazepine in summer, as it was expected. Computed and shifted measured concentrations of oxcarbazepine differed by a maximum of 2% and 1.5 ngL^{-1} during both samplings. Only the effluent stop, that was underestimated by the computation (see section 5.2.4), had the highest off-set with a -18% difference (6.0 ngL^{-1} computed for 5.1 ngL^{-1} actually measured). Triclosan and TAED showed minor differences between computed and shifted measured concentrations (less than 0.3 ngL^{-1}). No explanation for the higher differences found in the 8 h balances for TAED could be found. The quasi-perfect fit between computed and shifted measured concentrations thus indicated that dispersion effect was not perceptible on contaminant concentrations along the investigated segment during the two 24 h-sampling campaigns.

During the tracer-based experiment, transfer functions were used not only to compute expected concentrations at the different measurement stations but also to disentangle the effect of solar radiation from the photo-dependent elimination. Thus, the use of transfer functions was inherent to the analysis of tracer-based sampling data and the calculation of the specific decay constant k_i. But the decay constant k_{night} for the night data could also be calculated by simply fitting a first order decay using the measured concentrations at MS2, 3 and 4 and the corresponding values in the input function at MS1,

considering the mean travel time τ_m calculated from the transfer functions. k_{night} constants calculated by directly fitting first-order decay to measured data and using transfer functions for wastewater contaminants and a selection of inorganic ions are compared in Figure 27.

Negative k_{night} were removed by the computation procedure using transfer functions, and so were they for the direct fitting of first-order decay. This stems from the assumption that no contaminant input occurs along the investigated segment, the computation correcting negative k_{night} with 0 values.

Differences between removals calculated with and without using transfer functions were generally more pronounced for the tracer-based sampling than for the 24 h sampling (see the fungicide carbendazim or the bleaching agent TAED in Figure 27). Higher dispersion and low-velocity water parcels were expected during the tracer-based sampling due to the much lower discharge conditions and were reflected in the long tailing of transfer functions of both day- and night-time experiments (see Figure 12 in section 5.2.3).

CVs for the 6 h-time series in summer 2015 varied between 0.01 and 0.66 depending on the compound considered but no correlation was found with the absolute differences in calculated k_{night} using or not transfer functions. Thus, the disentangling of conservative transport to remove river transport effects such as dispersion seems only necessary when alteration is consequent. In River Steinlach, even at very low flow conditions, considering dispersion only brings small differences in calculated k_{night}. The method might be applied in other aquatic media where dispersion poses more of an issue, such as groundwater transport (Cirpka et al., 2007), flow through wetlands (Lange et al., 2011; Schuetz et al., 2012) or rivers with more complex features such as pools and consequent stagnant zones.

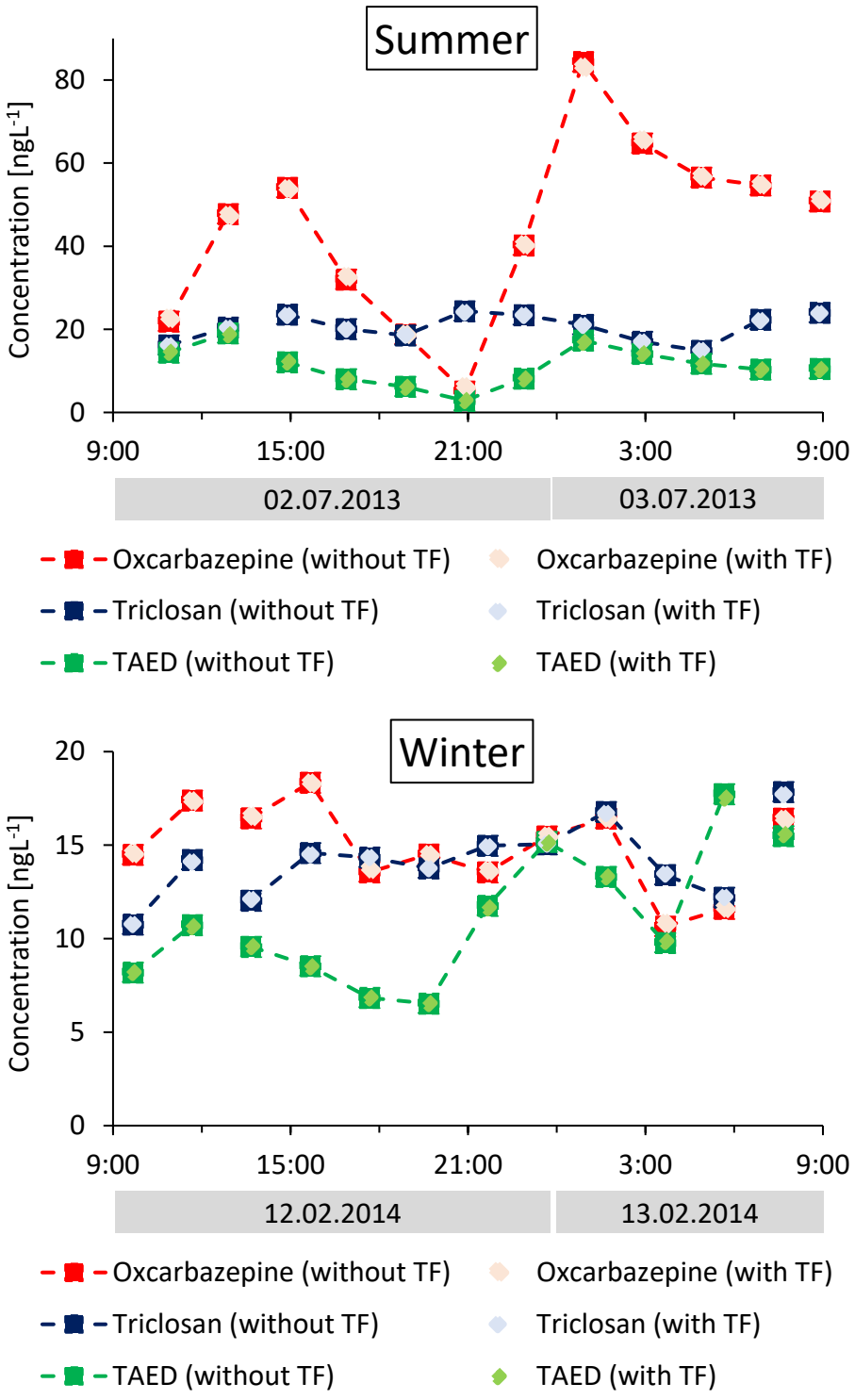

Figure 26. Comparison of concentrations measured at the upper control-cross section shifted by the travel time τ_m=3h53 (without using transfer functions (TF)) and the computed concentrations using transfer functions for oxcarbazepine, triclosan and TAED during the summer and winter 24 h-samplings.

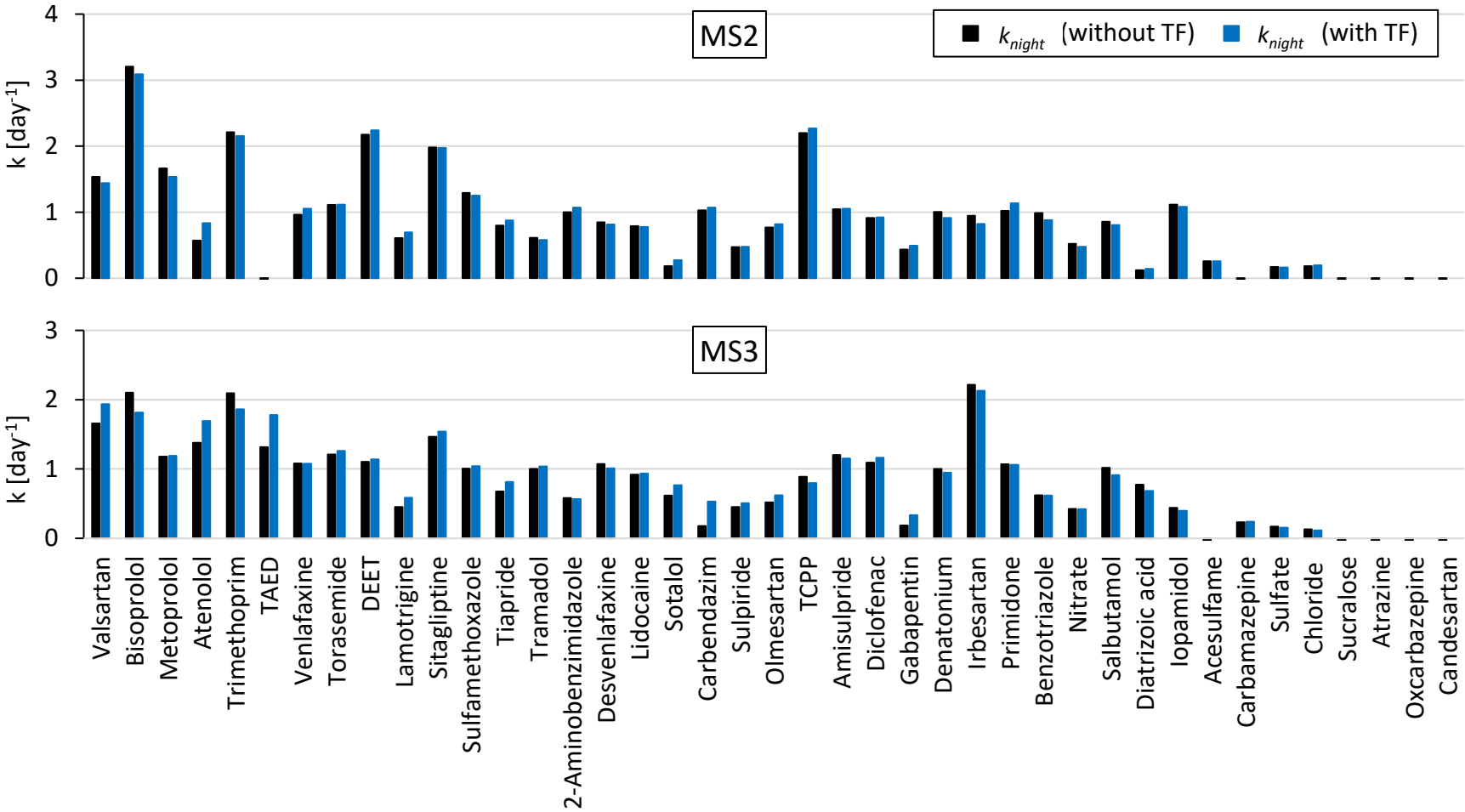

Figure 27. Comparison of night decay constants k_{night} calculated by directly fitting first order decay to measured concentrations (without using transfer functions (TF)) and calculated using TFs for MS2 and MS3.

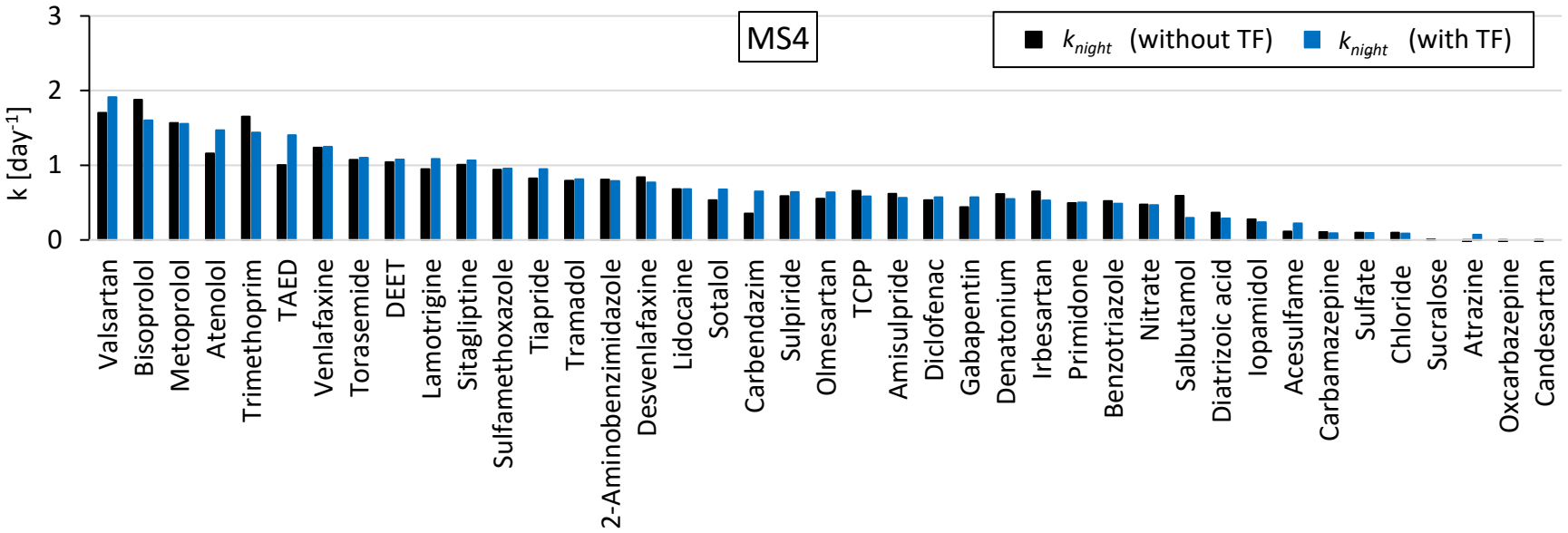

Figure 27 (continued). Comparison of night decay constants k_{night} calculated by directly fitting first order decay to measured concentrations (without using transfer functions (TF)) and calculated using TFs for MS2 and MS.

Field studies being sparse, one aim of this work was also to test different methods for the assessment of reactive transport. The use of a long water parcel was aimed at limiting the effect of dispersion or of error in travel time estimations. With a comparable number of samples, logistic and total duration, the tracer-based sampling allowed multiplying the number of monitoring stations along the investigated segment by using grab samples and correct the effect of dispersion and travel time inaccuracies by computation. The data from the tracer-based sampling could confirm that first-order kinetics could be fitted to the decay profiles of the investigated compounds in the studied segment. This can however only apply for transit time of a few hours but might not apply for longer contaminant transport, with the simple temporal variation of photo-dependent elimination processes. Unfortunately, volatile compounds like musk fragrances, that were assumed to be locally eliminated at turbulent zones such as the weirs and steps along the studied segment, were not analyzed during the tracer-based experiments and this hypothesis could not be validated. Finally, the calculated specific constant k_i of investigated contaminants during the tracer-based sampling was an indicator of the compound photodegradability independently from solar radiation but related to the river environment.

The use of EC or fluorescein as tracers to fit the transfer functions assumed that they behaved conservatively and would not undergo any retardation effect due to some sorption or trapping process. At River Steinlach pH, fluorescein was not sorbing and night-time tracer test indicated no loss or dilution of the tracer along the segment. But during day-time, fluorescein was photodegraded and computational transformation of the night-time data was needed to obtain day-time BTCs (see section 4.2.6). In addition, local authorities limited the performance of tracer tests to a few months of the year and each tracer injection had to be declared in advance for only given dates, whatever the field conditions, that cannot be for sure known in advance. It has been seen that even a reactive major ion like nitrate showed very limited transformation along the investigated segment of River Steinlach. EC being the resulting conductivity of naturally occurring inorganic ions dissolved in river water, it is a good tracer that would not vary along the river, besides through mixing with other entering water, which was ruled out for the study segment of River Steinlach. Indeed, in River Steinlach, balances for EC yielded -1.6 and 1.2% during the summer and winter 24 h samplings, respectively. As EC occurs naturally, there is no need of authorization to set divers in the river, and the monitoring can be performed over a long period (e.g. several months), only limited by the divers' battery duration. Only material defect had led to bias in the EC signal and the jamming of algae material in the divers had made its use to fit transfer functions impossible during the tracer-based experiments. Injecting a tracer in a river presents also the drawback to alter, even slightly, initial conditions in the river water, as fluorescein might absorb light in the water column and hinder photodegradation during the experiment or simply interact with other compounds. The fitting of transfer functions on the EC time series was however only possible thanks to the recognizable diurnal pattern from the WWTP and the limited dispersion that did not smooth the signal consequently. Thus, if using a tracer is necessary for the data exploitation, the choice would rather be a chemical species that is already present in the river water, if dispersion is limited and the tracer signal variable enough.

5.4 Assessment of particle-associated transport

5.4.1 Description of flood particles

Figure 28 shows the total suspended solid (TSS) concentration along both sampled flood events. The highest TSS value measured during the Steinlach flood was in sample 2 on the falling limb of the discharge peak ②. TSS concentration during the highest discharge peak (③) was lower and kept decreasing with discharge. In the Ammer flood, TSS concentration was the highest in sample 2 on the falling limb of the discharge peak ① to then decrease further with discharge.

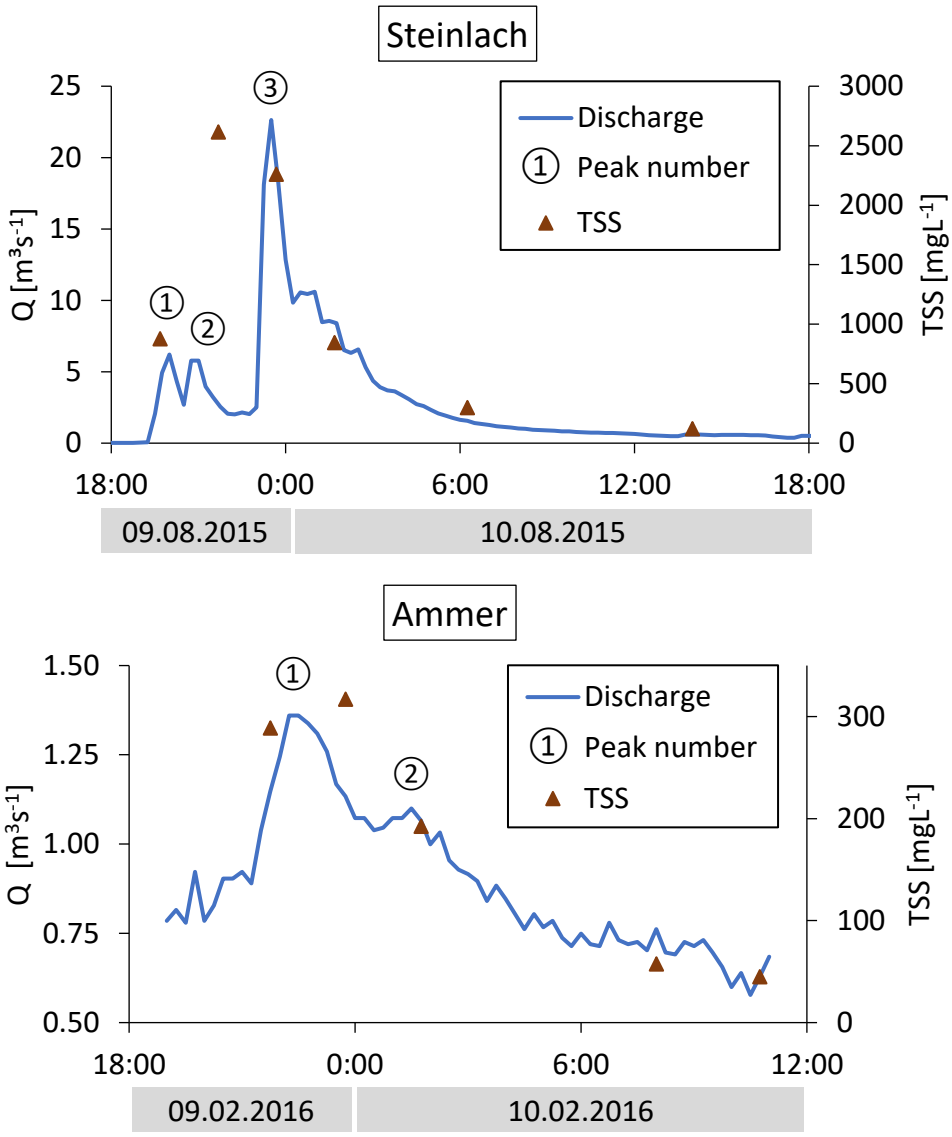

Figure 28. TSS concentration along discharge in samples taken during the Steinlach and the Ammer floods.

For both rivers, the main sediment fraction was constituted by silts with a median diameter d50 of 11 to 38 µm in the Steinlach and 19 to 24 µm in the Ammer flood. Samples 1 to 4 in River Steinlach and 1 to 3 in River Ammer were rather dark and looked like a mixture of yellowish grey and brownish grey sediments, respectively. All samples exhibited dark grains spread into the matrix. The first four

Steinlach samples presented plant debris that were not found in sample 5 and 6 or in any of the samples from the Ammer flood. In this latter, the absence of vegetal debris may indicate little surface run-off or catchment contribution to particles, presumably due to the weak precipitation and discharge, but might also be due to the reduced vegetation during February. The first four samples from the Steinlach flood exhibited similar variations of both the median diameter d50 and the organic content of captured particles (see Figure 29). Organic content did not decrease with d50 for Steinlach sample 5 and 6, which might indicate that the finer sediments host most of the organic matter. Ammer sediments had a rather stable organic content (4.2% to 4.7% in sample 1 to 4, 5.4% in sample 5 which is not shown in Figure 29) that slightly increased as d50 decreased and inversely, indicating again that finer sediments determined the organic content unlike coarser ones.

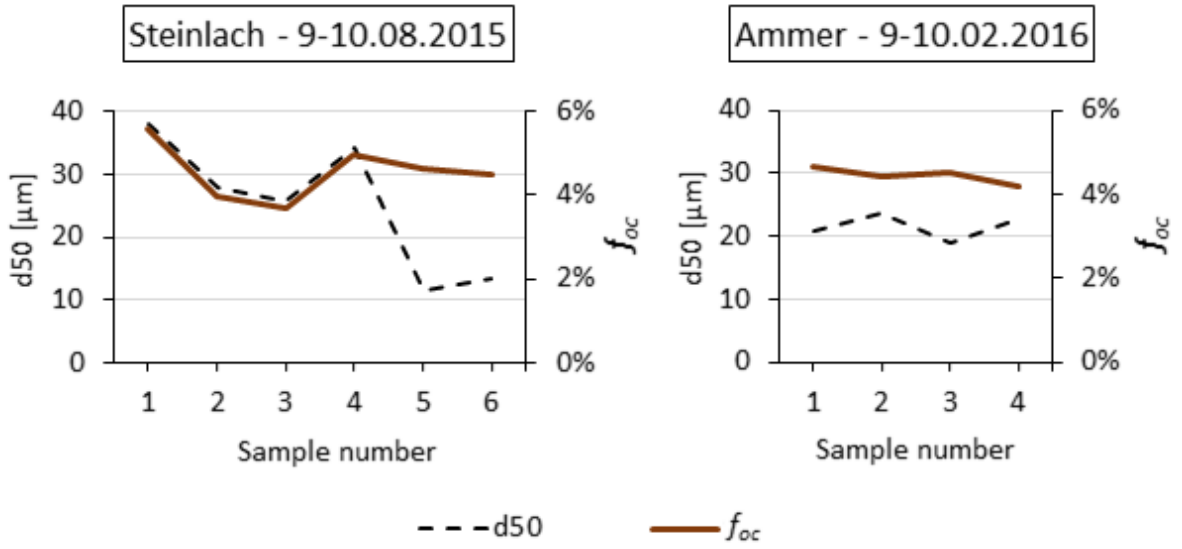

Figure 29. Median particle diameter (d50) and organic content (f_{oc}) measured from the particles in the Steinlach and Ammer flood samples.

Sediment granulometry is presented in Figure 30. The particle size distribution was stable over the Ammer event while the greater discharge range during the Steinlach flood might have caused the higher variability in the sediments of the Steinlach samples. The proportion of coarse sediments in Steinlach samples seemed independent from discharge but rather indicated sediment provenance. Particle size distribution was almost identical between sample 2 and 3, for discharges equal to 2.6 and 18.3 m^3s^{-1}, respectively, though both were also sampled on the falling limbs of a discharge peak. Steinlach samples 2 and 3 were separated by 2 h but showed also similar organic contents and sediment aspects, hinting that they may have stemmed from the same source. The coarser particle size in sample 1 and 4 could be due to the timing of the sampling, on the rising limb and on the top of a secondary discharge peak, respectively, where discharge still mobilized the neighboring coarse sediments. With a similar organic content as well, particles in sample 1 and 4 could indicate again a similar near source, different from particles in sample 2 and 3. The organic content being lower for the highest TSS values in samples 2 and 3 hints toward the release of rather mineral particles compared to the other samples, presumably from bank or surface erosion. The last two Steinlach samples, on the return to baseflow discharge, presented a finer fraction than what was observed at comparable or slightly lower discharge in the Ammer event. As smaller particles settle later than coarse and heavy ones, the sediments in Steinlach sample 5 and 6 were assumed to stem from the upper parts of the Steinlach catchment.

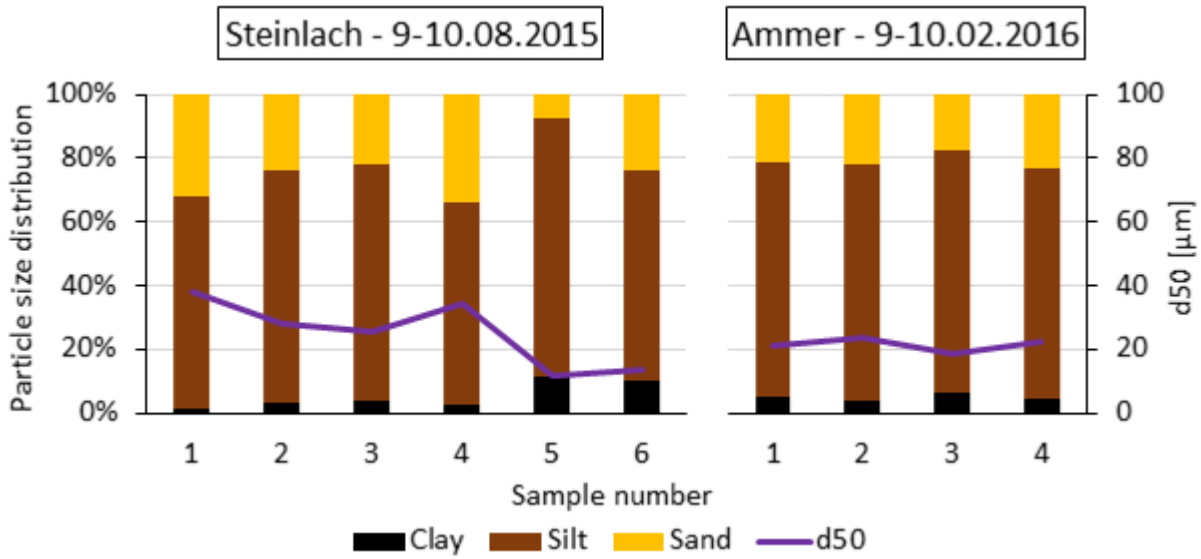

Figure 30. Particle size proportion in volume and median diameter d50 in suspended sediments recovered from the flood-event samples (the denominations "clay" – <2µm diameter – "silt" – 2-63µm – and "sand" – 63µm-2mm – correspond to the granulometric and not the mineralogic definition, according to the international ISO14688-1 (2002) *classification scales).*

5.4.2 Turbidity-TSS correlations during sampled floods

To verify the relationship between turbidity and TSS as for previous works on PAHs, turbidity measurements were plotted in Figure 31 versus TSS concentrations for floods sampled in River Steinlach and Ammer. Obtained negative intersects were forced to 0 for the results to remain realistic. R^2 and slopes m did not vary much with this change. Also, regression slopes m were comparable to the averaged m value from TSS-turbidity ratio of each sample (1.24 for the Steinlach flood and 1.35 for the Ammer flood).

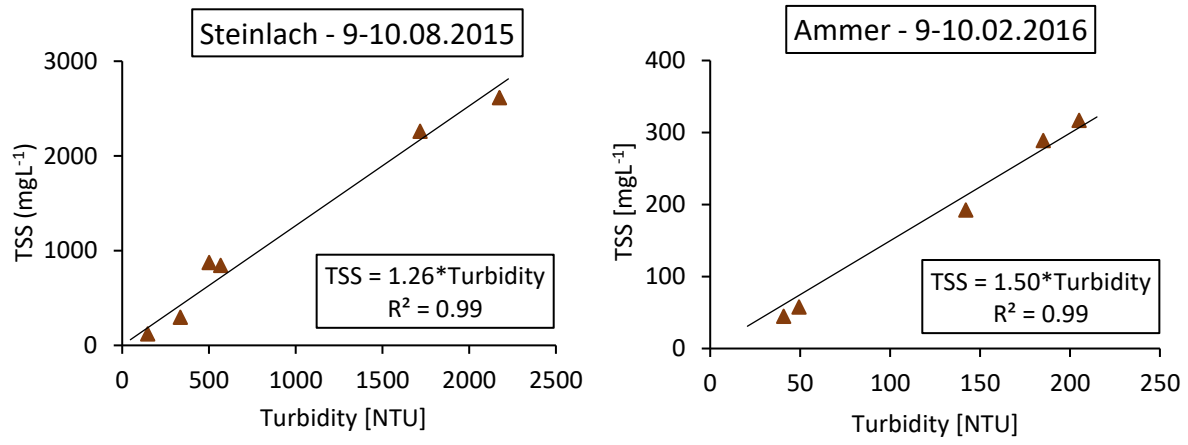

Figure 31. Total suspended solid concentration (TSS) versus turbidity in samples of the Steinlach and Ammer floods.

Table 12. Summary of turbidity-TSS correlations from current and previous works in River Steinlach and Ammer.

		Steinlach		Ammer	
		event sampling	monthly sampling	event sampling	monthly sampling
Present study	*m* [$mgL^{-1}NTU^{-1}$]	1.26	/	1.50	/
	R^2	0.99		0.99	
	Number of samples[1]	6		5	
	Discharge range [m^3s^{-1}]	0.6-18.3		0.6-1.2	
	Turbidity range [NTU]	147-2176		41-205	
	TSS range [mgL^{-1}]	120-2614		45-317	
Rügner et al. (2013)[2]	*m* [$mgL^{-1}NTU^{-1}$]	/	2.35 ± 0.11	/	1.62 ± 0.14
	R^2		0.97		0.75
	Number of samples		10		27
	Discharge range [m^3s^{-1}]		0.5-15		0.3-2.1
	Turbidity range [NTU]		0.4-114		1-76
	TSS range [mgL^{-1}]		1-239		2-150
Rügner et al. (2014)[3]	*m* [$mgL^{-1}NTU^{-1}$]	1.67 ± 0.04	/	2.79 ± 0.10	/
	R^2	0.97		0.94	
	Number of samples	26		31	
	Discharge range [m^3s^{-1}]	0.6-41.0		0.8-13.5	
	Turbidity range [NTU]	14-888		13-560	
	TSS range [mgL^{-1}]	19-1567		14-1590	

[1]Does not include the triplicate samples.
[2]Comprehends samples from October 2010 to January 2011.
[3]Three floods per river were sampled in 2012 and 2013.

Like in Rügner et al. (2013), the correlations observed were linear. Coefficients and some field parameters are compared to previous data in the same rivers (see Table 12).

The slope *m* obtained for the Steinlach flood was similar to the value reported from the flood samplings in the same river by Rügner et al. (2014) but half of the value reported by Rügner et al. (2013). Despite discharge event up to 15 m^3s^{-1} sampled, the authors of the 2013 publication stated that only low turbidity values were captured in River Steinlach and that the correlation determined might not hold for higher turbidity values. Indeed, as fine sediments create most turbidity, the *m* slope may get higher when mobilization and transport of coarse sediments increase with discharge. In the Ammer flood from this work, the rather low discharge conditions reflected the discharge range as during the sampling from Rügner et al. (2013) but turbidity was higher, similarly to the Rügner et al. (2014) study. The *m* slope calculated in this study was found close to the one in the Rügner et al. (2013) study, hinting that discharge may determine the coarseness of suspended particles in River Ammer. However, *m* slopes were quite similar between the Steinlach and Ammer floods captured in this work despite great differences of magnitude in both events.

5.4.3 Correlation between contaminant concentration and TSS

The total concentrations of contaminants were plotted against TSS to determine if a linear correlation was observable, similarly to PAHs (see section 4.1.4), indicating a constant loading of contaminants onto particles in the Steinlach and Ammer catchments.

5.4.3.1 River Steinlach

In the Steinlach flood, no linear relationship could be demonstrated from the plots of wastewater-contaminant concentrations versus TSS. But plotting the sampling order revealed a hysteresis phenomenon for some of the studied compounds. Hystereses were observable for three of the rather hydrophobic contaminants analyzed – triclosan, HHCB and AHTN – and for more soluble compounds – lidocaine, ibuprofen and carbamazepine (see in Figure 32 and Figure S9 of the Appendix). Unlike for triclosan and HHCB, the hystereses for the soluble compounds and AHTN displayed a noticeable difference between their concentrations in sample 2 and 3, despite similar grain size distribution, organic content of the particles and their assumed similar origin. Also, the course of the hystereses for lidocaine, ibuprofen and carbamazepine exhibited a concavity at sample 4 that was not observable for the more hydrophobic contaminants.

More complicated patterns were observed for the other investigated compounds. Among the four examples given in Figure 32, differences were also observed in the evolution of concentrations for each contaminant along TSS release. The concentration in sample 1 was among the highest measured for naproxen and TCPP, above sample 4's value unlike the compounds displaying a hysteresis, while it's among the lowest for caffeine and mecoprop. Generally, the concentration of naproxen and TCPP were rather high during the event but decreased at sample 5 and 6, with different pattern for each compound. Caffeine and mecoprop conserved rather low concentrations in sample 1 and 2, as well as 3 in the case of mecoprop, while the three last samples displayed higher concentration values. Caffeine being highly degraded in WWTP, it is often proposed as a tracer compound for untreated wastewater (Buerge et al., 2006; Kiguchi et al., 2016; Schirmer et al., 2011). However, it did not behave like contaminants such as pharmaceuticals or the bleaching agent TEAD (see Figure S10 in the Appendix) that should also be released solely through wastewater discharge but were found in high concentrations from the beginning of the event. Being an herbicide used in household gardens, mecoprop should come from urban surface run-off collected by the sewer but still behaved similarly to caffeine in the first two samples.

Concentrations of HHCB-lactone, diclofenac and TCPP remained quite high (>50 ngL^{-1}) at the end of the event, unlike the other compounds.

Though no linear correlations between concerned contaminants and particle concentrations was found, implying no constant particle loading of those contaminants, the existence of hystereses may still imply a partial relationship, i.e. a common release or association to particles. Considering that hydrophobic sorption is the major process for neutral substances (see section 3.6), the process can be considered for undissociated triclosan, HHCB, AHTN, carbamazepine and lidocaine exhibiting $\log D_{ow}$ above 2.6. However, according to Table S1 in the Appendix, HHCB-lactone and TCPP also exhibited significant $\log D_{ow}$ (i.e. 4.7 and 3.4, respectively) but did not show any correlation with TSS, despite their high concentrations during the flood event. Neither did DEET, which is also neutral and exhibited a $\log D_{ow}$ of 2.5. Hydrophobicity alone may thus not explain these hystereses found for neutral compounds. Dissociated lidocaine was the only investigated compound that should be found under cationic form at the Steinlach pH (between 26.4% and 52.6% according to www.chemicalize.com). Ibuprofen and the dissociated form of triclosan (between 56.8% and 76.8% at Steinlach pH, according to www.chemicalize.com) were the only anionic compounds which concentration exhibited hystereses with TSS. Still despite their contrasting properties, lidocaine, ibuprofen and carbamazepine exhibited a similar behavior along the Steinlach flood according to the samples collected. The other anionic (i.e. mecoprop, naproxen and diclofenac) and neutral compounds (i.e. TAED, TCEP and caffeine) have rather low $\log D_{ow}$, similarly to ibuprofen or lower. Thus, hydrophobicity, charge or the combination of both did not seem responsible for this hysteresis phenomenon for at least part of the investigated contaminants.

For compounds following this hysteresis pattern, no correlation was found between total concentrations of investigated compounds and organic content or particle diameter (see triclosan in Figure 32). The similarity between sample 2 and 3 assumed to stem from the same source was reflected only in the similar concentrations of triclosan and HHCB despite the lowest organic contents observed from the samples. Similarities between sample 1 and 4 might explain the concavities in total concentrations of lidocaine, ibuprofen and carbamazepine. No effect of the particle color or the presence of vegetal debris was reflected in the observed patterns. The finest sediments were found at the end of the event, their higher contact area but the low particle concentration could have been responsible for higher $C_{w,tot} = f(TSS)$ slopes but low concentration values in the correlations, if sorption would occur.

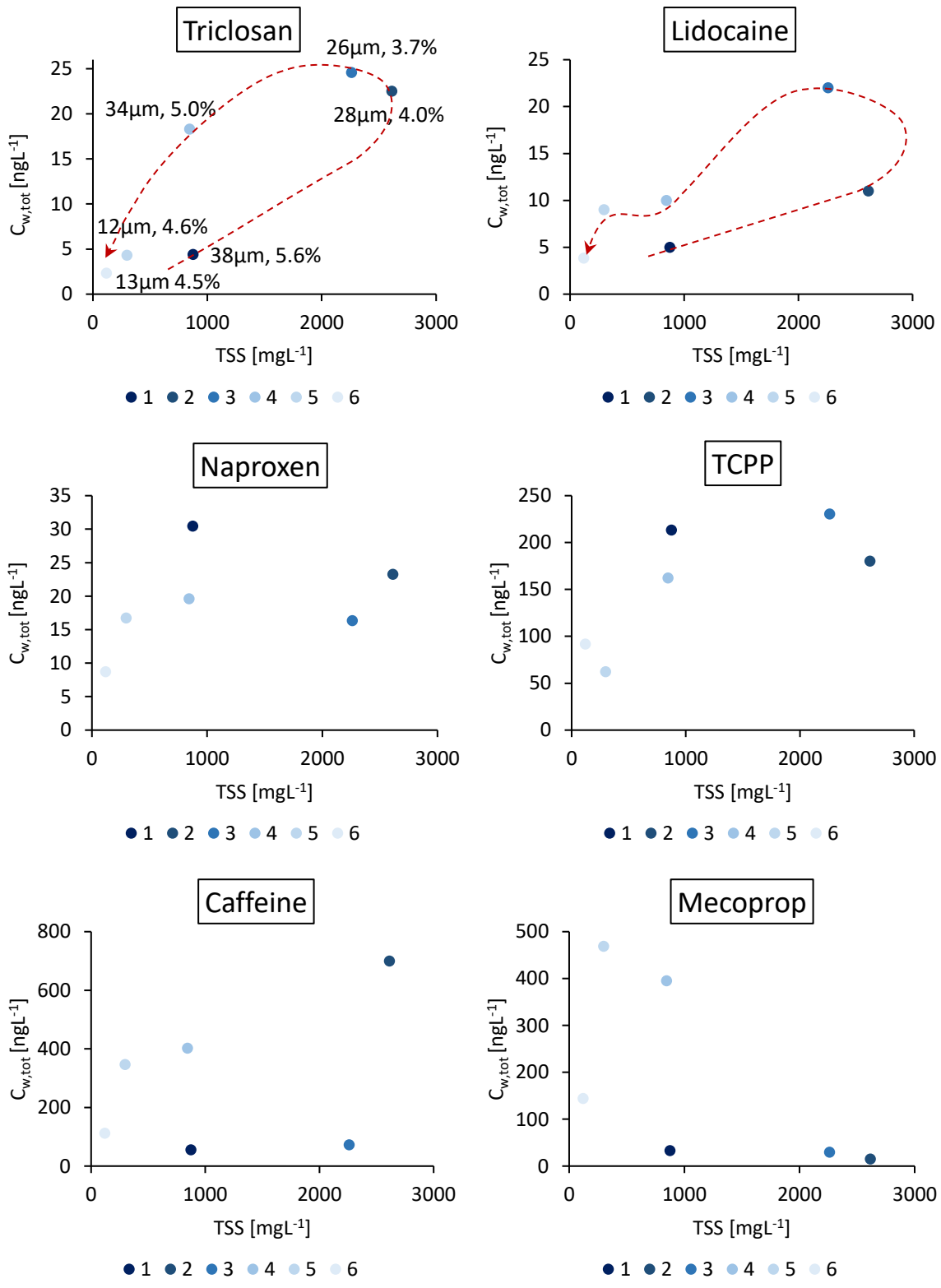

Figure 32. Concentration versus total suspended solid concentration (TSS) for example compounds in the Steinlach flood with sample number. The d50 and f_{oc} given for particles in µm and %, respectively, next to each sample for triclosan hold for the other compounds.

Inorganic ions being measured in filtered samples, their concentrations correspond directly to C_w and not $C_{w,tot}$ like for organic contaminants (see section 4.1.4). The dissolved concentration of inorganic ions sodium, calcium, potassium, magnesium and chloride showed hysteresis patterns versus TSS in a reverse order and direction as organic contaminants (see Figure 33). Nitrite was detected in the Steinlach event for all samples but the first one and showed a similar hysteresis as lidocaine, ibuprofen and carbamazepine, including the concavity from sample 4 low concentration, but exhibited a flat trend instead of a growing one. Dissolved concentration of potassium, considered to be a wastewater marker (Nödler et al., 2011), did not show a very strong decrease versus TSS and remained at rather low concentrations (i.e. 3 to 4 mgL^{-1}). Dissolved concentration of nitrate and sulfate were rather stable between sample 1 and 4 but increased with decreasing TSS (see Figure S11 in the Appendix).

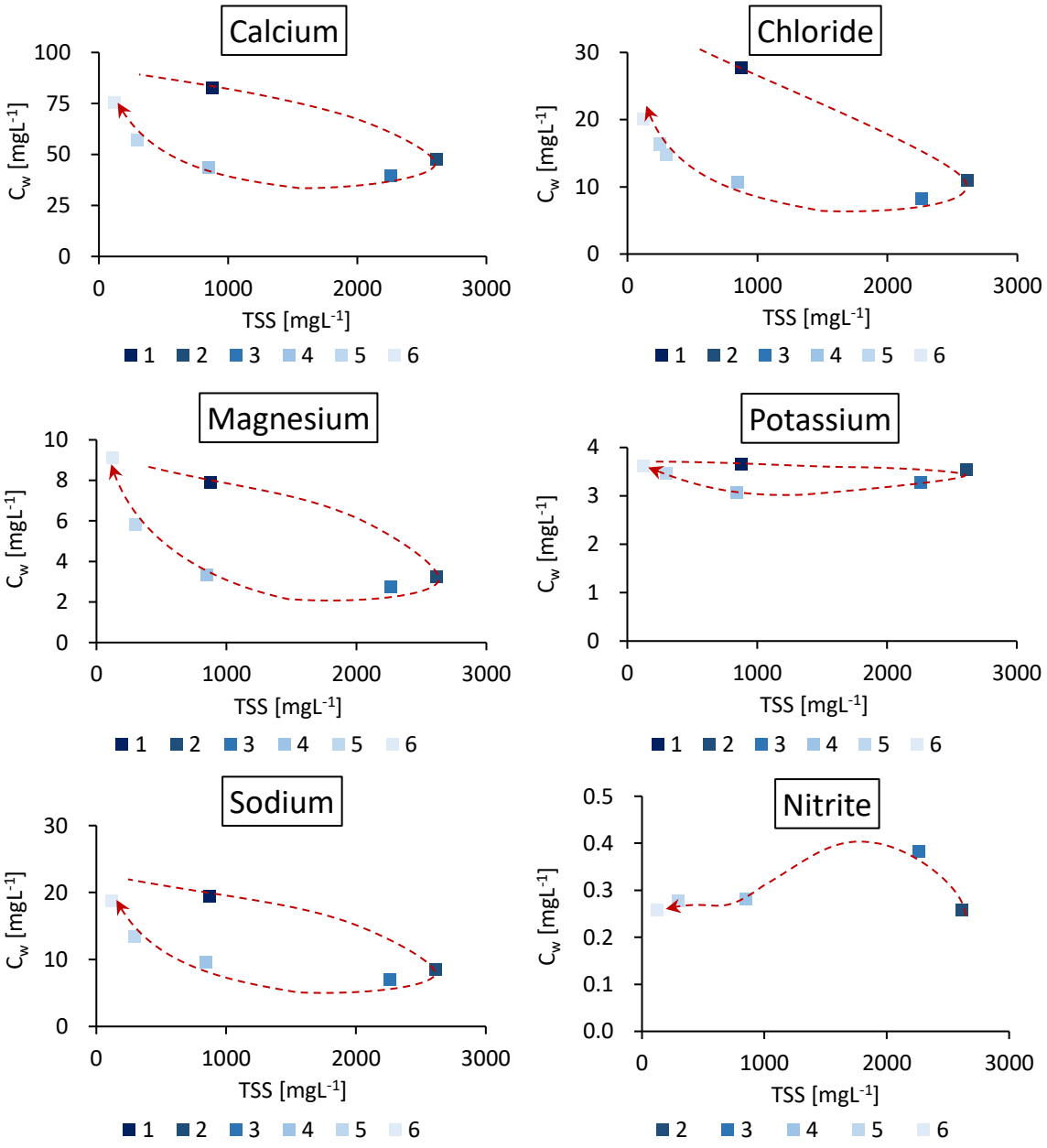

Figure 33. Concentration of inorganic ions presenting hysteresis behaviors versus TSS with sample number during the Steinlach flood.

The general decrease of dissolved concentrations of inorganic ions with increasing TSS indicated dilution of those ions, lower as TSS increased and higher as TSS decreased back along the hystereses. In contrast to the analyzed organic contaminants, that stem almost exclusively from the sewer system, most investigated inorganic ions have a consequent contribution from the catchment geology (see section 5.5.1). The decrease in dissolved concentration was the lowest for potassium that had the highest or second highest contribution from the sewer system of all inorganic ions measured at baseflow during the 24 h and tracer-based samplings, respectively. Reversely, magnesium had the lowest contribution from the sewer system and exhibited the highest dilution during the Steinlach flood. An increase of the potassium to magnesium concentration ratio, plotted along the Steinlach flood in Figure 34, thus should express an increase of the proportion of untreated wastewater over the catchment water. This proportion was highest in sample 2 and 3, where highest concentrations of wastewater contaminants were measured in observed contaminant hystereses. The similar ratios of 0.47 and 0.4 in sample 1 and 6, respectively, indicated a similar proportion of untreated wastewater over the catchment water at the beginning and at the end of the event. However, the strong release of magnesium captured in sample 1, described in the next paragraph, biased the potassium/magnesium ratio and underestimated the proportion of wastewater in the river in that sample. Finally, the fact that nitrite followed a similar pattern as organic contaminants confirmed that it mostly stemmed from the sewer system that was discharging untreated wastewater during the event.

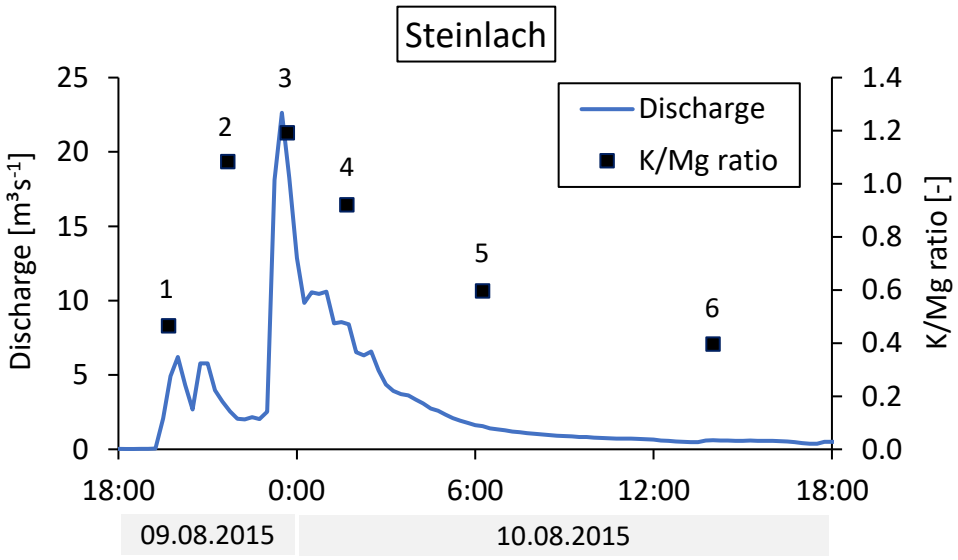

Figure 34. Potassium/magnesium concentration ratio along the flood event sampled in River Steinlach.

Fluxes of wastewater contaminants and inorganic ions generally increased with increasing discharge. The increase of most wastewater contaminants and TSS fluxes was not regular, showing various rises, drops and plateaus along the event. Only mecoprop and caffeine fluxes showed very random behaviors versus discharge. Fluxes of inorganic ions showed more linearity with discharge increase, particularly potassium and nitrite. Only sample 1 really stood out of the distribution with high fluxes of calcium, magnesium, sodium and chloride, hinting to the activation of a source particularly rich in those inorganic ions.

When plotting fluxes of investigated compounds against TSS, a rather resembling pattern was highlighted for fluxes of all investigated organic contaminants and inorganic ions but caffeine and mecoprop (see a selection of compounds in Figure 35). Differences were still observable. Fluxes of

organic contaminants that exhibited hystereses in $C_{w,tot} = f(TSS)$ plots as well as HHCB-lactone were stable between sample 1 and 2 while they were decreasing for all the other compounds (see naproxen, potassium and magnesium in Figure 35), increasing even for caffeine. A clear increase of fluxes was observed between sample 2 and 3 for all investigated compounds but caffeine, to decrease back to low fluxes until sample 6. The concavity observed at sample 4 in $C_{w,tot} = f(TSS)$ plots of lidocaine, ibuprofen and carbamazepine was observable in their fluxes, as well as for diclofenac.

Thus, the hystereses observed seemed more a peculiar result of dilution of compound concentrations for contaminants that had the particularity to exhibit very low fluxes in sample 1 and 2, that were only slightly higher than in sample 5 and 6. Similar particle characteristics and assumed origin in sample 1 and 4, 2 and 3 and 5 and 6 or TSS concentrations did not appear relevant in shaping these patterns. However, similar fluxes of naproxen, TCPP, DEET, TAED and all inorganic ions but nitrate (and nitrite) in sample 1 and 4 happened at similar d50, organic content and concentration of the particles. On the other hand, a great difference in fluxes of all compounds but caffeine was seen despite the similarity between sample 2 and 3, which displayed also the highest proportion of wastewater (see Figure 34). Differences in observed concentration patterns only stemmed from the particular amount of the concerned compound released and diluted in River Steinlach according to the sampling time, implying the existence of various sources releasing a specific composition of contaminant along the Steinlach flood event. As fluxes of inorganic ions decreased back to the sole catchment contribution, fluxes of organic contaminants always decreased towards detection limit at the end of the flood. But high fluxes were already observed for some compounds during sample 1 time as discharge started rising (see naproxen and magnesium in Figure 35). The sampling site being situated above the WWTP, CSOs with particular composition of contaminants and inorganic ions were already activated as discharge was rising and particles mobilized, but all CSOs inputs ceased as discharge came back to base flow and particles settled down.

In a nutshell, the absence of linear correlation between contaminant total concentration and TSS indicated no constant loading of the particles as for PAHs, if sorption of contaminants ever occurred. The precipitation event at the origin of the Steinlach flood induced a strong mobilization of particles parallel to contaminant release through CSOs upstream of the WWTP. Differences in compound concentrations and fluxes according to TSS hinted to a complex dynamic and a diversity of sources, each with specific composition in wastewater contaminants, forming mixtures in the river channel that were captured during the sampling. The dilution of concentration of investigated compounds by catchment water yielded distinctive patterns – e.g. hystereses – that were related neither to the compound properties nor the observed particle characteristics.

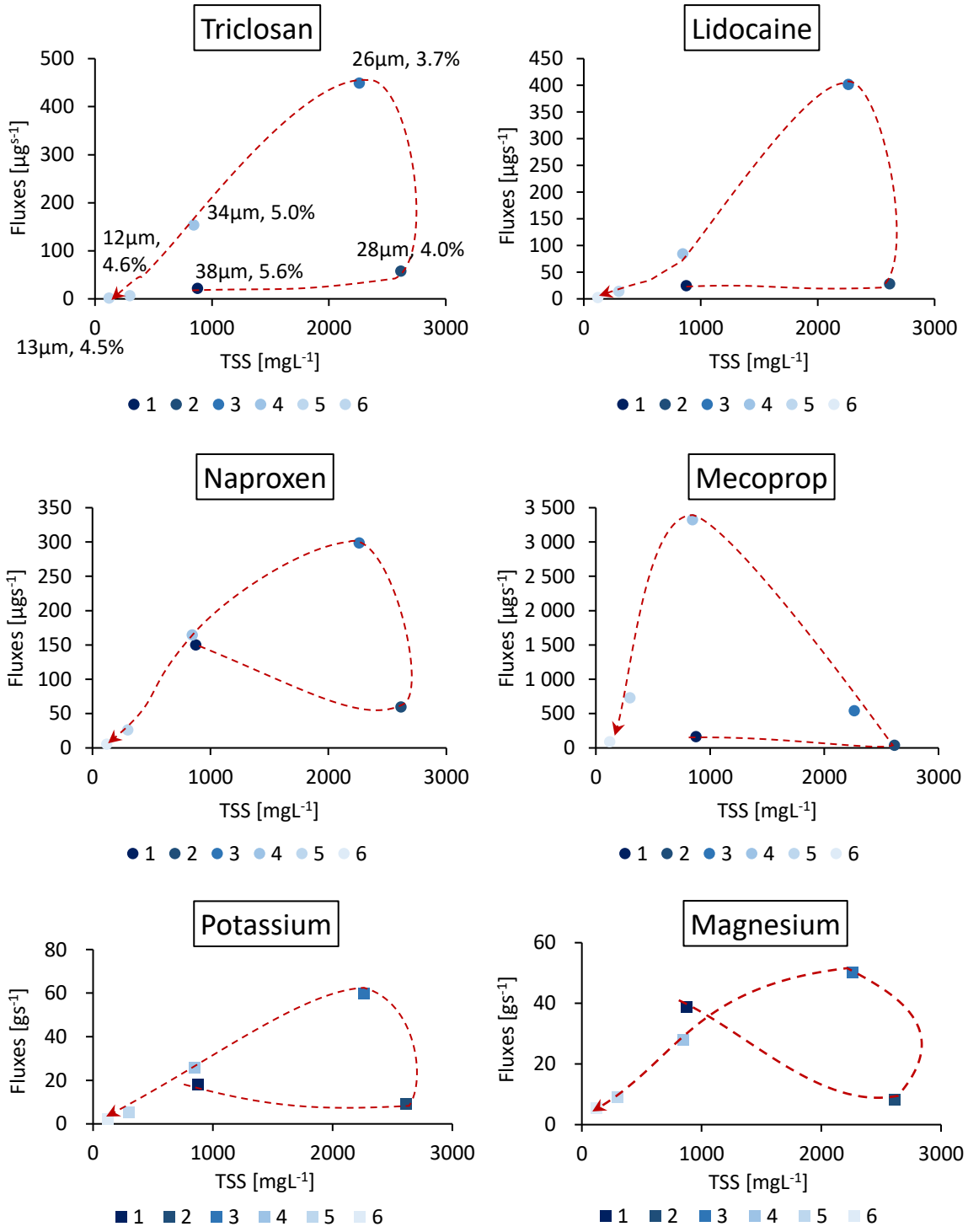

Figure 35. Fluxes versus total suspended solid concentrations (TSS) for example compounds in the Steinlach flood with sample number.

5.4.3.2 River Ammer

Concentrations of ten of the fourteen investigated wastewater contaminants exhibited clear patterns when plotted versus TSS in the flood event captured in River Ammer. Concentrations of caffeine, ibuprofen and TAED showed an anti-clockwise hysteresis behavior in the $C_{w,tot} = f(TSS)$ plots, with comparable concentrations at the beginning and the end of the event, for high and low TSS values (see Figure 36 and Figure S12 in the Appendix). Such circular hystereses implied that for a same compound concentration measured, more particles were released at the beginning than at the end of the Ammer event. In Figure 36, mecoprop concentration was stable over the TSS range observed. Concentrations of triclosan, TCPP, carbamazepine, lidocaine, diclofenac and naproxen increased rather linearly with increasing TSS (see Figure 36 and Figure S12 in the Appendix). However, four of the samples were grouped at the lowest and highest values of TSS with only sample 3 in the middle of the range. AHTN, HHCB, HHCB-lactone and DEET presented a similar distribution along TSS, at the difference that sample 3 was too low to be in alignment with the other samples (see HHCB in comparison with triclosan in Figure 36, and Figure S13 in the Appendix). Only atrazine and desethylatrazine exhibited a slightly higher concentration in sample 3 (see Figure S13 in the Appendix).

Moreover, high concentrations were measured for low TSS values, contrary to the Steinlach flood. Wastewater contaminants being released on a daily basis by WWTPs, concentrations reach up to micrograms per liter in the receiving rivers (e.g. see section 5.1.1). The sampling site of the Ammer flood event was situated 8 km downstream of both the Gäu-Ammer and the Bondorf-Hailfingen WWTPs. Considering the winter and cloudy conditions, it can be assumed that little or no degradation occurred during the transport of the contaminants between their release and Pfäffingen gauge, though musk fragrances might have evaporated into the atmosphere (see section 5.3.2).

Neither hydrophobicity nor electrical charge or the combination of both seemed to influence the correlation of contaminant concentrations with particle release. If triclosan, TCPP, carbamazepine and lidocaine exhibited $\log D_{ow}$ ranging from 2.6 to 4.7 that could induce significant hydrophobic binding to particles (see Table S1 in the Appendix), the musk fragrances AHTN, HHCB and HHCB-lactone, with their $\log D_{ow}$ ranging between 4.7 and 5, did not seem to relate to TSS release. Naproxen was negatively charged with a low $\log D_{ow}$ of -0.4-(-0.5), but so were mecoprop, diclofenac and ibuprofen. Despite being neutral, caffeine and TAED are very soluble, with a $\log D_{ow}$ of -0.6 and -1.8, respectively, but showed the same hysteresis pattern as ibuprofen. Dissociated lidocaine was again the only compound found under cationic form at Ammer pH (between 36.2% and 58.8% according to www.chemicalize.com) but showed a very linear relationship with TSS, similarly to naproxen. Sediment characteristics hardly varied along the discharge event, besides the organic content of sample 5, which d50 was not measured, about 1% higher than other sample particles.

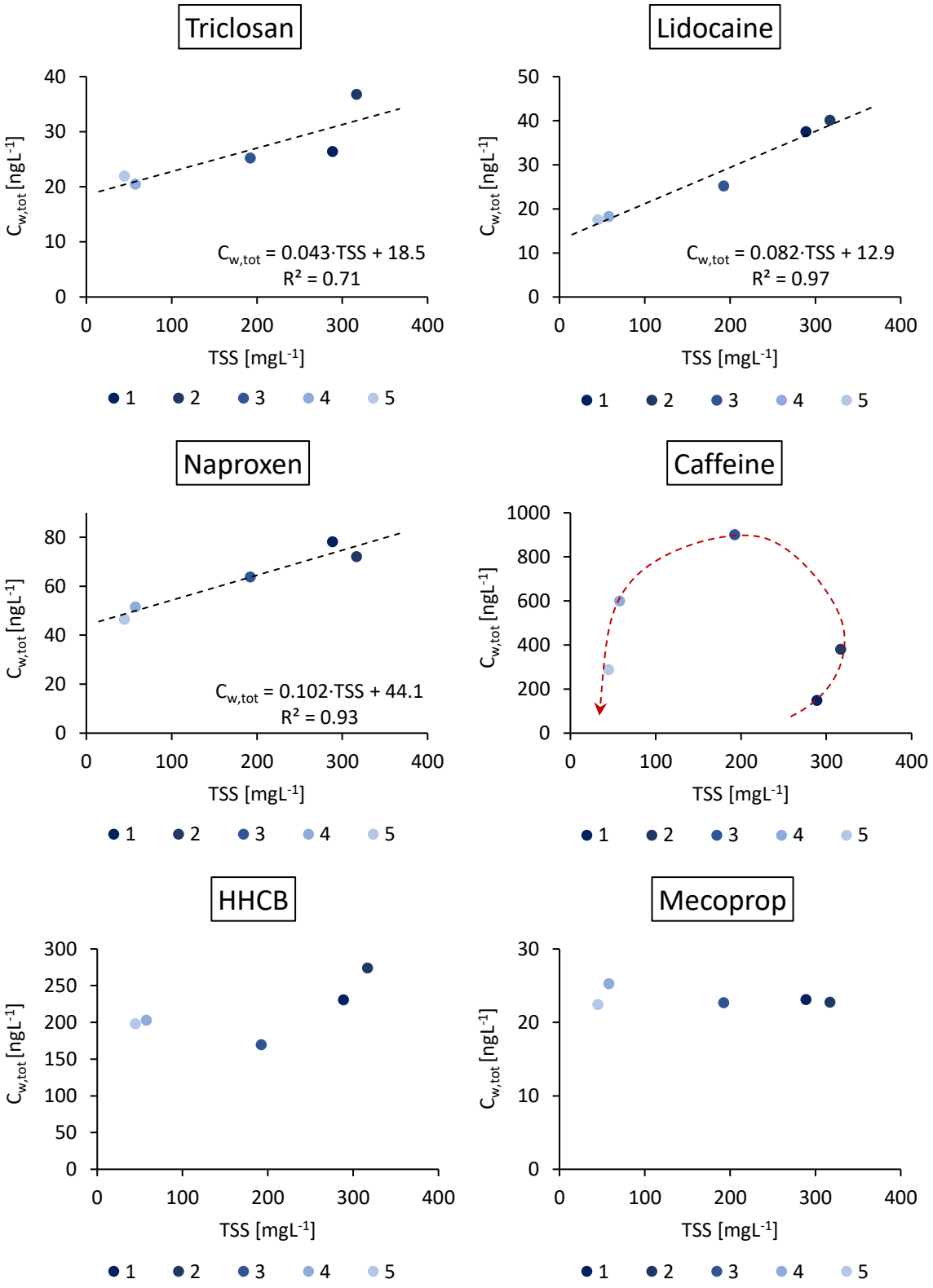

Figure 36. Concentration versus TSS of example contaminants with sample number during the Ammer flood.

The dissolved concentrations of inorganic ions sodium, ammonium, nitrite and chloride also increased linearly with TSS during the Ammer event (see Figure 37 and Figure S14 in Appendix). Only phosphate seemed to decrease with increasing TSS. Magnesium, calcium, sulfate, nitrate and fluoride did not seem

to correlate with TSS variations. Potassium was under the LOQ in the first two samples, as a measurement problem was suspected.

Again, the analysis of inorganic ions being done on filtered samples, the linear increase of their C_w versus TSS cannot indicate particle loading but a common release instead. No data regarding the contribution in inorganic ions from the WWTPs in the Ammer was provided by this work. However, the detection of ammonium and nitrite in every sample indicated the release of untreated wastewater. Sodium and chloride could also originate in higher proportion from wastewater input but also stem from pesticides spread onto crops. Conversely, concentrations of nitrate, fluoride, magnesium, calcium and sulfate might have remained mostly under the influence of the geology of the Ammer catchment during the event, similarly to the Steinlach. The fact that those latter did not correlate with TSS, unlike the more wastewater-related ions, might indicate that particle concentration increased as wastewater reached the sampling location.

It has been seen that particle concentration was rather high in the Ammer event captured in comparison to other works at similar or higher discharge conditions (see section 5.1.3). The limited discharge peak might indeed have a little incidence on bank erosion in the event sampled. Previous works in River Ammer actually proposed that discharge events and particle release were mainly introduced via CSOs while surface run-off from agricultural lands had a small contribution to Ammer discharge (Glaser et al., 2020a; Schwientek et al., 2013a). The decrease of phosphate concentration, primary ingredient in fertilizers that could have been spread in earlier months on agricultural plains of the Ammer catchment, versus TSS hints toward this conclusion. Finally, no hysteresis similar to TAED, ibuprofen and caffeine concentrations was found for inorganic ions.

The study of the EC online-time series during February 2016 showed that the conductivity variations consisted in three to four distinctive peaks per day at the Pfäffingen sampling site. The pattern is attributed to the drinking water exploitation discharging water into River Ammer in Poltringen, 1 km upstream of Pfäffingen. During the Ammer flood sampled, sample 1, 3 and 5 were on (diluted) peaks and 2 and 4 on (diluted) drops of the EC signal that could be recognized despite the dilution by the discharge increase (see Figure S15 in the Appendix). EC did not correlate with concentration of any of the investigated wastewater contaminants, inorganic ions (data not shown) or with TSS (see Figure 37). Still, dilution from water discharge by the drinking water production site might affect the correlations between TSS and concentrations of wastewater contaminants or inorganic ions, particularly as the discharge event captured remained small and concentrations stayed in the same order of magnitude during the event. In addition, a shorter residence time in the WWTPs upstream due to increase of incoming water from precipitation could have also caused a limited removal of contaminants and their release in higher quantities through the WWTP effluents.

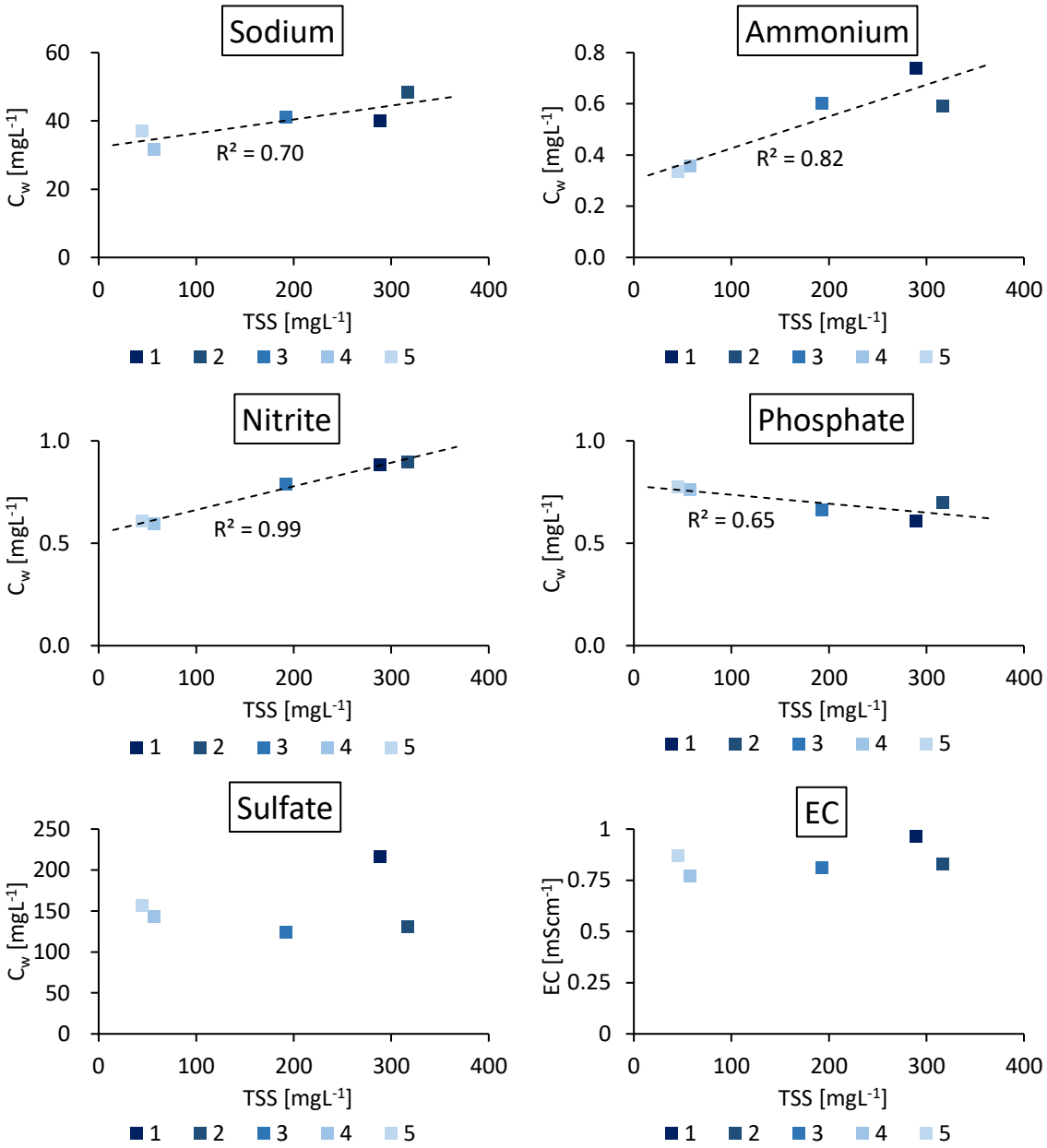

Figure 37. Concentration of inorganic ions and electrical conductivity (EC) versus TSS with sample number during the Ammer flood.

Fluxes of TAED, caffeine and ibuprofen increased up to the third sample before decreasing until the end of the event, with similar fluxes in sample 1 and 5 for TAED and caffeine (data not shown). Despite the small discharge range, fluxes of all other compounds but pesticides generally decreased steeply with decreasing discharge, though HHCB, AHTN, lidocaine, diclofenac and TSS had their highest fluxes in the second sample. Fluxes of HHCB, AHTN, HHCB-lactone and TSS remained similar in the last two samples while a decrease was still observable for the other compounds. Fluxes of pesticides mecoprop, atrazine and desethylatrazine decreased more gradually with discharge. Mecoprop being an herbicide spread over gardens in urban areas and atrazine being applied on crops before its ban in Germany in 1991, they and desethylatrazine should stem from run-off from both urban and agricultural surfaces unlike the more wastewater-derived compounds. Fluxes of calcium, magnesium and sulfate decreased steeply and stabilized towards the end of the event while ammonium, nitrate and fluoride still exhibited

a decrease in the late samples. Phosphate, nitrite, chloride and sodium had a more gradual distribution with their highest fluxes in sample 2. Thus, the highest release of most analyzed contaminants and inorganic ions was seen in the first two samples, at the beginning of the event, and a gradual, more limited release was mostly linked to compounds related to agriculture. The common stabilization of fluxes of particles and some wastewater contaminants in sample 4 and 5 comforts the hypothesis on the sewer provenance of particles captured in the Ammer event and the occurrence of a flush effect responsible for high TSS concentrations. However, not all wastewater contaminants followed this pattern, hinting towards the existence of specific composition of various CSO releases. Finally, the gradual decrease of fluxes of herbicide-related compounds with discharge revealed a small contribution of the urban and agricultural lands of the Ammer catchment.

In a nutshell, particle-associated transport could not be confirmed as a linear increase of total concentration of six organic contaminants versus TSS was also observed for dissolved concentrations of more wastewater-related inorganic ions. Though a small participation of the catchment was observed, a flush effect from the CSOs (or WWTPs) was assumed to be responsible for the strong release of particles parallel to contaminants in the discharge event of River Ammer. Particle-associated transport, if any, could not be related to properties of the particles captured or of the organic contaminants involved.

5.4.3.3 The Steinlach pre-sampling campaign

TSS was not measured for the "pre-sampling" in River Steinlach of June 2013 but measured turbidity was converted to TSS. According to the *m* value of 1.26 determined in section 5.4.2, TSS ranged from 1.2 to 16.5 mgL^{-1}, the lowest values corresponding to the WWTP effluent samples.

The samples downstream of the effluent had a turbidity range of 11.5 to 12 NTU (TSS=14.5-15.1 mgL^{-1}) that did not allow correlation with particle concentration. The samples taken upstream of the WWTP and in the tributaries offered a bigger range of turbidity but no correlation between contaminant concentrations and turbidity variations was found.

The filtration of water samples showed that part of the contaminants was retained with the particles during the filtration process (see Table 13). The highest percentages were found for artificial musk fragrances AHTN, HHCB and its metabolite HHCB-lactone – up to 33% – and to a lower extent for the flame retardant TCPP and the bleaching agent TAED. Besides TAED that is highly soluble, those compounds have $\log D_{ow}$ higher than 3 (see Table S1 in the Appendix). Artificial musk fragrances being volatile, except HHCB-lactone according to observations in section 5.3.2, there is the possibility that filtration have allowed their evaporation from the water samples. The other compounds exhibited less than 10% difference between filtered and unfiltered samples. However, the filtration retained very variable proportions of contaminants between the different locations, even for samples of the main stem, that had similar contaminant concentrations and turbidities.

Table 13. Differences between concentrations measured on filtered and unfiltered samples (over the concentration measured on unfiltered samples) during the "pre-sampling" in River Steinlach.

	Carbamazepine	Caffeine	HHCB	HHCB-lactone	AHTN
Upstream of the WWTP effluent (-5 m)	-1%	1%	5%	28%	12%
Steinlach 1 (+930 m)	6%	12%	6%	16%	4%
Steinlach 2 (+1740 m)	6%	3%	12%	14%	33%
Steinlach 3 (+2740 m)	1%	-2%	20%	24%	6%
Steinlach 4 (+3490 m)	7%	-5%	6%	30%	29%
Steinlach confluence (+4240 m)	6%	0%	2%	2%	31%
1st Effluent sample	2%	5%	18%	21%	49%
2nd Effluent sample	2%	7%	13%	21%	45%
Ehrenbach	9%	-1%	-1%	5%	0%
Tributary ②	11%	9%	20%	20%	5%
Tributary ④	/	23%	-14%	-2%	5%

	TCEP	TCPP	DEET	TAED
Upstream of the WWTP effluent (-5 m)	-4%	10%	/	17%
Steinlach 1 (+930 m)	7%	9%	4%	26%
Steinlach 2 (+1740 m)	3%	15%	3%	2%
Steinlach 3 (+2740 m)	4%	9%	8%	15%
Steinlach 4 (+3490 m)	10%	3%	6%	-2%
Steinlach confluence (+4240 m)	6%	8%	2%	1%
1st Effluent sample	-1%	5%	7%	9%
2nd Effluent sample	-2%	8%	10%	2%
Ehrenbach	0%	16%	13%	0%
Tributary ②	-1%	10%	/	/
Tributary ④	-3%	21%	/	/

5.4.4 Discussion

Data from the Steinlach and Ammer floods investigated could not help distinguishing whether correlations of contaminant concentrations with TSS implied the occurrence of sorption or only a common release. In River Steinlach, hystereses patterns observed for total concentrations of triclosan, HHCB, AHTN, lidocaine, ibuprofen and carbamazepine and dissolved concentrations of inorganic ions versus TSS were attributed to the varying dilution of releases from the compound sources in the Steinlach catchment upstream of the WWTP. Assumed particle provenance seemed to differ from contaminant release and particle-associated transport could not be confirmed. If any, the hystereses observed ruled out constant loading of the particles along the flood event. In the Ammer event, the increase of total concentration of triclosan, lidocaine, carbamazepine, naproxen, diclofenac and TCPP was assumed to be synchronous with particle release, presumably from sewer systems or the WWTPs upstream. The same was observed for dissolved concentrations of inorganic ions that were presumed rather wastewater-related, such as sodium, ammonium, nitrite and chloride, ruling out their particle-associated transport.

Each flood from each river exhibited a relationship between some wastewater contaminants and particle release, though different patterns were observed, and different compounds were concerned. Despite not being highly hydrophobic, carbamazepine and lidocaine followed a similar hysteresis pattern versus TSS in the Steinlach while concentrations of carbamazepine and lidocaine linearly increased versus TSS in river Ammer. If the hysteresis observed for ibuprofen concentrations in the Steinlach event showed a similar hysteresis pattern versus TSS, ibuprofen circular hysteresis in the Ammer event implied a temporal pattern independent from TSS release. HHCB and AHTN showed hysteresis behaviors in the Steinlach flood but no correlation versus TSS in the Ammer event. Conversely, naproxen, diclofenac and TCPP showed linear correlations versus TSS in the Ammer flood but more erratic behaviors in River Steinlach. Concentration of caffeine, TAED and mecoprop did not correlate versus TSS concentration in the Steinlach event while in the Ammer flood, concentration of caffeine and TAED showed a circular hysteresis shape versus TSS, similarly to ibuprofen, and mecoprop was stable over the TSS range.

The particle characteristics assessed during the present study did not explain either why some contaminants showed a correlation with TSS. Common particle characteristics at similar TSS concentrations and of assumed similar provenance led to different concentrations of wastewater contaminants in the Steinlach flood. Finer particles in the Ammer, with higher contact area and homogeneous characteristics except for the higher organic content in the last flood sample, could have led to the clearer correlation of total concentrations with TSS than the Steinlach. The average organic content was similar between particles captured in the Steinlach and the Ammer flood, but organic contaminants did not react similarly, besides triclosan that generally increased with TSS in both floods.

As it was assumed in section 5.4.3, an increase of TSS parallel to contaminant concentration could either be concomitant with the arrival of untreated wastewater at the sampling location or be due to a flushing of sewer particle as CSO occurs. In the first case, short transit times through the river network appointed to equilibration of wastewater with environmental particles due to fast flow conditions may limit sorption. Sorption of ionic species involved weak binding processes (see section 3.6.2) with sediments that may be even more hindered by turbulences met during higher discharge conditions. Sewer particles may have reached equilibrium due to their storage in the sewer network where wastewater constantly flows. But the release of particles, contaminated or not occurred as wastewater and thus dissolved contaminants were released as well. If input of contaminants under dissolved form is not fully compensated by dilution from increased river discharge, solely C_w or both C_w and C_{sus} can increase with TSS during the floods captured. C_w of wastewater-related inorganic ions increased indeed with TSS during the Ammer flood and the same can be expected from wastewater contaminants. That neither hydrophobicity nor the charge or the combination of both could be identified as a certain factor

explaining a relationship between contaminant and TSS concentration would also orient conclusions towards a common release of contaminants and particles rather than purely particle-associated transport.

Still sorption mechanism can occur. The increase in concentration of wastewater contaminants was rather low compared to PAHs in former studies (Rügner et al., 2014; Schwientek et al., 2013b). Unlike PAHs, which are highly hydrophobic compounds mostly transported in rivers bound to particles during high discharge conditions, concentrations of wastewater contaminants remained in the same order of magnitude, similarly to what was observed in Kolpin et al. (2004), or increased by a factor of ten. TSS increased up to three orders of magnitude during the events sampled (up to 317 mgL^{-1} in the Ammer flood and up to 2614 mgL^{-1} in the Steinlach flood). An overestimation of contaminant partitioning to particles was calculated from the data collected in the Ammer flood to assess the maximum proportion of particle-bound contaminants during the event. To do so, constant particle loading and a negligible increase of C_w during the Ammer flood compared to the increase of $C_{sus} \cdot TSS$ was assumed, as for PAHs in Schwientek et al. (2013b). The slopes of the linear $C_{w,tot} = f(TSS)$ regressions for wastewater contaminants would then represent solely C_{sus}. An apparent K_d was calculated for each concerned contaminant using this apparent C_{sus} concentration and the intercept of the linear regression as C_w using equation (1). The maximum proportion of wastewater contaminants on the solid phase during the Ammer flood was estimated from these same terms, still assuming that only contaminated particles but no contaminated water were released. Table 14 shows that the maximum proportion of wastewater contaminants bound to particles in the flood samples of the Ammer event remained under 51% for TSS of about 300 mgL^{-1}, except for lidocaine with up to 67%. The share of particle-bound transport decreased then for lower values of TSS in the late samples to reach a similar value as for the pre-sampling campaign (see Table 13). In addition, that raw wastewater was discharged during the event and that C_w would increase would lessen this estimated proportion of particle-bound contaminants over dissolved ones.

Table 14. Maximum proportion of contaminant mass sorbed onto particles in samples of the Ammer flood, estimated using apparent K_d and measured TSS.

		Apparent K_d [Lkg^{-1} TSS]					
		2464	1769	6357	2313	3341	2324
Sample	TSS [mgL^{-1}]	Carbamazepine	Diclofenac	Lidocaine	Naproxen	TCPP	Triclosan
1	289	42%	34%	65%	40%	49%	40%
2	317	44%	36%	67%	42%	51%	42%
3	192	32%	25%	55%	31%	39%	31%
4	57	12%	9%	27%	12%	16%	12%
4	58	12%	9%	27%	12%	16%	12%
4	58	12%	9%	27%	12%	16%	12%
5	45	10%	7%	22%	9%	13%	9%

5.4.5 Investigation method discussion

$C_{w,tot} = f(TSS)$ cannot be used to identify and quantify particle-associated transport of wastewater contaminants, as it was done for PAHs, as wastewater contaminants can be released both under dissolved and sorbed state during CSO discharge. PAHs, on the other hand, are almost exclusively sorbed onto land-surface particles through atmospheric deposition and released in rivers exclusively on washed-off surface particles during precipitation events, or from concomitant resuspension of contaminated sediment reserves in the river network during flood events (Schwientek et al., 2013b). Repeating flood sampling and adding analysis of field-filtered and unfiltered samples would give a definitive answer on whether wastewater contaminants actually bind to the particles transported during flood events.

The study of discharge patterns during previous floods in the investigated catchments during the preparation phase of the samplings allowed dimensioning the sampling but the capture of the right peaks remained a question of luck. The saturation of soils at the time of the rain, the duration, intensity and temporal variation of the precipitation causing a flood has a strong influence on the shape of the hydrograph obtained, in addition to catchment specificities such as its morphology or slope. The Steinlach discharge peak ③ would have not been so well captured if the two minor discharge peaks ① and ② had not triggered the autosampler before, and at the right timing. The minimum sampling pace of 2 h could also have missed variations in the contaminant fluxes and concentrations. A higher sampling pace could increase the chances to capture the interesting steps of contaminant release during flood events and provide more points for correlations with TSS, which was however not feasible with the sample volume required.

Finally, the choice of the location should be oriented upstream of WWTPs if possible, to prevent the interference of contaminant background concentrations caused by the diurnal pattern from effluent discharge in the correlations with TSS, as it was the case in River Ammer.

5.5 Fluxes of wastewater contaminants in investigated rivers

5.5.1 Contribution of the WWTP during dry weather conditions

Estimated contributions of the Steinlach-Wiesaz WWTP to fluxes monitored during the tracer-based and the 24 h-sampling campaigns in River Steinlach are given in Table 15 and 16, respectively.

During the tracer-based experiment, the contribution of the WWTP to fluxes of most organic contaminants reached ~99-100% with a lowest value of 94% for DEET, besides atrazine with 71 to 78%. The contribution of the WWTP to investigated compounds did not vary between day and night, due to the similar proportions of treated water in the two experiments (74% and 77% of the discharge flowing into the studied segment, respectively). The Steinlach-Wiesaz contributed to more than 90% of fluxes of chloride, nitrate, phosphate, potassium and sodium during the tracer based-sampling.

During both 24 h campaigns, the WWTP contributed more than 90% of the fluxes of most organic contaminants entering the studied segment. Oxcarbazepine and mecoprop in winter, AHTN and TAED constituted exceptions that could be explained by the low concentrations measured (less than 20 ngL^{-1}) in the main reach and considering the few ngL^{-1} measured upstream of the WWTP and in tributaries. TCEP, atrazine, desethylatrazine as well as all inorganic ions had contributions of the WWTP under 90%. Contribution of the WWTP for compound fluxes was comparable between summer 2013 and winter 2014 for all compounds but mecoprop, DEET, oxcarbazepine, triclosan, calcium and sulfate, that had a lower WWTP contribution during the winter campaign. TAED was the only analyzed compound with a significantly higher contribution of the WWTP during the winter campaign. The WWTP contributed to more than 50% of fluxes of chloride, nitrate, potassium and sodium during both 24 h-sampling campaigns with a maximum of 76% (for potassium).

According to WWTP contributions calculated for investigated compounds, the WWTP is the main source of organic contaminants during dry weather conditions. Indeed during dry-weather conditions, besides potential leaks of the sewer system (Musolff et al., 2010; Rutsch et al., 2006; Wolf et al., 2012) in the Steinlach catchment, the contaminants produced from urban areas are directed to the WWTP and only exit through the effluent by resisting treatment. The higher contribution of the WWTP to compound fluxes measured in summer compared to winter and in summer 2015 compared to summer 2013 could be linked to lower discharge and subsurface flow that transfer the contaminants in soils and groundwater to the river network. The decrease of WWTP contribution to pesticide fluxes such as DEET, mecoprop or atrazine with decreasing discharge conditions would support this conclusion. The presence of wastewater contaminants in water bodies that are not impacted by WWTP effluent discharge (i.e. upstream of the WWTP and in tributaries), could as well be explained by such diffuse intrusion of the contaminants into the river network. Additionally, combined sewer overflows occurring during strong rain events all over the catchment can discharge large amounts of wastewater-related contaminants (Musolff et al., 2010; Radke et al., 2010) that might be stored bound to particles of the riverbed or in the hyporheic zone.

The inorganic ions with highest WWTP contribution were in all baseflow campaigns potassium, sodium, nitrate, chloride as well as phosphate while fluxes of magnesium, calcium and sulfate seemed more influenced by the catchment geology. Potassium was the inorganic ion with the highest WWTP contribution and has been reported as tracer ion for wastewater discharge in literature (Nödler et al., 2011).

Table 15. Contribution [%] of the Steinlach-Wiesaz WWTP in the fluxes of investigated compounds entering the studied river segment of River Steinlach during the day- and night-time experiments of the tracer-based samplings.

	2-Aminobenzimidazole	Acesulfame	Amisulpride	Atenolol	Atrazine	Benzotriazole	Bisoprolol
Day experiment	100	96-97	100	100	75-78	100	100
Night experiment	100	96-97	100	100	71-73	100	100
	Candesartan	Carbamazepine	Carbendazim	DEET	Denatonium	Desvenlafaxine	Diatrizoic acid
Day experiment	100	100	100	94-96	100	100	98
Night experiment	100	100	100	95	100	100	98
	Diclofenac	Gabapentin	Iopamidol	Irbesartan	Lamotrigine	Lidocaine	Metoprolol
Day experiment	100	100	98-99	100	100	100	100
Night experiment	100	100	99	100	100	100	100
	Olmesartan	Oxcarbazepine	Primidone	Salbutamol	Sitagliptine	Sotalol	Sucralose
Day experiment	100	100	100	100	100	100	100
Night experiment	100	100	100	100	100	100	100
	Sulfamethoxazole	Sulpiride	TAED	TCPP	Tiapride	Torasemide	Tramadol
Day experiment	100	100	100	99-100	100	100	100
Night experiment	100	100	100	99-100	100	100	100
	Trimethoprim	Valsartan	Venlafaxine	Calcium	Chloride	Magnesium	Nitrate
Day experiment	100	100	100	80	90-91	81-82	98-99
Night experiment	100	99-100	100	77	90	78-79	98
	Phosphate	Potassium	Sodium	Sulfate			
Day experiment	95-96	96-97	93	87-89			
Night experiment	94-95	96	92	87			

Table 16. Contribution [%] of the Steinlach-Wiesaz WWTP to the total mass fluxes of investigated compounds entering the studied river segment in River Steinlach during the summer and winter 24 h-sampling campaigns.

	AHTN	Atrazine	Carbamazepine	DEET	Desethylatrazine	Diclofenac	HHCB
Summer[1]	81-89	/	98-99	99-100	/	100	96-98
Winter	89-92	48-84	97-98	90-93	0	/	98-99
	HHCB-lactone	Lidocaine	Mecoprop	Naproxen	OTNE	Oxcarbazepine	TAED
Summer[1]	96-98	/	98-99	99-100	96-98	98-100	41-77
Winter	98	96-97	54-71	97-98	98	80-89	87-95
	TCPP	TDCPP	TCEP	Triclosan	Calcium	Chloride	Magnesium
Summer[1]	96-98	92-95	/	97-99	29-45	50-64	16-32
Winter	98-99	94-95	39-77	93-95	18-27	54-62	19-27
	Nitrate	Potassium	Sodium	Sulfate			
Summer[1]	51-66	65-76	57-69	30-50			
Winter	60-69	68-75	53-62	27-34			

[1]The calculation did not account for the samples impacted by the effluent stop of the WWTP.

5.5.2 Monthly sampling

Turbidity captured during the monthly sampling being mostly low, no relationship between contaminant concentrations and turbidities could be identified.

In River Goldersbach, the suspected analytical problem hindered the proper estimation of fluxes of contaminants at least at the WESS-gauge location. Despite unrealistic contaminant detection, a calculation from the measured data provided very limited fluxes of contaminants at both Goldersbach sampling sites, displayed in Table 17. The potential overestimation of fluxes at the WESS gauge and maybe also at the mouth location in Tübingen City due to possible analytical bias did not allow concluding on the expected influence of the urban areas between the two locations. Still, an increase of fluxes between the two locations could be seen mostly during the snow melting events, for musk fragrances, caffeine, TCEP and TCPP, where CSOs were expected. Concentrations of contaminants used were similar in those samples as in the others, which can either be explained by cross-contamination or dilution of CSO releases in the lower section of River Goldersbach by a sufficient proportion of catchment water.

In River Steinlach, fluxes of musk fragrances, caffeine, TCPP, TAED and triclosan upstream of the WWTP remained low at discharge up to 4.5 m^3s^{-1} and only increased by up to two orders of magnitude at 12 m^3s^{-1} during the first snow-melting event in December 2010. Fluxes of pharmaceuticals showed a small scattering at low discharge and were not measurable at higher discharge presumably due to high dilution. Fluxes of TCEP, TDCPP and DEET did not show any pattern versus discharge. Downstream of the WWTP, higher fluxes of contaminants exhibited a scattered distribution in all samples. Only TAED, triclosan, flame retardants, caffeine and HHCB showed significantly higher fluxes than during baseflow conditions at the 15 and 6 m^3s^{-1} discharge captured by the December 2010 and January 2011 samples, respectively.

In River Ammer, none of the contaminant fluxes besides atrazine correlated with discharge conditions, and only TAED and, to a lower extent, HHCB showed significantly higher fluxes during the snow-melting events in December 2010 and January 2011. During dry weather conditions, elimination was expected within the 8 km separating the WWTPs and Pfäffingen (Glaser et al., 2020b). However, besides atrazine, fluxes of which decreased from winter to fall as discharge decreased, fluxes of no contaminant showed a seasonal pattern, even DEET which is principally used during summer.

The data provided by the monthly sampling confirmed conclusions obtained from the present work. During dry-weather conditions, differences in fluxes (see Table 17) between upstream and downstream of the Steinlach WWTP showed that WWTPs were major sources of contaminants, though factors driving their input could not be understood with the given data. The snow-melting events in December 2010 and January 2011 created a significant increase of fluxes for only some wastewater contaminants. Those contaminant releases being unrelated to the contaminant degradability (e.g. TAED, caffeine or HHCB against the persistent flame retardants) highlighted the activation of specific sources, presumably CSOs, with particular compositions within the investigated catchments.

Table 17 also presents fluxes of the sum of 15 PAHs (PAH15) analyzed in Schwientek et al. (2013b). The study highlighted the predominant transport of PAHs on particles, released into river networks through CSO discharge of urban surface run-off and resuspension of contaminated sediments during precipitation and consequent high-discharge events. Minimum fluxes of PAH15 were indeed measured at low-flow conditions during dry-weather and were similar to lowest fluxes of single wastewater contaminants in River Goldersbach and Steinlach upstream of the WWTP. But fluxes of PAH15 met during high discharge conditions following precipitation events were up to two orders of magnitude higher than highest fluxes met during those conditions for single wastewater contaminants.

Table 17. Ranges of fluxes in [µgs^{-1}] calculated from the discharge estimations and concentrations measured during the monthly sampling in Rivers Goldersbach, Steinlach and Ammer between 2009 and 2011.

		AHTN	Caffeine	Carbamazepine	DEET	Diclofenac	HHCB	HHCB-lactone
Goldersbach	WESS gauge	0-3.7	0-81	0	0-3.8	0	0-4.2	0-12
	Mouth	0-7	0-300	0	0-0.8	0	0-4.6	0-11
Steinlach	upstream of the WWTP	0-46	3-4155	0-6	0-18	0	0-135	1-89
	downstream of the WWTP	10-142	3-11398	15-116	9-105	16-55	53-534	20-650
Ammer	WESS gauge	7-127	8-1431	43-282	9-89	6-69	33-380	19-653
		Lidocaine	TAED	TCEP	TCPP	TDCPP	Triclosan	PAH15*
Goldersbach	WESS gauge	0	0-4.4	0-28	0-8.0	0-0.4	0-8.8	0.3-88
	Mouth	0-0.1	0-8	1.6-30	0-30	0-3.1	0	/
Steinlach	upstream of the WWTP	0-1	0-1611	1-136	0-353	0-18	0-48	0-5100
	downstream of the WWTP	0-34	7-3888	24-511	147-737	12-265	0-159	3-5592
Ammer	WESS gauge	5-68	0-993	34-189	159-647	14-320	0-27	39-989

*(Schwientek et al., 2013b).

5.5.3 Estimation of fluxes in the Steinlach and other contrasting catchments

Section 5.3 showed how attenuation processes, driven by environmental parameters, reduced fluxes of wastewater contaminants in River Steinlach, reaching up to complete removal at the end of the investigated segment. This decrease of contaminant fluxes with distance from the source follows the temporal variability of environmental conditions favorizing attenuation processes. In addition, though section 5.5.1 confirmed that the Steinlach-Wiesaz WWTP was the major source of wastewater contaminants in River Steinlach during dry-weather conditions, section 5.4 showed that the occurrence of precipitation activated other sources of contaminants in the Steinlach catchment. Thus, to estimate fluxes of wastewater contaminants, one must also account for spatial heterogeneities in contaminant release (i.e. point sources) and the temporal variation of sources activation and outflow (Musolff et al., 2009).

Temporal patterns observed in fluxes right downstream of the Steinlach-Wiesaz WWTP effluent, reflecting variations of WWTP input, varied from one compound to another, along one single day as well as between seasons (see Table 19). Daily variability was higher for wastewater contaminants, that had the WWTP as main contributor compared to most inorganic ions, and during summer 2013 compared to winter 2014. The release patterns over 24 h or according to season did not seem to correspond to compound degradability observed in the Steinlach stretch downstream of the WWTP in section 5.3. Flux variability may stem from the high variability in composition of wastewater-contaminant sources identified from flood sampling data (see sections 5.4.4 and 5.5.2) that mixing of wastewater within the treatment basins of the WWTP may have only partly homogenized. Sorption to activated sludge or enhanced degradation during WWTP treatment might also have affected each compound differently. Similarly, the higher efficiency of WWTPs expected in summer did not lead automatically to lower input fluxes of contaminants compared to winter season. Fluxes of persistent TCPP and carbamazepine were similar between the two seasons, but also for TAED and triclosan. Fluxes of TDCPP, oxcarbazepine, HHCB-lactone, DEET and mecoprop were lower in average in winter. The influence of the contaminant use in such case was recognizable for DEET, released fluxes of the insect repellent, applied mostly during the summer season, being very low in winter.

Within 24 h-time series and between 24 h loads measured from the winter and summer samplings downstream of the Steinlach-Wiesaz WWTP, fluxes varied with less than a factor of three for all compounds (see Table 18). From the data of the monthly sampling taken at low-flow conditions downstream of the WWTP, the minimum variability was found for TCPP fluxes, varying within a factor of 2.3, while fluxes of HHCB-lactone varied within 33 folds. Though higher discharge conditions were removed from the dataset, rain events might have preceded some samplings, but it was assumed that the low-flow samples from the monthly sampling captured a representative variability of contaminant fluxes during dry-weather conditions. The larger scatter of the monthly data was thus attributed to the larger variability of environmental conditions captured compared to the two 24 h-sampling spans. Also, ranges of fluxes of TCPP, triclosan and diclofenac monitored by the monthly sampling downstream of the WWTP in River Steinlach did not overlap fluxes captured during the 24 h-sampling campaigns (see Table 19). Either the range from the monthly sampling was not representative or fluxes of those compounds changed between 2009-2011 and 2013-2014.

The contrast between carbamazepine and HHCB-lactone illustrates difficulties in estimating yearly loads from such variable dataset. HHCB-lactone results from the metabolization of the artificial musk fragrance HHCB by bacteria in the sewer network and during the WWTP treatment, being itself susceptible to seasonally variable photo-independent elimination (see section 5.3.2). Fluxes of the persistent carbamazepine, which as a pharmaceutical has a different production path from HHCB-lactone, has less absolute and relative variability (see Table 18 and Figure 38). If considering using mean fluxes monitored at low flow conditions during the monthly sampling to extrapolate to yearly

loads of contaminants, the less dispersed distribution of carbamazepine fluxes would be more reliable than the one of HHCB-lactone.

Table 18. Ratio between maximum and minimum fluxes calculated downstream of the WWTP in River Steinlach during the summer and winter 24 h samplings and during the monthly sampling at low flow, and ratio of 24 h-loads between winter and summer for a selection of compounds.

	AHTN	Carbamazepine	DEET	Diclofenac
Summer 24 h sampling[1]	1.7	1.7	2.2	1.8
Winter 24 h sampling	1.4	1.5	1.6	/
Winter/summer 24 h sampling	2.1	1.1	0.1	/
Monthly sampling	14.2	7.9	12.0	3.5
	HHCB	HHCB-lactone	TAED	TCEP
Summer 24 h sampling[1]	1.6	1.8	2.6	2.4
Winter 24 h sampling	1.4	1.8	2.6	/
Winter/summer 24 h sampling	2.7	1.1	1.6	/
Monthly sampling	3.5	32.7	7.3	6.6
	TCPP	TDCPP	Triclosan	
Summer 24 h sampling[1]	2.0	1.6	1.8	
Winter 24 h sampling	1.6	2.0	1.7	
Winter/summer 24 h sampling	1.0	0.9	1.2	
Monthly sampling	2.3	10.1	6.7	

[1]Flux calculation did not account for the effluent stop.

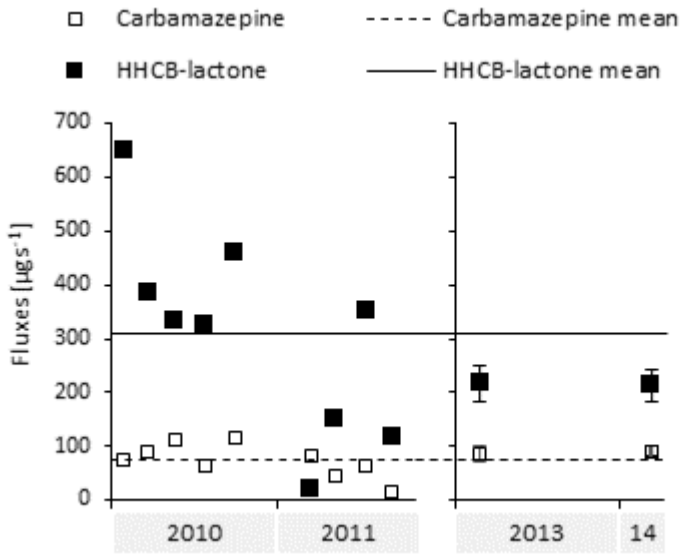

Figure 38. Fluxes of carbamazepine and HHCB-lactone downstream of the WWTP in River Steinlach at baseflow during the monthly (2010-2011) and the 24 h samplings (2013 and 2014).

Table 19. Comparison of fluxes in [µgs^{-1}] of a selection of organic contaminants during various flow conditions in River Steinlach downstream of the WWTP and in the Steinlach flood upstream of the WWTP.

	AHTN	Carbamazepine	DEET	Diclofenac
Summer 24h sampling[1]	5-9	65-110	26-56	173-309
Winter 24h sampling	13-18	70-102	4-6	/
Monthly sampling - low flow	10-142	15-116	9-105	16-55
Dec.2010 ; Jan.2011*	116 ; 69	86 ; 74	81 ; 39	48 ; 35
Steinlach flood[2]	4-833	8-872	4-346	18-73
	HHCB	HHCB-lactone	Lidocaine	TAED
Summer 24h sampling[1]	34-54	150-272	/	5-13
Winter 24h sampling	97-134	132-244	8-20	7-17
Monthly sampling - low flow	53-185	20-650	0-34	7-49
Dec.2010 ; Jan.2011*	534 ; 297	534 ; 233	0 ; 12	3888 ; 691
Steinlach flood[2]	7-1502	35-2111	2-402	3-566
	TCPP	TDCPP	Triclosan	
Summer 24h sampling[1]	71-140	20-31	9-16	
Winter 24h sampling	71-112	13-26	11-18	
Monthly sampling - low flow	147-339	12-116	0-7	
Dec.2010 ; Jan.2011*	737 ; 208	265 ; 69	159 ; 21	
Steinlach flood[2]	26-1219	/	1-449	

*Snow-melting events captured during the monthly sampling.
[1]The flux range did not account for samples impacted by the effluent stop.
[2]The Steinlach flood was sampled upstream of the WWTP, unlike the other campaigns presented in this table.

In addition to the variability of wastewater contaminant release along a single day, between seasons or along a year, long-term estimates of fluxes must consider the existence of secondary contaminant sources with specific compositions that are only activated during precipitation events. The fluxes measured during the Steinlach flood of August 9-10, 2015 showed that quantities by-passing the WWTP during that particular event were up to two orders of magnitude higher than the fluxes measured downstream of the WWTP during the 24 h-sampling campaigns (see Table 19). On year 2015, only one other flood event, occurring in January of the same year, showed a similar discharge as the event sampled in August, with about 25 m^3s^{-1}. The comparison of the fluxes measured during the minor Ammer discharge events of February 9-10, 2016 and during the monthly sampling showed that little floods with presumably a smaller return period, yielded a small or no increase of contaminant fluxes flowing through Pfäffingen (see Table 20). Only exceptions were diclofenac, which fluxes increased by up to five folds, and TAED, by up to ten folds, during the snow-melting events and the Ammer flood captured. Fluxes of atrazine and desethylatrazine were quite minor during the Ammer flood captured in February 2016 compared to what was measured during the monthly sampling. This only confirms that the increase of discharge during the Ammer flood was due to additional wastewater input, and that direct land surface or sub-surface run-off contribution was limited.

Table 20. Comparison of fluxes in [µgs^{-1}] of a selection of organic contaminants during various flow conditions in River Ammer.

	AHTN	Atrazine	Caffeine	Carbamazepine	DEET
Monthly sampling - low flow	7-127	3-9	8-617	43-282	9-89
Dec.2010 ; Jan.2011*	64 ; 52	9 ; 9	1431 ; 457	116 ; 80	38 ; 39
Ammer flood	26-60	0.7-1.4	170-960	51-173	5-17
	Desethylatrazine	Diclofenac	HHCB	HHCB-Lactone	Lidocaine
Monthly sampling - low flow	5-31	6-69	33-214	19-653	5-68
Dec.2010 ; Jan.2011*	19 ; 34	37 ; 32	380 ; 273	528 ; 227	22 ; 21
Ammer flood	2.5-4.0	132-362	151-310	256-561	11-45
	TAED	TCEP	TCPP	TDCPP	Triclosan
Monthly sampling - low flow	0-37	34-189	159-647	14-222	0-12
Dec.2010 ; Jan.2011*	993 ; 310	121 ; 117	505 ; 372	320 ; 75	27 ; 11
Ammer flood	43-333	51-156	60-217	13-30	14-42

*Snow-melting events captured during the monthly sampling.

As it was concluded in section 5.4.3, flux increase during high discharge events was not proportional to discharge due to composition specificity of triggered contaminant sources and particle-associated transport could not be confirmed, disabling the use of turbidity as a proxy for extrapolating fluxes of particle-bound contaminants. A rough estimate of the contribution by the Steinlach and Ammer captured floods to yearly loads of contaminants during baseflow conditions downstream of the Steinlach-Wiesaz WWTP and in Pfäffingen (presented in Figure 39) is presented in Table 21. Assuming that sampling captured a certain representativeness of contaminant input variations, a "back-of-the-envelop" calculation of the contribution of the floods captured was done by integrating contaminant fluxes measured in each flood sample over the duration separating each sample. As a comparison, the respective 22 h and 15 h durations of the Steinlach and Ammer floods would represent 0.3% and 0.2% of a year.

Table 21. Estimate of flux contribution by the Steinlach and Ammer floods to minimum yearly loads of contaminants monitored downstream of the Steinlach-Wiesaz WWTP and in Pfäffingen, respectively.

	AHTN	Atrazine	Caffeine	Carbamazepine	DEET	Diclofenac	HHCB
Steinlach	1.0%	/	12.1%	0.5%	0.5%	2.6%	0.7%
Ammer	0.2%	0.04%	1.0%	0.1%	0.0%	1.0%	0.3%
	HHCB-lactone	Lidocaine	TAED	TCEP	TCPP	TDCPP	Triclosan
Steinlach	0.4%	1.1%	2.1%	1.0%	1.0%	/	7.0%
Ammer	0.2%	0.3%	3.0%	0.2%	0.1%	0.05%	1.3%

In Table 21, despite the high fluxes of contaminants monitored during the Steinlach flood, the quantities by-passing the WWTP reached up to 2.6% (for diclofenac) of minimum estimations from what is released by the WWTP over a year. Only exception was caffeine with 12.1%, known to be highly removed during the WWTP treatment process, and triclosan with 7%. In the Ammer flood, loads of caffeine hardly contributed to 1% of minimum yearly loads monitored at Pfäffingen. Thus, considering the time span of the Steinlach flood and the long return period of such flood, the activation of secondary

sources during such event were assumed to have negligible effect on yearly loads of most compounds but caffeine and triclosan in River Steinlach downstream of the WWTP. The small Ammer discharge event contributed to minimum yearly loads up to ten times less than the Steinlach flood, still reaching up to 1.3% (for triclosan) of minimum yearly loads and even 3% for TAED. The rather high contribution of the small Ammer flood to yearly loads could be partly explained by the mitigation of contaminant input from the two WWTPs by natural attenuation, between effluent discharge and Pfäffingen. For Pfäffingen control cross-section, the recurrent occurrence of such small wastewater induced floods may have an impact on contaminant loads of compounds like triclosan and TAED when cumulated on the long term.

Only the monthly data was available for estimating yearly loads in River Goldersbach. If no contaminant can be released upstream of Bebenhausen, a release of contaminants during precipitation events between Bebenhausen and the Goldersbach mouth in Tübingen might impact the generally low fluxes measured in the stream. For this lower section, missing wet-weather conditions could cause an underestimation of the real loads flowing through River Goldersbach, as it was highlighted for PAHs (Schwientek et al., 2013b).

In Figure 39, only minimum yearly loads of organic contaminants could be estimated for the three investigated rivers based on the average fluxes of the monthly samplings, considering only low flow conditions and excluding discharge events triggering CSO releases. The sum of yearly loads of 15 PAHs species (PAH15), estimated using average sediment loads for the years 2014 to 2016 and C_{sus} provided by Schwientek et al. (2017), was also shown in Figure 39 as a comparison. Locations for estimation of yearly loads were chosen to limit the impact of CSO input in order to approach the reality the most closely to the minimum estimations here. Loads in River Goldersbach were monitored at the WESS gauge above Bebenhausen. Loads in River Steinlach were calculated downstream of the WWTP to measure the impact of the higher urban pressure and neglect erratic input from CSO events in comparison to daily input from the WWTP. The data from the monthly sampling only allowed the WESS gauge in Pfäffingen as monitoring location in River Ammer, downstream of the two WWTPs. Pfäffingen location presented however the disadvantage of offering a certain residence time for natural attenuation of contaminants after their release by WWTPs making the impact of small recurrent CSO releases due to precipitation even more consequent when cumulated. The population in the catchment of each location were 0, 50000 and 68700 inhabitants for River Goldersbach, Steinlach and Ammer, respectively, at the time of the sampling.

In Figure 39, while no release of contaminant should be observed in River Goldersbach downstream of the pristine Schönbuch forest, minimum yearly loads estimated by using raw concentration data were still very limited, with loads under 0.10 kg a^{-1} (for TCEP). In comparison, minimum yearly loads in the Steinlach and Ammer catchments downstream of WWTPs reached up to 10 kg a^{-1} (for HHCB-lactone and TCPP). The yearly PAH15 load ranked third in the dataset of the sixteen organic species investigated, after HHCB-lactone and TCPP, with its 4 and 6 kg a^{-1} in River Steinlach and Ammer, respectively.

Error bars for wastewater compounds represented the standard deviation of the compound flux distribution, the mean of which was used to estimate minimum yearly loads. Error bars for PAHs were based on the standard deviation provided in Schwientek et al. (2017), illustrating the scattering of the $C_{w,tot} = f(TSS)$ correlations used for the determination of C_{sus}. PAH15 being mainly released during precipitation events, the temporal variability of their release is higher than for wastewater contaminants. But the use of turbidity as a proxy and the correlation between PAH and particle concentrations, benefiting many data points, provided a more robust method for load estimation, yielding the small error bars in Figure 39. As seen on error bars of the other compounds in Figure 39, the high variability of fluxes measured during the monthly sampling led to high uncertainties in load estimations by using an average value, particularly for HHCB-lactone in River Steinlach and Ammer and for TCPP and

caffeine in River Ammer. This variability being partly linked to contaminant attenuation in streams, fluxes of vulnerable compounds will be affected further spatially as contaminants get eliminated downstream. In addition to HHCB-lactone, HHCB, AHTN, diclofenac, TAED and triclosan demonstrated elimination from the water column (see section 5.3) and their fluxes, though presenting a lower uncertainty, may be affected by environmental conditions further downstream. Diclofenac, TAED and triclosan may show particular temporal variability as they undergo photo-dependent degradation. More persistent compounds with less variability in their fluxes, such as carbamazepine and the flame retardants TCEP and TDCPP, would provide more stable fluxes within each catchment for yearly estimations.

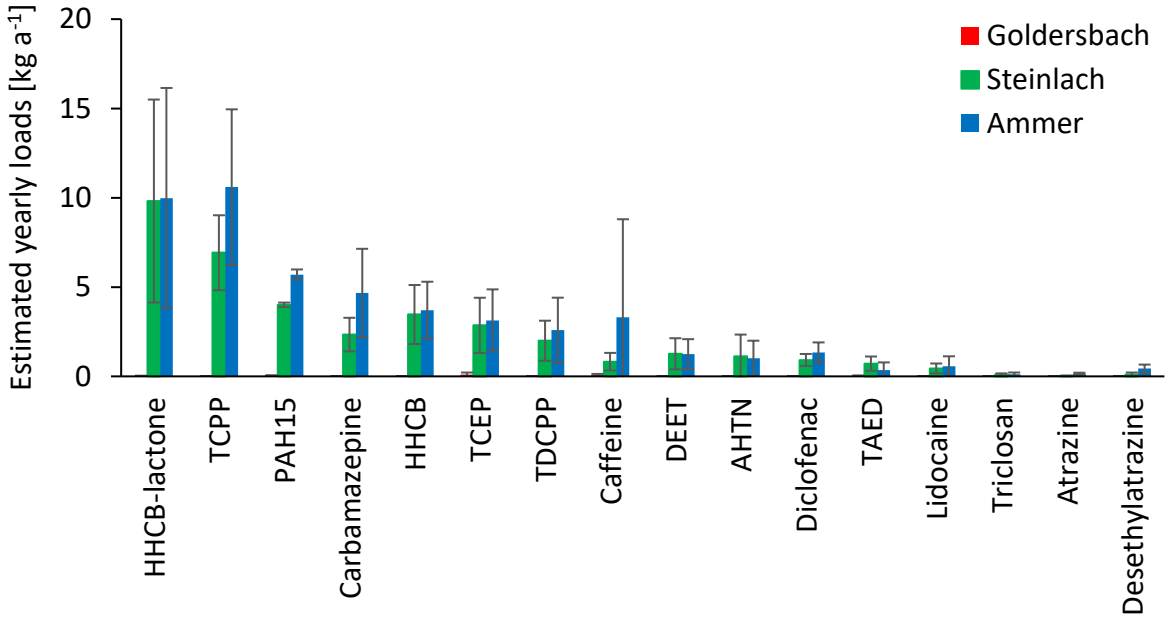

Figure 39. Estimated minimum yearly loads in River Goldersbach at the WESS gauge above Bebenhausen, in River Steinlach downstream of the Steinlach-Wiesaz WWTP and in River Ammer at the gauge in Pfäffingen.

The Ammer catchment is more populated than the Steinlach but a similar population equivalent was handled by their treatment facilities due to the higher industrialization of the Steinlach catchment. Higher loads were observed in River Ammer for persistent compounds like TCPP, carbamazepine and PAHs, as well as the highly degradable caffeine. Caffeine can indeed only be produced by the human population but was not proportional to population difference between the two catchments while the big error bar indicated high uncertainties in its load estimation. The other contaminants, persistent and degradable, presented rather similar yearly loads between the two catchments, maybe due to natural attenuation in River Ammer.

In a nutshell, from the data gathered in this work, the estimation of contaminant loads presented various challenges from the temporal and spatial variability of contaminant input. Estimating loads of organic contaminants without the temporal resolution necessary to capture the temporal variability of their input in the investigated streams thus demonstrates the need of an easily measurable proxy, such as turbidity for suspended sediments and particle-associated compounds like PAHs. The distance from the contaminant source would also allocate the contaminants residence time for their elimination and comparison between catchments could be biased according to the monitoring location chosen.

6 Summary and Conclusions

This work was based on field measurements and sampling of river water to observe the variability of contaminant input and elimination in rivers.

Lagrangian sampling allowed following water parcels along the investigated segments of River Steinlach and observing contaminant attenuation during various environmental conditions. Long water parcels and modelling of river transport through transfer functions were used to take into account dispersion effects and reduce inaccuracies in travel time estimations. Assuming that photo-independent elimination processes did not vary significantly over the sampling day, the comparison between day- and night-time removals revealed the occurrence of photo-dependent elimination for some of the investigated contaminants during the summer season. During the winter season, photo-dependent elimination was absent and removals were reduced or non-existent for compounds that showed reactivity in summer. The investigated contaminants exhibited various reactivities, from the rather persistent carbamazepine to the highly reactive oxcarbazepine. The latter exhibited both photo-dependent and independent elimination and removals up to 100% at the end of the investigated river segment. Volatile artificial musk fragrances left aside, dominant elimination processes for the examplary compounds taken for this study were supposedly photodegradation and biodegradation in the sediment or at the bed surface. Although temperature variations did not seem to exhibit a strong influence at the scale of a day, the bigger temperature difference between seasons might explain lower photo-independent elimination during the winter sampling compared to summer observations. Besides the influence of day-night alternation and seasons, high removal rates observed during the 2013 and particularly during the 2015 summer samplings highlighted the influence of favorable local parameters, e.g., the high fraction of treated wastewater with adapted wastewater bacteria, relatively high contaminant, DOC and nitrate concentrations and elevated water temperature. More generally, the low flow conditions caused a high ratio of reactive surface to water volume, with a relatively large fraction of water flowing through the shallow hyporheic zone and the occurrence of stagnant surface-water zones, as well as a reduced water column favorizing sun ray penetration of the water body. Finally, during the tracer-based sampling, photo-dependent degradation of some compounds was highly efficient during the short time of favorable conditions met on the day-time campaign but depended on the amount of solar radiation reaching the river water. In addition to cloud cover and seasonal variations, simple day-night alternation makes photodegradation a highly variable elimination process, the efficiency of which was mostly comparable or inferior to photo-independent elimination processes when averaged over 24 h of a cloudless day in summer-time.

Sampling to assess particle-associated transport targeted turbid waters during discharge events triggered by precipitation in Rivers Steinlach and Ammer. The expected linear correlation between total concentrations of organic contaminants and TSS was found for six of the fourteen investigated contaminants during the flood sampled in River Ammer. While such correlation was attributed to hydrophobicity for PAHs in previous works, it seemed independent from hydrophobicity or charge of the concerned wastewater compounds in the present study. In the Ammer flood, the release of untreated wastewater through CSOs was assumed to cause an increase of the concentration of contaminants in the dissolved phase parallel to the release of particles, which may have led to an apparent correlation between contaminant total concentration and TSS. Without directly analyzing compounds on the sediments, particle-associated transport could thus not be confirmed. Assuming that sorption at equilibrium and constant loading of contaminants on particles did occur, less than 51% of carbamazepine, diclofenac, naproxen, TCPP and triclosan and less than 67% of lidocaine was sorbed at a particle concentration around 300 mgL^{-1}. This proportion would quickly drop as turbidity decreased while CSO releases ceased and WWTPs became the main contaminant sources again. The particle-associated transport of wastewater contaminants, if any, was thus more limited than what was observed for PAHs or may have not reached equilibrium in the studied conditions.

The observation of contaminant fluxes through the various campaigns and in the different investigated catchments showed both spatial and temporal variabilities of contaminant input. During dry weather conditions, the Steinlach-Wiesaz WWTP was the main source of wastewater contaminants and minor concentrations and fluxes were measured in water bodies that did not receive effluent discharge. Input fluxes of contaminants varied over a single day, between seasons and all year round according to variations of WWTP releases. During the monthly sampling performed in River Steinlach between 2010 and 2011, fluxes of the persistent TCPP varied by only 2 folds against 33 folds for HHCB-lactone. But during sufficiently heavy rain events, erratic combined-sewer overflows in the whole catchment release untreated wastewater and presumably contaminated sewer particles into the investigated streams. During the flood captured in River Steinlach, fluxes of wastewater contaminants went up to two orders of magnitude higher than fluxes measured downstream of the WWTP during dry weather conditions. But considering the rare occurrence of such events, the input of most analyzed contaminants during the duration of the flood was negligible in comparison to the estimated yearly loads. The up to ten times lower input of contaminants by minor untreated wastewater releases during the event captured in River Ammer could have a higher impact on yearly loads when considering the recurrent occurrence of such small event. Finally, minimum annual loads were estimated using average values of fluxes during dry-weather conditions of the monthly sampling. While no contaminant source was known in the pristine section of River Goldersbach, minimum estimations of annual loads yielded up to 10 kg a^{-1} for HHCB-lactone and TCPP in River Steinlach and Ammer downstream of WWTPs.

The spatial and temporal variability of contaminant input from the WWTP, the interference and variability of natural attenuation processes and the erratic activation of additional point-sources by precipitation challenged the assessment of transport and fate of wastewater contaminants in streams. The present work observed almost ideal conditions for natural attenuation of contaminants (e.g. baseflow conditions, sunny and dry weather) or their particle-associated transport (e.g. significant particle concentration in the water column). However, differences in prevailing environmental conditions showed that contaminant fate and transport was highly dependent on environmental parameters that vary in time (e.g. discharge, temperature, sunlight), implying that contaminant transport in a given river cannot be defined by a single campaign. As a step following laboratory experiments under controlled conditions and before comparing catchments as it is often done in literature, single river systems should be further assessed over a variability of environmental conditions including also less favorable ones. Besides, the impact of CSOs on yearly loads of wastewater contaminants shall be further investigated. With no correlation established so far between contaminant fluxes and discharge or contaminant and TSS concentrations, methods to capture the erratic occurrence of CSO releases and their actual impact on yearly contaminant loads should be explored. A first step could pursue the present work on the determination of particle-associated transport, by the analysis on field-filtered and unfiltered samples this time.

References

Acuña, V., von Schiller, D., García-Galán, M.J., Rodríguez-Mozaz, S., Corominas, L., Petrovic, M., Poch, M., Barceló, D., Sabater, S., 2015. Occurrence and in-stream attenuation of wastewater-derived pharmaceuticals in Iberian rivers. Sci. Total Environ. 503–504, 133–141. https://doi.org/10.1016/j.scitotenv.2014.05.067

Adolfsson-Erici, M., Pettersson, M., Parkkonen, J., Sturve, J., 2002. Triclosan, a commonly used bactericide found in human milk and in the aquatic environment in Sweden. Chemosphere 46, 1485–1489. https://doi.org/10.1016/S0045-6535(01)00255-7

Ahel, M., Giger, W., Schaffner, C., 1994. Behaviour of alkylphenol polyethoxylate surfactants in the aquatic environment-II. Occurrence and transformation in rivers. Water Res. 28, 1143–1152. https://doi.org/10.1016/0043-1354(94)90201-1

Al-Khazrajy, O.S.A., Boxall, A.B.A., 2016. Impacts of compound properties and sediment characteristics on the sorption behaviour of pharmaceuticals in aquatic systems. J. Hazard. Mater. 317, 198–209. https://doi.org/10.1016/j.jhazmat.2016.05.065

Alexy, R., Kümpel, T., Kümmerer, K., 2004. Assessment of degradation of 18 antibiotics in the Closed Bottle Test. Chemosphere 57, 505–512. https://doi.org/10.1016/j.chemosphere.2004.06.024

Andreozzi, R., Marotta, R., Pinto, G., Pollio, A., 2002. Carbamazepine in water: persistence in the environment, ozonation treatment and preliminary assessment on algal toxicity. Water Res. 36, 2869–2877. https://doi.org/10.1016/S0043-1354(01)00500-0

Antweiler, R.C., Writer, J.H., Murphy, S.F., 2014. Evaluation of wastewater contaminant transport in surface waters using verified Lagrangian sampling. Sci. Total Environ. 470–471, 551–558. https://doi.org/10.1016/j.scitotenv.2013.09.079

Aymerich, I., Acuña, V., Barceló, D., García, M.J., Petrovic, M., Poch, M., Rodriguez-Mozaz, S., Rodríguez-Roda, I., Sabater, S., von Schiller, D., Corominas, L., 2016. Attenuation of pharmaceuticals and their transformation products in a wastewater treatment plant and its receiving river ecosystem. Water Res. 100, 126–136. https://doi.org/10.1016/j.watres.2016.04.022

Baena-Nogueras, R.M., González-Mazo, E., Lara-Martín, P.A., 2017. Degradation kinetics of pharmaceuticals and personal care products in surface waters: photolysis vs biodegradation. Sci. Total Environ. 590–591, 643–654. https://doi.org/10.1016/j.scitotenv.2017.03.015

Bahnmüller, S., von Gunten, U., Canonica, S., 2014. Sunlight-induced transformation of sulfadiazine and sulfamethoxazole in surface waters and wastewater effluents. Water Res. 57, 183–192. https://doi.org/10.1016/j.watres.2014.03.019

Baker, D.R., Kasprzyk-Hordern, B., 2013. Spatial and temporal occurrence of pharmaceuticals and illicit drugs in the aqueous environment and during wastewater treatment: New developments. Sci. Total Environ. 454–455, 442–456. https://doi.org/10.1016/j.scitotenv.2013.03.043

Barber, L.B., Antweiler, R.C., Flynn, J.L., Keefe, S.H., Kolpin, D.W., Roth, D.A., Schnoebelen, D.J., Taylor, H.E., Verplanck, P.L., 2011. Lagrangian mass-flow investigations of inorganic contaminants in wastewater-impacted streams. Environ. Sci. Technol. 45, 2575–2583. https://doi.org/10.1021/es104138y

Barber, L.B., Keefe, S.H., Brown, G.K., Furlong, E.T., Gray, J.L., Kolpin, D.W., Meyer, M.T., Sandstrom, M.W., Zaugg, S.D., 2013. Persistence and potential effects of complex organic contaminant mixtures in wastewater-impacted streams. Environ. Sci. Technol. 47, 2177–2188. https://doi.org/10.1021/es303720g

Barber, L.B., Keefe, S.H., LeBlanc, D.R., Bradley, P.M., Chapelle, F.H., Meyer, M.T., Loftin, K.A.,

Kolpin, D.W., Rubio, F., 2009. Fate of sulfamethoxazole, 4-nonylphenol, and 17β-estradiol in groundwater contaminated by wastewater treatment plant effluent. Environ. Sci. Technol. 43, 4843–4850. https://doi.org/10.1021/es803292v

Bayer, A., Asner, R., Schüssler, W., Kopf, W., Weiß, K., Sengl, M., Letzel, M., 2014. Behavior of sartans (antihypertensive drugs) in wastewater treatment plants, their occurrence and risk for the aquatic environment. Environ. Sci. Pollut. Res. 21, 10830–10839. https://doi.org/10.1007/s11356-014-3060-z

Benotti, M.J., Trenholm, R. a, Vanderford, B.J., Holady, J.C., Stanford, B.D., Snyder, S. a, 2009. Pharmaceuticals and endocrine disrupting compounds in U.S. drinking water. Environ. Sci. Technol. 43, 597–603. https://doi.org/10.1021/es801845a

Bertani, I., Del Longo, M., Pecora, S., Rossetti, G., 2016. Longitudinal variability in hydrochemistry and zooplankton community of a large river: A lagrangian-based approach. River Res. Appl. 32, 1740–1754. https://doi.org/10.1002/rra.3028

Bester, K., 2005. Polycyclic musks in the Ruhr catchment area - transport, discharges of waste water, and transformations of HHCB, AHTN and HHCB-lactone. J. Environ. Monit. 7, 43–51. https://doi.org/10.1039/b409213a

Bester, K., 2004. Retention characteristics and balance assessment for two polycyclic musk fragrances (HHCB and AHTN) in a typical German sewage treatment plant. Chemosphere 57, 863–870. https://doi.org/10.1016/j.chemosphere.2004.08.032

Birgand, F., Skaggs, R.W., Chescheir, G.M., Gilliam, J.W., 2007. Nitrogen removal in streams of agricultural catchments—a literature review. Crit. Rev. Environ. Sci. Technol. 37, 381–487. https://doi.org/10.1080/10643380600966426

Boreen, A.L., Arnold, W.A., McNeill, K., 2004. Photochemical fate of sulfa drugs in then aquatic environment: Sulfa drugs containing five-membered heterocyclic groups. Environ. Sci. Technol. 38, 3933–3940. https://doi.org/10.1021/es0353053

Bouwer, E., Durant, N., Wilson, L., Zhang, W., Cunningham, A., 1994. Degradation of xenobiotic compounds in situ: Capabilities and limits. FEMS Microbiol. Rev. 15, 307–317. https://doi.org/10.1111/j.1574-6976.1994.tb00142.x

Brown, J.B., Battaglin, W.A., Zuellig, R.E., 2009. Lagrangian sampling for emerging contaminants through an urban stream corridor in colorado. JAWRA J. Am. Water Resour. Assoc. 45, 68–82. https://doi.org/10.1111/j.1752-1688.2008.00290.x

Buerge, I.J., Buser, H.-R., Müller, M.D., Poiger, T., 2003. Behavior of the Polycyclic Musks HHCB and AHTN in Lakes, Two Potential Anthropogenic Markers for Domestic Wastewater in Surface Waters. Environ. Sci. Technol. 37, 5636–5644. https://doi.org/10.1021/es0300721

Buerge, I.J., Poiger, T., Müller, M.D., Buser, H., 2006. Combined sewer overflows to surface waters detected by the anthropogenic marker caffeine. Environ. Sci. Technol. 40, 4096–4102. https://doi.org/10.1021/es052553l

Burke, V., Treumann, S., Duennbier, U., Greskowiak, J., Massmann, G., 2013. Sorption behavior of 20 wastewater originated micropollutants in groundwater - Column experiments with pharmaceutical residues and industrial agents. J. Contam. Hydrol. 154, 29–41. https://doi.org/10.1016/j.jconhyd.2013.08.001

Chebbo, G., Gromaire, M.C., 2004. The experimental urban catchment 'Le Marais' in Paris: what lessons can be learned from it? J. Hydrol. 299, 312–323. https://doi.org/10.1016/j.jhydrol.2004.08.011

Chowdhury, R.R., Charpentier, P., Ray, M.B., 2010. Photodegradation of estrone in solar irradiation. Ind. Eng. Chem. Res. 49, 6923–6930. https://doi.org/10.1021/ie901796x

Cirpka, O.A., Fienen, M.N., Hofer, M., Hoehn, E., Tessarini, A., Kipfer, R., Kitanidis, P.K., 2007. Analyzing bank filtration by deconvoluting time series of electric conductivity. Ground Water 45, 318–328. https://doi.org/10.1111/j.1745-6584.2006.00293.x

Cladière, M., Bonhomme, C., Vilmin, L., Gasperi, J., Flipo, N., Tassin, B., 2014. Modelling the fate of nonylphenolic compounds in the Seine River — part 1: determination of in-situ attenuation rate constants. Sci. Total Environ. 468–469, 1050–1058. https://doi.org/10.1016/j.scitotenv.2013.09.028

DIN38409-2, 1987. German Standard Methods for Examination of Water, Waste Water and Sludge, Summary Action and Material Characteristic Parameters (Group H) - Determination of Filterable Matter and the Residue on Ignition.

Dingman, S.L., 1984. Fluvial hydrology.

Drillia, P., Dokianakis, S.N., Fountoulakis, M.S., Kornaros, M., Stamatelatou, K., Lyberatos, G., 2005. On the occasional biodegradation of pharmaceuticals in the activated sludge process: the example of the antibiotic sulfamethoxazole. J. Hazard. Mater. 122, 259–265. https://doi.org/10.1016/j.jhazmat.2005.03.009

Durán-Álvarez, J.C., Prado, B., González, D., Sánchez, Y., Jiménez-Cisneros, B., 2015. Environmental fate of naproxen, carbamazepine and triclosan in wastewater, surface water and wastewater irrigated soil — Results of laboratory scale experiments. Sci. Total Environ. 538, 350–362. https://doi.org/10.1016/j.scitotenv.2015.08.028

Einsele, G., Agster, G., 1986. Überblick zur Geologie und Morphologie des Schönbuchs, in: Das Landschaftsökologische Forschungsprojetkt Naturpark Schönbuch. pp. 1–13.

Fono, L.J., Kolodziej, E.P., Sedlak, D.L., 2006. Attenuation of wastewater-derived contaminants in an effluent-dominated river. Environ. Sci. Technol. 40, 7257–7262. https://doi.org/10.1021/es061308e

Freese, H.M., Karsten, U., Schumann, R., 2006. Bacterial abundance, activity, and viability in the eutrophic River Warnow, Northeast Germany. Microb. Ecol. 51, 117–127. https://doi.org/10.1007/s00248-005-0091-5

Gao, J., Pedersen, J.A., 2005. Adsorption of Sulfonamide Antimicrobial Agents to Clay Minerals. Environ. Sci. Technol. 39, 9509–9516. https://doi.org/10.1021/es050644c

García-Armisen, T., İnceoğlu, Ö., Ouattara, N.K., Anzil, A., Verbanck, M.A., Brion, N., Servais, P., 2014. Seasonal variations and resilience of bacterial communities in a sewage polluted urban river. PLoS One 9, e92579. https://doi.org/10.1371/journal.pone.0092579

Gasperi, J., Gromaire, M.C., Kafi, M., Moilleron, R., Chebbo, G., 2010. Contributions of wastewater, runoff and sewer deposit erosion to wet weather pollutant loads in combined sewer systems. Water Res. 44, 5875–5886. https://doi.org/10.1016/j.watres.2010.07.008

Gasperi, J., Sebastian, C., Ruban, V., Delamain, M., Percot, S., Wiest, L., Mirande, C., Caupos, E., Demare, D., Kessoo, M.D.K., Saad, M., Schwartz, J.J., Dubois, P., Fratta, C., Wolff, H., Moilleron, R., Chebbo, G., Cren, C., Millet, M., Barraud, S., Gromaire, M.C., 2014. Micropollutants in urban stormwater: occurrence, concentrations, and atmospheric contributions for a wide range of contaminants in three French catchments. Environ. Sci. Pollut. Res. 21, 5267–5281. https://doi.org/10.1007/s11356-013-2396-0

Gilbreath, A.N., McKee, L.J., 2015. Concentrations and loads of PCBs, dioxins, PAHs, PBDEs, OC pesticides and pyrethroids during storm and low flow conditions in a small urban semi-arid watershed. Sci. Total Environ. 526, 251–261. https://doi.org/10.1016/j.scitotenv.2015.04.052

Glaser, C., Zarfl, C., Rügner, H., Lewis, A., Schwientek, M., 2020a. Analyzing particle-associated pollutant transport to identify in-stream sediment processes during a high flow event. Water 12,

1794. https://doi.org/10.3390/w12061794

Glaser, C., Zarfl, C., Werneburg, M., Böckmann, M., Zwiener, C., Schwientek, M., 2020b. Temporal and spatial variable in-stream attenuation of selected pharmaceuticals. Sci. Total Environ. 741, 139514. https://doi.org/10.1016/j.scitotenv.2020.139514

Grathwohl, P., Rügner, H., Wöhling, T., Osenbrück, K., Schwientek, M., Gayler, S., Wollschläger, U., Selle, B., Pause, M., Delfs, J.O., Grzeschik, M., Weller, U., Ivanov, M., Cirpka, O.A., Maier, U., Kuch, B., Nowak, W., Wulfmeyer, V., Warrach-Sagi, K., Streck, T., Attinger, S., Bilke, L., Dietrich, P., Fleckenstein, J.H., Kalbacher, T., Kolditz, O., Rink, K., Samaniego, L., Vogel, H.J., Werban, U., Teutsch, G., 2013. Catchments as reactors: A comprehensive approach for water fluxes and solute turnover. Environ. Earth Sci. 69, 317–333. https://doi.org/10.1007/s12665-013-2281-7

Grenni, P., Patrolecco, L., Ademollo, N., Tolomei, A., Barra Caracciolo, A., 2013. Degradation of gemfibrozil and naproxen in a river water ecosystem. Microchem. J. 107, 158–164. https://doi.org/10.1016/j.microc.2012.06.008

Guillet, G., Knapp, J.L.A., Merel, S., Cirpka, O.A., Grathwohl, P., Zwiener, C., Schwientek, M., 2019. Fate of wastewater contaminants in rivers: using conservative-tracer based transfer functions to assess reactive transport. Sci. Total Environ. 656, 1250–1260. https://doi.org/10.1016/j.scitotenv.2018.11.379

Gutowski, L., Olsson, O., Lange, J., Kümmerer, K., 2015. Photolytic transformation products and biological stability of the hydrological tracer Uranine. Sci. Total Environ. 533, 446–453. https://doi.org/10.1016/j.scitotenv.2015.07.002

Hanamoto, S., Nakada, N., Jürgens, M.D., Johnson, A.C., Yamashita, N., Tanaka, H., 2018. The different fate of antibiotics in the Thames River, UK, and the Katsura River, Japan. Environ. Sci. Pollut. Res. 25, 1903–1913. https://doi.org/10.1007/s11356-017-0523-z

Hari, A.C., Paruchuri, R.A., Sabatini, D.A., Kibbey, T.C.G., 2005. Effects of pH and Cationic and Nonionic Surfactants on the Adsorption of Pharmaceuticals to a Natural Aquifer Material. Environ. Sci. Technol. 39, 2592–2598. https://doi.org/10.1021/es048992m

Heberer, T., Gramer, S., Stan, H.-J., 1999. Occurrence and distribution of organic contaminants in the aquatic system in Berlin. Part III: Determination of synthetic musks in Berlin surface water applying solid-phase microextraction (SPME) and gas chromatography-mass spectrometry (GC-MS). Acta Hydrochim. Hydrobiol. 27, 150–156. https://doi.org/10.1002/(SICI)1521-401X(199905)27:3<150::AID-AHEH150>3.0.CO;2-H

Herzog, B., Lemmer, H., Horn, H., Müller, E., 2013. Characterization of pure cultures isolated from sulfamethoxazole-acclimated activated sludge with respect to taxonomic identification and sulfamethoxazole biodegradation potential. BMC Microbiol. 13, 276. https://doi.org/10.1186/1471-2180-13-276

Hou, J., Pan, B., Niu, X., Chen, J., Xing, B., 2010. Sulfamethoxazole sorption by sediment fractions in comparison to pyrene and bisphenol A. Environ. Pollut. 158, 2826–2832. https://doi.org/10.1016/j.envpol.2010.06.023

Huang, X., Wu, C., Hu, H., Yu, Y., Liu, J., 2015. Sorption and degradation of triclosan in sediments and its effect on microbes. Ecotoxicol. Environ. Saf. 116, 76–83. https://doi.org/10.1016/j.ecoenv.2015.03.002

Huang, X., Wu, C., Xiong, X., Zhang, K., Liu, J., 2014. Partitioning and degradation of triclosan and formation of methyl-triclosan in water-sediment systems. Water, Air, Soil Pollut. 225, 2099. https://doi.org/10.1007/s11270-014-2099-2

ISO14688-1, 2002. Geotechnical investigation and testing — Identification and classification of soil —

Part 1: Identification and description.

Kassotaki, E., Buttiglieri, G., Ferrando-Climent, L., Rodriguez-Roda, I., Pijuan, M., 2016. Enhanced sulfamethoxazole degradation through ammonia oxidizing bacteria co-metabolism and fate of transformation products. Water Res. 94, 111–119. https://doi.org/10.1016/j.watres.2016.02.022

Kiguchi, O., Sato, G., Kobayashi, T., 2016. Source-specific sewage pollution detection in urban river waters using pharmaceuticals and personal care products as molecular indicators. Environ. Sci. Pollut. Res. 23, 22513–22529. https://doi.org/10.1007/s11356-016-7437-z

Kile, D.E., Chiou, C.T., Zhou, H., Li, H., Xu, O., 1995. Partition of nonpolar organic pollutants from water to soil and sediment organic matters. Environ. Sci. Technol. 29, 1401–1406. https://doi.org/10.1021/es00005a037

Kirk, J., 1981. Monte Carlo study of the nature of the underwater light field in, and the relationships between optical properties of, turbid yellow waters. Mar. Freshw. Res. 32, 517. https://doi.org/10.1071/MF9810517

Knapp, J.L.A., Osenbrück, K., Cirpka, O.A., 2015. Impact of non-idealities in gas-tracer tests on the estimation of reaeration, respiration, and photosynthesis rates in streams. Water Res. 83, 205–216. https://doi.org/10.1016/j.watres.2015.06.032

Kolpin, D., Skopec, M., Meyer, M., Furlong, E., Zaugg, S., 2004. Urban contribution of pharmaceuticals and other organic wastewater contaminants to streams during differing flow conditions. Sci. Total Environ. 328, 119–130. https://doi.org/10.1016/j.scitotenv.2004.01.015

Kuehn, W., Müller, U., 2000. Riverbank filtration: An overview. J. / Am. Water Work. Assoc. 92, 60–69.

Kunkel, U., Radke, M., 2012. Fate of pharmaceuticals in rivers: deriving a benchmark dataset at favorable attenuation conditions. Water Res. 46, 5551–5565. https://doi.org/10.1016/j.watres.2012.07.033

Kunkel, U., Radke, M., 2011. Reactive tracer test to evaluate the fate of pharmaceuticals in rivers. Environ. Sci. Technol. 45, 6296–6302. https://doi.org/10.1021/es104320n

la Farré, M., Pérez, S., Kantiani, L., Barceló, D., 2008. Fate and toxicity of emerging pollutants, their metabolites and transformation products in the aquatic environment. TrAC - Trends Anal. Chem. 27, 991–1007. https://doi.org/10.1016/j.trac.2008.09.010

Lahti, M., Oikari, A., 2011. Pharmaceuticals in settleable particulate material in urban and non-urban waters. Chemosphere 85, 826–831. https://doi.org/10.1016/j.chemosphere.2011.06.084

Lam, M.W., Mabury, S.A., 2005. Photodegradation of the pharmaceuticals atorvastatin, carbamazepine, levofloxacin, and sulfamethoxazole in natural waters. Aquat. Sci. 67, 177–188. https://doi.org/10.1007/s00027-004-0768-8

Lam, M.W., Young, C.J., Brain, R.A., Johnson, D.J., Hanson, M.A., Wilson, C.J., Richards, S.M., Solomon, K.R., Mabury, S.A., 2004. Aquatic persistence of eight pharmaceuticals in a microcosm study. Environ. Toxicol. Chem. 23, 1431. https://doi.org/10.1897/03-421

Landrum, P.F., 1989. Bioavailability and toxicokinetics of polycyclic aromatic hydrocarbons sorbed to sediments for the amphipod Pontoporeia hoyi. Environ. Sci. Technol. 23, 588–595. https://doi.org/10.1021/es00063a012

Lange, C., Kuch, B., Metzger, J.W., 2015. Occurrence and fate of synthetic musk fragrances in a small German river. J. Hazard. Mater. 282, 34–40. https://doi.org/10.1016/j.jhazmat.2014.06.027

Lange, J., Schuetz, T., Gregoire, C., Elsässer, D., Schulz, R., Passeport, E., Tournebize, J., 2011. Multi-tracer experiments to characterise contaminant mitigation capacities for different types of artificial

wetlands. Int. J. Environ. Anal. Chem. 91, 768–785. https://doi.org/10.1080/03067319.2010.525635

Larcher, S., Yargeau, V., 2011. Biodegradation of sulfamethoxazole by individual and mixed bacteria. Appl. Microbiol. Biotechnol. 91, 211–218. https://doi.org/10.1007/s00253-011-3257-8

Launay, M.A., Dittmer, U., Steinmetz, H., 2016. Organic micropollutants discharged by combined sewer overflows – Characterisation of pollutant sources and stormwater-related processes. Water Res. 104, 82–92. https://doi.org/10.1016/j.watres.2016.07.068

Leclercq, M., Mathieu, O., Gomez, E., Casellas, C., Fenet, H., Hillaire-Buys, D., 2009. Presence and Fate of Carbamazepine, Oxcarbazepine, and Seven of Their Metabolites at Wastewater Treatment Plants. Arch. Environ. Contam. Toxicol. 56, 408–415. https://doi.org/10.1007/s00244-008-9202-x

Li, Z., Gomez, E., Fenet, H., Chiron, S., 2013. Chiral signature of venlafaxine as a marker of biological attenuation processes. Chemosphere 90, 1933–1938. https://doi.org/10.1016/j.chemosphere.2012.10.033

Li, Z., Sobek, A., Radke, M., 2016. Fate of pharmaceuticals and their transformation products in four small european rivers receiving treated wastewater. Environ. Sci. Technol. 50, 5614–5621. https://doi.org/10.1021/acs.est.5b06327

Lin, A.Y.-C., Lin, C.-A., Tung, H.-H., Chary, N.S., 2010. Potential for biodegradation and sorption of acetaminophen, caffeine, propranolol and acebutolol in lab-scale aqueous environments. J. Hazard. Mater. 183, 242–250. https://doi.org/10.1016/j.jhazmat.2010.07.017

Lin, A.Y., Plumlee, M.H., Reinhard, M., 2006. Natural attenuation of pharmaceuticals and alkylphenol polyethoxylate metabolites during river transport: photochemical and biological transformation. Environ. Toxicol. Chem. 25, 1458–1464. https://doi.org/10.1897/05-412R.1

Lindström, A., Buerge, I.J., Poiger, T., Bergqvist, P.-A., Müller, M.D., Buser, H.-R., 2002. Occurrence and environmental behavior of the bactericide triclosan and its methyl derivative in surface waters and in wastewater. Environ. Sci. Technol. 36, 2322–2329. https://doi.org/10.1021/es0114254

Loos, R., Gawlik, B.M., Locoro, G., Rimaviciute, E., Contini, S., Bidoglio, G., 2009. EU-wide survey of polar organic persistent pollutants in European river waters. Environ. Pollut. 157, 561–568. https://doi.org/10.1016/j.envpol.2008.09.020

Lu, B., Feng, Y., Gao, P., Zhang, Z., Lin, N., 2015. Distribution and fate of synthetic musks in the Songhua River, Northeastern China: influence of environmental variables. Environ. Sci. Pollut. Res. 22, 9090–9099. https://doi.org/10.1007/s11356-014-3973-6

Mader, B.T., Uwe-Goss, K., Eisenreich, S.J., 1997. Sorption of nonionic, hydrophobic organicchemicals to mineral surfaces. Environ. Sci. Technol. 31, 1079–1086. https://doi.org/10.1021/es960606g

Madrid, Y., Zayas, Z.P., 2007. Water sampling: Traditional methods and new approaches in water sampling strategy. TrAC Trends Anal. Chem. 26, 293–299. https://doi.org/10.1016/j.trac.2007.01.002

Mandaric, L., Kalogianni, E., Skoulikidis, N., Petrovic, M., Sabater, S., 2019. Contamination patterns and attenuation of pharmaceuticals in a temporary Mediterranean river. Sci. Total Environ. 647, 561–569. https://doi.org/10.1016/j.scitotenv.2018.07.308

Matamoros, V., Duhec, A., Albaigés, J., Bayona, J.M., 2009. Photodegradation of Carbamazepine, Ibuprofen, Ketoprofen and 17α-Ethinylestradiol in Fresh and Seawater. Water. Air. Soil Pollut. 196, 161–168. https://doi.org/10.1007/s11270-008-9765-1

Matamoros, V., Rodríguez, Y., 2017. Influence of seasonality and vegetation on the attenuation of

emerging contaminants in wastewater effluent-dominated streams. A preliminary study. Chemosphere 186, 269–277. https://doi.org/10.1016/j.chemosphere.2017.07.157

McDonough, C.A., Helm, P.A., Muir, D., Puggioni, G., Lohmann, R., 2016. Polycyclic musks in the air and water of the lower great lakes: spatial distribution and volatilization from surface waters. Environ. Sci. Technol. 50, 11575–11583. https://doi.org/10.1021/acs.est.6b03657

Meade, R.H., Stevens, H.H.J., 1990. Strategies and equipment for sampling suspended sediment and associated toxic chemicals in large rivers — with emphasis on the Mississippi river. Sci. Total Environ. 97–98, 125–135. https://doi.org/10.1016/0048-9697(90)90235-M

Merel, S., Nikiforov, A.I., Snyder, S.A., 2015. Potential analytical interferences and seasonal variability in diethyltoluamide environmental monitoring programs. Chemosphere 127, 238–245. https://doi.org/10.1016/j.chemosphere.2015.02.025

Merel, S., Snyder, S.A., 2016. Critical assessment of the ubiquitous occurrence and fate of the insect repellent N,N-diethyl-m-toluamide in water. Environ. Int. 96, 98–117. https://doi.org/10.1016/j.envint.2016.09.004

Mompelat, S., Le Bot, B., Thomas, O., 2009. Occurrence and fate of pharmaceutical products and by-products, from resource to drinking water. Environ. Int. 35, 803–814. https://doi.org/10.1016/j.envint.2008.10.008

Moody, J.A., 1993. Evaluation of the lagrangian scheme for sampling the Mississippi River during 1987-90. US Department of the Interior, US Geological Survey.

Moreno-González, R., Rodríguez-Mozaz, S., Gros, M., Pérez-Cánovas, E., Barceló, D., León, V.M., 2014. Input of pharmaceuticals through coastal surface watercourses into a Mediterranean lagoon (Mar Menor, SE Spain): Sources and seasonal variations. Sci. Total Environ. 490, 59–72. https://doi.org/10.1016/j.scitotenv.2014.04.097

Morrall, D., McAvoy, D., Schatowitz, B., Inauen, J., Jacob, M., Hauk, A., Eckhoff, W., 2004. A field study of triclosan loss rates in river water (Cibolo Creek, TX). Chemosphere 54, 653–660. https://doi.org/10.1016/j.chemosphere.2003.08.002

Müller, E., Schüssler, W., Horn, H., Lemmer, H., 2013. Aerobic biodegradation of the sulfonamide antibiotic sulfamethoxazole by activated sludge applied as co-substrate and sole carbon and nitrogen source. Chemosphere 92, 969–978. https://doi.org/10.1016/j.chemosphere.2013.02.070

Müller, M.E., Escher, B.I., Schwientek, M., Werneburg, M., Zarfl, C., Zwiener, C., 2018. Combining in vitro reporter gene bioassays with chemical analysis to assess changes in the water quality along the Ammer River, Southwestern Germany. Environ. Sci. Eur. 30, 20. https://doi.org/10.1186/s12302-018-0148-y

Musolff, A., Leschik, S., Möder, M., Strauch, G., Reinstorf, F., Schirmer, M., 2009. Temporal and spatial patterns of micropollutants in urban receiving waters. Environ. Pollut. 157, 3069–3077. https://doi.org/10.1016/j.envpol.2009.05.037

Musolff, A., Leschik, S., Reinstorf, F., Strauch, G., Schirmer, M., 2010. Micropollutant Loads in the Urban Water Cycle. Environ. Sci. Technol. 44, 4877–4883. https://doi.org/10.1021/es903823a

Navarro, A., Endo, S., Gocht, T., Barth, J.A.C., Lacorte, S., Barceló, D., Grathwohl, P., 2009. Sorption of alkylphenols on Ebro River sediments: Comparing isotherms with field observations in river water and sediments. Environ. Pollut. 157, 698–703. https://doi.org/10.1016/j.envpol.2008.08.007

Niu, J., Zhang, L., Li, Y., Zhao, J., Lv, S., Xiao, K., 2013. Effects of environmental factors on sulfamethoxazole photodegradation under simulated sunlight irradiation: kinetics and mechanism. J. Environ. Sci. 25, 1098–1106. https://doi.org/10.1016/S1001-0742(12)60167-3

Nödler, K., Hillebrand, O., Idzik, K., Strathmann, M., Schiperski, F., Zirlewagen, J., Licha, T., 2013.

Occurrence and fate of the angiotensin II receptor antagonist transformation product valsartan acid in the water cycle - A comparative study with selected β-blockers and the persistent anthropogenic wastewater indicators carbamazepine and acesulfame. Water Res. 47, 6650–6659. https://doi.org/10.1016/j.watres.2013.08.034

Nödler, K., Licha, T., Fischer, S., Wagner, B., Sauter, M., 2011. A case study on the correlation of micro-contaminants and potassium in the Leine River (Germany). Appl. Geochemistry 26, 2172–2180. https://doi.org/10.1016/j.apgeochem.2011.08.001

Nödler, K., Tsakiri, M., Licha, T., 2014. The impact of different proportions of a treated effluent on the biotransformation of selected micro-contaminants in river water microcosms. Int. J. Environ. Res. Public Health 11, 10390–10405. https://doi.org/10.3390/ijerph111010390

Osenbrück, K., Wöhling, T., Lemke, D., Rohrbach, N., Schwientek, M., Leven, C., Castillo Alvarez, C., Taubald, H., Cirpka, O.A., 2013. Assessing hyporheic exchange and associated travel times by hydraulic , chemical , and isotopic monitoring at the Steinlach Test Site , Germany. Environ. Earth Sci. 69, 359–372. https://doi.org/10.1007/s12665-012-2155-4

Rabiet, M., Margoum, C., Gouy, V., Carluer, N., Coquery, M., 2010. Assessing pesticide concentrations and fluxes in the stream of a small vineyard catchment - Effect of sampling frequency. Environ. Pollut. 158, 737–748. https://doi.org/10.1016/j.envpol.2009.10.014

Radke, M., Lauwigi, C., Heinkele, G., Mürdter, T.E., Letzel, M., 2009. Fate of the antibiotic sulfamethoxazole and its two major human metabolites in a water sediment test. Environ. Sci. Technol. 43, 3135–3141. https://doi.org/10.1021/es900300u

Radke, M., Ulrich, H., Wurm, C., Kunkel, U., 2010. Dynamics and attenuation of acidic pharmaceuticals along a river stretch. Environ. Sci. Technol. 44, 2968–2974. https://doi.org/10.1021/es903091z

Readman, J.W., Mantoura, R.F.C., Rhead, M.M., Brown, L., 1982. Aquatic distribution and heterotrophic degradation of Polycyclic Aromatic Hydrocarbons (PAH) in the Tamar Estuary. Estuar. Coast. Shelf Sci. 14, 369–389. https://doi.org/10.1016/S0272-7714(82)80009-7

Reemtsma, T., Weiss, S., Müller, J., Petrovic, M., González, S., Barcelo, D., Ventura, F., Knepper, T.P., 2006. Polar pollutants entry into the water cycle by municipal wastewater: A European perspective. Environ. Sci. Technol. 40, 5451–5458. https://doi.org/10.1021/es060908a

Rúa-Gómez, P.C., Püttmann, W., 2013. Degradation of lidocaine, tramadol, venlafaxine and the metabolites O-desmethyltramadol and O-desmethylvenlafaxine in surface waters. Chemosphere 90, 1952–1959. https://doi.org/10.1016/j.chemosphere.2012.10.039

Ruff, M., Müller, M.S., Loos, M., Singer, H.P., 2015. Quantitative target and systematic non-target analysis of polar organic micro-pollutants along the river Rhine using high-resolution mass-spectrometry - identification of unknown sources and compounds. Water Res. 87, 145–154. https://doi.org/10.1016/j.watres.2015.09.017

Rügner, H., Schwientek, M., Beckingham, B., Kuch, B., Grathwohl, P., 2013. Turbidity as a proxy for total suspended solids (TSS) and particle facilitated pollutant transport in catchments. Environ. Earth Sci. 69, 373–380. https://doi.org/10.1007/s12665-013-2307-1

Rügner, H., Schwientek, M., Egner, M., Grathwohl, P., 2014. Monitoring of event-based mobilization of hydrophobic pollutants in rivers: calibration of turbidity as a proxy for particle facilitated transport in field and laboratory. Sci. Total Environ. 490, 191–198. https://doi.org/10.1016/j.scitotenv.2014.04.110

Rügner, H., Schwientek, M., Milačič, R., Zuliani, T., Vidmar, J., Paunović, M., Laschou, S., Kalogianni, E., Skoulikidis, N.T., Diamantini, E., Majone, B., Bellin, A., Chiogna, G., Martinez, E., López de Alda, M., Díaz-Cruz, M.S., Grathwohl, P., 2019. Particle bound pollutants in rivers: results from

suspended sediment sampling in Globaqua river basins. Sci. Total Environ. 647, 645–652. https://doi.org/10.1016/j.scitotenv.2018.08.027

Rühmland, S., Wick, A., Ternes, T.A., Barjenbruch, M., 2015. Fate of pharmaceuticals in a subsurface flow constructed wetland and two ponds. Ecol. Eng. 80, 125–139. https://doi.org/10.1016/j.ecoleng.2015.01.036

Rutsch, M., Rieckermann, J., Krebs, P., 2006. Quantification of sewer leakage: a review. Water Sci. Technol. 54, 135–144. https://doi.org/10.2166/wst.2006.616

Ryan, C.C., Tan, D.T., Arnold, W.A., 2011. Direct and indirect photolysis of sulfamethoxazole and trimethoprim in wastewater treatment plant effluent. Water Res. 45, 1280–1286. https://doi.org/10.1016/j.watres.2010.10.005

Sangster, J.L., Oke, H., Zhang, Y., Bartelt-Hunt, S.L., 2015. The effect of particle size on sorption of estrogens, androgens and progestagens in aquatic sediment. J. Hazard. Mater. 299, 112–121. https://doi.org/10.1016/j.jhazmat.2015.05.046

Sangster, J.L., Zhang, Y., Hernandez, R., Garcia, Y.A., Sivils, J.C., Cox, M.B., Snow, D.D., Kolok, A.S., Bartelt-Hunt, S.L., 2014. Bioavailability and fate of sediment-associated trenbolone and estradiol in aquatic systems. Sci. Total Environ. 496, 576–584. https://doi.org/10.1016/j.scitotenv.2014.07.040

Schaffer, M., Börnick, H., Nödler, K., Licha, T., Worch, E., 2012a. Role of cation exchange processes on the sorption influenced transport of cationic β-blockers in aquifer sediments. Water Res. 46, 5472–5482. https://doi.org/10.1016/j.watres.2012.07.013

Schaffer, M., Boxberger, N., Börnick, H., Licha, T., Worch, E., 2012b. Sorption influenced transport of ionizable pharmaceuticals onto a natural sandy aquifer sediment at different pH. Chemosphere 87, 513–520. https://doi.org/10.1016/j.chemosphere.2011.12.053

Schaper, J.L., Posselt, M., McCallum, J.L., Banks, E.W., Hoehne, A., Meinikmann, K., Shanafield, M.A., Batelaan, O., Lewandowski, J., 2018. Hyporheic exchange controls fate of trace organic compounds in an urban stream. Environ. Sci. Technol. 52, 12285–12294. https://doi.org/10.1021/acs.est.8b03117

Schirmer, M., Reinstorf, F., Leschik, S., Musolff, A., Krieg, R., Strauch, G., Molson, J.W., Martienssen, M., Schirmer, K., 2011. Mass fluxes of xenobiotics below cities: Challenges in urban hydrogeology. Environ. Earth Sci. 64, 607–617. https://doi.org/10.1007/s12665-010-0880-0

Schmadel, N.M., Ward, A.S., Kurz, M.J., Fleckenstein, J.H., Zarnetske, J.P., Hannah, D.M., Blume, T., Vieweg, M., Blaen, P.J., Schmidt, C., Knapp, J.L.A., Klaar, M.J., Romeijn, P., Datry, T., Keller, T., Folegot, S., Marruedo Arricibita, Amaia I. Krause, S., 2016. Stream solute tracer timescales changing with discharge and reach length confound process interpretation. Water Resour. Res. 52, 3227–3245. https://doi.org/10.1002/2015WR018062

Schuetz, T., Weiler, M., Lange, J., 2012. Multitracer assessment of wetland succession: Effects on conservative and nonconservative transport processes. Water Resour. Res. 48, 1–15. https://doi.org/10.1029/2011WR011292

Schultz, M.M., Furlong, E.T., Kolpin, D.W., Werner, S.L., Schoenfuss, H.L., Barber, L.B., Blazer, V.S., Norris, D.O., Vajda, A.M., 2010. Antidepressant pharmaceuticals in two U.S. effluent-impacted streams: occurrence and fate in water and sediment, and selective uptake in fish neural tissue. Environ. Sci. Technol. 44, 1918–1925. https://doi.org/10.1021/es9022706

Schwarzenbach, R.P., Gschwend, P.M., Imboden, D.M., 2003. Environmental organic chemistry, John Wiley & Sons, New Jersey.

Schwientek, M., Guillet, G., Rügner, H., Kuch, B., Grathwohl, P., 2016. A high-precision sampling scheme to assess persistence and transport characteristics of micropollutants in rivers. Sci. Total

Environ. 540, 444–454. https://doi.org/10.1016/j.scitotenv.2015.07.135

Schwientek, M., Osenbrück, K., Fleischer, M., 2013a. Investigating hydrological drivers of nitrate export dynamics in two agricultural catchments in Germany using high-frequency data series. Environ. Earth Sci. 69, 381–393. https://doi.org/10.1007/s12665-013-2322-2

Schwientek, M., Rügner, H., Beckingham, B., Kuch, B., Grathwohl, P., 2013b. Integrated monitoring of particle associated transport of PAHs in contrasting catchments. Environ. Pollut. 172, 155–162. https://doi.org/10.1016/j.envpol.2012.09.004

Schwientek, M., Rügner, H., Scherer, U., Rode, M., Grathwohl, P., 2017. A parsimonious approach to estimate PAH concentrations in river sediments of anthropogenically impacted watersheds. Sci. Total Environ. 601–602, 636–645. https://doi.org/10.1016/j.scitotenv.2017.05.208

Schwientek, M., Selle, B., 2016. Quantifying in-stream retention of nitrate at catchment scales using a practical mass balance approach. Environ. Monit. Assess. 188, 111. https://doi.org/10.1007/s10661-016-5097-6

Seeland, A., Oetken, M., Kiss, A., Fries, E., Oehlmann, J., 2012. Acute and chronic toxicity of benzotriazoles to aquatic organisms. Environ. Sci. Pollut. Res. 19, 1781–1790. https://doi.org/10.1007/s11356-011-0705-z

Selle, B., Rink, K., Kolditz, O., 2013a. Recharge and discharge controls on groundwater travel times and flow paths to production wells for the Ammer catchment in southwestern Germany. Environ. Earth Sci. 69, 443–452. https://doi.org/10.1007/s12665-013-2333-z

Selle, B., Schwientek, M., Lischeid, G., 2013b. Understanding processes governing water quality in catchments using principal component scores. J. Hydrol. 486, 31–38. https://doi.org/10.1016/j.jhydrol.2013.01.030

Simonich, S.L., Federle, T.W., Eckhoff, W.S., Rottiers, A., Webb, S., Sabaliunas, D., De Wolf, W., 2002. Removal of fragrance materials during U.S. and European wastewater treatment. Environ. Sci. Technol. 36, 2839–2847. https://doi.org/10.1021/es025503e

Stein, K., Ramil, M., Fink, G., Sander, M., Ternes, T.A., 2008. Analysis and sorption of psychoactive drugs onto sediment. Environ. Sci. Technol. 42, 6415–6423. https://doi.org/10.1021/es702959a

Ternes, T.A., 1998. Occurrence of drugs in German sewage treatment plants and rivers. Water Res. 32, 3245–3260. https://doi.org/10.1016/S0043-1354(98)00099-2

Tixier, C., Singer, H.P., Canonica, S., Müller, S.R., 2002. Phototransformation of triclosan in surface waters: a relevant elimination process for this widely used biocide - laboratory studies, field measurements, and modeling. Environ. Sci. Technol. 36, 3482–3489. https://doi.org/10.1021/es025647t

van der Veen, I., de Boer, J., 2012. Phosphorus flame retardants: Properties, production, environmental occurrence, toxicity and analysis. Chemosphere 88, 1119–1153. https://doi.org/10.1016/j.chemosphere.2012.03.067

Villinger, E., 1982. Grundwasserbilanzen im Karstaquifer des Oberen Muschelkalks im Oberen Gäu (Baden-Württemberg). Geol. Jahrbücher - R. C 32, 43–61.

Walling, D.., Owens, P.., Carter, J., Leeks, G.J.., Lewis, S., Meharg, A.., Wright, J., 2003. Storage of sediment-associated nutrients and contaminants in river channel and floodplain systems. Appl. Geochemistry 18, 195–220. https://doi.org/10.1016/S0883-2927(02)00121-X

Webb, S., Ternes, T., Gibert, M., Olejniczak, K., 2003. Indirect human exposure to pharmaceuticals via drinking water. Toxicol. Lett. 142, 157–167. https://doi.org/10.1016/S0378-4274(03)00071-7

Weyrauch, P., Matzinger, A., Pawlowsky-Reusing, E., Plume, S., von Seggern, D., Heinzmann, B.,

Schroeder, K., Rouault, P., 2010. Contribution of combined sewer overflows to trace contaminant loads in urban streams. Water Res. 44, 4451–4462. https://doi.org/10.1016/j.watres.2010.06.011

Wilson, B.A., Smith, V.H., DeNoyelles, F., Larive, C.K., 2003. Effects of three pharmaceutical and personal care products on natural freshwater algal assemblages. Environ. Sci. Technol. 37, 1713–1719. https://doi.org/10.1021/es0259741

Winkler, M., Kopf, G., Hauptvogel, C., Neu, T., 1998. Fate of artificial musk fragrances associated with suspended particulate matter (SPM) from the River Elbe (Germany) in comparison to other organic contaminants. Chemosphere 37, 1139–1156. https://doi.org/10.1016/S0045-6535(98)00110-6

Wolf, L., Zwiener, C., Zemann, M., 2012. Tracking artificial sweeteners and pharmaceuticals introduced into urban groundwater by leaking sewer networks. Sci. Total Environ. 430, 8–19. https://doi.org/10.1016/j.scitotenv.2012.04.059

Writer, J.H., Antweiler, R.C., Ferrer, I., Ryan, J.N., Thurman, E.M., 2013. In-stream attenuation of neuro-active pharmaceuticals and their metabolites. Environ. Sci. Technol. 47, 9781–9790. https://doi.org/10.1021/es402158t

Writer, J.H., Ryan, J.N., Keefe, S.H., Barber, L.B., 2012. Fate of 4-Nonylphenol and 17β-Estradiol in the Redwood River of Minnesota. Environ. Sci. Technol. 46, 860–868. https://doi.org/10.1021/es2031664

Yamamoto, H., Nakamura, Yudai, Moriguchi, S., Nakamura, Yuki, Honda, Y., Tamura, I., Hirata, Y., Hayashi, A., Sekizawa, J., 2009. Persistence and partitioning of eight selected pharmaceuticals in the aquatic environment: Laboratory photolysis, biodegradation, and sorption experiments. Water Res. 43, 351–362. https://doi.org/10.1016/j.watres.2008.10.039

Yang, Y.Y., Toor, G.S., Williams, C.F., 2015. Pharmaceuticals and organochlorine pesticides in sediments of an urban river in Florida, USA. J. Soils Sediments 15, 993–1004. https://doi.org/10.1007/s11368-015-1077-7

Field-based measurement and characterization of transport and turn-over of wastewater contaminants in streams

-

Appendix

Table S1. Usage and physico-chemical properties of investigated contaminants (chemicalize.com). Values are given only when the compound is investigated in the given campaign.

Compound name	Usage	pk_a	Log D_{ow}[2]				
			Steinlach 24 h sampling		Steinlach tracer-based sampling	Flood sampling	
			Summer	Winter	Summer	Steinlach	Ammer
			pH = 7.6-8.6	/[1]	pH = 8 / pH = 7.6-7.8[3]	pH = 7.8-8.2	pH = 7.6-8.0
2-Aminobenzimidazole	pesticide	8.1[5] & 12.6[4]			0.8 / 0.5-0.7		
Acesulfame	artificial sweetener	3[4]			-1		
AHTN	artificial musk fragrance	/	5	x		5	5
Amisulpride	antipsychotic agent	7[5] & 14[4]			0.1 / 0.2-0.2		
Atenolol	cardiovascular drug	9.7[5] & 14.1[4]			1.0		
Atrazine	pesticide	4.2[5] & 14.5[4]		x (2.2)	2.2		2.2
Benzotriazole	pesticide	0.6[5] & 8.6[4]			1.2 / 1.3-1.2		
Bisoprolol	antihypertensive agent	9.7[5] & 14.1[4]			0.5 / 0.2-0.3		
Caffeine	stimulant	-1.2[5]				-0.6	-0.6
Candesartan	antihypertensive agent	1.5[5] & 3.5[4]			0.3 / 0.5-0.4		
Carbamazepine	anticonvulsant	16[4]	2.8	2.8	2.8	2.8	2.8
Carbendazim	fungicide	4.3[5] & 9.7[4]			1.8		
DEET	insect repellant	-1[5]	2.5	2.5	2.5	2.5	2.5
Denatonium	bittering agent	12.4[4]			0.4		
Desethylatrazine	Atrazine metabolite	4.4[5] & 14.6[4]		x (1.5)			1.5
Desvenlafaxine	antidepressant	8.9[5] & 10.1[4]			1.6 / 1.3-1.5		
Diatrizoic acid	contrast agent	2.2[4]			-0.6		

[1]pH was not measured during the winter 24 h sampling but was expected to be in the same range as the summer 24 h sampling. Crosses were left to indicate that the compound was analyzed during the winter campaign and log D_{ow} values between parentheses were given in case it was not analyzed during the summer campaign.
[2]log D_{ow} is the logarithmic octanol-water distribution coefficient.
[3]day-time experiment pH / night-time experiment pH range.
[4]strongest acidic pK_a.
[5]strongest basic pK_a.

Table S1. (continued) Usage and physico-chemical properties of investigated contaminants (chemicalize.com). Values are given only when the compound is investigated in the given campaign.

Compound name	Usage	pk_a	Log D_{ow}[2]				
			Steinlach 24 h sampling		Steinlach tracer-based sampling	Flood sampling	
			Summer	Winter	Summer	Steinlach	Ammer
			pH = 7.6-8.6	/[1]	pH = 8 / pH = 7.6-7.8[3]	pH = 7.8-8.2	pH = 7.6-8.0
Diclofenac	anti-inflammatory drug	4[4]	1-0.8		0.9 / 1-0.9	0.9-0.8	1-0.9
Gabapentin	anticonvulsant drug	4.6[5] & 9.9[4]			-1.3		
HHCB	artificial musk fragrance	/	4.7	x		4.7	4.7
HHCB-lactone	HHCB metabolite	/	4.7	x		4.7	4.7
Ibuprofen	anti-inflammatory drug	4.9[4]				1.0-0.7	1.2-0.9
Iopamidol	contrast agent	-1.6[5] & 11[4]			-0.7		
Irbesartan	antihypertensive agent	4.1[5] & 5.9[4]			4 / 4.1-4.1		
Lamotrigine	anticonvulsant	5.9[5] & 15[4]			1.9		
Lidocaine	local anesthetic	7.8[5] & 13.8[4]		x (2.5-2.8)	2.6 / 2.5-2.6	2.6-2.6	2.5-2.6
Mecoprop	herbicide	3.5[4]	-0.5	x		-0.5	-0.5
Metoprolol	antihypertensive agent	9.7[5] & 14.1[4]			0.1 / -0.3-(-0.1)		
Naproxen	anti-inflammatory drug	4.2[4]	-0.5	x		-0.5-(-0.4)	-0.5-(-0.4)
Olmesartan	antihypertensive agent	5.3[5] & 0.9[4]			-1.2 / -0.2-(-0.3)		
OTNE	artificial musk fragrance	/	3.6				
Oxcarbazepine	anticonvulsant	13.2[4]	1.8	x	1.8		
Primidone	anticonvulsant	11.5[4]			1.1		
Salbutamol	bronchodilator	9.4[5] & 10.12[4]			-0.8/ -1.1-(-1)		

[1]pH was not measured during the winter 24 h sampling but was expected to be in the same range as the summer 24 h sampling. Crosses were left to indicate that the compound was analyzed during the winter campaign and log D_{ow} values between parentheses were given in case it was not analyzed during the summer campaign.
[2]log D_{ow} is the logarithmic octanol-water distribution coefficient.
[3]day-time experiment pH / night-time experiment pH range.
[4]strongest acidic pK_a.
[5]strongest basic pK_a.

Table S1. (continued) Usage and physico-chemical properties of investigated contaminants (chemicalize.com). Values are given only when the compound is investigated in the given campaign.

Compound name	Usage	pk_a	Log D_{ow}[2]				
			Steinlach 24 h sampling		Steinlach tracer-based sampling	Flood sampling	
			Summer	Winter	Summer	Steinlach	Ammer
			pH = 7.6-8.6	/[1]	pH = 8 / pH = 7.6-7.8[3]	pH = 7.8-8.2	pH = 7.6-8.0
Sitagliptin	antidiabetic drug	8.8[5]			0.4 / 0.1-0.2		
Sotalol	antihypertensive agent	9.4[5] & 10.1[4]			-1.6 / -1.9-(-1.8)		
Sucralose	artificial sweetener	11.9[4]			-0.5		
Sulfamethoxazole	corrosion inhibitor	2[5] & 6.2[4]			-0.1 / 0-(-0.1)		
Sulpiride	antidepressant	8.4[5] & 10.2[4]			-0.2 / -0.5 -0.4		
TAED	bleaching agent	/	-1.8	-1.8	-1.8	-1.8	-1.8
TCEP	flame retardant	/	2.1			2.1	2.1
TCPP	flame retardant	/	3.4	3.4	3.4	3.4	3.4
TDCPP	flame retardant	/	4.3	x			4.3
Tiapride	antipsychotic	7.6[5] & 13.2[4]			0.3 / 0.1-0.2		
Torasemide	antihypertensive agent	4.2[5] & 5.92[4]			1.1		
Tramadol	analgesic	9.2[5] & 13.8[4]			1.2 / 0.8-1		
Triclosan	biocide	7.7[4]	4.7-4.0	x		4.6-4.4	4.7-4.5
Trimethoprim	antibiotic	7.16[5]			1.2		
Valsartan	antihypertensive agent	-0.6[5] & 4.4[4]			0.5 / 0.9-0.7		
Venlafaxine	antidepressant	8.9[5] & 14.4[4]			1.8 / 1.4-1.6		

[1]pH was not measured during the winter 24 h sampling but was expected to be in the same range as the summer 24 h sampling. Crosses were left to indicate that the compound was analyzed during the winter campaign and log D_{ow} values between parentheses were given in case it was not analyzed during the summer campaign.
[2]log D_{ow} is the logarithmic octanol-water distribution coefficient.
[3]day-time experiment pH / night-time experiment pH range.
[4]strongest acidic pK_a.
[5]strongest basic pK_a.

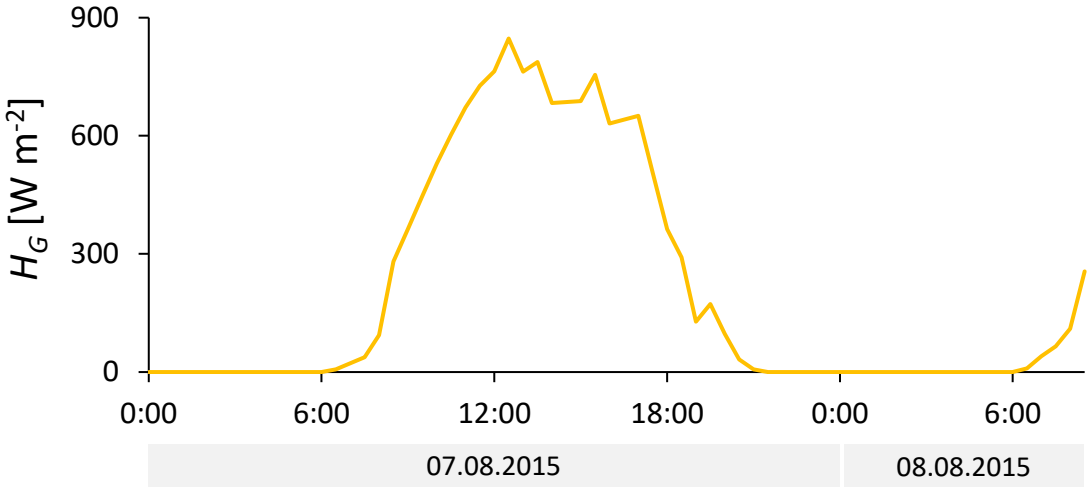

Figure S1. Global solar radiation time series used for the computation of contaminant removal during the tracer-based sampling (Source: LUBW http://udo.lubw.baden-wuerttemberg.de).

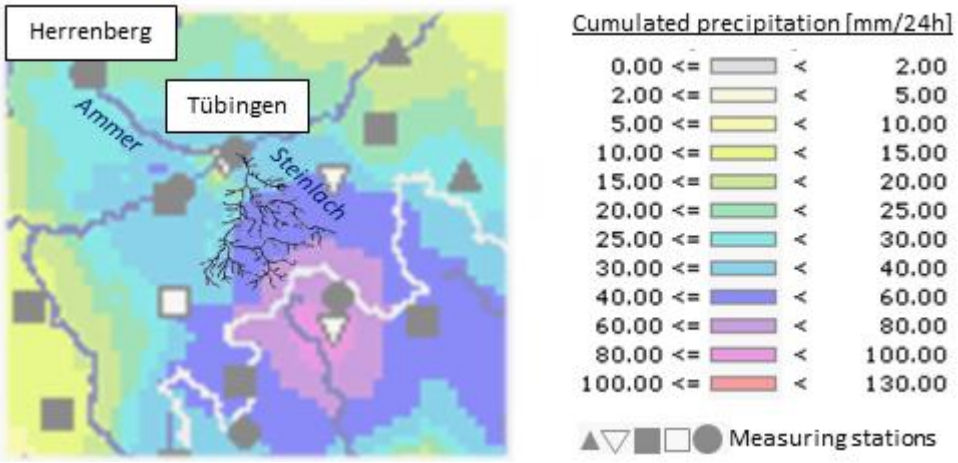

Figure S2. Interpolated cumulated precipitation over 24 h from 09.08.15 to 10.08.15 05:00 (Source: LUBW www.hvz.baden-wuerttemberg.de).

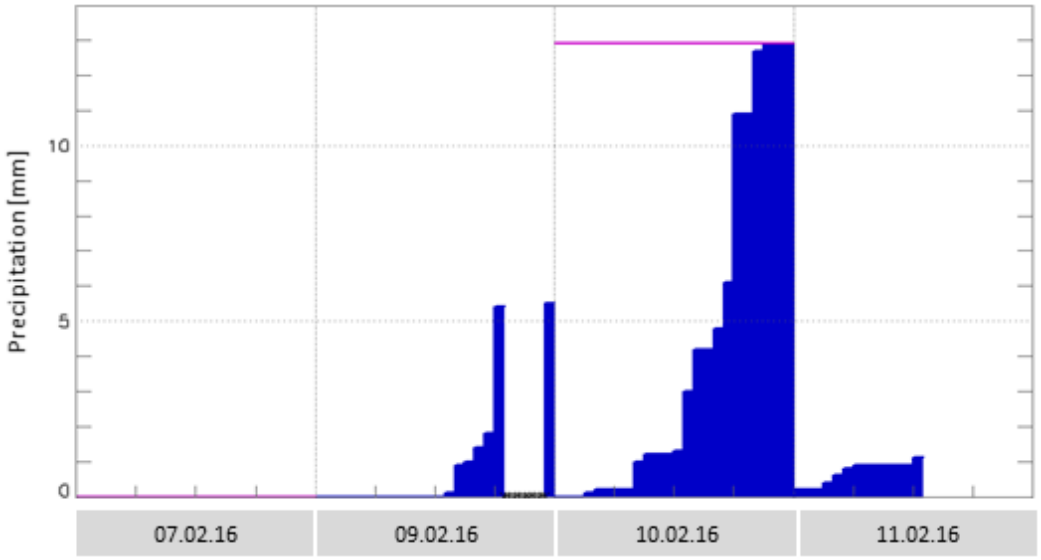

Figure S3. Precipitation measurement in Herrenberg measurement station for the period of the 07.02.16 until the 11.2.16 13:45 (Source: LUBW www.hvz.baden-wuerttemberg.de).

Table S2. Summary of calculated k_i and k_{night} decay constants for investigated compounds for the segments comprised between MS1 and MS2, MS3 and MS4 during the tracer-based sampling.

	MS1-2		MS1-3		MS1-4	
	$k_i.10^{-8}$ [m^2J^{-1}]	k_{night} [day^{-1}]	$k_i.10^{-8}$ [m^2J^{-1}]	k_{night} [day^{-1}]	$k_i.10^{-8}$ [m^2J^{-1}]	k_{night} [day^{-1}]
2-Aminobenzimidazole	b.t.*	1.1	b.t.	0.6	b.t.	0.8
Acesulfame	b.t.	0.3	0.3	b.t.	0.2	0.2
Amisulpride	b.t.	1.1	b.t.	1.2	0.8	0.6
Atenolol	1.7	0.8	1.6	1.7	1.4	1.5
Atrazine	b.t.	b.t.	b.t.	b.t.	b.t.	0.1
Benzotriazole	b.t.	0.9	b.t.	0.6	b.t.	0.5
Bisoprolol	2.9	3.1	7.2	1.8	5.0	1.6
Candesartan	1.2	b.t.	b.t.	b.t.	0.4	b.t.
Carbamazepine	b.t.	b.t.	b.t.	0.2	b.t.	0.1
Carbendazim	b.t.	1.07	b.t.	0.5	b.t.	0.7
DEET	11.5	2.2	6.3	1.1	3.2	1.1
Denatonium	2.4	0.9	0.7	0.9	0.1	0.5
Desvenlafaxine	1.0	0.8	1.3	1.0	1.1	0.8
Diatrizoic acid	0.2	0.1	b.t.	0.7	b.t.	0.3
Diclofenac	3.8	0.9	5.6	1.2	5.6	0.6
Gabapentin	0.6	0.5	b.t.	0.3	b.t.	0.6
Fluorescein	15.8	0	18.0	0	16.0	0
Iopamidol	b.t.	1.1	b.t.	0.4	b.t.	0.2
Irbesartan	2.9	0.8	2.0	2.1	2.6	0.5
Lamotrigine	b.t.	0.7	b.t.	0.6	b.t.	1.1
Lidocaine	b.t.	0.8	b.t.	0.9	b.t.	0.7
Metoprolol	1.1	1.5	3.9	1.2	4.4	1.6
Olmesartan	b.t.	0.8	b.t.	0.6	b.t.	0.6
Oxcarbazepine	36.6	b.t.	58.9	b.t.	38.3	b.t.
Primidone	b.t.	1.1	b.t.	1.1	0	0.5
Salbutamol	1.5	0.8	0.7	0.9	1.0	0.3
Sitagliptin	b.t.	2.0	b.t.	1.5	b.t.	1.1
Sotalol	0.5	0.3	0.1	0.8	0.9	0.7
Sucralose	b.t.	b.t.	b.t.	b.t.	b.t.	b.t.
Sulfamethoxazole	b.t.	1.3	b.t.	1.0	b.t.	1.0
Sulpiride	b.t.	0.5	b.t.	0.5	b.t.	0.6
TAED	13.4	b.t.	17.1	1.8	9.4	1.4
TCPP	b.t.	2.3	b.t.	0.8	b.t.	0.6

*b.t. for "below threshold". When the contaminant displayed a downstream concentration equal or higher – presumably due to chemical uncertainty – than the concentration in the input time series, the model released a threshold value for constants k_i (=$2.57.10^{-11}$ m^2J^{-1}) and k_{night} (=$2.22.10^{-14}$ day^{-1}), that is corrected to 0 for further calculations.

Table S2 (continued). Summary of calculated k_i and k_{night} decay constants for investigated compounds for the segments comprised between MS1 and MS2, MS3 and MS4 during the tracer-based sampling.

	MS1-2		MS1-3		MS1-4	
	$k_i.10^{-8}$ [m^2J^{-1}]	k_{night} [day^{-1}]	$k_i.10^{-8}$ [m^2J^{-1}]	k_{night} [day^{-1}]	$k_i.10^{-8}$ [m^2J^{-1}]	k_{night} [day^{-1}]
Tiapride	b.t.*	0.9	0.2	0.8	b.t.	1.0
Torasemide	b.t.	1.1	b.t.	1.3	b.t.	1.1
Tramadol	0.8	0.6	2.4	1.0	2.9	0.8
Trimethoprim	b.t.	2.2	b.t.	1.9	b.t.	1.4
Valsartan	b.t.	1.4	b.t.	1.9	b.t.	1.9
Venlafaxine	1.1	1.1	3.2	1.1	3.2	1.2
Calcium	1.0	b.t.	0.3	0.1	0.3	0.1
Chloride	b.t.	0.2	b.t.	0.1	b.t.	0.1
Magnesium	1	0	b.t.	0	0	0
Nitrate	b.t.	0.5	b.t.	0.4	b.t.	0.5
Phosphate	b.t.	1	b.t.	2	b.t.	1
Potassium	b.t.	1	0	0	b.t.	1
Sodium	b.t.	0	b.t.	0	b.t.	0
Sulfate	b.t.	0.2	b.t.	0.2	b.t.	0.1

*b.t. for "below threshold". When the contaminant displayed a downstream concentration equal or higher – presumably due to chemical uncertainty – than the concentration in the input time series, the model released a threshold value for constants k_i (=2.57.10^{-11} m^2J^{-1}) and k_{night} (=2.22.10^{-14} day^{-1}), that is corrected to 0 for further calculations.

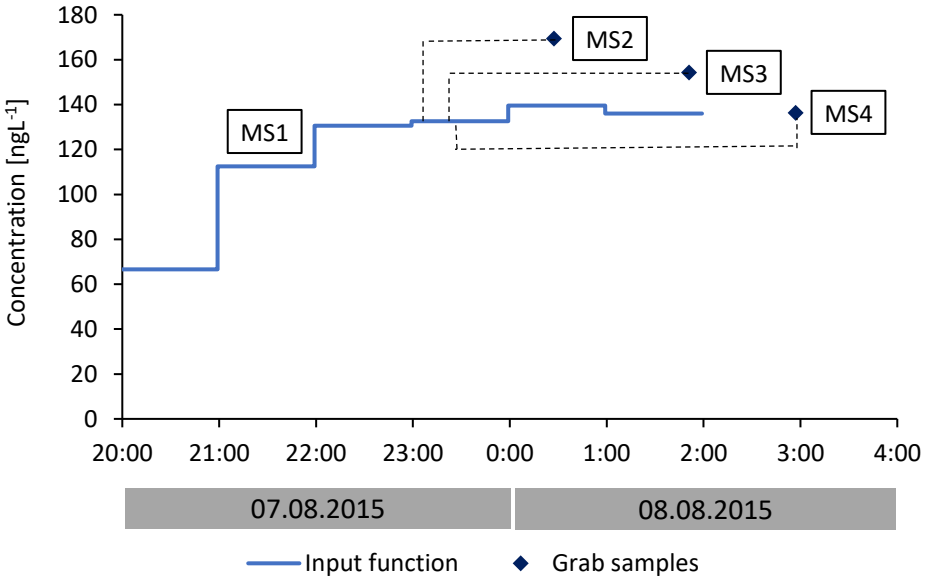

Figure S4. Oxcarbazepine raw data from the tracer-based sampling. The dotted lines link the grab samples taken at MS2, MS3 and MS4 to the corresponding initial concentration of the input function at MS1 at t-τ.

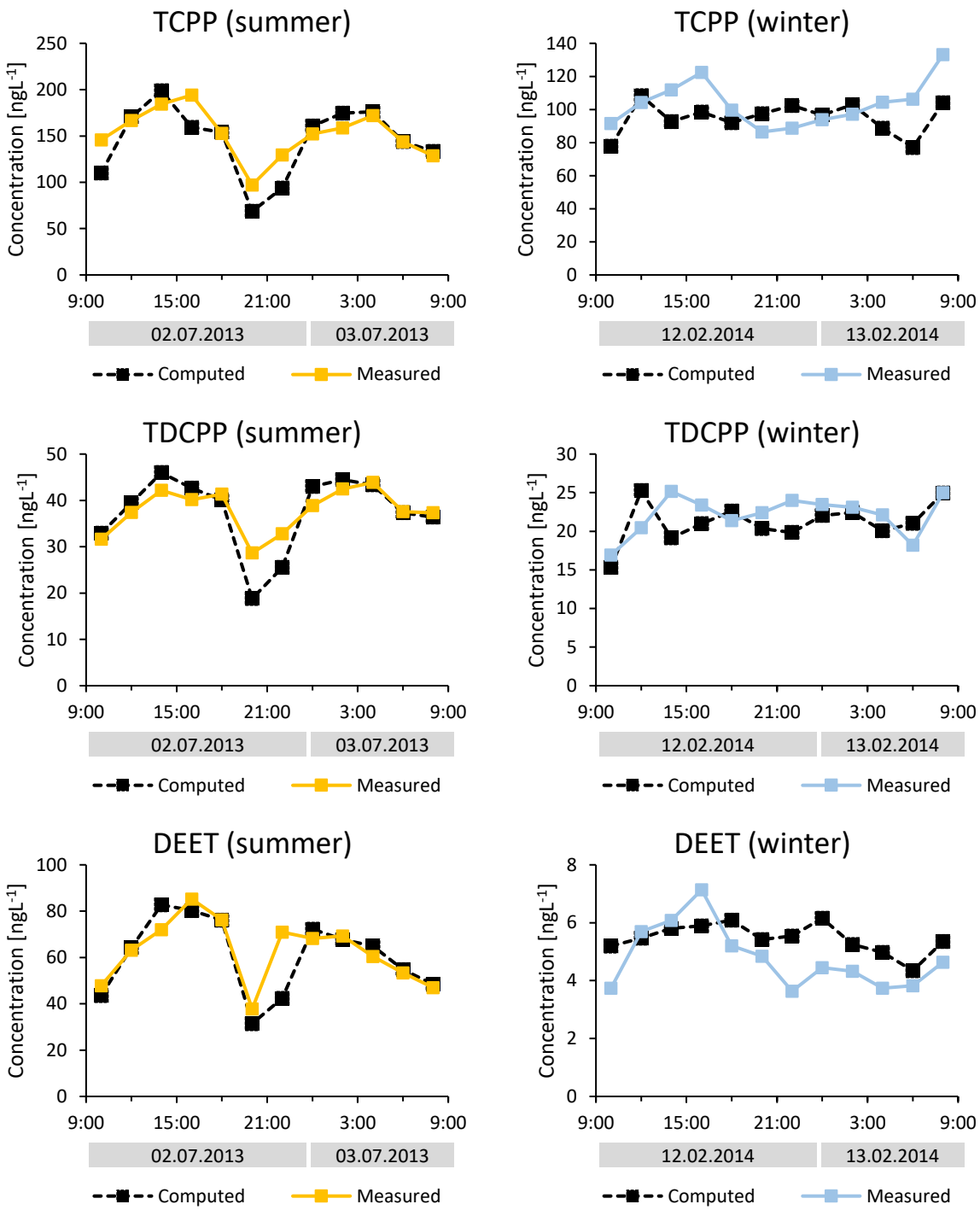

Figure S5. Computed and measured concentrations for the remaining compounds with conservative behaviors observed during the summer and winter 24 h-sampling campaigns.

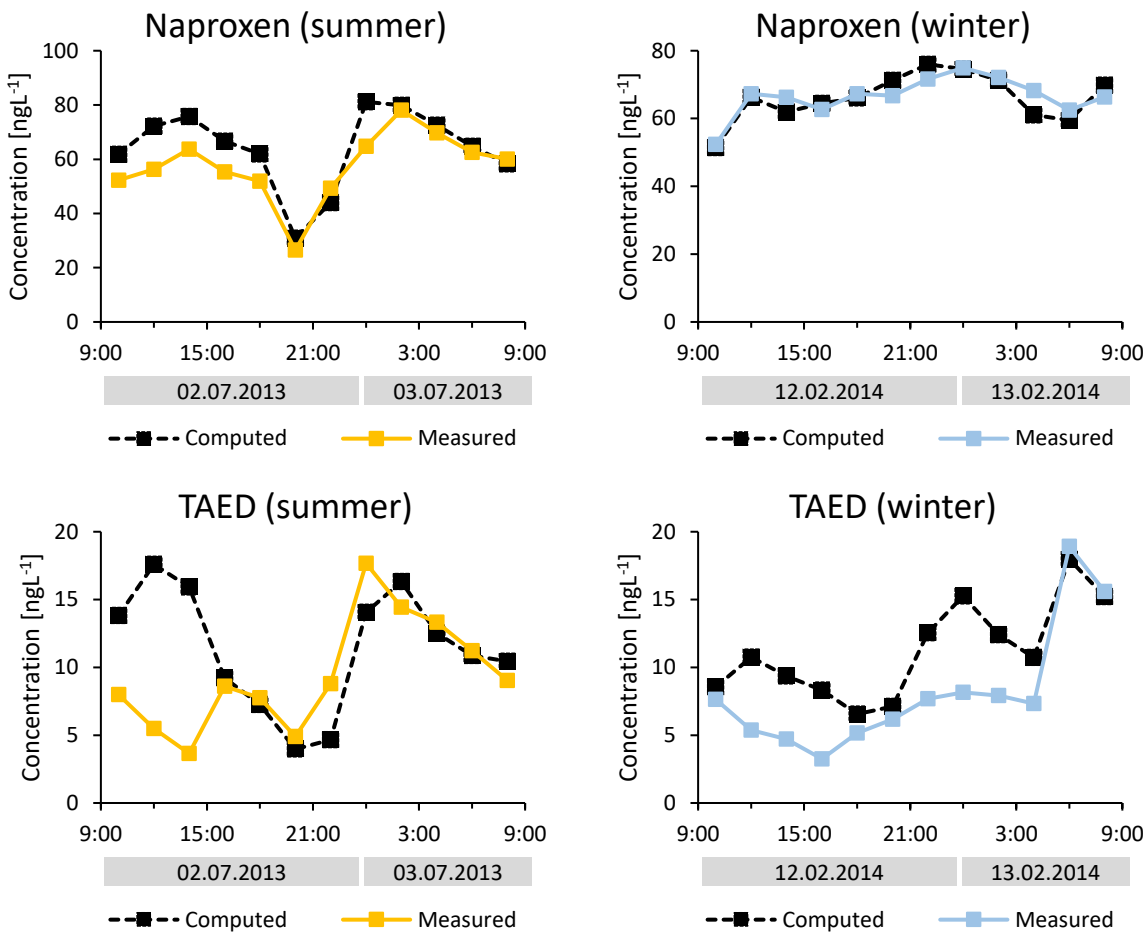

Figure S6. Computed and measured concentrations during the summer and winter 24 h-sampling campaigns for the remaining examples photo-reactive compounds.

Table S3. Henry's law volatility constant (K_H) estimated using US Environmental Protection Agency's EPISuite™ (www.chemspider.com).

	K_H [m^3atm $mole^{-1}$]
OTNE	$3.2 \cdot 10^{-4}$
AHTN	$2.3 \cdot 10^{-4}$
HHCB	$1.8 \cdot 10^{-4}$
HHCB-lactone	/
DEET	$1.3 \cdot 10^{-6}$
Carbamazepine	$1.6 \cdot 10^{-9}$
TAED	$2.8 \cdot 10^{-14}$

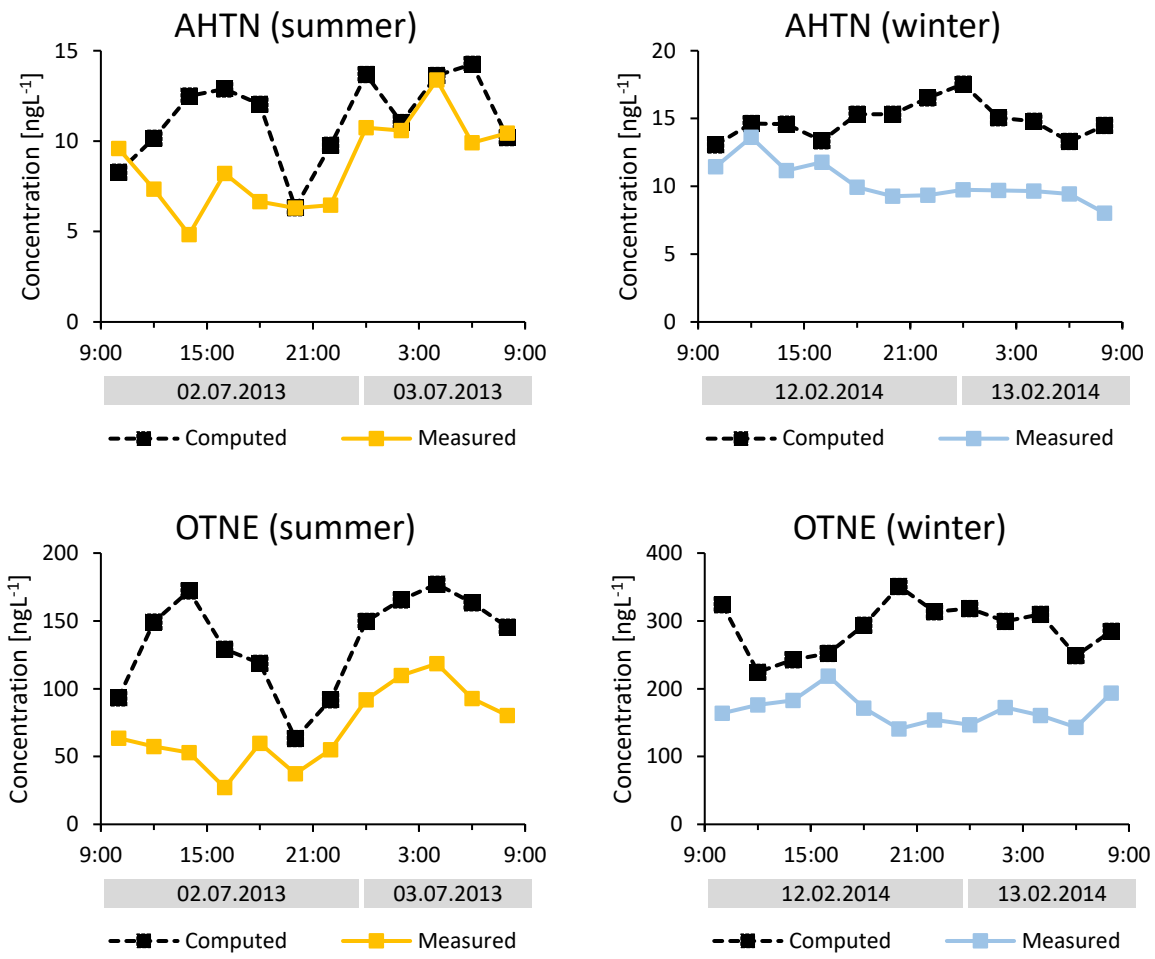

Figure S7. Patterns observed for the musk fragrances OTNE and AHTN during the summer and winter 24 h-sampling campaigns.

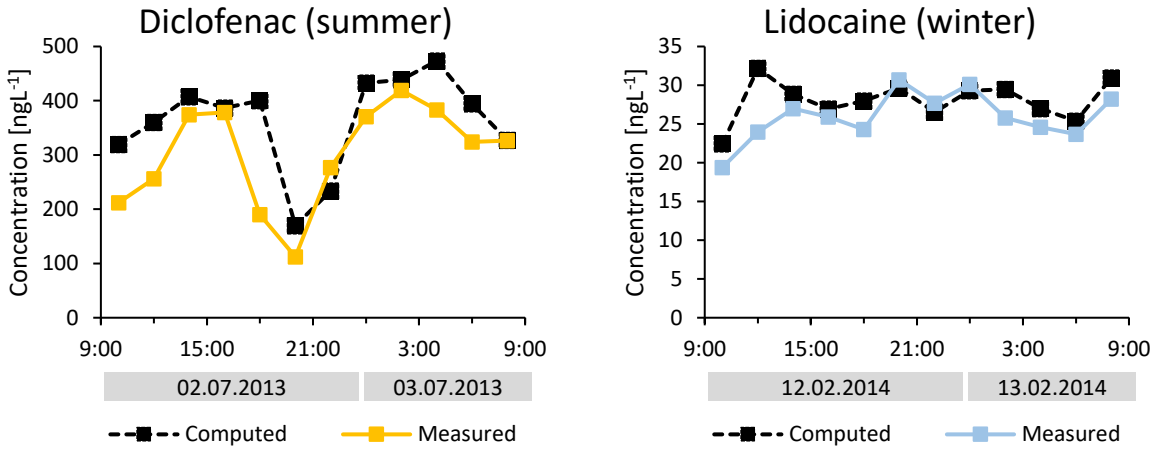

Figure S8. Patterns observed for diclofenac and lidocaine during the summer and winter 24 h-sampling campaigns, respectively.

Table S4. Summary of calculated k and corresponding half-life $t_{1/2}$, k_{day} and k_{night} decay constants for compounds investigated in the studied River Steinlach segment during the summer and winter 24 h-sampling campaigns.

	Summer campaign (2-3.07.2013)				**Winter campaign (12-13.02.2014)**			
	24 h		Day-time	Night-time	24 h		Day-time	Night-time
	k [day^{-1}]	$t_{1/2}$ [days]	k_{day} [day^{-1}]	k_{night} [day^{-1}]	k [day^{-1}]	$t_{1/2}$ [days]	k_{day} [day^{-1}]	k_{night} [day^{-1}]
AHTN	1.7	0.4	2.6	0.9	3.4	0.2	2.1	4.3
Carbamazepine	0.2	3.8	0.5	0.1	0.1	5.7	0.3	0.1
DEET	-0.1	/	0.4	0.0	1.2	0.6	-0.3	2.3
Diclofenac	1.2	0.6	1.3	0.8	/			
Lidocaine	/				0.7	1.0	1.3	0.3
Naproxen	0.7	0.9	1.2	0.4	-0.1	/	-0.1	-0.3
HHCB	2.4	0.3	3.9	1.9	4.1	0.2	3.3	4.7
HHCB-lactone	1.2	0.6	1.4	1.3	0.6	2.1	1.1	0.5
Mecoprop	0.6	1.2	0.4	0.7	-2.4	/	-2.6	-2.1
OTNE	4.2	0.2	6.3	2.9	5.0	0.1	2.8	6.0
Oxcarbazepine	5.7	0.1	11.7	3.9	1.4	0.5	1.1	1.2
TAED	1.3	0.5	4.6	-0.2	2.9	0.2	6.2	2.6
Triclosan	2.9	0.2	4.6	0.4	0.7	1.0	0.0	1.3
TCEP	0.7	0.7	1.2	0.3	/	0.0	0.0	0.0
TCPP	-0.1	/	-0.3	0.2	-0.8	/	-0.9	-0.8
TDCPP	0.1	7.1	0.5	0.2	-0.5	/	-0.2	-0.2
Calcium	0.0	/	0.0	0.0	0.1	7.0	0.3	0.1
Chloride	0.0	57.2	0.1	0.0	0.0	105.7	0.1	0.1
Magnesium	-0.9	/	-1.0	-0.8	0.0	95.2	0.1	-0.1
Nitrate	0.3	2.5	0.4	0.2	0.3	2.6	0.4	0.3
Potassium	0.1	12.2	0.2	0.0	0.1	6.8	0.1	0.1
Sodium	0.0	18.5	0.0	0.1	0.0	23.6	0.1	0.0
Sulfate	0.0	48.0	0.1	0.0	0.1	8.9	0.1	0.2

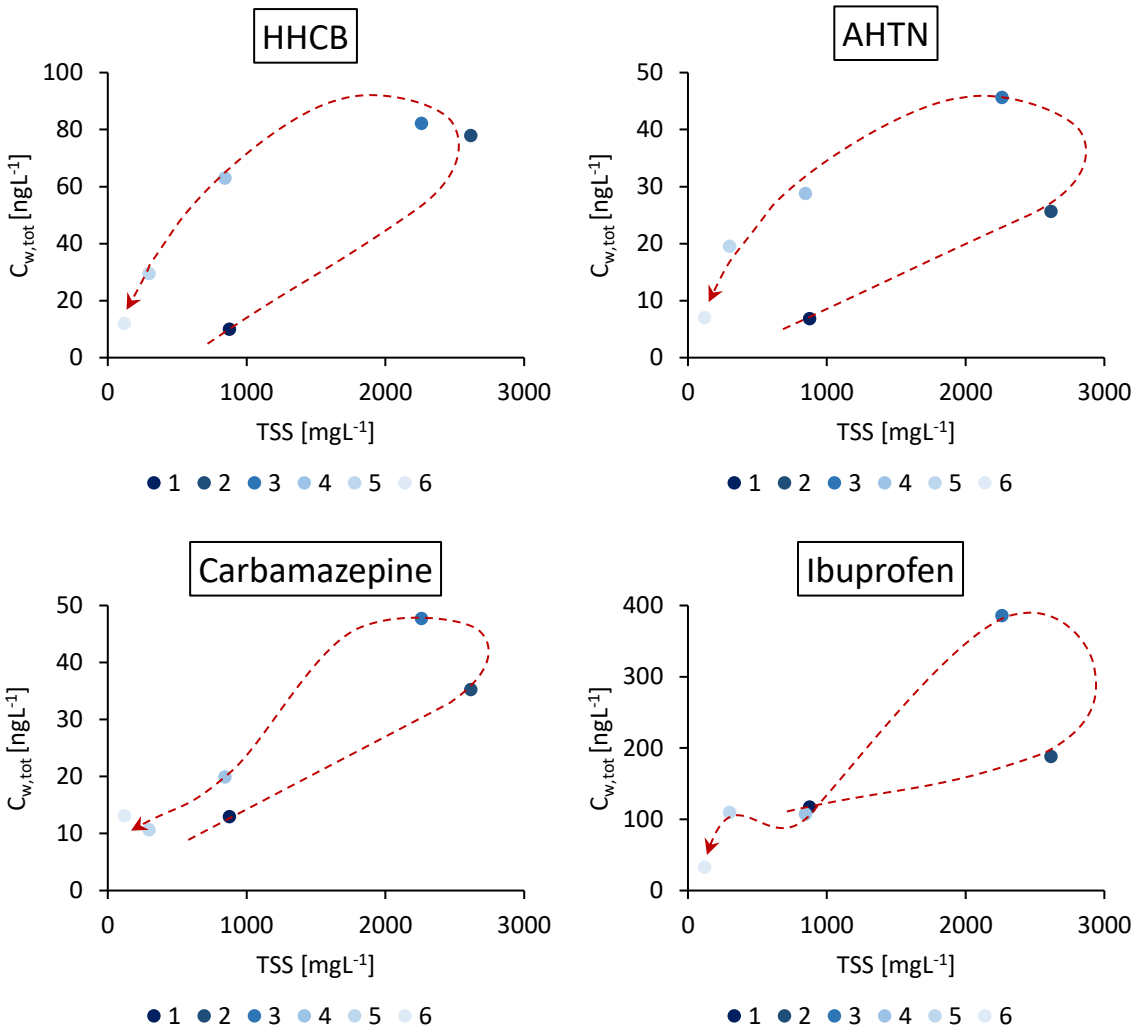

Figure S9. Concentrations of wastewater contaminants presenting hysteresis behaviors versus TSS with sample number during the Steinlach flood.

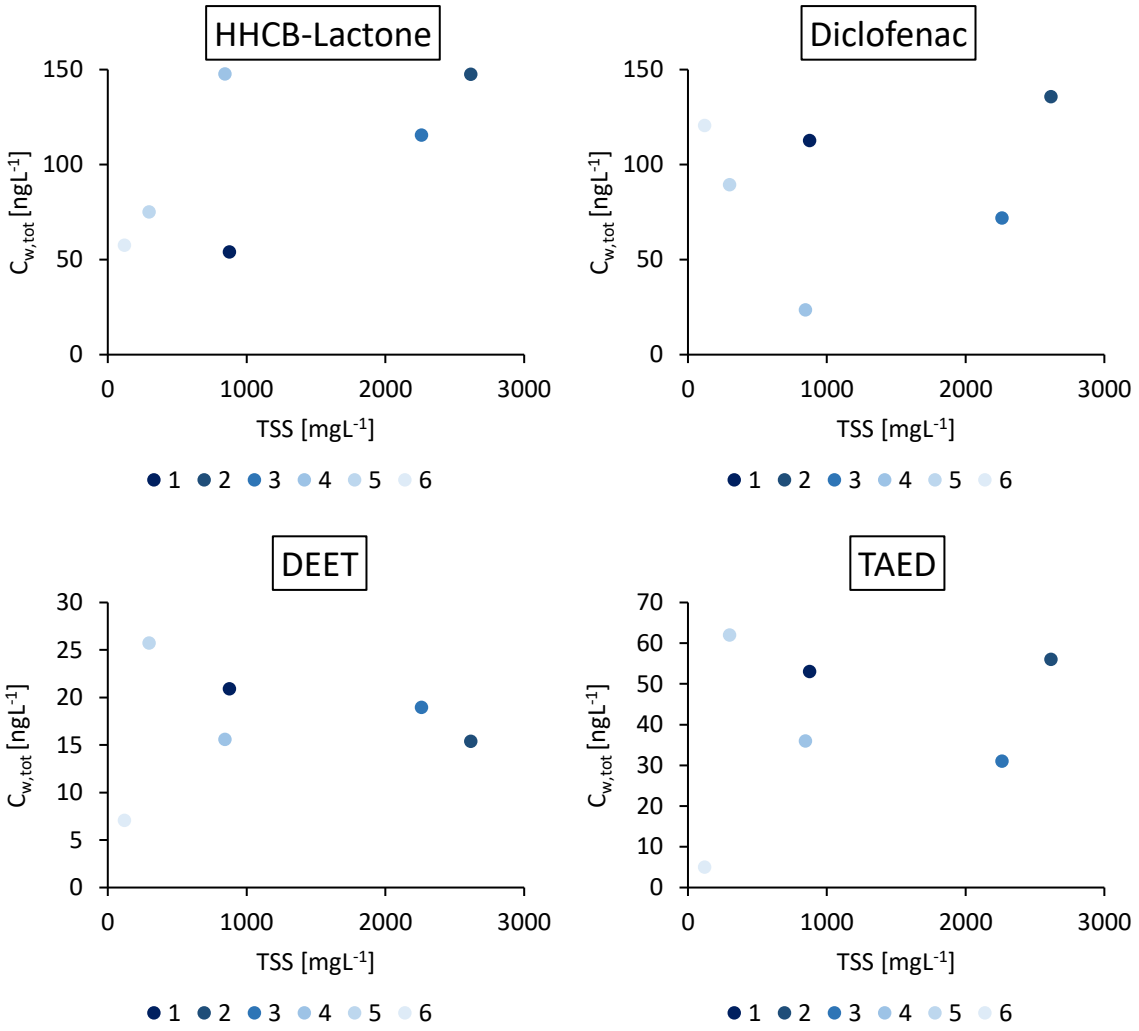

Figure S10. Concentrations of wastewater contaminants presenting no hysteresis behavior versus TSS with sample number during the Steinlach flood.

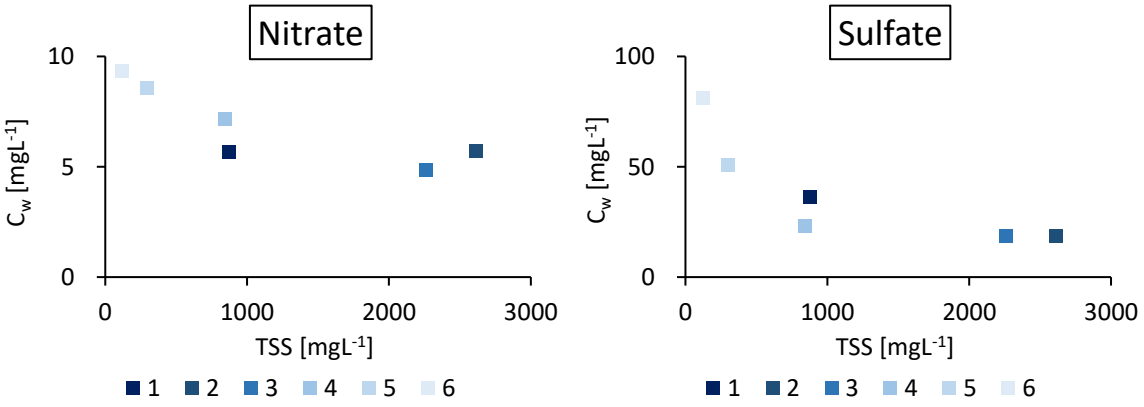

Figure S11. Concentration of inorganic ions presenting no hysteresis behavior versus TSS with sample number during the Steinlach flood.

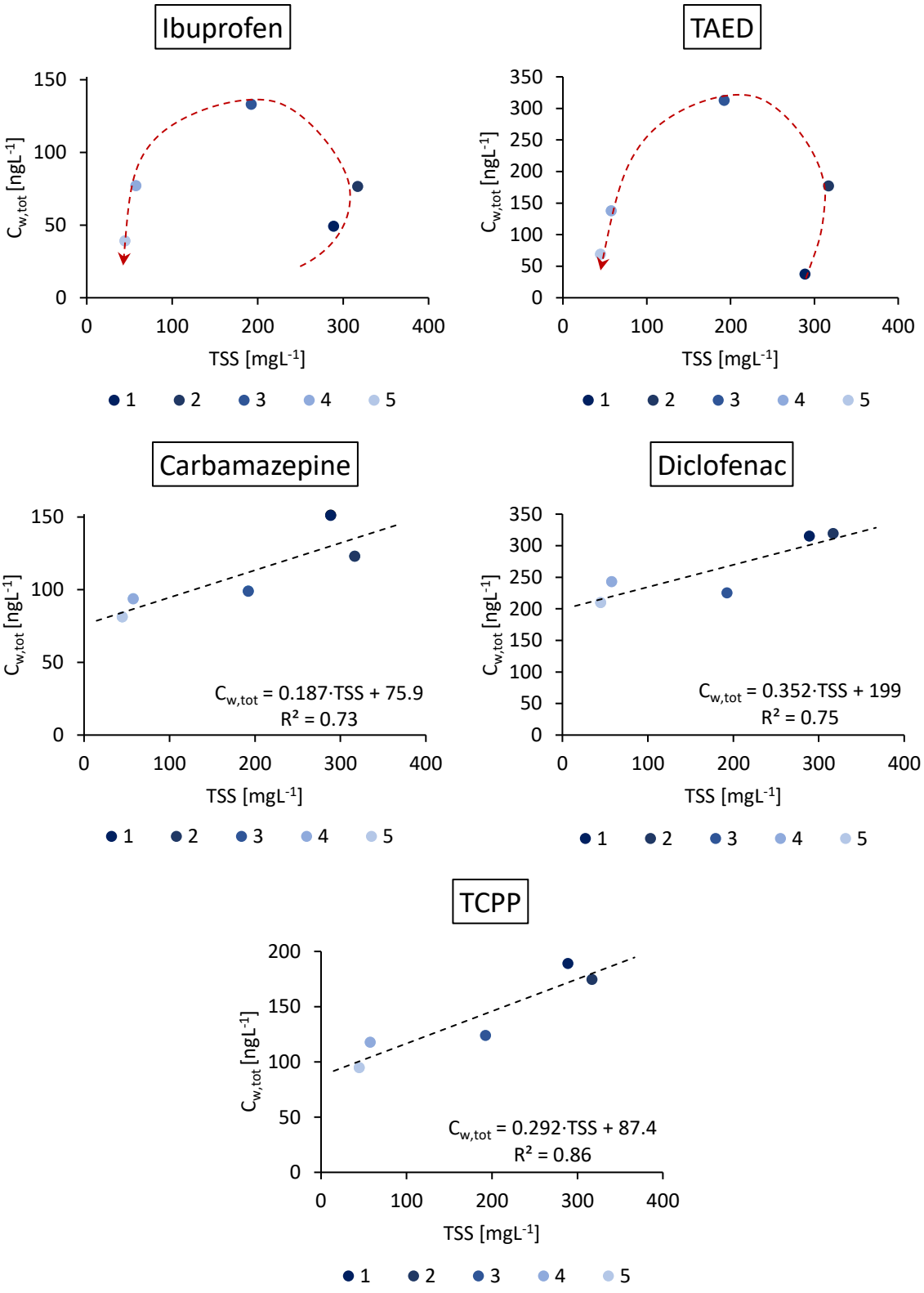

Figure S12. Concentration of wastewater contaminants versus TSS with sample number during the Ammer flood.

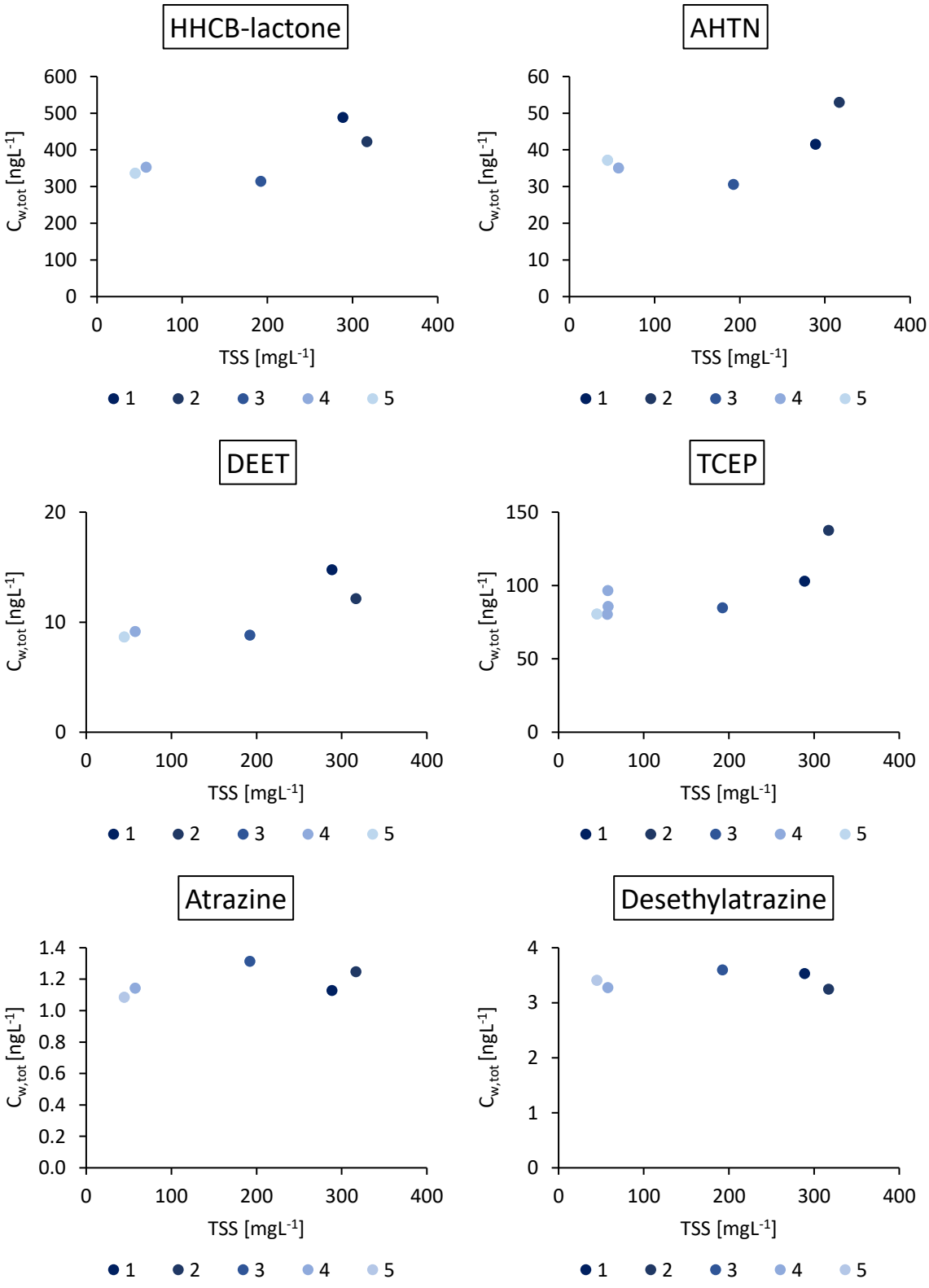

Figure S13. Concentration of organic contaminants versus TSS with sample number during the Ammer flood.

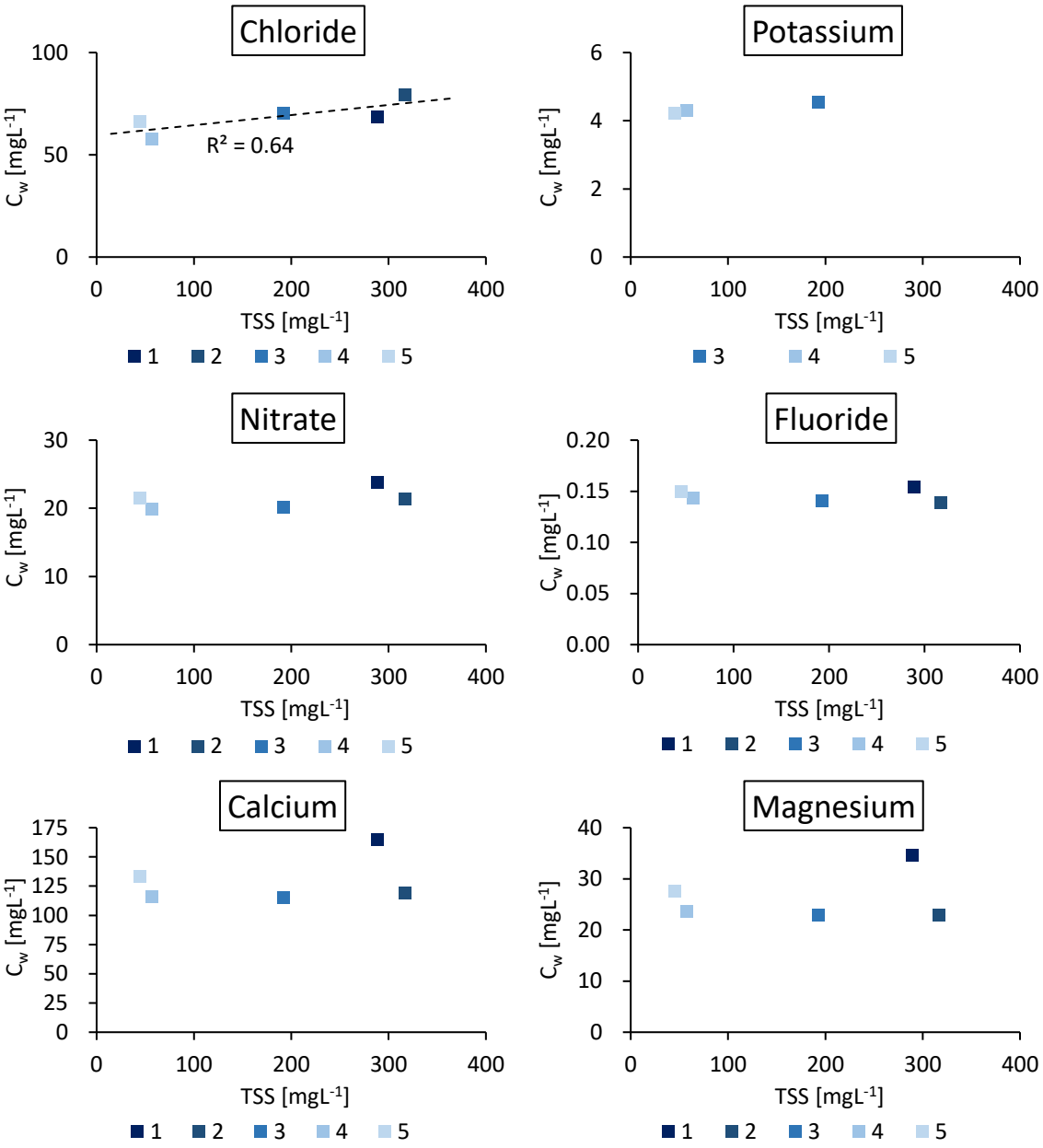

Figure S14. Concentration of inorganic ions versus TSS with sample number during the Ammer flood.

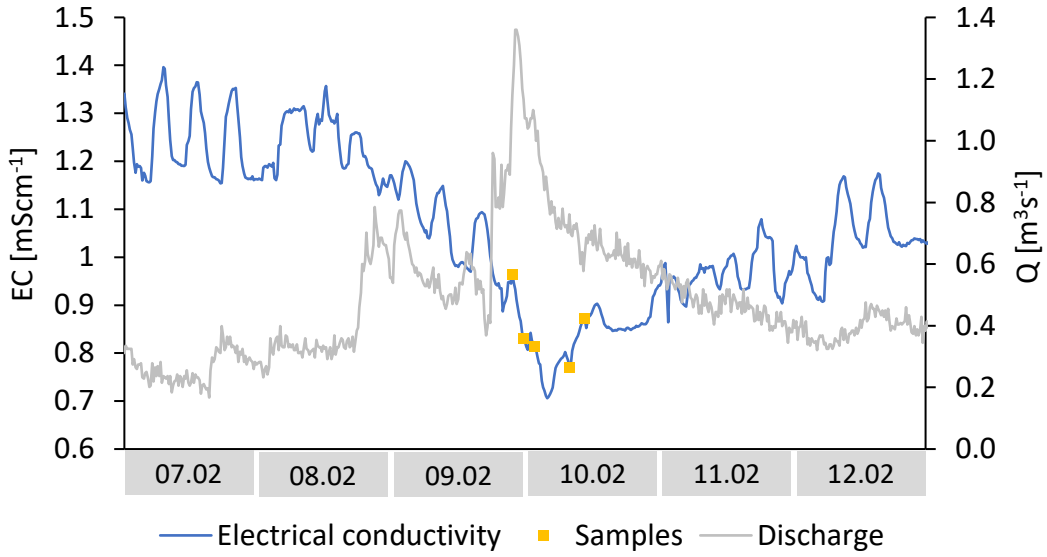

Figure S15. Specific electrical conductivity (EC) and discharge (Q) measured at the Pfäffingen gauge in the days preceding and following the Ammer flood sampled.